Stress Evaluation in Web Gap Details Prone to Distortion Induced Fatigue

by

Mohamad Najari

A thesis submitted in partial fulfillment of the requirements for the degree of

Doctor of Philosophy

in

Structural Engineering

Department of Civil and Environmental Engineering
University of Alberta

Abstract

The most common fatigue problem in steel structures is fatigue cracking caused by distortion. Although methods of repair for structures that suffer from distortion induced fatigue do exist, our ability to assess the resistance of existing structures is lacking. Consequently, it is difficult to assess whether structures with details that are known to be prone to distortion induced fatigue should be rehabilitated or not; costly repairs are often executed without knowing whether these rehabilitations are necessary.

An investigation of prediction methods for web gap stresses indicated that the governing web gap stress is a function of several parameters (e.g. lateral stiffness of the flange, stiffness of the stiffener, magnitude of the differential displacement, and several other factors that have been identified to affect the stresses developed in the web gap) and a simple method of analysis that incorporates all these parameters does not exist.

In this study the web gap stress prediction equation was built upon the knowledge gained in earlier projects and finite element investigation to develop an accurate method of assessing resistance to distortion induced fatigue and to develop a model that can assess the stress in details subjected to distortion induced fatigue. Dimensional analysis approach is used to obtain the equation to calculate the magnitude of stress in these details as a function of geometrical variables and applied loads. The results of this research will be used to assess the fatigue resistance of these details in order to extend the service life of aging bridge steel structures without compromising their level of safety.

Although the proposed empirical equations are analytically more complicated than the previously used equations to calculate the stress, they predict the stress in the web gap within 20 percent and cover a wide range of parameters which almost includes all the steel multi-girder bridges with bend plate diaphragm. Considering all the complexity in the web gap details, this is an acceptable accuracy for the stress calculation.

Linear elastic fracture mechanics approach, used in this study to investigate fatigue behavior of the web gap detail, proved that even though the fracture in the detail is a mixed-mode fracture, Mode I is the governing mode for these details.

ACKNOWLEDGEMENTS

This project was mostly funded by Natural Sciences and Engineering Research Council of Canada and AECOM Technology Corporation. I would like to acknowledge their support.

I would like to express my sincere gratitude to Dr. Marwan El-Rich for his constant support, guidance, insightful comments. He was always there for me to help and provide more than sufficient support without which this work would not be carried out.

I would like to thank Dr. Gilbert Y. Grondin for his technical support and guidance throughout different stages of the project.

I would also like to appreciate my supervisory committee, Dr. Samer Adeeb, Dr. Carlos Cruz Noguez, as well as the examining committee, Dr. Caroline Bennett, and Dr. Ben Jar for their comments and guidance.

In addition, I would like to extend my deepest thanks and gratitude to my caring and supporting family in Iran for always providing me with an opportunity to succeed in life.

And the greatest thanks to my wonderful wife, Saba, who, by her patience, support, encouragement and with a heart full of love has contributed to the fulfillment of this work. She sacrificed the best years of her life and so much more to help me accomplish my aspirations.

TABLE OF CONTENTS

LIST OF FIGURES

LIST OF TABLES

Chapter 1

Introduction

1.1. Motivation

Canada has well-developed and countrywide transportation system such as roads, rails and bridges; but almost 50% of Canadian highway bridges were built prior to 1970 to cope with increasing demand arising from a strong growth in population, increased urbanization, and increased car usage (Gagnon et. al. (2008)). These bridges have reached or are nearing the end of their service life. Fatigue of steel highway and railway bridges is a common problem with aging infrastructures, which results in important overall economic losses, either from costs of repair or loss of use of the structure. Therefore, with ageing of our bridge infrastructure it is crucial to assess current bridges more accurately both to avoid unnecessary expenditures and to make sure they are in a safe operating condition.

In multi-girder steel bridges, to transfer lateral loads and distribute live loads among the girders, diaphragm members are used at the location of transverse stiffeners welded to the girder web. Prior to 1985, connection between these diaphragms connection stiffeners and the girder tension flange was rarely provided to avoid a potential load fatigue prone detail. Therefore, the gap between the tension flange and the stiffener leaves the girder web unstiffened in the connection detail. This gap is known as "Web Gap". While applying cyclic traffic loads which are not uniformly distributed among girders, there is always a differential deflection between two adjacent girders. This differential vertical deflection causes a racking motion in the diaphragm connecting the two girders. This rotation is resisted by a couple of horizontal forces and results in cyclic out-of-plane distortion and large stress ranges in the web gap. This intense stress gradient accelerates initiation and propagation of cracks in both longitudinal and vertical

directions in that region. These cracks are the most common fatigue deficiency in highway and railway bridges. It is estimated that 90% of all fatigue cracking is the result of out-of-plane distortion at fatigue prone details (Connor & Fisher, 2006). Longitudinal web gaps are also presented in most gusset plate connections. These details are designed for lateral bracing and also reported as a distortional-induced fatigue prone detail (Fisher, 1990). Further explanation and details about this problem is discussed in Chapter 2.

1.2. Objectives and Scope

There are many factors that affect web gap stresses which are discussed in the following. These factors make the stress assessment in the details subjected to out-of-plane stress even more complicated. Although many researchers have investigated the local stress due to out-of-plane deformation in the web gaps, a method to find the magnitude of distortional stresses is still not well developed. Moreover, it has been shown that the stress is very difficult and expensive to predict from field investigations and experimental studies. Therefore, a simple and comprehensive method should be developed to assess the stress in the web gap details. This method has to consider the most significant parameters affecting the stress magnitude in the details and to be applicable to any multi-girder steel bridges with these web gaps.

Loading, material properties, geometrical configuration, residual stresses, and initial imperfections of the component subjected to cyclic loading are some of the factors affecting the performance of the steel structures. The more information we have in this regard, the more accurately we can assess distortion-induced fatigue prone details. Material properties and geometrical details can be obtained by experimental tests and measurements. For the details subjected to stress-induced (load-induced) fatigue loading, the stress range is also a known factor. Therefore, from simple approaches such as S-N fatigue life prediction curves, the details can be assessed and the remaining life can be predicted. Without using a simple method such as fatigue curves, it is costly to assess and evaluate the fatigue resistance of the details. For the details subjected to distortion induced fatigue, current S-N fatigue curves cannot be used as they do not account for parameters affecting these fatigue prone details. Even with a fatigue curve for distortion induced fatigue, the details still have to be investigated to obtain the stress range. Therefore, first of all, the magnitude of the stress in the web gap should be obtained to be able to assess the fatigue life of the detail. In addition the suitable S-N fatigue curve should be

developed for the details prone to distortion induced fatigue, in future researches as well, as engineers are still left without guidance when evaluating an existing bridge with distortion induced fatigue.

The objectives of this research are to develop a model that can assess the stress in details subjected to distortion induced fatigue and to investigate the fatigue life of the web gap details using fracture mechanics. The results of this research will be used to assess the fatigue resistance of these details in order to properly assess the service life of aging bridge steel structures without compromising their level of safety. Finite element (FE) analysis will be conducted to perform parametric study and obtain the stress states in the details. The results will be compared to existing experimental findings of former experimental researches to develop and verify the equation to evaluate the web gap stress.

In this study, steel multi-girder bridges with staggered bend plate diaphragm are assessed. The angle of skew is assumed to be zero. Therefore, the girders are considered as none-skewed. This makes the calculation more straightforward. Moreover, in future studies the effect of the skew angle can be investigated and a modification factor can be proposed.

The distortion induced fatigue (or fatigue due to cyclic out of plane movements) problems present many challenges in the fatigue assessment, when it comes to evaluating the magnitude of stress in the detail, the crack initiation and growth behaviour, and to assess the repairing technique. Although, there are numerous researches in this area, the web gap stress in steel multi-girder bridges cannot be accurately calculated yet without a detailed FE analysis and having a simple and comprehensive approach to evaluate fatigue resistance of the detail considering all the mentioned parameters, is still lacking.

Based on the knowledge gained in earlier projects on steel members with stress induced fatigue cracks, the main objective of this research is to develop an accurate method of assessing resistance of details subjected to distortion induced fatigue. Calculating the stress in these details is considered as the initial step of this assessment.

The main scope of the research is to develop a simple, but comprehensive method to predict the structural stress in the web gap details. This will be used in combination to a proper S-N curve to assess the fatigue life of the details prone to distortion induced fatigue. The results of

this study will propose guidelines to be considered in the assessment of steel details subjected to out-of-plane deformation under cyclic load.

1.3. Methodology

The literature review in Chapter 2 indicates that the governing web gap stress is a function of several parameters (e.g. lateral stiffness of the flange, stiffness of the stiffener, magnitude of the differential displacement, and several other factors) and a simple method of analysis that incorporates all these parameters does not exist. Therefore, a method to predict the maximum web gap stress in multi-girder steel bridges is developed at the first step of this research. This method includes parameters such as lateral and torsional stiffness of the tension flange, stiffness of the stiffener, diaphragm spacing, and web gap stiffness

In the next step, detailed FE models of full-size girders that mimic the experimental tests described in references (Hartman et al, 2013) will be constructed using ABAQUS 13. These models will serve as global models for further detailed analysis. To reduce modeling time and cost, local models of the web gaps will be developed. Refined mesh will be used in these models to determine the localized strains and stresses at that region. The boundary conditions in the local models are based on the analysis results from the global models. Obtained stresses and strains from the local models will be used in order assess the accuracy of the proposed equation. The local model will be used to assess the fatigue life of details subjected to distortion induced fatigue. It should be noted that data from other available experimental test results (D'Andrea, Grondin, & Kulak, 2001; Fraser, Grondin, & Kulak, 2000) and field measurements (Jajich, Schultz, Bergson, & Galambos, 2000; Severtson, Beukema, & Schultz, 2004) will be used to evaluate the proposed web gap stress prediction model.

In the parametric study stage, geometric dimensions are varied according to Chapter 5. These ranges are selected to cover the common web gap dimensions and global bridge geometries reported in the bridge inventories (Berglund & Schultz, 2001).

1.4. Organization of Thesis

This thesis consists of 7 chapters including *Introduction* which is included in the Chapter 1.

In Chapter 2, a brief background of distortion induced fatigue, details prone to this problem, models used in order to calculate the stress in these details, and parameter affecting the magnitude of this stress are presented. It should be noted that the background of fracture mechanics approach which is used in fatigue life assessment of the web gap, dimensional analysis, design of experiments, and regression methods are presented in the thesis body and in the corresponding chapters and prior to their applications. In addition, theories of plates and shells used in order to obtain the web plate stiffness in steel multi-girder bridges and the required calculations are presented in Appendix A.

Finite element modeling techniques are discussed in Chapter 3. A comprehensive finite element model of a steel bridge with three 9.1 m girders is created. This model was constructed in order to serve as the global model for the sub models used in this study to investigate the behavior of the web gap details. This chapter also includes the experimental tests results as well as the analytical results used to verify the finite element modeling procedures.

Using the mentioned global model developed in Chapter 3, the fatigue life of the web gap detail is assessed using fracture mechanics and the findings of this investigation is compared with the observed life of the detail. These results which are presented in Chapter 4 confirm the accuracy of the modeling procedure once again and provide a better understanding of the governing failure mode of the cracks prone to distortion induced fatigue.

Chapter 5 includes a brief background of dimensional analysis and its application in structural engineering field. The dimensionless π-parameters used in the experimental design are formed in this chapter and the results of the scale independency study required for dimensional analysis are also included here.

The screening study for each dimensionless parameter was conducted in Chapter 6 to obtain a better idea for the influence of each dimensionless parameter on the response function (the magnitude of stress in the web gap). Using the information gained from the screening study, the

experiments were designed to generate data using finite element analysis for regression analysis. Non-linear exponential regression applied on the data and the empirical web gap stress prediction equations are developed in Chapter 6. This chapter also provides the assessment of the proposed equations using two experimental programs at University of Alberta and University of Kansas, as well as a finite element study at University of Minnesota which was validated using field measurements and monitoring.

The last chapter (Chapter 7) includes a summary of the work, conclusions obtained from this study, in addition to some recommendations for further studies.

The appendixes are presented at the end of the thesis. Appendix A includes the method used to calculate and obtain the web plate stiffness at the web gap detail. Appendix B and C present the models dimensions and results of the finite element analysis for the screening study and the design of experiments, respectively.

Chapter 2

Background and Literature Review

2.1. Fatigue in Structural Engineering

Most engineering structures and machines such as bridges, cranes, drilling equipment, etc., are under dynamic load such as traffic load, reciprocal and rotational load. Fatigue in these structures is the weakening of the material by initiating micro-cracks and propagating the cracks in their structural members caused by these repeatedly applied loads. These cracks propagate further by continued application of cyclic load and cause the failure of the member and eventually, in the worse cases, the failure of the structures themselves. Depending on the applied load, the location and the deformation of the fatigue prone detail, fatigue can be divided in two categories, load-induced fatigue and distortion induced fatigue. The most common fatigue problem in steel structures is fatigue cracking caused by distortion which is introduced in the following section.

In terms of fatigue life which is simply defined as the number of load cycles, or more specifically stress cycles, that the member sustains before failure, there are high cycle fatigue and low cycle fatigue. There is no distinguishing number of cycles that can specify these types of fatigue. High cycle fatigue is characterized by low amplitude high frequency elastic strains. For instance, tuning fork under a strike vibrates at several cycles a second and eventually it maintain the original shape. Conversely, low cycle fatigue is characterized by high amplitude low frequency plastic strains. Fatigue in a thin aluminum bar under bending can be considered to be low cycle fatigue as it deforms the bar plastically and after some load plastic deformation remains in the bar.

2.2. Distortion Induced Fatigue

As it is mentioned in previous section, distortion induced fatigue is the most common fatigue problem in steel structures specifically multi-still girder bridges built prior to 1985 (Fisher, Fisher, & Kostem, 1979). It is mostly caused by out-of-plane distortion in the structural member because of the nature of three-dimensional stress developed in the member. In another words, the life of a detail prone to distortion induced fatigue is shorter than another member with the same material and under the same stress range but under load induced fatigue load.

In multi-girder steel bridges, to transfer lateral loads and to distribute live loads among the girders, diaphragm members are used at the location of transverse stiffeners welded to the girder web. Prior to 1985, connection between these transverse stiffeners and the girder tension flange was rarely provided to avoid a potential fatigue prone detail. Therefore, the gap between the tension flange and the stiffener leaves the girder web unstiffened in the connection detail. While applying cyclic traffic loads which are not uniformly distributed among girders, there is always a differential deflection between two adjacent girders. This differential vertical deflection causes a racking motion in the diaphragm that connects the two girders. This rotation is resisted by a couple of horizontal forces and results in cyclic out-of-plane distortion and large stress ranges in the web gap. This intense stress gradient accelerates initiation and propagation of cracks in both longitudinal and vertical directions in that region. These cracks are the most common fatigue deficiency in highway and railway bridges to the extent that Connor and Fisher (Connor & Fisher, 2006) estimated that 90% of all fatigue cracking is the result of out-of-plane distortion at fatigue prone details. Longitudinal web gaps are also presented in most gusset plate connections. These details are designed for lateral bracing and also reported as a distortion-induced fatigue prone detail (Fisher, 1990). Figure 2- 1 and Figure 2- 2 illustrate the location of the web gap in multi-girder bridges and in lateral gusset plate connections, respectively.

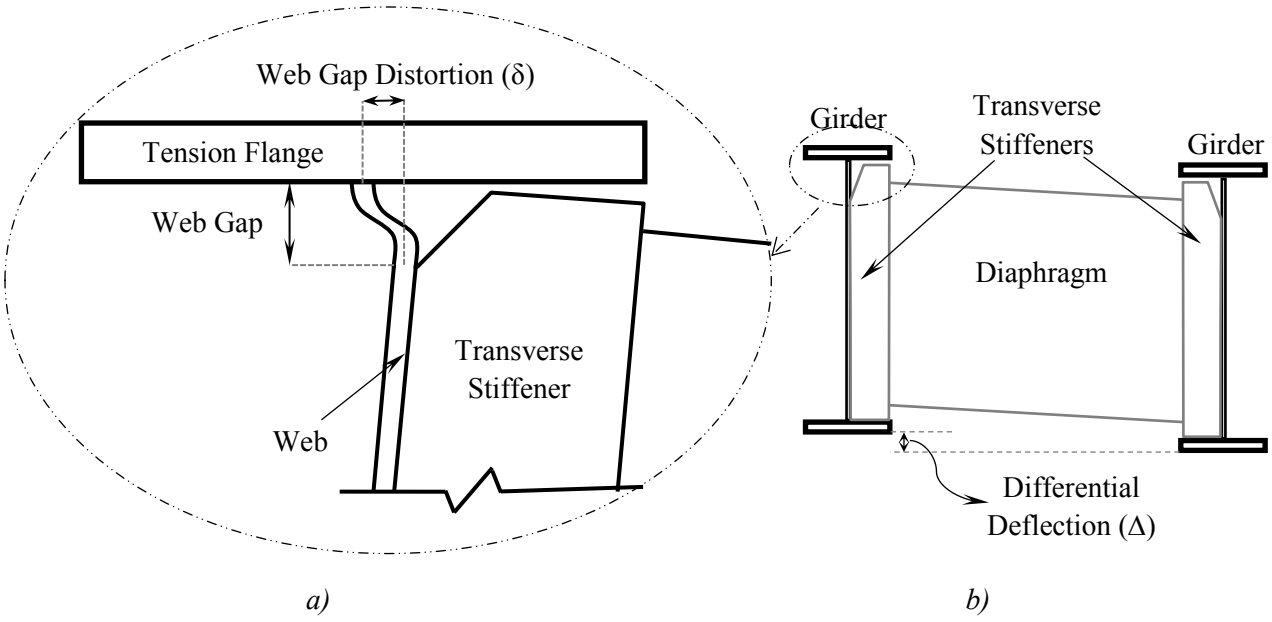

Figure 2- 1: a) Web gap distortion, b) Differential deflection of two adjacent girders.

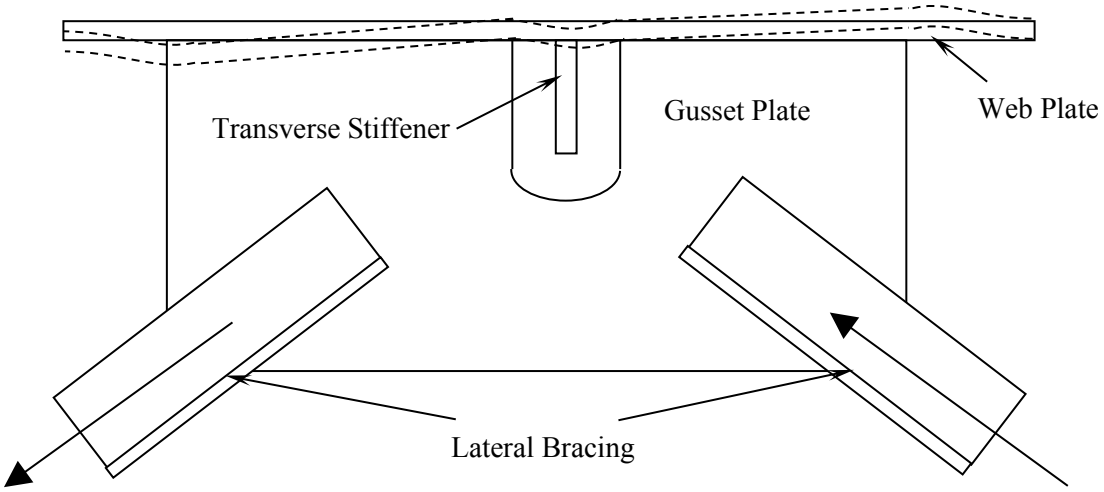

Figure 2- 2: Lateral gusset plate connections distortion.

2.3. Web Gaps in Multi-Girder Bridges

In this study the web gap details in steel multi-girder bridges are considered as details prone to distortion induced fatigue, and are investigated further. These details are located in web plate adjacent to the girder flanges. They are mostly in top portion of web in negative moment segments of the girders and in the bottom portion of the web plate in positive segments of the girders. Because of the short length of this gap and the relatively huge out of plane distortion which should be transferred to the web plate, the large vertical in plane stress as well as out of

plane stress are created in the web gap. The locations of the maximum and minimum stresses are at the top and bottom parts of the web gap. In another words, for web gaps located in positive moment segment of the girder, the cracks can possibly located at stiffener to web weld toe and top of bottom flange to web weld toe. This can also occur at top web gaps. This is well described in Figure 2-3. For the negative moment segments of the girder, the locations of the maximum and minimum stresses are below the top flange and web weld toe and top of the stiffener and web weld toe. This high cyclic stress magnitude in the detail leads the detail to be cracked at these locations. This crack sometimes propagates through the thickness of the web and sometimes the propagation stops and doesn't continue through the web thickness. The most common shapes of the cracks are shown in Figure 2-3. The initiation and propagation of these cracks as well as fatigue assessment of these details are described in Chapter 3.

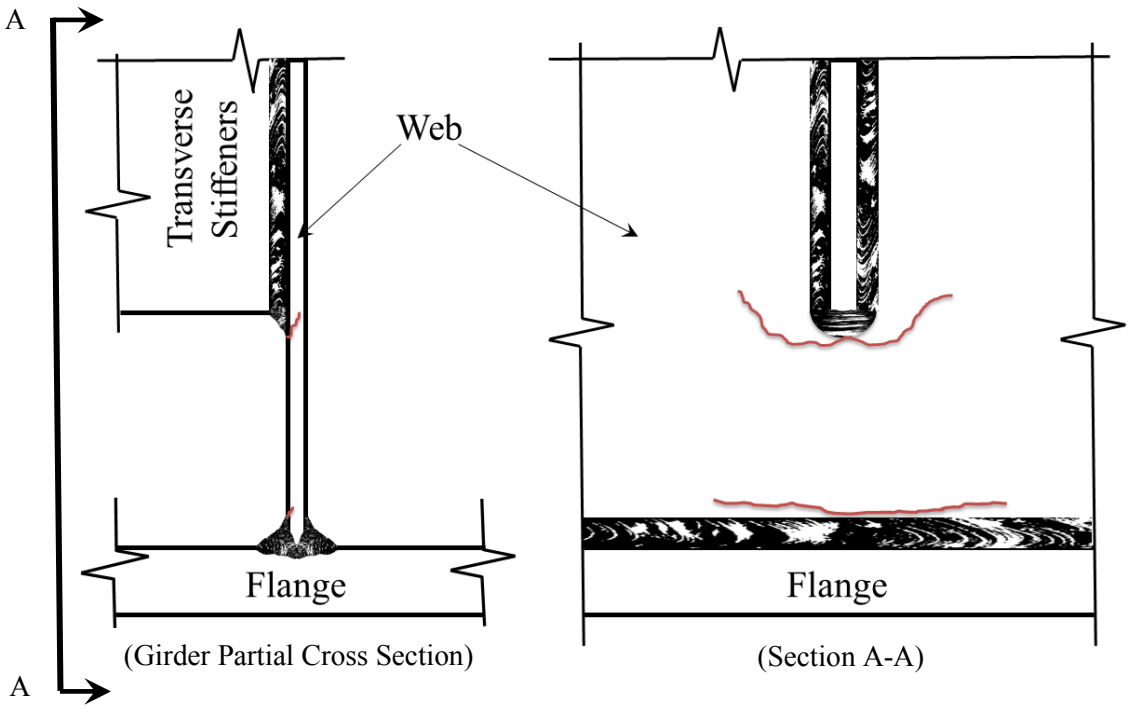

Figure 2- 3: Location of a web gap in positive moment segments of the girder and possible location of cracks

2.4. Parameters Affecting Web Gap Stress

There are many factors that affect web gap stresses which are discussed in this section. These factors make the stress assessment in the details subjected to a complex out-of-plane stress distribution. Loading, material properties, geometrical configuration, residual stresses, and initial imperfections of the component subjected to cyclic loading are some of the factors affecting the performance of the steel structures.

In general, the parameters affecting the web gap stress can be divided in two groups depending on their relative location to the web gap. These two groups are named as local parameters and global parameters.

Although weld geometry, weld deficiency, and residual stress affect the magnitude of the stress and the fatigue life of a crack, they are not included in this study.

2.4.1. Local Parameters

Geometrical dimensions of web plate, tension flange, and stiffener directly affect the magnitude of the vertical stress as well as the magnitude of the web gap distortion. These parameters are presented in this section. The practical ranges of these parameters are presented in the following chapters.

2.4.1.1. Web Gap Length

Web gap length can be considered as one of the most critical parameters to assess the web gap stress. The longer the web gap, the more flexible the detail and it can absorb the distortion and deform easier.

2.4.1.2. Web Thickness

This parameter is also one of the principal parameters in web gap stress calculation. The thicker the web plate, the stiffer the web gap will be. This decreases the deformability of the web gap which creates higher stress at weld toes in the detail (Li and Schults 2005). Web thickness and web gap length can also be combined to form a unique parameter named web gap plate stiffness.

2.4.1.3. Tension Flange Lateral and Torsional Stiffnesses

Depending on the positive or negative moment segment of the girder, a web gap can be either located in the top portion of the web and below the top flange, or, in the bottom portion of the web and above the bottom flange. When the transverse stiffener is pulled by the diaphragm plate or cross brace frame as a result of differential deformation, the web gap is both under lateral deformation and longitudinal rotation. The mentioned deformation and rotation are transferred to the tension flange. In the case where the top flange is in tension and the web gap is in the top portion of the web plate, as the top flange is totally constrained in the concrete deck, the boundary condition at the flange can be considered as a fixed support. In such a case, the deformation and rotation do not transfer to the tension flange and the stiffness of the top flange does not affect the stress in the web gap detail.

In the positive segment of the girder where the bottom flange is in tension, the web gap is located in the bottom portion of the web plate. In this case, the bottom flange plays a significant role in deformation of the web gap. A main portion of the transformed lateral displacement from the transverse stiffener is transferred to the bottom flange as it is not laterally supported at the web gap location. The rotation of the bottom part of the web gap also creates torsion in the bottom web gap (Severtson *et. al*. 2004). Therefore, the lateral torsional stiffness and out of plane bending stiffness of the bottom flange are also very important parameters in the web gap stress calculation. The stiffer the bottom flange, the more rigid the boundary condition it provides for the bottom part of the web gap. This results in higher stress in the web gap detail. The tension flange lateral and torsional stiffnesses can be calculated using the dimensions of the flange plate including flange plate thickness, flange plate width, and the transverse stiffener spacing.

2.4.1.4. Transverse Stiffener Stiffness

Transverse stiffener stiffness is also an important parameter and has significant effect on the stress in the web gap detail. The transverse stiffener is directly attached to the web plate and creates a stress concentrated prone detail at the connection. A thin plate for the stiffener increases the concentrated stress in the web plate. This is because the load from the transverse stiffener is

applied in a very small area in comparison to a thicker stiffener plate. Stiffener in comparison with the web plate is relatively rigid and without a noticeable deformation transfers the rotation created by differential deflection of adjacent girders. The effect of the transverse stiffeners is not studied anywhere in the literature. This will be discussed further in the following chapters.

2.4.1.5. Diaphragm and Cross Brace Frame Stiffness

Diaphragm plate and cross frame members are present for construction purposes, to transfer lateral loads and, to some extent, distribute live loads among the girders. The load created by differential deflection between the two adjacent girders resulting from these live loads is transferred by diaphragm plates or the cross brace frames to the web gap and results in distortion in the detail.

If the diaphragm plate and cross brace frame members are flexible, less rotation from the differential deflection is transferred to the web gap and this deferential displacement mostly deforms the diaphragm plate or cross brace frame member itself. In other words, the adjacent girders would deform almost independently which reduces the magnitude of distortion in the web gap, significantly.

2.4.2. Global Parameters

These parameters indirectly affect the magnitude of the web gap distortion. They play a significant role in the magnitude of the differential deflection which is transformed to the web gap by diaphragm plate or cross frame brace.

2.4.2.1. Girder Spacing

Differential deflection is transferred and becomes web gap distortion by almost a rigid rotation of the diaphragm plate as shown in Figure 2-1. Therefore, the girder spacing can be another important parameter in web gap stress calculation. This parameter can be inherently

considered as diaphragm stiffness and has the same effect on the web gap distortion. The longer the girder spacing the less rotation in the diaphragm and less distortion in the web gap detail.

2.4.2.2. Deck Thickness

Deck thickness has a direct effect on the magnitude of differential deflection. Even though a very thick or an almost rigid deck can reduce the differential deflection, a small rotation is still created in the diaphragm plate or the cross brace frame. Therefore, if the differential deflection is a known parameter and is already available, the effect of stiffness of the bridge deck has already been considered in the calculation and there is no need to investigate this parameter any further.

2.4.2.3. Span Length

Span length is also one of the primary bridge characteristics used to calculate the deflection of the bridge girders. Therefore, it is very important in order to find the differential deflection between two adjacent girders and consequently calculate the web gap distortion and stress magnitude. Longer span length results in more flexible girders. These girders have higher differential deflection under none uniform distributed load.

2.4.2.4. Angle of Skew

Hassel et al. (H. L. Hassel, Hartman, Bennett, Matamoros, & Rolfe, 2010) and (H. Hassel, Bennett, Matamoros, & Rolfe, 2012) examined the relationships between skew angle (0°, 20°, and 40°), cross-frame spacing (at 2.29 to 9.14 m (7.50 to 30.0 ft.)), and stresses on distortion-induced fatigue susceptibility using numerical models. The cross-frame configurations examined included staggered perpendicular to the girder line as well as parallel to the support skew. Equal-leg angle cross-frame elements were selected for skewed bridges on the basis of both slenderness ratio and stiffness. Connections between girder webs and flanges as well as girder webs and connection plates were modeled with 15.9 mm welds and were rigidly connected with surface-to-surface tie constraints. It was found that, although in every model the 20° skew resulted in the

highest web-gap principal stresses, no clear trend was established between skew angle and web-gap stress.

2.4.2.5. Bracing Spacing, Types, and Configurations

Wang et al (Wang, Yan, & Cheng, 2013) established numerical analysis models (using the finite element solver, ANSYS) of a three-span (25, 35, and 25 m) continuous curved steel girder bridge with five welded plate girders spaced at 2.7m to investigate the fatigue stress at the web gaps. Cross frames were placed in the radial direction every 5m in the longitudinal direction of the bridge. They applied five different AASHTO fatigue truck load cases (AASHTO, 2007) but only presented the results of load case I (the last axis of AASHTO fatigue truck was located at cross-frame I longitudinal). Different web gap length, web thickness, curvature radius, and cross-frame layout (X and K) were investigated to find web gap deflection and vertical bending stresses in different web gap height at various locations. They found that under applied loads, different out-of-plane distortion occurred at various positions in web gaps, and the web gap was subject to double curvature; both the bottom web gap at middle span area and the top web gap at support were poor fatigue details, however, only the top web gap at support was poor fatigue detail in straight bridge. It was also found that out-of-plane bending stresses in X layouts were a little higher than in layouts with K cross-frames.

One of the most common bracing systems for I-shape-girder bridges is a discrete torsional system consisting of cross frames with a K- or X-configuration. These braces are usually fabricated from angles or of solid diaphragms constructed with channel-type sections for ease in attachment to girder stiffeners. In addition, solid plate (plate diaphragm) or channel diaphragms are used in some bridges. Top or bottom lateral truss bracing (a relative brace system) may be needed as temporary bracing during construction or permanent bracing to mainly resist wind loads (Chen & Duan, 2014).

Web gaps in multi-girder bridges are subjected to a transverse load applied through the stiffener at one end of the web gap which is resisted at the other end by tension flange. Top and bottom of the web gaps have the highest tension and compression stresses and most of the fatigue cracks are discovered in these locations (Connor & Fisher, 2006).

Keating & Fisher (1985) performed several field studies of various bridge details to determine the stresses and out-of-plane distortions in the web gap. The web distortion between the end of the stiffener and the flange ranged from 0.013 mm to 0.025 mm under service loading conditions and the measured bending stresses in the web gap ranged from 10 MPa to 97 MPa. Furthermore, all strain measurements taken in the web gaps showed that reverse curvature bending was present. The field investigations indicated that the relatively high stress levels in the gap region usually caused cracking within the first ten years of the service life of the bridges. They found that cracks initiated at the web gap boundaries, where the maximum bending stresses, induced by the relatively small deformations are located.

Fisher (1990) investigated fatigue cracks in the web gaps of bridge girders at the connection of transverse beams, too. Transverse beams were connected to the girders through stiffeners which were not connected to the girder flanges. The cracks had developed due to out-of-plane deformation of the web gaps. The strains in the web gap were measured using strain gauges. The strain measurements indicated that the transverse beam was pushing the web out-of-plane and the web gap was subjected to double curvature (Fisher 1990).

Castiglioni, Fisher, & Yen (1988) presented a numerical investigation of web gaps subjected to out-of-plane displacements in multi-girder steel bridges. A parametric study was carried out to determine the effects of web gap length and web thickness on web gap stress. They found that increasing the web gap length and decreasing its stiffness may decrease the stresses in the web gap enough to reduce the probability of developing distortion induced fatigue cracks in these areas.

Shifferaw & Fanous (2013) conducted field testing and numerical studies to examine the behaviour of web-gap distortion of a skewed multi-girder steel bridge. They found that the shorter web gap resulted in higher vertical and principal strain due to increased bending by diaphragm forces in the web. They also found that by connecting the transverse stiffener to the top flange of the girder the out-of-plane distortion can be effectively reduced.

2.5. Web Gap Stress Assessment

The magnitude of distortional stresses has been shown to be difficult to predict from field investigations and experimental studies (Jajich, Schultz, Bergson, & Galambos, 2000). Fisher et al., (1979) assumed that web gaps behave like a short, rotationally fixed beam undergoing lateral distortion δ. By using the slope deflection equation an approximation for the relationship between differential deflection, Δ, an approximation of distortional stresses in the web gap was obtained. It was assumed that the deep diaphragm undergoes a rigid body rotation about its base, and the relatively thin web gap takes up all out-of-plane deflection. The assumed relationship between δ and Δ is shown in Figure 2- 4.

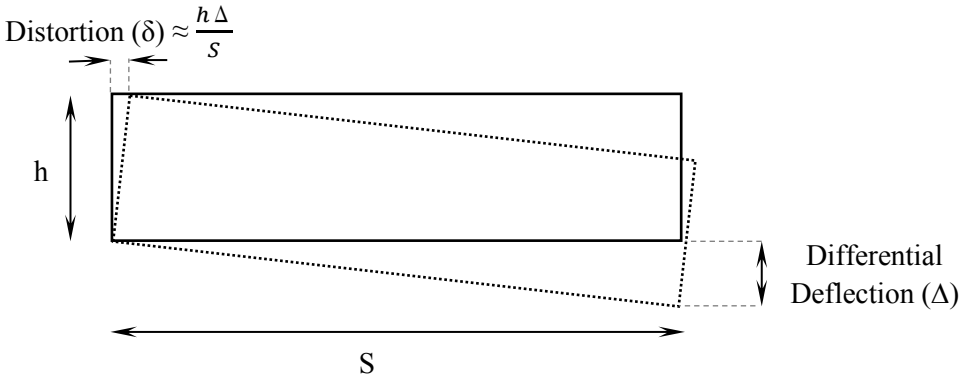

Figure 2- 4: Diaphragm Rotation

The stress due to rotation of the ends of the web gap has also been neglected under the assumptions to drive the equation. By using Equation (2-1) the maximum out-of-plane web gap stress in vertical direction can be calculated.

$$\sigma_{wg} = \frac{3Ew}{g^2}\delta = \frac{3Ew}{g^2}\left(\frac{h\Delta}{S}\right) \qquad (2\text{-}1)$$

where E is Young's modulus, w is the thickness of the web, h is the depth of the diaphragm, S is the girder spacing, g is the length of the web gap and Δ is the differential deflection between adjacent girders, as shown in Figure 2- 1 and Figure 2- 4. Web gap stress is not necessarily well predicted by Equation 1 even if differential deflection is known. This is because the diaphragm, stiffeners and surrounding structural elements such as bridge deck and

tension flange are also involved while transferring differential deflection to the girder web. For the web gaps at the bottom portion of the web, near the bottom flange, the out-of-plane deflection of the lower flange which depends on the lateral stiffness of the bottom flange can accommodate most of the diaphragm rotation and allow the web gap to rotate further. This rotation decreases the maximum web gap stress in the web gap by modeling the web gap more flexible.

In 1998 the Minnesota Department of Transportation (Mn/DOT) funded a research study to instrument and monitor Bridge #27734 (I94/1694) to determine the stresses in the web gap of the bridge which was subjected to distortion induced fatigue (Jajich et al., 2000). It was found that obtained web gap stresses from the field measurements were 2 to 2.5 times larger than the flange stresses. No clear relation between web gap stresses and the flange stresses was reported. They developed a detailed FE model of the web gap region and validated it using field measurements. To validate the FE model, they obtained the stress from the model at the same location of the mounted strain gauges in the field and compared it with the stress obtained from measured strain multiplies by Young's modulus. They found good agreement between the FE results and field measurements. They found that Equation (2-1) predicted much higher maximum stresses than the measured one. They recommended using Equation (2-2) to calculate the maximum stress in the web gap. In this equation it was assumed that all of the differential deflection between girders is transferred into the diaphragm rotation and yields a rotation of θ equal to Δ/S. This simple assumption neglects the effect of distortion in the web gap.

$$\sigma_{wg} = \frac{2Ew}{g}\left(\frac{\Delta}{S}\right) \qquad (2\text{-}2)$$

The terms used in Equation (2-2) are the same as the parameters described for Equation (2-1). For the mentioned bridge, this equation gave much more realistic results for maximum web gap stress (72MPa) than Equation (2-1) (1021MPa), and correlated well with their FE analysis (83MPa) and field measurements (56MPa). This equation was based on field data taken from the aforementioned bridge which was a three-span bridge with staggered bent-plate diaphragms and a skew angle of 60°. The problem with using this estimation is that, this equation is suitable for bridges whose geometry and support conditions near a diaphragm

connection closely resemble the Bridge #27734 (I94/1694) which had staggered bend-plate diaphragms with skewed configuration.

To overcome this problem, Berglund & Schultz (2001) used a three-dimensional FE model of the entire bridge validated with field measurements conducted by Jajich et al. (2000) to study the influence of various parameters on the differential deflection of adjacent bridge girders. They investigated the effect of girder spacing, angle of skew, main span length, concrete deck thickness, adjacent span length and diaphragm depth. It was observed that the maximum value of Δ/S mainly depends on skew angle and span length.

To determine the relevance of Equation (2-2) to other steel multi-girder bridges in the Mn/DOT inventory, Severtson *et al.* (Severtson, Beukema, & Schultz, 2004) instrumented two additional bridges (Bridge #27796 which was a five-span bridge and had a 45.5° skew and staggered cross-brace diaphragms, and Bridge #62028 which was a non-skew bridge and had five spans with no-staggered bent-plate diaphragms) to monitor the distortional fatigue response. Again, the stresses and differential deflections found by field study could not be well predicted by Equation (2-1), and Equation (2-2). The main reason is that the mode of out-of-plane deformation of these bridges was different from that assumed by previous prediction methods. They found that the web gap stress was primarily generated by rotation of the top of the web gap, θ_t, and rotation of the bottom of the web gap, θ_b (Figure 4). With the assumptions of linear beam theory, and considering the web gap as a fixed-fixed isotropic beam, the slope deflection Equation (2-3) was recommended as an idealized representation of this system.

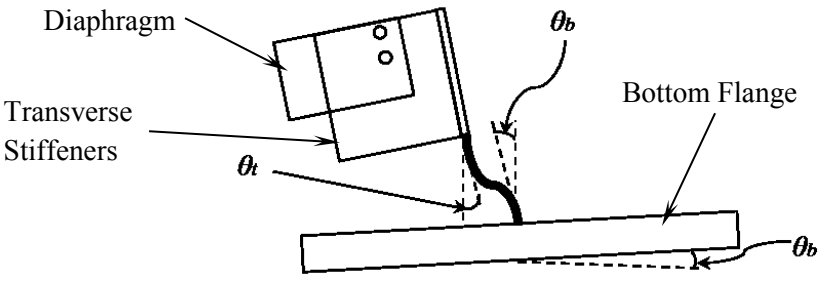

Figure 2- 5: Rotation of Top and Bottom of the Web gap.

$$\sigma_{wg} = \frac{Ew}{g}(2\theta_b + \theta_t + 3\frac{\delta}{g}) \quad (2\text{-}3)$$

By creating a FE model of a portion surrounding an instrumented diaphragm of Bridge #27796, and normalizing the values θ_t and θ_b by Δ/S, Equation (2-3) was simplified to Equation (2-4). Values of 1.7 and 0.9, were proposed for the normalized rotations $\theta_t / (\Delta / S)$ and $\theta_b / (\Delta / S)$, respectively. In their FE models, only one parameter was varied at a time. For example, to investigate the effect of web gap length, all the other geometrical parameters remained constant. Web gap length was varied from 1.7 in to 3.3 in. The web thickness was also varied from 0.4 in to 1.7 in. They also investigated three different span lengths (100, 112, and 124 ft.). To find the relation between Δ and σ_{wg}, they applied various differential deflection to the girders and found the maximum web gap while all the geometric parameters remained constant. The magnitude of differential deflection was varied between one-half and twice the amount measured during truck testing in order to simulate a variety of loading conditions. They found that web thickness, w, has the largest influence on web gap stress, while girder spacing, S, has the least effect.

$$\sigma_{wg} = \frac{3.5Ew}{g}(\frac{\Delta}{S}) \quad (2\text{-}4)$$

As the accuracy of Equation (2-4) relative to field measurements was not significantly affected by neglecting the web gap distortion (δ), this equation neglected the influence of lateral deflection of the web gap, δ. Previously, the neglected web gap deflection was accredited as the major cause of the out-of-plane distortion of the web gap (Fisher et al., 1979). The effect of cross-braces on differential deflection in addition to bent-plate diaphragms was also investigated. Severtson *et al.* (2004) found that the use of cross-braces significantly reduces maximum differential deflection. Therefore, they recommended a modification factor for reducing the deflection prediction for bridges with cross-brace diaphragms.

Li and Schults (Li & Schultz, 2005), from the same research group, performed FE analyses of the aforementioned bridges. The FE results were verified with the field measurements. They studied the sensitivity of diaphragm stress response to prototypical variations of typical diaphragm and bridge parameters. In their FE study, only one parameter was varied at a time to investigate its effect on the maximum web gap stress. They proposed a refined calibration of the constant coefficient (C in Equation (2-5)) in the stress formulas proposed by Jajich (Jajich et al., 2000) and Severtson (Severtson et al., 2004) for similar bridges

$$\sigma_{wg} = C\frac{Ew}{g}(\frac{\Delta}{S}) \qquad (2\text{-}5)$$

The magnitude of C is highly sensitive to bridge and web gap geometrical parameters. They recommended using average value of 2.25 and 2.75 for C for bridges similar to the Bridge #27734 (I94/1694) with bent-plate diaphragms and Bridge #27796 with cross-brace diaphragms, respectively. They also studied the effect of lateral deflection of the web gap, δ, in the prediction and found that neglecting δ does not significantly reduce the accuracy of the stress prediction equation, except for extreme cases of short web gap lengths, very thin and very thick web thicknesses. They recommended neglecting δ in the stress prediction equation until a more comprehensive investigation of this parameter can be made. Although their web gap stress prediction formula was calibrated for some specific bridges, the prediction results are still sometimes different from the FE models up to 220%.

To find the relation between differential deflection and web gap distortion, Li & Schultz (2005) applied different differential deflection values. In these models, all the geometrical parameters of web gap and the girders remained the same. By increasing the differential deflection, it is expected to get higher web gap distortion. Investigating the FE results of the work done by Severtson *et al.* (Severtson et al., 2004) and Li and Schults (Li & Schultz, 2005) showed an opposite trend. Therefore, these results are not reliable to investigate the ability of mentioned models for predicting the maximum web gap stress as a linear relation between differential deflection and web gap distortion was assumed in these models. Moreover, the web gap stress prediction models should be able to predict the results from other research programs as well.

The magnitude of web gap stress cannot be easily assessed with these simple assumptions as several various parameters are affecting this stress. Although these equations are simple to used, assuming the beam behavior for a thin plate subjected to a double curvature would lead to totally unrealistic results for the stress calculation. Therefore, a closer look and assessment is needed in order to resemble the behavior of the web plate in the web gap location. As the web plate has very thin wall, it can be considered as shell or a thin plate which goes under the double curvature distortion. The theory of plates and shell is studied in order to get a better assessment of the behavior of the web plate in the web gap region. The results of this study and the method to resemble the stiffness of the web plate are presented in Appendix A.

2.6. Introduction to Dimensional Analysis

As it was mentioned in the previous sections, the magnitude of the stress in the web gap detail is influenced by several parameters. The influence of these parameters should be considered simultaneously in order to investigate the overall behavior of the detail. These parameters are explained in detail in Chapter 5.

When the response function is unknown and the relations among the parameters are complicated, dimensional analysis can be a method to obtain the response function. This method has been proven very efficient and reliable in engineering and science fields. The most well-known application of the dimensional analysis is in hydraulic engineering area. It was utilized in order to drive the Darcy–Weisbach equation which relates the pressure loss, length of pipe, friction, to the average velocity of the fluid flow for an incompressible fluid (Darcy 1857).

In structural engineering this method has also been used occasionally. For instance, DiBattista et al. (2002) utilized this method to develop simplified equation to predict the behavior of sleeper-supported piping system. The results from this approach predict the results of the experimental data as well as the FE results, reliably. The description of the dimensional analysis method is presented in Chapter 5.

Chapter 3

Finite Element Modeling Techniques and Procedures

3.1. Experimental Program

The experiment was conducted at Kansas University (Hartman et al, 2013). A 9.1-m (30-ft) long three-girder test bridge was constructed and tested. The girders were spaced at 1.5 m and connected with X-type cross frame braces at the two simple support locations and at mid-span. A total of 12 test trials were performed with varying load ranges. Static loading was applied to the bridge correlated with the upper bound load of 267 kN from the first test trial in their physical test sequence. Loading was applied at mid-span over the interior girder and was applied at rates varying between 1.0 – 2.0 Hz. For each test trial, data for girders maximum deflection, girders lateral deflection, girders bottom flange normal bending stress and uncracked and cracked web gap strains as well as the number of cycle for crack initiation and propagation were collected.

3.2. Bridge Description

The dimensions and the detail of the bridge and connections are presented in Figure 3- 1 and Figure 3- 2. The girders are comprised of a 16 x 279 mm top flange, 6 x 876 mm web, and 25 x 279 mm bottom flange. All girders were supported on rollers to minimize axial forces with a center-to-center span length of 8.7 m between supports.

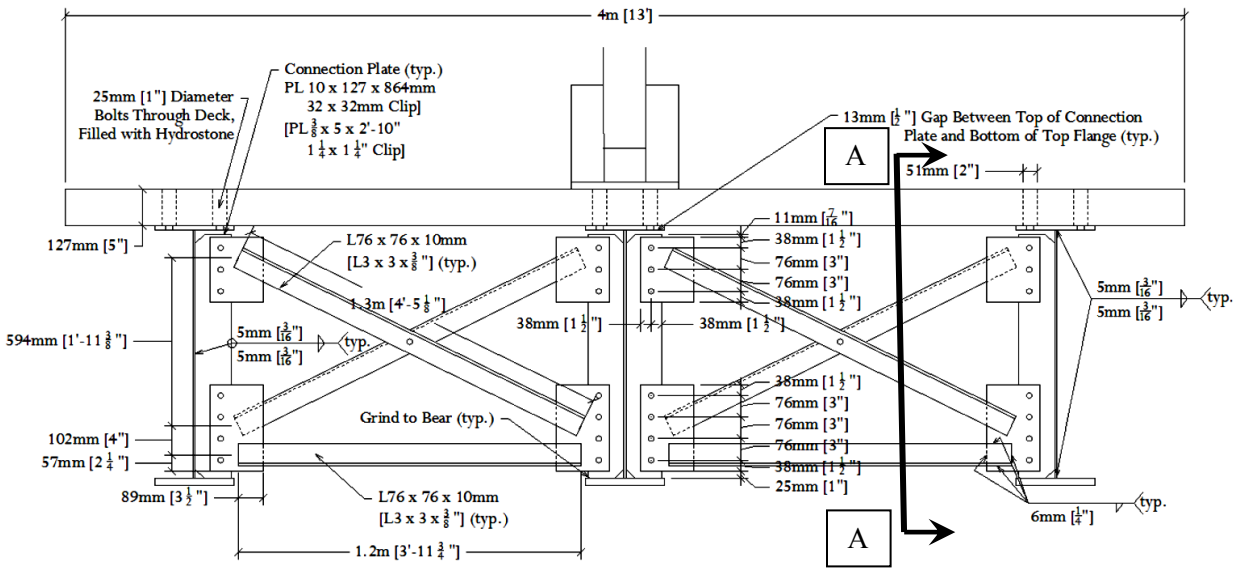

Figure 3- 1: Dimensions of the bridge at cross frames section (Hartman et al (2013))

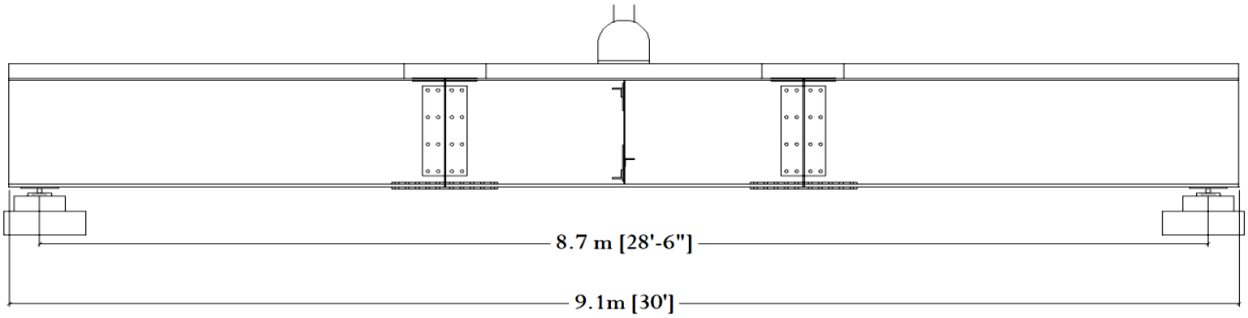

Figure 3- 2: Girder span (Section A-A) and load application (Hartman et al (2013))

3.3. Loading and Instrumentations

Cyclic loading was applied to the bridge by a MTS 201.70 actuator. A 25-mm thick steel plate was also centered on the bridge deck to distribute the applied concentrated force. In the static loading test (Trial #1) 267 kN downward load was applied to the middle girder and the girders maximum deflection, girders lateral deflection, girders bottom flange normal bending stress and uncracked and cracked web gap strains as well as the number of cycle for crack initiation and propagation were recorded.

The strain in the web gap was measured using five different strain gauges which are 6 mm long. The locations of these strain gauges are shown in Figure 3-3.

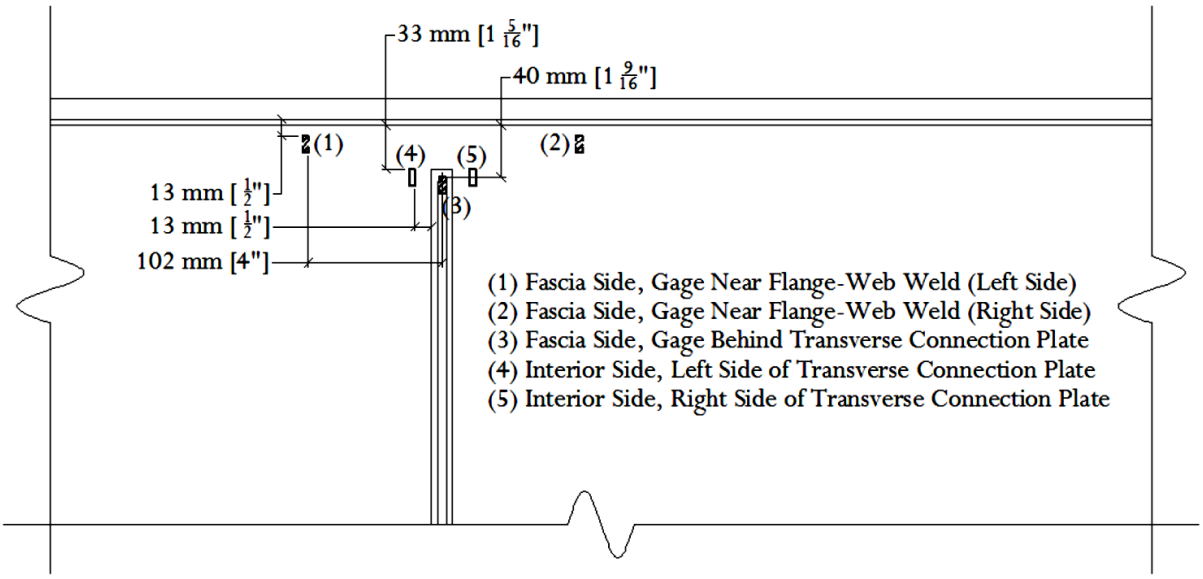

Figure 3- 3: Location of the strain gauges in the web gap (Hartman et al (2013))

3.4. Experimental Measurements

Although the results of several tests are available for this experimental program, most of them are for retrofitted web gap details. Therefore only the first trial of these tests would be useful for this study. In this trial, a 267 kN concentrated force was applied and the corresponding measurements were reported. Under this load, the 2 mm and 0.8 mm girder deflections are measured for the mid spans of middle girder and the side girders, respectively. These deflections lead to 1.2 mm differential deflection for the two adjacent girders. The mid span normal bending stress for the bottom flanges are also calculated based on the measured strains. For the middle girders the normal bending stress at the bottom flange is found to be equal to 29.6 MPa and for the side girders are 8.3 MPa and 9.7 MPa for the south side girder and the north side girder respectively. The girders deflection and the calculated stress are summarized in

Table 3- 1. Strain in the web gaps were also measured for both the north and the south girders and presented in this table.

Table 3- 1: Experimental measurement of the girders for the deflections, web gap and bottom flange stresses

Girder	Δ_i (mm)	σ_n (MPa)	ε_3, σ_3 (με, MPa)	ε_4, σ_4 (με, MPa)	ε_5, σ_5 (με, MPa)
North	0.8	9.7	-705	285	352
Center	2.0	29.6	N/A	N/A	N/A
South	0.8	8.3	-839	522	556

where Δ_i is the maximum deflection for the corresponding girder, in millimetres, σ_n is the girder maximum bottom flange stress, in MPa, and ε_3 , ε_4 , and ε_5 are the measured vertical strains in the web gap at strain gauge location of 3, 4, and 5 according to Figure 3-3. These measurements are for 267 kN applied load.

3.5. Finite Element Model of The Bridge

ABAQUS 6.13 is used to create the 3D finite element model of the three-girder bridge with cross frame braces. As shell elements are much more computationally efficient in many cases then solid elements would be and the model is a detailed model with more than hundred parts including girders, connectors, stiffeners, etc., it was decided to use shell elements. This model is used as a global model for a more refined model of web gap called sub-model to investigate the stress in the detail more accurately and efficiently.

4-node doubly curved thin shell element (S4R) is used to mesh different parts of the model using reduced integration, hourglass control, and finite membrane strains.

In order to represent the real material properties in the model, cyclic material properties used in this model. The steel strain-stress relationship is best described by Ramberg-Osgood equation presented in Equation (3-1).

$$\varepsilon = \frac{\sigma}{E} + \left(\frac{\sigma}{K'}\right)^{1/n'} \qquad (3\text{-}1)$$

where, E is the Young's modules, $K'$is the cyclic strength coefficient, and n' is the cyclic strain hardening exponent which are obtained from an experimental program at University of Alberta (Wang .Y, 2010) and presented in Table 3- 2.

Table 3- 2: Experimental results of cyclic material properties used in finite element models (Wang .Y (2010)).

Parameter	E (GPa)	K' (MPa)	n'
Value	213	727	0.150

The plastic strain used in the plastic material properties in finite element models are calculated based on Equation (3-2). In this equation, ε, is defined in Equation (3-1).

$$\varepsilon_{pl} = \varepsilon - \frac{\sigma}{E} \qquad (3\text{-}2)$$

Using the mentioned cyclic material constants the Stress-Strain curves are obtained based on both elastic strain and plastic strain. These relations are graphed in Figure 3-4.

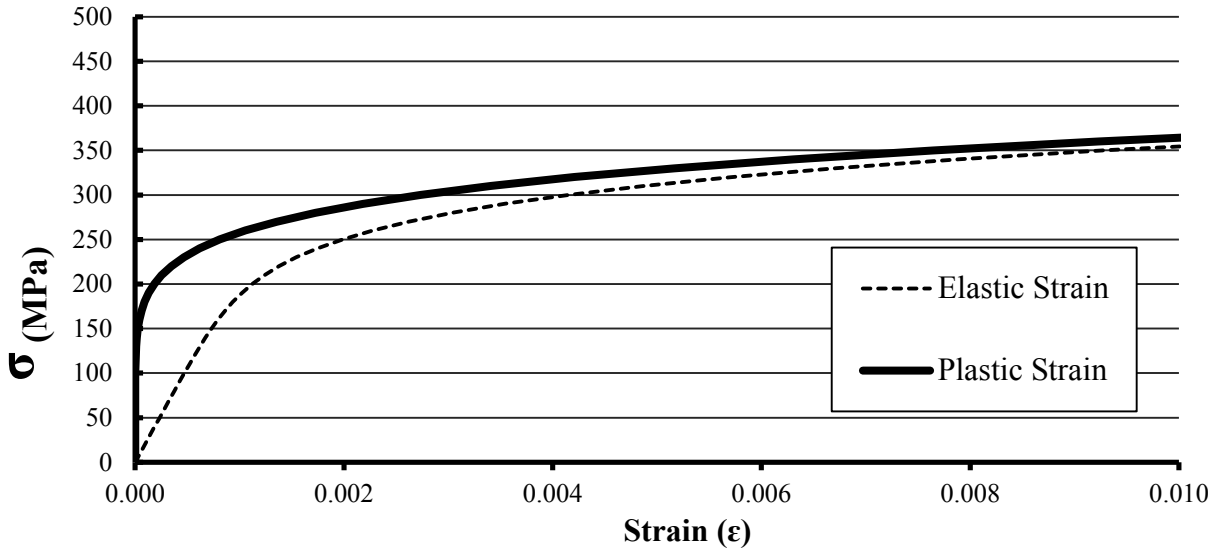

Figure 3- 4: Steel Strain-Stress Relationship Used in FEA.

The steel material used in the models has Young's modules of 200 GPa and Poisson's ratio of 0.3. The girders are simply supported at both ends of the bottom flanges. The bridge deck is also modeled as homogeneous shells with the concrete material with Young's modules of 25 GPa and Poisson's ratio of 0.16. It was decided to use shell element for the bridge deck because the thickness to both sides length ration of the deck were less than 5% and using shell element does not reduce the accuracy of the results. There was no crack reported for the concrete slab and the 267 kN load is not high enough to cause any damage to the concrete slab. Therefore, the elastic material behaviour can represent the real concrete behaviour in this model.

The top and bottom flanges are rigidly tied to the web plate to create the girders. Surface to surface tie method is also used to connect the stiffeners to web and bottom flanges, gusset plates to stiffeners, and cross frame members to gusset plates. The same method is used to model the slab connections to top surfaces of the top flanges.

Piers are also modeled by simply supported boundary condition which restricts the displacements of the ends of bottom flanges in perpendicular directions to girders longitudinal direction. The concentrated load is applied to the center of the slab. To distribute the load and represent the load actuator, the 267 kN load is applied to a rigid plate which is centered and connected to the slab. This also helps to faster convergence in the model as it reduces the very high stress concentration under the load.

General static procedure and direct solving method is used to analyze the model. Large displacements and deformations are also taken into account in the model analysis.

In this model, welds are not modeled for connecting the details as the main purpose was to use the results of the model for the sub-model. This saves a significant computational time in the model. In contrast, the detailed model including the welds with a refined mesh is used for the sub-model to investigate the stress in the web gap more accurately. There are several methods to model the welds in the detail which are investigated and compared in the following sections. Some of these methods are used only for shell elements.

The finite element model of the bridge is shown in Figure 3- 5. This model is named Global Model and will be referred to the same name for the rest of this chapter.

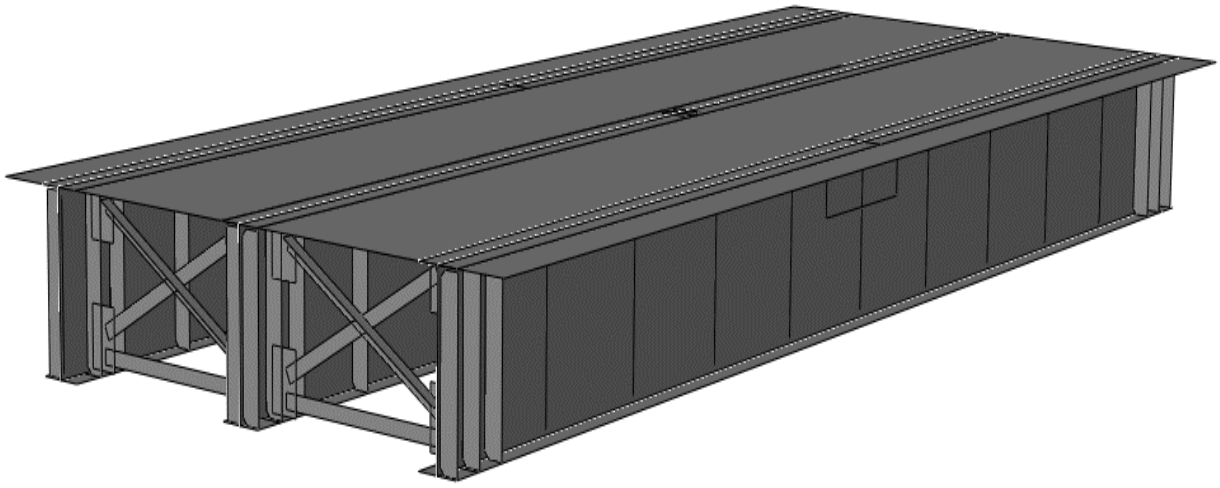

Figure 3- 5: Finite element model of the three girder steel bridge

3.6. Verification of The Bridge Finite Element Model

After applying 267 kN concentrated force to the center of the bridge, the girders deflection are calculated as well as the maximum normal bending stress in each bottom flange of the girders. The results of the finite element model and comparison of them with the experimental measurements are presented in Table 3- 3.

Table 3- 3: Finite element results and experimental measurement of the girders for the deflections and bottom flange stresses

Girder	$\Delta_{Experiment}$ (mm)	Δ_{FEA} (mm)	$\sigma_{Experiment}$ (MPa)	σ_{FEA} (MPa)
North	0.8	0.77	9.7	9
Center	2.0	1.99	29.6	30
South	0.8	0.78	8.3	9

The results of the finite element analysis are also presented in Figure 3- 6 and Figure 3- 7. The vertical deformation is scaled 100 timed.

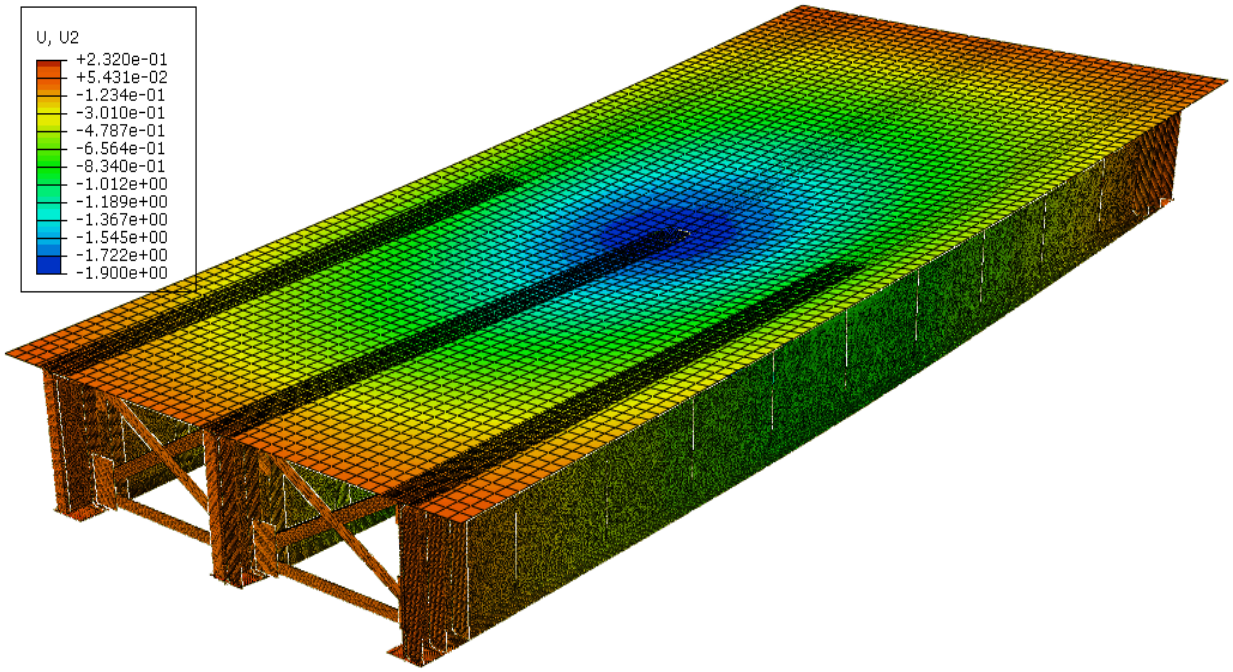

Figure 3- 6: Scaled vertical deflection of the bridge under 267kN load

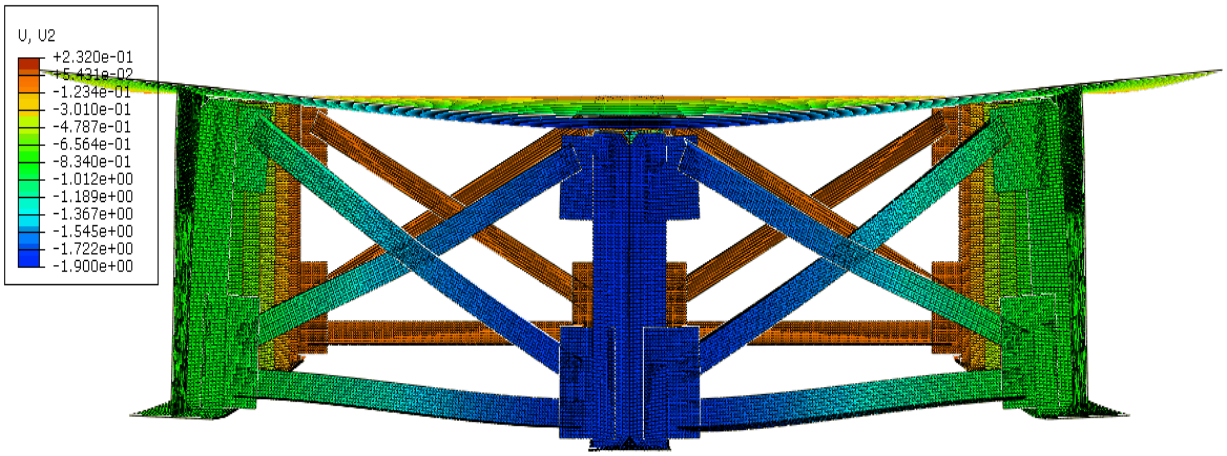

Figure 3- 7: Scaled vertical deflection of the bridge under 267kN load at the middle cross frame section

3.7. Finite Element Model of The Web Gap

To investigate the stress in the web gap detail a model with fine mesh is used in which more details including the welds are also modeled to provide more accurate results. In order to save computational time, a technique called "Sub-Modeling" is used for the detail. To use this method, it is needed to have a global model to provide the initial boundary conditions for the sub-model. The global model for the web gap sub-model is the verified full scale finite element model of the three girders bridge. Details of the location, mesh size, as well as the boundary condition for the sub-model is presented in the following section.

3.7.1. Sub-Model of The Three Girders Bridge

The sub-model of the web gap detail includes a portion of web plate, stiffener, and top flange as it is shown in Figure 3- 8. This detail is found in both sides of the bridge for the north and south girders.

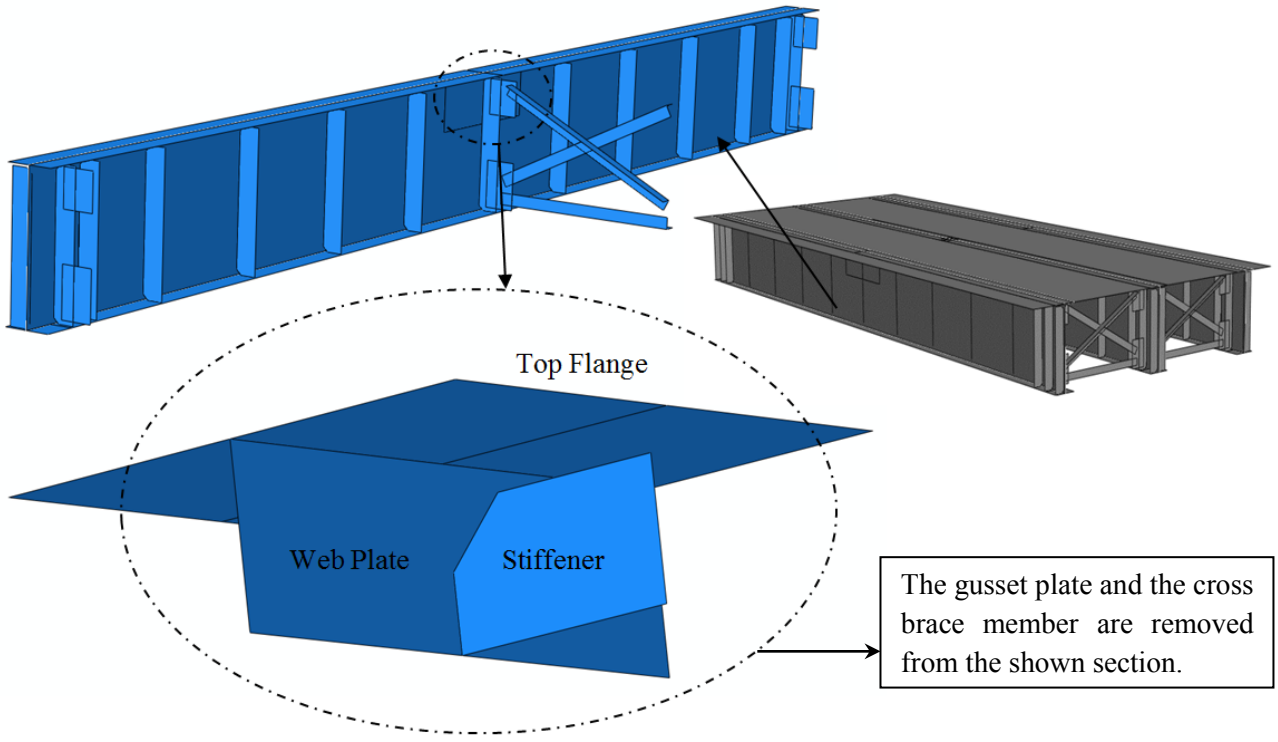

Figure 3- 8: Location of the web gap model (sub-model) and different components of the model

Boundary condition for the web gap sub-model is applied by the interface nodes between global model and the sub-model itself. Interface nodes are the nodes from which the sub-model is detached from the global model. The displacement and the rotation of the interface nodes are extracted from the global model and are applied to the sub-model as an initial loading condition. This boundary condition is shown in Figure 3- 9. The density of these nodes depends on the elements size of each component. Both displacements and rotational degrees of freedom for each interface node in the sub-model are tied to the nodes in the global model.

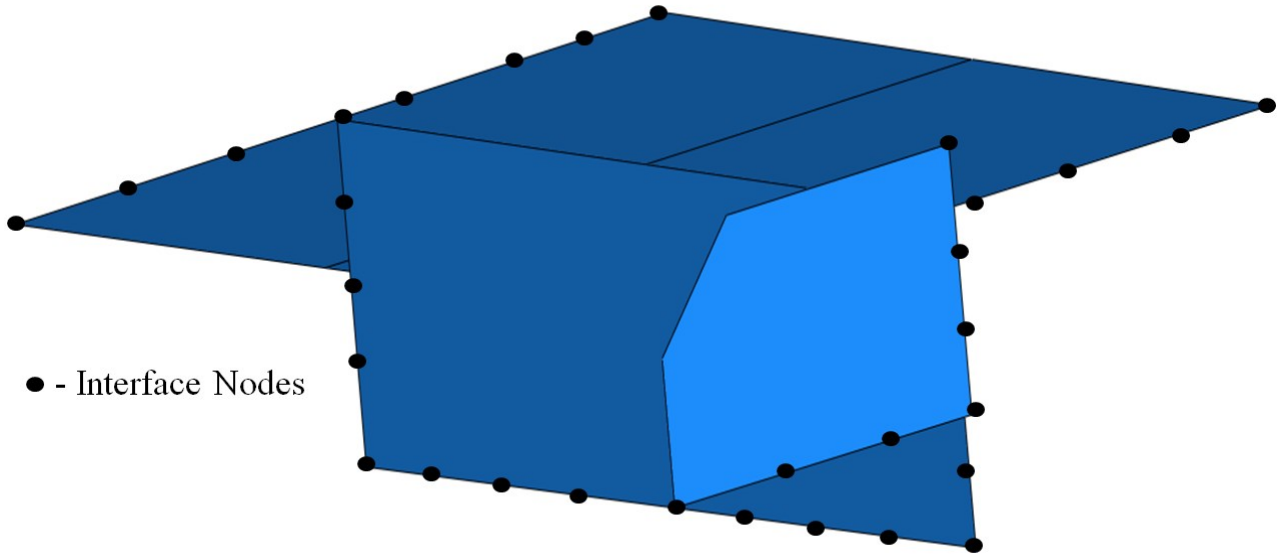

Figure 3- 9: Location of interface nodes connecting the sub-model to the global model.

In the sub-model there are only two fillet welds connecting the components together. One welds the stiffener to the web plate and the other one connects the web plate to top flange. The fillet welds have 5 mm weld throat thickness. These welds are shown in Figure 3- 10. There are several techniques to model the weld in finite element models which are explained and compared in the following section. Then according to this investigation, the most suitable technique will be selected and used to model the weld in the sub-model.

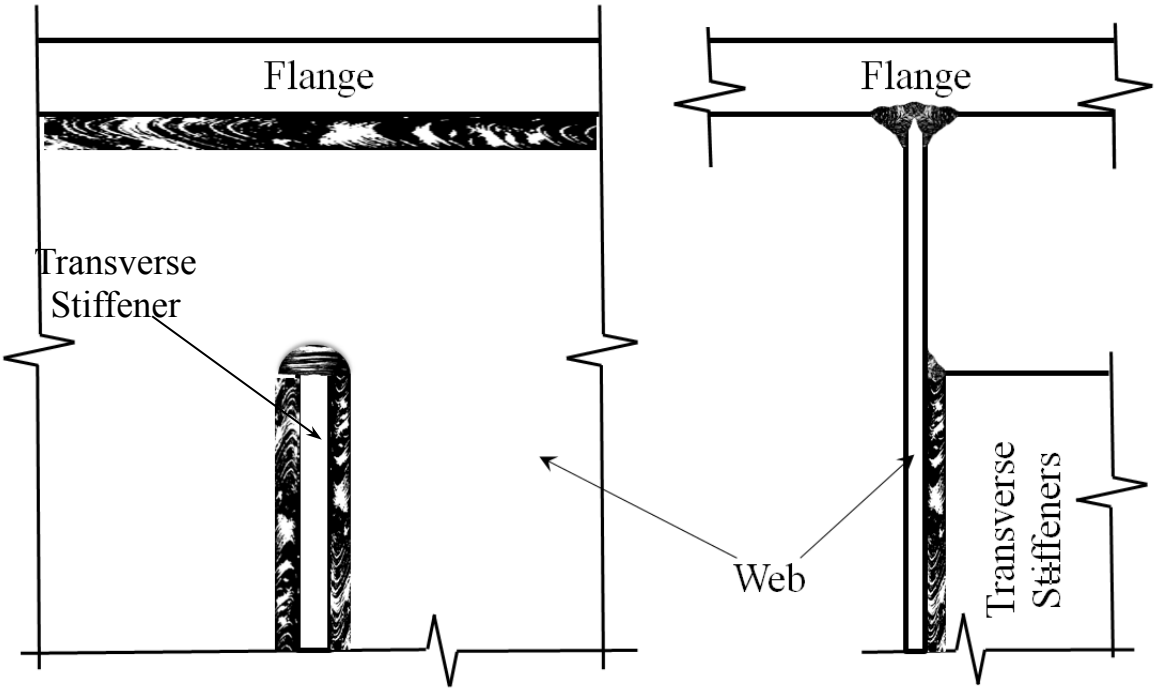

Figure 3- 10: Fillet welds in the web gap location. Left figure shows the cross section of the girder at the web gap.

3.7.2. Weld Modeling Techniques

In welded details in steel structures under cyclic loading cracks most likely initiate at weld toes which are highly stressed zones. At these critical points which are named hotspots, it is difficult to determine the local stress states and standard fatigue criteria are very difficult to apply for fatigue life prediction. Therefore, the stress state in these regions should be well defined using appropriate finite element models. To create these models, the details under investigation should be modeled as accurate and realistic as possible. This includes the welds geometry as well. Depends on the method used, sometimes the geometry of the welds are modeled and sometimes only the stiffness or the effect of them in the detail is modeled.

If solid elements are used in the model, the welds are usually modelled since the geometry and stiffness of the welds can be easily modelled using solid elements. In contrast, in shell elements models, it is not easy to model the welds and it requires some modelling effort in which the stress value at welded regions can be dependent on the weld modeling technique. In simple shell element models in which the stress distribution is not significantly influenced by the

local stiffness of the joint, the welds do not need to be modeled. In multi girder steel bridges, the stresses in the web gap details are affected by bending stress and because of stress concentration effects emanating from nonlinear deformation (out of plane double curvature deformation) the welds should be modeled and the stiffness of the weld should be taken into account. There are several modeling techniques to model the welds in the details and are presented in the following.

3.7.2.1. Rigid Links Method

This technique was proposed by Fayard, Bignonnet, & Van (1996) to find hot spot stress at the weld toes. It is used when using shell elements in the finite element model and it only models the local rigidity of the weld joints. Using this technique, weld toe stress is directly found from element's centers of gravity instead of the surface stress extrapolation which is the most common way to calculate the stress. This method is well described in Figure 3- 11 for single-side weld modeling. In this figure, the plates are also shown for better explanation as well as the shell elements (the bold lines with dots representing the elements nodes).

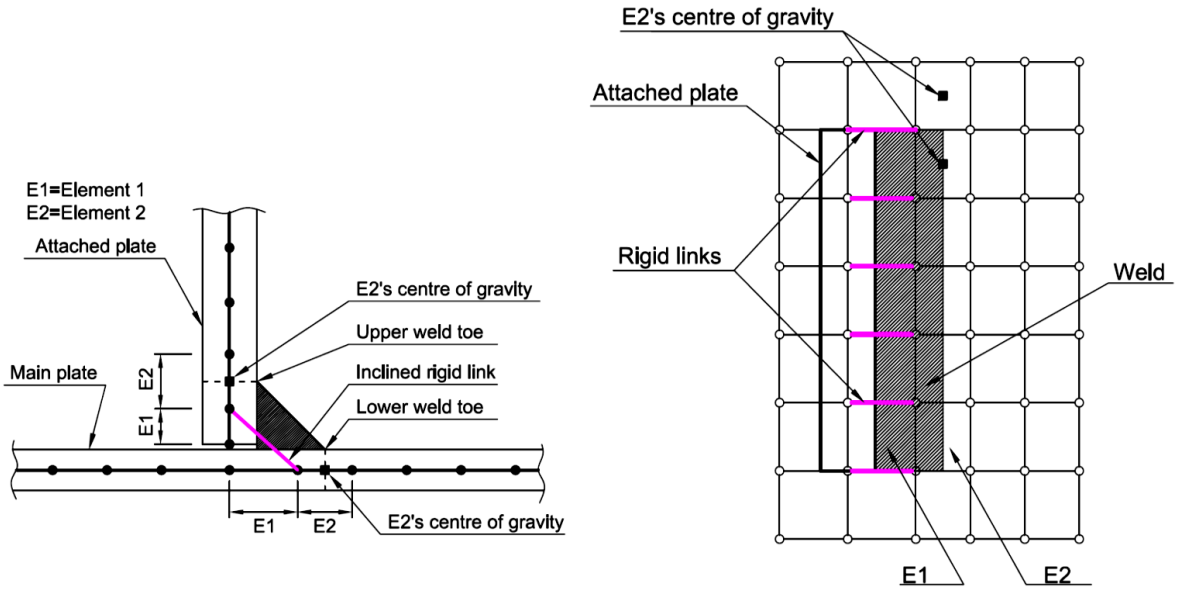

Figure 3- 11: Single-side weld modelling with rigid links Proposed by Fayard et al. (1996), (Aygül, 2012)

The lengths of adjacent shell elements, E1 and E2, should be selected correctly to represent the location of weld toes. The common nodes of these elements are used to link each element by rigid links. These links are shown by the dark pink color lines in the figure.

3.7.2.2. Oblique Shell Elements Method

In this method which is proposed by Niemi (1995), the weld joint is modeled using oblique shell elements. These elements are able to represent both the stiffness and geometry of the welds. As it is shown in Figure 3- 12, the length of inclined shell elements should be chosen in a way to represent the weld toes locations. The thickness of oblique shell elements is also equal to the throat thickness of welds.

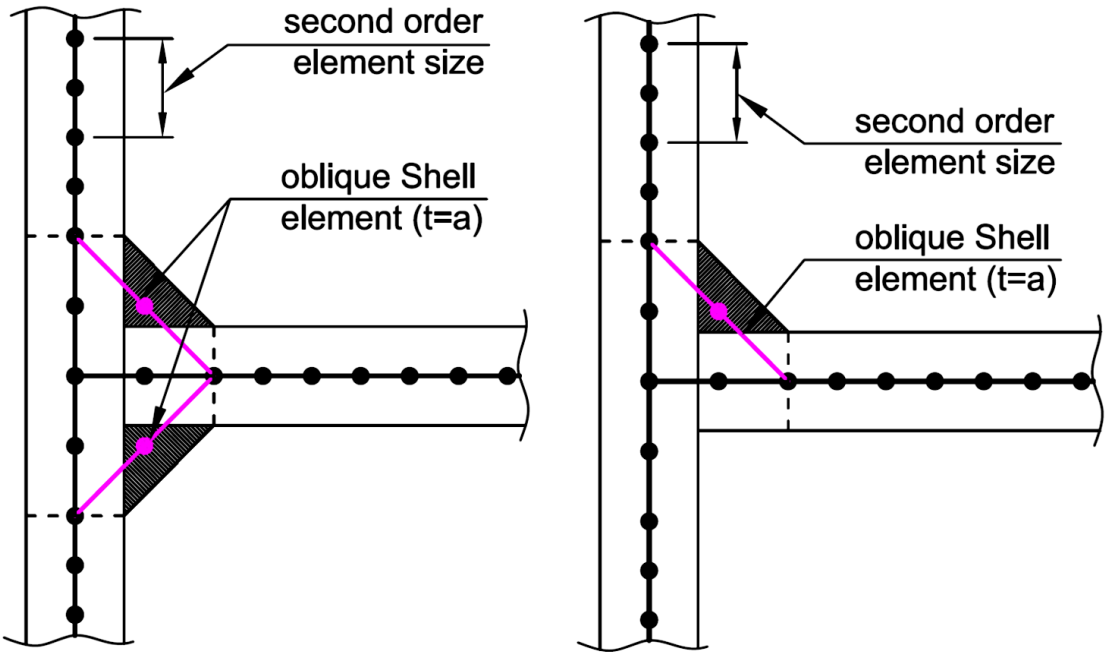

Figure 3- 12: Weld modeling using oblique shell elements proposed by Niemi (1995), (Aygül, 2012)

3.7.2.3. Increased Thickness Method

Another method to model weld in models with shell elements is using the shell elements with variable thickness in the intersection region of welded joints. In this method the geometry of the weld is not modeled and only the stiffness is taken in to the consideration. Depending on the mesh size in the weld location, the thickness can gradually (linearly) increase from "t" to "t+a" where, t, is the plate thickness and, a, is the weld throat thickness. These dimensions and the method are described by Niemi (1995) and Figure 3- 13.

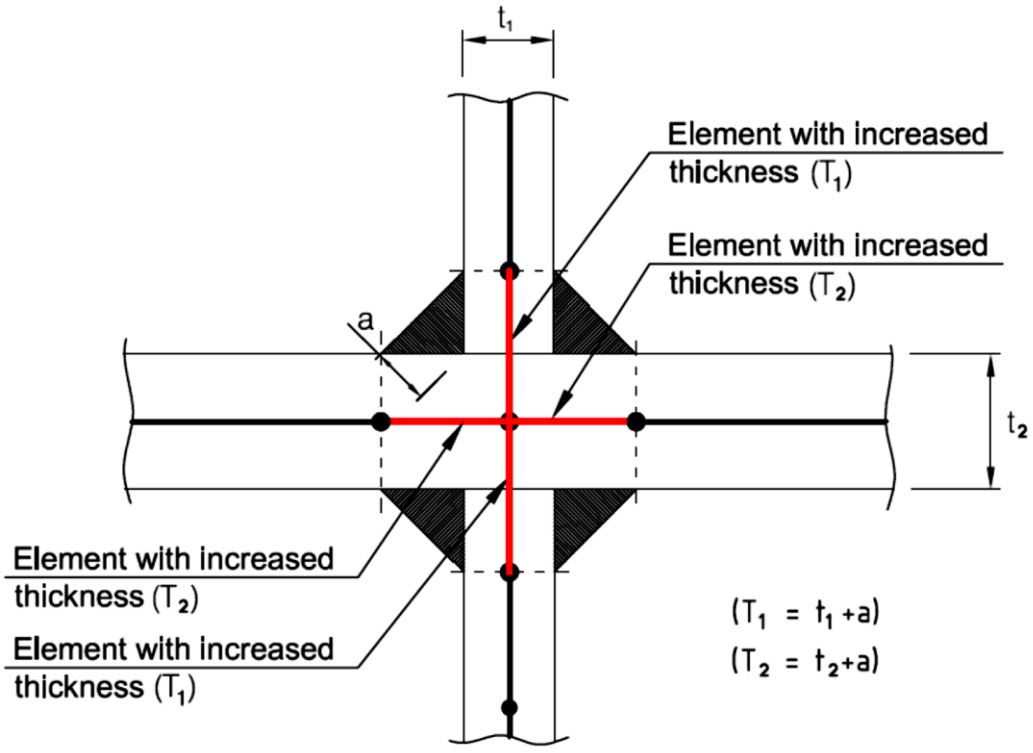

Figure 3- 13: Modelling welds using shell elements with increased thickness (Aygül, 2012)

3.7.2.4. Solid Elements Method

Solid elements are the most accurate and simplest elements to model both shell and solid bodies. Using this method, both the dimension and stiffness of the weld is modeled and detailed geometry can be represented by this method. The only issue with this type of elements is the computational cost of it in comparison with shell elements.

To optimize the model, it is also common practice to use a combination of shell and solid elements in the model but this technique needs some extra considerations. This is because connecting these elements can lead to some numerical error in the model as the shell elements have 5 degree of freedom and the solid elements have only 3 degree of freedom in each node. This can cause some convergence issues in the model. There are some techniques to connect shell elements to solid elements in numerical models. Instead of connecting the connecting shell directly to the solid surface, it can be connected to another shell surface perpendicular to the connecting shell surface. The width of this shell surface is equal to the thickness of the connecting surface and the length of it is the same as the length of the connecting surface and the solid part. The thickness of this surface can be chosen in a way to provide a relatively rigid surface to transfer the bending moments and the rotations to the solid elements. There is another method called Multi Point Constraint (MPC). The MPC equations are needed to be generated to transfer rotation from shell elements to solid elements which involve time consuming and work effort.

3.7.2.5. Comparing the weld modeling techniques

In a study conducted by Akhlaghi (2009), the mentioned weld modeling techniques are investigated and the accuracy of the weld toe stress computing are compared to the results from the experiments performed to evaluate the fatigue resistance of a bridge detail. In this study the structural hot spot stress (SHSS) approach was used to calculate the stress in the weld toe. The weld was modeled using 3 different modeling techniques: solid elements (Model 1), oblique shell elements with a thickness equal to weld throat thickness (Model 2) in which the geometry and stiffness of the weld were modeled, and shell elements with an increasing thickness (Model 3). In addition, a shell model was also investigated in which the weld were not modeled at all and the shell elements were tied together (Model 4). It was found that the model with solid elements computes the stress in the weld toe more accurately. The model with shell elements with an increasing thickness also provided very acceptable results. In contrast, the other two models, the model without any weld and the one with oblique shell elements, had unacceptable and unrealistic stress in the weld toe. The results of the hot spot stress calculated using these models are presented in Table 3- 4.

Table 3- 4: Comparison of computed and measured structural hot spot stresses (Akhlaghi, 2009)

Model	Hot Spot #1			Hot Spot #2		
	SHSS (MPa)	Ratio of SHSS value to solid element model	Ratio of SHSS value to measurement	SHSS (MPa)	Ratio of SHSS value to solid element model	Ratio of SHSS value to measurement
Solid Elements (Model 1)	230	1.00	1.14	268	1.00	1.43
Oblique Shell Elements (Model 2)	126	0.55	0.62	72	0.27	0.38
Shell Elements with Varying Thickness (Model 3)	158	0.69	0.78	223	0.83	1.19
Shell Elements with No Weld (Model 4)	873	3.80	4.32	848	3.16	4.51
Measurement	202	0.89	1.00	188	0.70	1.00

Hot Spot #1 and Hot Spot #2 are for the stresses at two different weld toe locations. As it is shown in the table, the model with shell elements with an increasing thickness to model the weld (Model 3) predicts the results very well. Therefore, it is decided to use this technique in the sub-model.

Therefore, using shell elements with an increasing thickness to model the weld, the web gap geometry is as shown in Figure 3-14. The red dashed lines symbolically represent the thickness of the web plate at different sections. The web gap is divided to four sections. The top section which is 8 mm long has thickness of 279 mm which is as thick as the flange width. The second section from top which is 5 mm long (the size of the weld throat thickness) has thickness of 11 mm. The longest section which is the web plate itself has the thickness of 6 mm and the last section with 5 mm length has thickness of 8.5 mm which is the thickness of the summation of web plate thickness and half of weld throat thickness. Half of weld throat thickness is added to the web plate as there is only one weld at the detail. The weld has a triangular cross section and an average of the weld throat thickness is taken in to consideration according to Figure 3-13. In this figure there are two welds at the joint and the thickness is increased by two times of half of weld throat thickness.

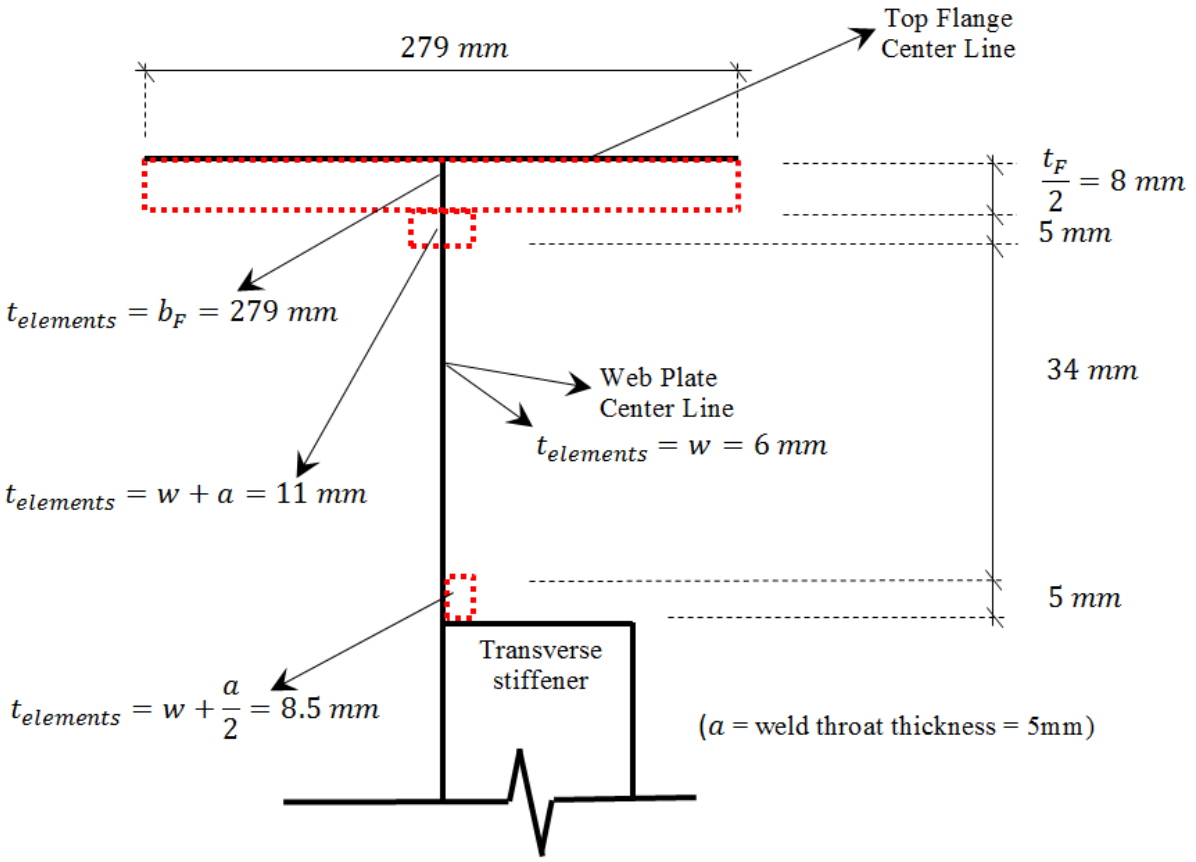

Figure 3- 14: Different thicknesses of the web plate shell elements at the web gap to represent welds

3.7.3. Sub-Model Finite Element Results

After applying the load boundary condition to the sub-model, the vertical stress in the web gab, deformation of the web plate is calculated and compared with the experimental measurements (Table 3-1). The stress obtained from FE analysis at the corresponding strain gauges location is the average stress calculated from the stress in the elements at the location of the strain gauges. For instance to obtain the strain in the web gap at location of strain gauges number 3, 4, and 5 the average of strains for a 6 mm long elements strip is taken in to account. The results are presented in Table 3-6. The calculated stresses are based on the measured strain in the experimental program. The strain for the specific location is simply multiplied by steel Young's Modulus (200GPa).

Table 3- 5: Experimental measured stress and analytically calculated stress in the web gap

	Measured Strain, ε (με)		Calculated Stress, σ.E (MPa)		Vertical Stress From FEA
Web Gap	North Girder	South Girder	North Girder	South Girder	North and South
Strain Gauge 3	-705	-839	141	168	162
Strain Gauge 4	285	522	57	105	135
Strain Gauge 5	352	556	70	112	134

3.7.3.1. Sub-Model Mesh sensitivity Analysis

To study the effect of the mesh size and density on the stress calculation in the web gap, a mesh sensitivity analysis or a mesh convergence study is performed on the sub-model. As the model is a small finite element model and very efficient in terms of computational time cost, the mesh size is uniform in every component for mesh sizes as small as 0.5 mm. Therefore, the effect of having a coarse mesh in these models is omitted from the results. For smaller mesh density (0.2 and 0.1 mm) the web gap itself is meshed with fine mesh and the rest of the local model is meshed using 0.5 mm mesh size. The result of mesh sensitivity analysis is presented in Figure 3- 15 to Figure 3- 16.

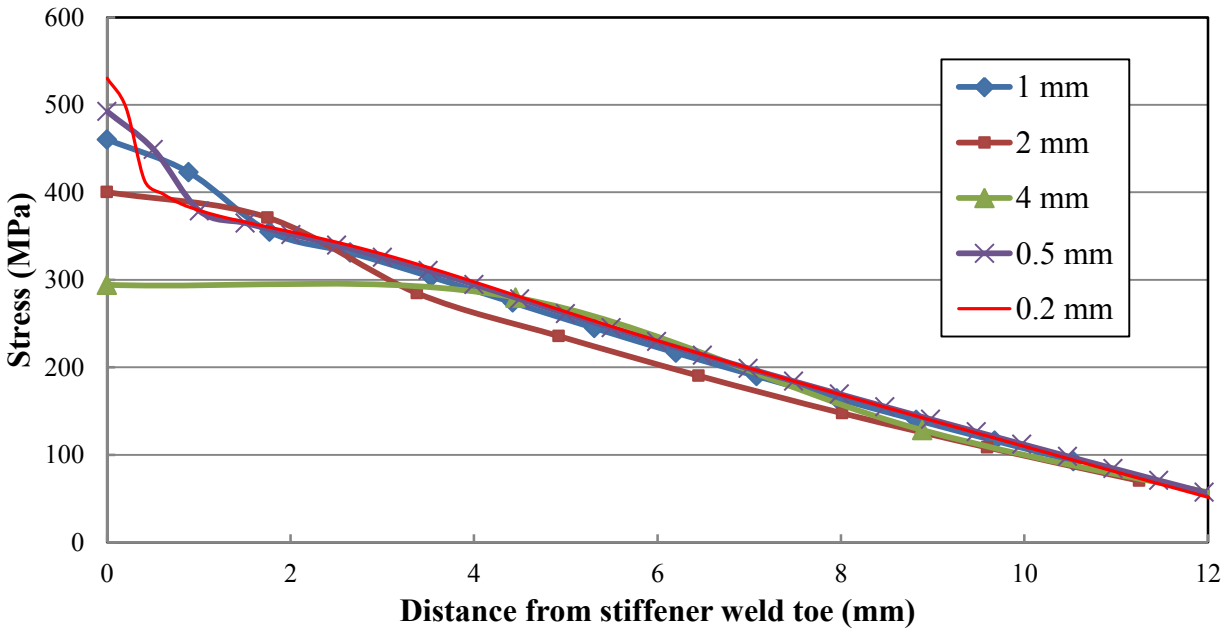

Figure 3- 15: Vertical stress vs. distance from stiffener weld toe for various mesh sizes

As shown in Figure 3- 15 the maximum vertical stress in the web gap at the weld toe highly depends on mesh size. The smaller the mesh size and the denser it is, the higher the calculated vertical stress. This maximum vertical stress is located at the stiffener weld toe and is plotted in Figure 3- 16.

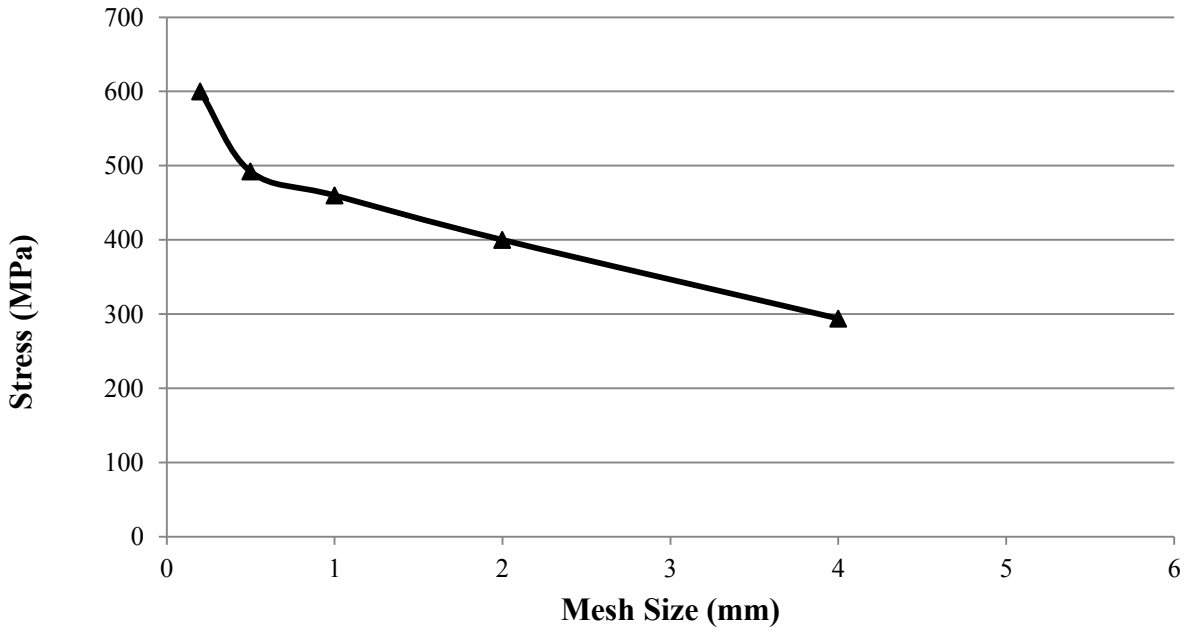

Figure 3- 16: Maximum Vertical Stress at Weld Toe vs. Mesh Size

Another method to compare the stress at weld toe is Hot Spot Stress (HSS). This is recommended by BSI standards (BSI, 2014). According to this guideline, The HSS can be obtained by Equation (3-3). It recommends that for stress analysis based on measured strains or FEA of a relatively fine mesh model, quadratic extrapolation from stresses on the plate edge at distances 4 mm, 8 mm and 12 mm from the weld toe should be used.

$$HSS = 3\sigma_{4mm} - 3\sigma_{8mm} + \sigma_{12mm} \quad (3\text{-}3)$$

Using this equation, the HSS for different mesh sizes are calculated and compared in Figure 3- 17, and Table 3- 6.

Table 3- 6: HSS calculation for different mesh sizes using Equation (3-3)

Mesh Size (mm)	σ_{4mm} (MPa)	σ_{8mm} (MPa)	σ_{12mm} (MPa)	**HSS** (MPa)
4	280	159	59	422
2	265	148	53	404
1	288	163	55	430
0.5	295	169	56	434
0.2	297	169	52	436

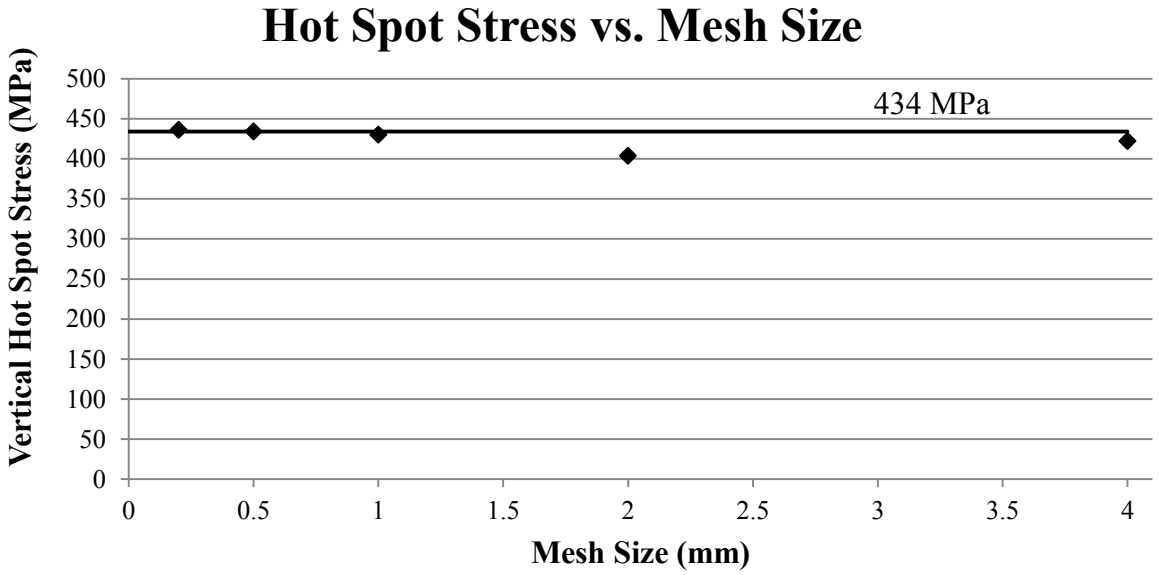

Figure 3- 17: HSS at stiffener weld toe for different mesh sizes

Although stress distribution pattern changes slightly at the weld toe by varying the mesh size and density, the vertical stress along the web gap 2 mm away from the weld toe varies with the same pattern for mesh sizes smaller than 2 mm. The difference between these stress distributions while using different mesh sizes and densities is presented in Figure 3- 18 and Figure 3- 19 for 0.2 mm and 1.0 mm mesh sizes.

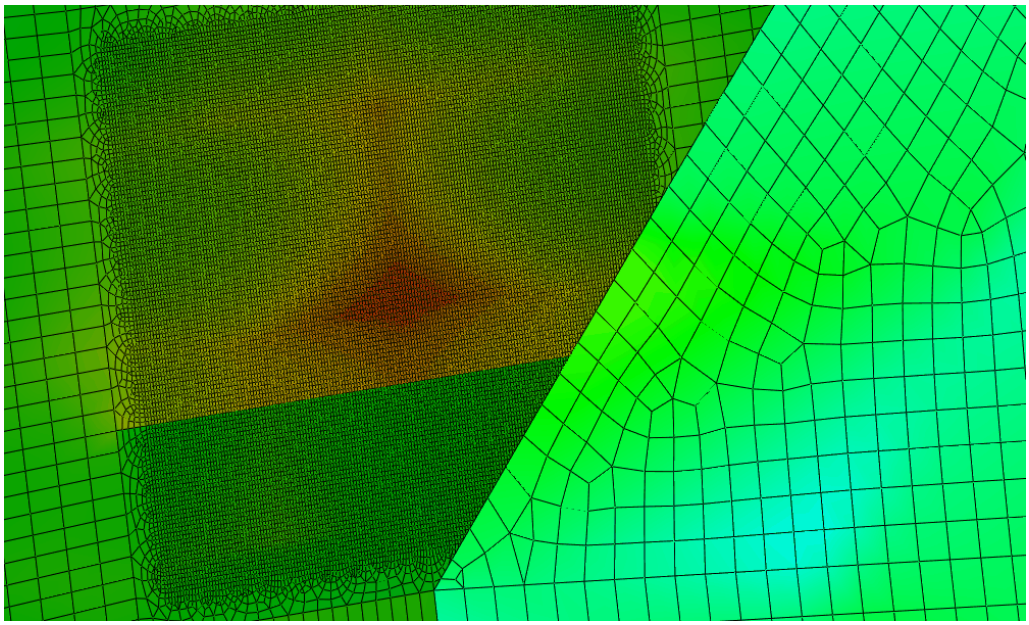

Figure 3- 18: Stress distribution in the web gap using 0.2 mm mesh size

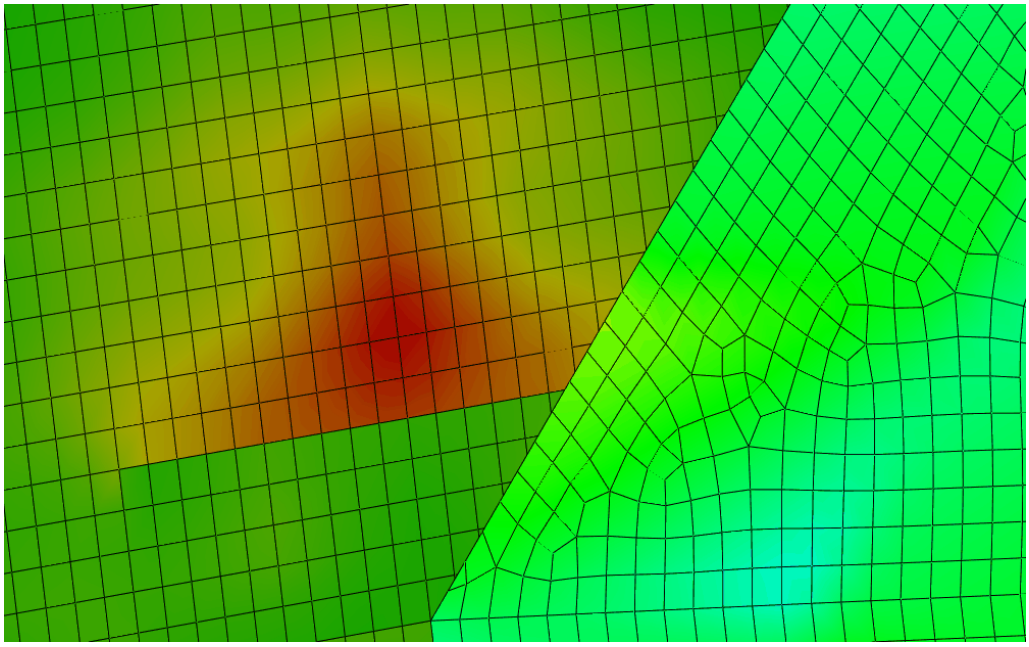

Figure 3- 19: Stress distribution in the web gap using 1 mm mesh size

3.7.3.2. Vertical Stress Distribution in The Web Gap

In web gap details, maximum stress occurs in vertical direction and the Von-Mises and maximum principal stress are mostly governed by the vertical stress. In addition, the approach used to calculate the vertical stress using HSS methods is already developed in the literature. Therefore, it was decided to use vertical stress as the representative of the stress state in the detail in this study.

The distribution of the vertical stress in the web gap is also presented in Figure 3-20. As it is shown in this figure, the maximum tension stress is located in the weld toe at the transverse stiffener and the web plate connection weld as it was originally expected. The maximum compression stress is also located at the weld toe near the weld connecting the web plate to the top flange.

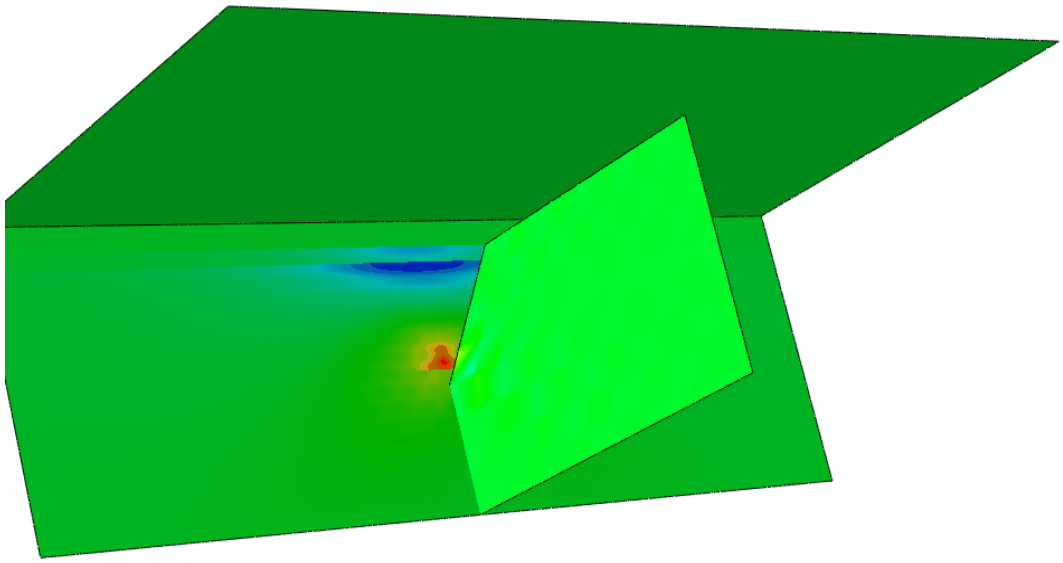

Figure 3- 20: Web gap vertical stress distribution

To investigate the effect of the welds in the web gap detail, another sub-model is also created for the web gap without any weld modeled. The vertical stress along the path shown in Figure 3- 21 is monitored for both sub models (with and without weld modeled). The path is defined along the web gap and is started from top flange center line to transverse stiffener.

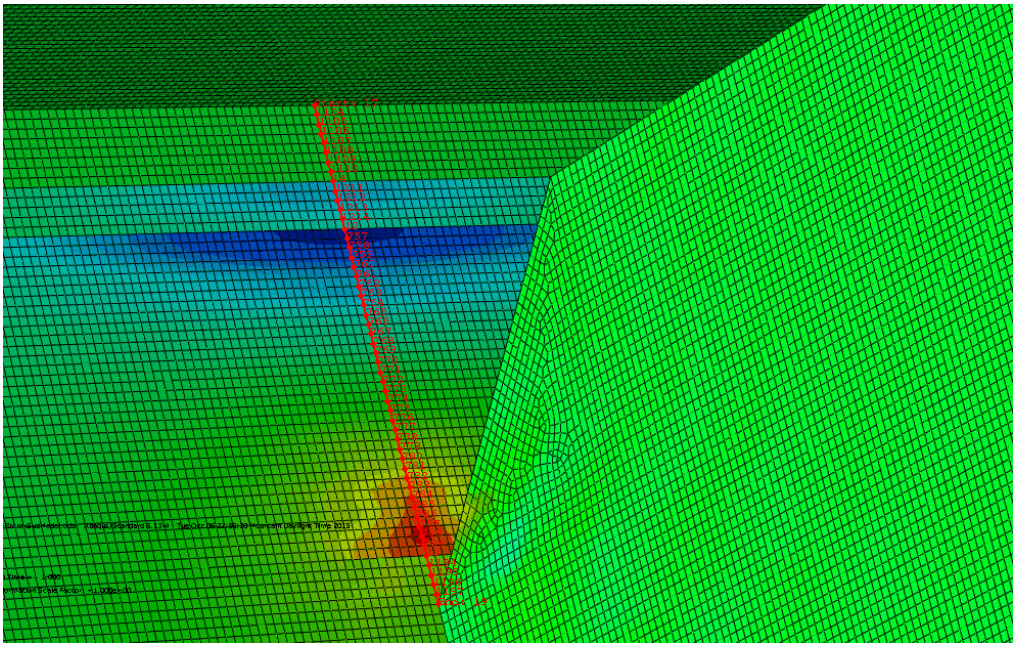

Figure 3- 21: The path used in the web gap to monitor the variation of vertical stress in web plate

In this chapter, the FE modeling procedure and different weld modeling technique were investigated to obtain a reliable and accurate FE model for further study. According to the findings from this chapter, it was decided to use shell elements with an increasing thickness to model the weld at the web gap detail in the following chapters. The cyclic material property is also used to define the material properties in FE models. 1 mm mesh size at the web gap seems to provide accurate results and there is no need to have finer mesh in the detail as it does not influence the results. Therefore, 1 mm local mesh and smoothly growing global mesh is used in the web gaps for both models used in parametric studies and the design of experiments. The path shown in Figure 3-20 is used to calculate HSS for the models in the following chapters by obtaining the stresses at 4, 8, and 12 mm away from the weld toe at the transverse stiffener to web connection.

Chapter 4

Fatigue Assessment of Web Gap Detail

4.1. Fatigue Life Assessment Methods

There are generally two methods to assess fatigue life of a detail. First one is using the conventional S-N curves method which is mostly based on experimental test. The second method is using fracture mechanics approach. These methods have some limitations and assumptions of which the assessor must be aware before utilizing them. These methods are explained in the following sections and the application of them to assess the fatigue life of web gap details in multi-girder steel bridge is discussed.

4.1.1. S-N Curve

For the details subjected to stress-induced (load-induced) fatigue loading, the stress range is a known factor. Therefore, by means of simple approaches such as S-N fatigue life prediction curves, the details can be assessed and the remaining life can be predicted. In this method, first of all, the magnitude of the stress in the web gap should be obtained in order to assess the fatigue life of the detail. Then by using the appropriate and already developed S-N curve, the life of the detail can be estimated.

In S-N curves graphs, the X-axis is the logarithmic scale of cycles to failure (N) and the Y-axis is the magnitude of applied cyclic stress ranges (S). Different steel design codes have developed their own S-N curves which are somehow very similar to each other. The differences between theses curves are the number of categories, the slope of the graphs, and the constant amplitude fatigue limit (CAFL) for each graph. CAFL is the horizontal portions of the S− N curves and it means if the stress ranges applied to a detail are lower than this value for the specific detail, it does not taken into account for fatigue life calculation and if all the applied stress ranges are less than the CAFL for the detail, the fatigue life is infinite for the detail.

Canadian Highway Bridge Design Code CAN/CSA S6-11 (CSA-S6, 2014) provides S-N curves for very common details and categorizes them from “A” to “E”. Category A represents the highest fatigue strengths and category E represents the lowest fatigue strengths.

Although the S-N curves in Canadian Highway Bridge Design Code are very similar to S-N curves used in AASHTO, there are some differences as well. For example, fatigue curves in AASHTO have a constant amplitude fatigue limit for each fatigue category which can lead to an overestimation of the fatigue life prediction when the majority of the applied stress ranges are below the CAFL. In contrast, the Canadian Highway Bridge Design Code does not have these constant lines for its detail categories. Instead, each graph has two portions, one with a slope of m = 3 used above the CAFL which continuous with the second portion with a slope of m = 5 which is used below the CAFL. Using these curves includes the effect of small applied stress ranges into fatigue life calculation. The S-N curves in Canadian Highway Bridge Design Code and AASHTO are presented in Figure 4- 1 and Figure 4- 2, respectively. In Figure 4- 1, the dashed line represents the CAFL for each category and only A, C, D, E1 categories are graphed.

These curves are obtained from a regression analysis of several comprehensive full-scale tests and graphed as the mean minus two standard deviations from the mean. There are some shortcomings according to Josi & Grondin (2010). For instance, the failure criteria such as the number of cycles to first detection of a crack, specific length of a crack, multiple detection of multiple cracks, etc. is not clearly defined. Crack initiation and propagation lives are not distinguished for a detail in the corresponding S-N curves. Therefore, the remaining life of details with an existing crack is vaguely predictable and S-N curves approach only provides reasonable approximation for new structures for the similar details as the ones used to develop the fatigue curves. The current slope used for S-N curves (m = 3) is not applicable to all details as it is found that some details follow smaller slopes than 3 (Stephens, Fatemi, Stephens, & Fuchs, 2000). In addition, assuming straight lines even for log-log plot is not a realistic trend for fatigue behavior of the details. In addition, the suitable S-N fatigue curve is not yet developed for the details prone to distortion induced fatigue too and the engineers are still left without guidance when conducting an evaluation of an existing bridge with distortion induced fatigue. For the details subjected to distortion induced fatigue, current S-N fatigue curves cannot be used as the

experimental test conducted to obtain these curves as they do not represent the details prone to distortion induced fatigue .

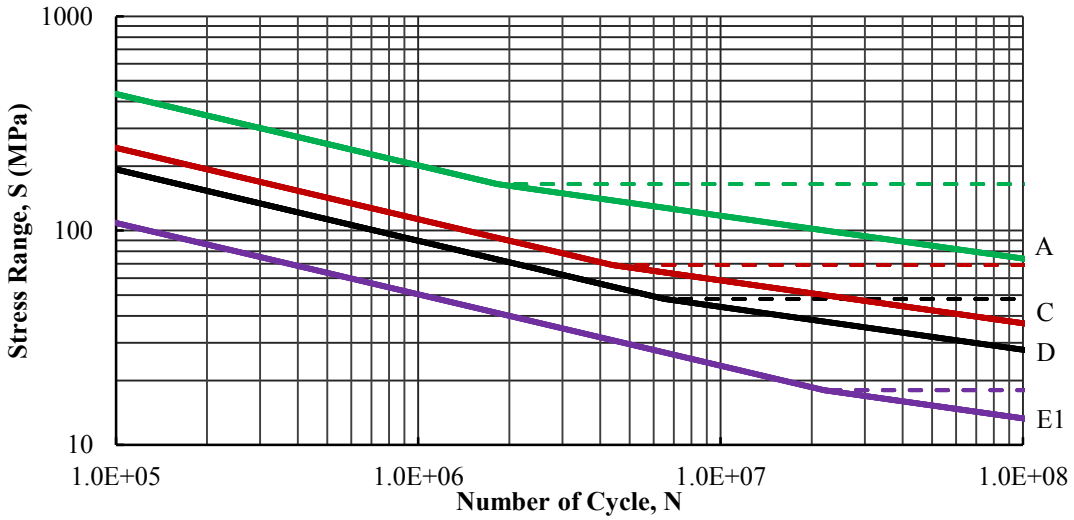

Figure 4- 1: S-N curves according to Canadian Highway Bridge Design Code (CSA-S6, 2014)

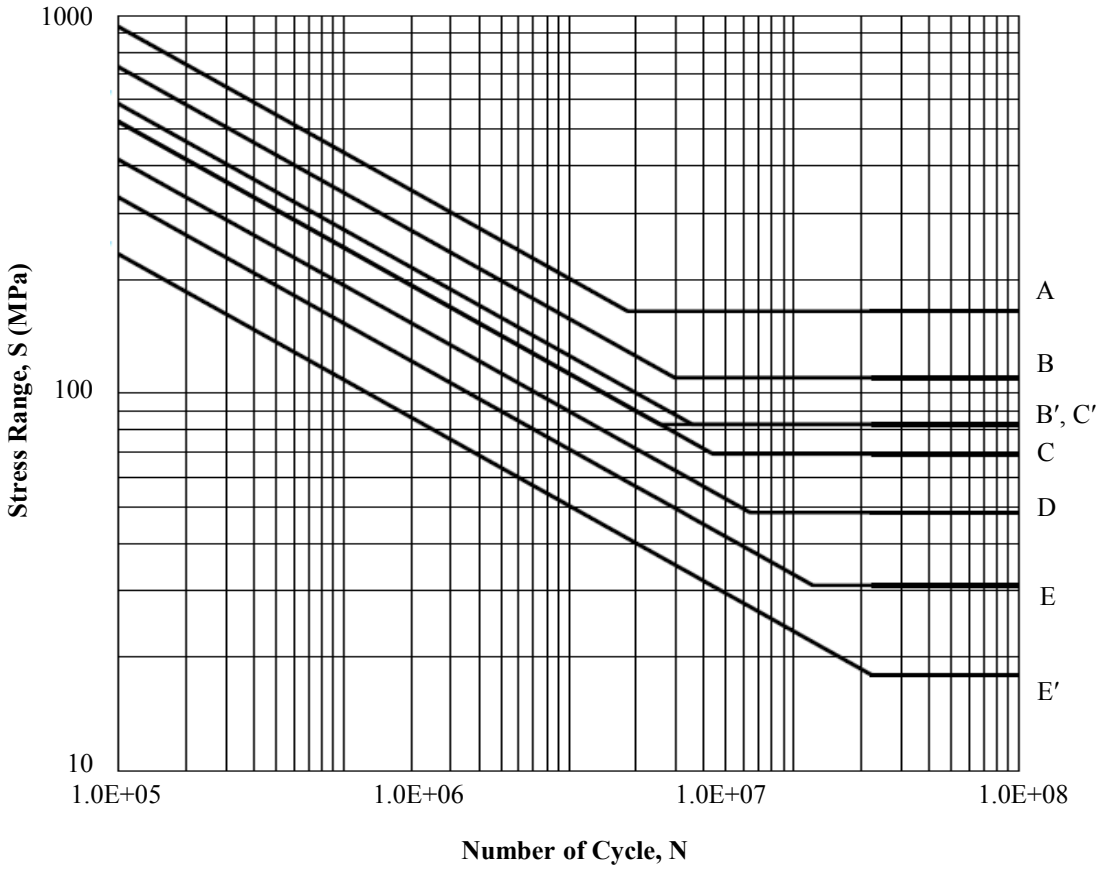

Figure 4- 2: S-N curves according to AASHTO (AASHTO 2014)

4.1.2. Fracture Mechanics

Fracture mechanics is a branch of continuum mechanics and according to Harris (1995), Fracture Mechanics as an engineering discipline which quantifies the conditions under which a structure, or part thereof, fails due to the growth of a crack. This approach does not need to take into account the prior history of the investigated component. Therefore, it is an appropriate but sometimes expensive and challenging tool to investigate the current condition of a detail and predict the remaining life it. Fracture mechanics accounts for the crack initiation and propagation stages, separately which makes it useful for assessing the new structures as well to find the life of the detail prior to formation of any crack. The methods to obtain the crack initiation life and propagation life are presented in the following sections.

4.1.2.1. Crack Initiation Life

Crack initiation life can be determined using empirical correlation approaches such as stress-based approach, strain-based approach, and energy-based approach. In high stress low cycle fatigue problem such as web gap detail under distortion induced cyclic load, the initiation life of the detail is not a main concern as it does not take numerous cycles to form and grow a crack to a visible size. Therefore, Just a brief review of the crack initiation life calculation is brought in this section.

Although energy-based approach is the most accurate and reliable method for details with complex stress and strain fields, it requires more complex computations and is very time consuming. For welded details which have localized high stresses and drastic changes in stress fields, According to Chen, Grondin, & Driver (2005), the strain-based method provides more accurate results than the stress-based method. Therefore, it is decided to utilize strain-based method to calculate the crack initiation life of web gap detail in steel multi-girder bridges.

Generally strain-based method uses the measured strain in the detail and by knowing the fatigue material properties, calculates the crack initiation life. According to Stephens et al. (2000) strain-based method is a very suitable method for low cycle fatigue of ductile materials and low to high cycle fatigue where small plastic strains exist. Based on the strain-based method, crack initiation life can be calculated using Equation (4-1).

$$\frac{\Delta\varepsilon}{2} = \frac{(\sigma'_f)^2}{\sigma_{max}E}(N_i)^{2b} + \frac{\sigma'_f\varepsilon'_f}{\sigma_{max}}(N_i)^{b+c} \quad (4\text{-}1)$$

where $\frac{\Delta\varepsilon}{2}$ is the strain amplitude ($\frac{\varepsilon_{max}-\varepsilon_{min}}{2}$) in the detail, σ_{max} is the maximum local stress accounting for plasticity, σ'_f is fatigue strength coefficient, ε'_f is fatigue ductility coefficient, b is fatigue strength exponent, c is fatigue ductility exponent, and finally N_i is the number of initiation cycles.

The crack in web gap detail initiates either in the weld body or at the weld toe where the transverse stiffener is connected to the web plate (Fisher, 1978). Some cracks in the web gap detail are also reported in the literature located at the weld toe near the tension flange but the crack at transverse stiffener weld toe location is almost inevitable in web gap details prone to distortion induced fatigue (Fisher, 1978).

In order to use Equation (4-1) the proper material properties for the steel should be obtained. The material properties used in this study are for weld metal obtained in an experimental program conducted at University of Alberta (Josi & Grondin, 2010) and presented in Table 4- 1.

Table 4- 1: Crack Initiation material properties (Josi & Grondin, 2010)

Crack Initiation Parameters	
σ'_f	630 MPa
ε'_f	0.34
b	-0.059
c	-0.63

4.1.2.2. Crack Propagation Life

There are several parameters defined as the fracture criteria such as Energy release rate parameter (G), crack-tip-opening displacement (CTOD), J-Integral, and stress intensity factor (K). J-Integral and stress intensity factor (K) are the most common parameters as can be obtained using finite element analysis. In this section these parameters are briefly explained.

4.1.2.2.1. Crack-Tip-Opening Displacement (CTOD)

Crack-Tip-Opening Displacement (CTOD) is an empirical parameter and can be found by performing experimental tests. In order to find this parameter, the magnitude of the crack tip should be measured. It is almost impractical for structural tests with limited equipment to measure the actual crack tip itself. To measure the crack tip opening, some test procedures are developed. The standard test to find CTOD is performed by three-point bending on a single-edge-notched specimen. These tests are usually done on materials with plastic deformation before the failure. The plastic deformation of the material at the crack tip allows the tip of a crack to stretch and open for measurements. The specimen has visible crack in the middle where bending moment and deformation are maximums. When the load is being applied, the crack tip plastically deforms until a critical load is reached. The magnitude of the load in which the fracture occurs and the opening of the crack mouth are recorded. Knowing the crack length and the dimensions of the specimen, and by assuming that the specimen halves are rigid and rotate about a hinge point, the crack tip opening can be calculated. Moreover, by monitoring the magnitude of the applied load and the crack tip opening, one can realize if the specimen is fractured in a brittle or in ductile manner.

4.1.2.2.2. J-Integral Approach

Any system in thermodynamic equilibrium tends to maintain its energy equilibrium. If under a certain condition this energy equilibrium changes or is disrupted, the system retains its energy equilibrium by releasing the excessive energy and decreasing the energy level. In the state of non-equilibrium, a crack can occur and propagate to release the excessive energy and to regain the equilibrium state. Therefore, the critical conditions for fracture can be defined as the point where crack growth occurs under equilibrium conditions, with no net change in total energy (Anderson, 2005).

As it was discussed previously, there are basically two types of materials in terms of fractural behavior; brittle and ductile. This is based on the amount of energy that the material needs to develop a crack. For example materials such as glass do not need much energy to grow a crack when the crack is initiated in the system. The energy stored in the body of material with brittle fracture behavior is a function of two independent variables: the displacement of the load, and the area of the crack. Linear elastic fracture mechanics (LEFM) theory can be applied and utilized for materials with brittle fracture behavior. This is because the material still behaves in an elastic manner even though it is in plastic phase very close to the crack tip location. Therefore, fracture analysis of these materials can be fairly simple. On the other hand, for the material with ductile behavior, it is needed to consider the plasticity theory. This makes the calculation and fracture analysis of the crack challenging. To overcome this issue and as an alternative approach for performing the fracture analysis for ductile materials, the J-Integral energy approach is widely used.

The J integral is a line integral (path-independent) around the crack tip and mostly used in problems with large plastic zone around the crack tip. This is relatively large compared to dimensions of specimen. When the crack grows, J-Integral represents the rate of change of the net potential energy which is a measure of singularity strength at the crack tip.

In the J-Integral approach, crack grows when the energy at the crack location exceeds a certain amount known as the critical energy. The magnitude of the critical energy depends on the material properties. The energy method was first introduced by Griffith (1921). He basically proposed an energy-based failure criterion and compared the work required to break atomic

bonds to the strain energy released as a crack grows. Griffith performed experimental tests on glass and his theorem provides excellent agreement with experimental data for brittle materials but not for ductile material such as steel. His method predicts an infinite magnitude for stress at crack tip when linear elastic material property is used. In reality, material at the crack tip goes into a plastic phase before crack grows. Therefore, plasticity around the crack tip must be considered in these materials. There are mainly two assumptions for Griffith energy balance approach:

1. Work for the formation of crack must be done against the cohesive forces of the molecules on either side of the crack;
2. If the crack opening is greater than a very small distance called the "radius of molecular action", the energy per unit area is a constant of material, called its surface tension.

This is all about utilizing the concept of work and energy. Work which is a mechanical form of energy has a physical definition. The work is calculated by multiplying the force by the amount of movement of an object in the direction of the applied force. As the magnitude of the force and the displacement can vary during the load application, the amount of work is calculated using Equation (4-2).

$$W = \int F.dx \tag{4-2}$$

where W, is the total work done on the object, F, is the magnitude of the force, and dx, is the instantaneous displacement of the force. This equation can be represented in terms of stress and strain simply by dividing and multiplying the right hand side of the equation by the volume of the object. Equation (4-3) presents the work in terms of stress and strain.

$$W = V \int \sigma.d\varepsilon \tag{4-3}$$

$$\sigma = f(\varepsilon) \tag{4-4}$$

where, σ is the stress which is a function of strain as shown in Equation (4-4), and ε, is the corresponding strain in the system.

As strain and stress are used in this equation, the work calculated in Equation (4-3) is equal to strain energy, U which is presented in Equation (4-5).

$$W = U = V \int \sigma . d\varepsilon \tag{4-5}$$

The integral in Equation (4-5) is called strain energy density which is defined as strain energy per unit volume and is represented in Equation (4-6).

$$W' = U' = \int \sigma . d\varepsilon \tag{4-6}$$

$$W = U = U' \times V \tag{4-7}$$

where, U' is strain energy density and for linear elastic material in uniaxial tension is calculated using Equation (4-7). Figure 4- 3 graphically represents the calculation of U', for linear elastic material.

$$U' = \frac{1}{2} E \varepsilon^2 \tag{4-8}$$

To calculate the strain energy, Equation (4-7) can be simply substituted in Equation (4-8).

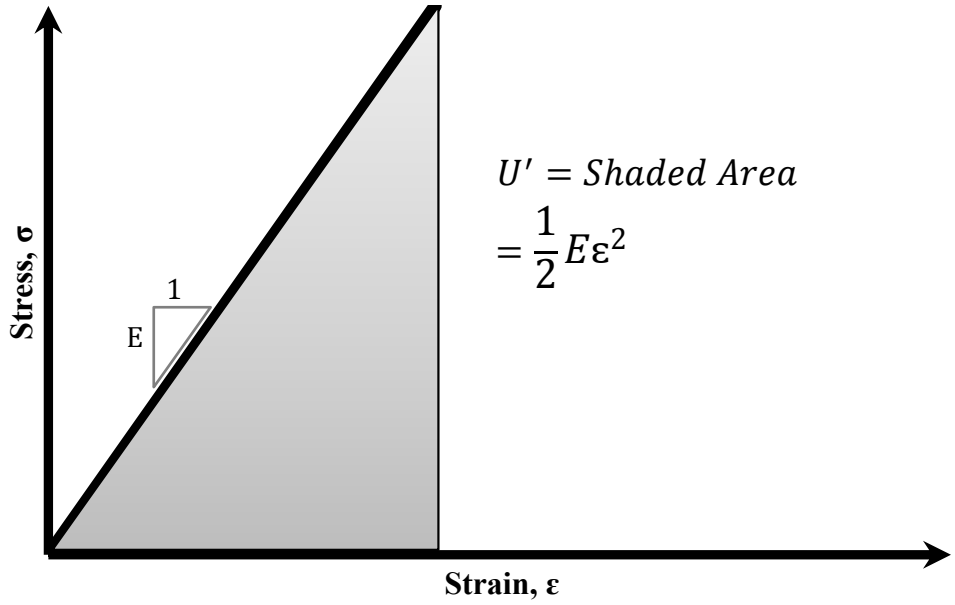

Figure 4- 3: Strain Energy Density Calculation for Linear Elastic Material

In order for a crack to propagate to a certain length, a, the atomic bonds should be broken along the crack length. The amount of work needed for the crack propagation to length of a is equal to the energy required to break the atomic bonds along the crack length which can be calculated using Equation (4-9).

$$E_{bond} = 2\gamma_s aB \tag{4-9}$$

where γ_s, is the energy required to break atomic bonds per unit surface area, a, is the crack length, and B, is the crack width or the member thickness in case the crack is a complete through thickness crack.

Griffith defined a failure criterion in which the elastic energy is related to the atomic bond energy. This relation is shown in Equation (4-10).

$$\sigma_f = \sqrt{\frac{G_c E}{\pi a}} \tag{4-10}$$

where σ_f, is the remote stress at failure for the crack with length of "a", E, is the material modulus of elasticity (Young's modulus), and G_c, is the energy release rate which is defined as the magnitude of energy required to break atomic bonds per unit surface area (γ_s) multiplied by two which is shown in the following equation:

$$G_c = 2 \times \gamma_s \tag{4-11}$$

Critical energy release rate is a material property which is independent of the applied loads and the geometry of the body. As soon as the energy release rate in the material exceeds critical energy release rate, the crack propagates. Energy release rate is obtained experimentally and is defined in Equation (4-12).

$$G_c = -\frac{\partial U(\Delta, A)}{\partial A} \tag{4-12}$$

where U, is the potential elastic energy in the body available for crack growth, and A, is the crack area. Elastic material behavior is the main assumption to find G.

Using the energy release rate parameter, the failure load in which the crack grows can be obtained. This parameter is only valid when LEFM is used for fracture analysis. In order to investigate the inelastic material behavior, J-Integral approach is used. J-Integral calculates the rate of change of net potential energy with respect to crack propagation per unit thickness of crack tip for a non-linear elastic material. In other words J-Integral is the energy flow into the crack tip. It is also an indication of the singularity strength at the crack tip for the case of elastic-plastic material behavior. The J-Integral can be obtained using Equation (4-13).

$$J = \int_{\Gamma} (W\, dx_2 - t_i \frac{\partial u_i}{\partial x_1} ds) \tag{4-13}$$

where x_2 and x_1 are the coordinate directions, W is the strain energy density which is a function of x_2 and x_1 , t_i is the surface traction tensor and defined in Equation (4-14), Γ is the closed path (curve) on which the integral is being taken along, and u is the displacement vector.

$$t_i = [\sigma].n_i = \begin{bmatrix} \sigma_{11} & \sigma_{12} & \sigma_{13} \\ \sigma_{21} & \sigma_{22} & \sigma_{23} \\ \sigma_{31} & \sigma_{32} & \sigma_{33} \end{bmatrix}.n_i \tag{4-14}$$

where [σ] is the Cauchy stress tensor, and σ_{ij} is the component of the stress tensor.

For isotropic, perfectly brittle, linear elastic materials, the J-integral can be directly related to the fracture toughness if the crack extends straight ahead with respect to its original orientation (Yoda, 1980). Fracture toughness is a material property which can be obtained by experimental test and is defined as the ability of the cracked material to resist the propagation of the crack or the material fracture.

As Griffith theory is not very practical for engineering problems with large plastic zone, Irwin (1965) proposed and developed energy release rate concept. He found that the plastic zone develops at the crack tip for both ductile materials and brittle materials. By increasing the magnitude of the applied load, the plastic zone grows and leads to reduction of the stresses and displacements near the crack-tip. This was the introduction to Stress intensity factor parameter which is presented in the next section.

4.1.2.2.3. Stress Intensity Factor

In fracture mechanics, to evaluate the stress near the crack tip which is caused by the remote applied stress, a factor called Stress Intensity Factor (SIF) is used. This factor is a function of the magnitude of the remotely applied stress, crack length, the geometry of the detail, and the location of the crack in the detail. SIF can be calculated using Equation (4-15).

$$K = \sigma_{ij}(r,\theta)\sqrt{2\pi r} \times \frac{1}{f_{ij}(\theta)} + \gamma(r,\theta) \qquad (4\text{-}15)$$

where K is the stress intensity factor, r is the distance from the crack tip, σ_{ij} is the stress distribution around the crack, f_{ij} is a dimensionless quantity that is a function of the remote applied load and the geometry of the body containing the crack. γ is also a higher order function of r and θ.

Stress intensity factor is defined for all three modes of fracture; opening mode (Mode I), in-plane shear mode (Mode II), and out-of-plane shear or tearing mode (Mode III). The corresponding stress intensity factor for these modes are K_I, K_{II}, and K_{III}, respectively. These modes are illustrated in Figure 4- 4 and defined in Equation (4-16) to (4-18).

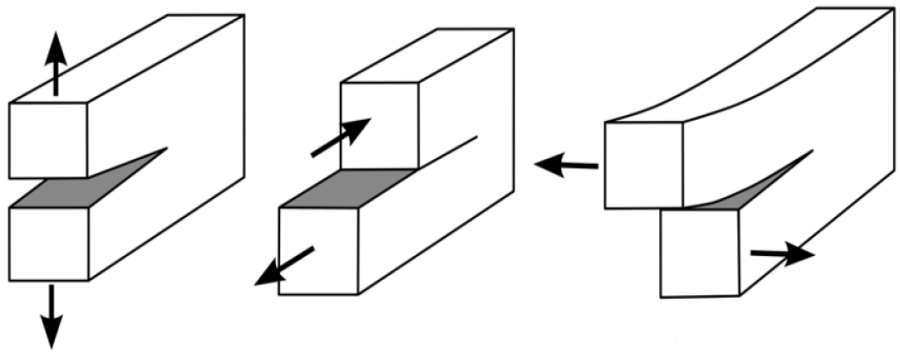

Mode I Mode II Mode III

Figure 4- 4: Various Loading Condition and Modes in Fracture Mechanics (Aygül, Al-Emrani, Barsoum, & Leander, 2014)

$$K_I = \lim_{r\to 0} \sigma_{yy}(r,\theta)\sqrt{2\pi r}, \qquad \text{when } \theta = 0 \qquad (4\text{-}16)$$

$$K_{II} = \lim_{r\to 0} \sigma_{yx}(r,\theta)\sqrt{2\pi r}, \qquad \text{when } \theta = 0 \qquad (4\text{-}17)$$

$$K_{III} = \lim_{r\to 0} \sigma_{yz}(r,\theta)\sqrt{2\pi r}, \qquad \text{when } \theta = 0 \qquad (4\text{-}18)$$

In these equations, it is assumed that the crack is in the X-Y plane. By knowing the magnitude of the stress intensity factor for a specific crack and under a known loading scenario, the stresses near the crack tip can be calculated. For example the stresses near crack tip (r), in direction of θ, and only under crack opening Mode I is presented in Figure 4- 5.

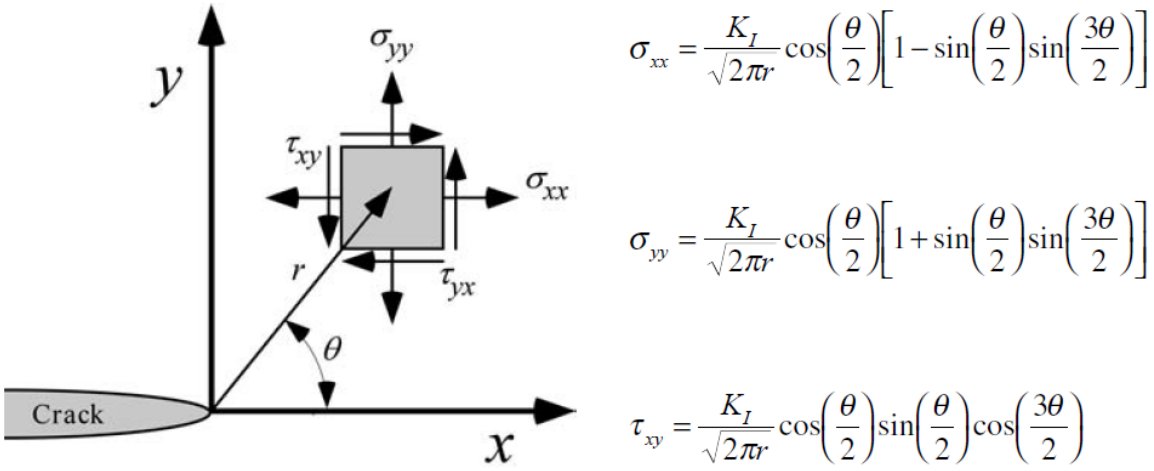

Figure 4- 5: Stresses near the Tip of a Crack in an Elastic Material (Anderson, 2005).

Finding the stress intensity factor (in this case, K_I) is the most challenging part. For several specimens with predefined simple geometry and location for the crack, the empirical and closed form solutions to calculate K were derived and are available in the literature. For instance, for an existing through crack in a semi-finite plate with an edge crack subjected to a remote

tensile stress, the closed form solution for stress intensity factor for Mode I is presented in Equation (4-19).

$$K_I = 1.12\,\sigma\sqrt{\pi a} \tag{4-19}$$

In case of a complex problem, one needs to either perform experimental tests or conduct numerical analysis to estimate the stress intensity factor for a given crack and loading condition. It should be noted that the obtained stress intensity factor would only be valid for the same specimen with exactly the same crack size and shape, at the same location. In case the crack propagates, the obtained stress intensity factor is not valid anymore and it should be estimated again.

When the stress intensity factor is calculated, it is compared with the critical stress intensity factor (K_{cr}) to assess the crack failure. This occurs when K_i (corresponding stress intensity factor for the fracture mode) is equal or greater than K_{cr}. Despite of K_i, which is a function of applied load and geometry, K_{cr} is a measure of material resistance and is already obtained for most of engineering materials.

In case of having mixed mode crack opening and fracture, the failure criterion is presented in Equation (4-20).

$$K_{Mixed-Mode} = G_c = {K_I}^2 + {K_{II}}^2 + \frac{E'}{2G}{K_{III}}^2 \tag{4-20}$$

where G_c is the energy release rate, $E'=\frac{E}{(1-\nu)^2}$ for plane strain and $E' = E$ for plane stress, E is the material Young's modulus, ν is the Poisson's ratio, and G is the shear modulus.

4.1.2.2.4. The Relation between G and J-Integral, K

Irwin (1965) found that LEFM can be used to calculate the energy required for fracture and crack propagation, even for materials with relatively small plastic zone at the crack tip. Therefore, using this assumption, the fracture energy (strain energy release rate) can be obtained from stress intensity factor. For instance, for opening mode (Mode I) the energy release rate can be calculated using Equation (4-21).

$$G_c = G_I = \frac{K_I^2}{E'} \tag{4-21}$$

where K_I is the stress intensity factor for Mode I, $E'=\frac{E}{(1-\nu)^2}$ for plane strain and $E' = E$ for plane stress, E is the material Young's modulus, and ν is the Poisson's ratio, and G is the shear modulus.

By using linear elastic assumption for the crack growth, the energy release rate is equal to the J-Integral as well. This relationship is presented in Equation (4-22).

$$G_c = J - Integral = \frac{K_c^2}{E'} \tag{4-22}$$

4.1.2.2.5. Crack Propagation Life Calculation

In this study linear elastic fracture mechanics (LEFM) approach is used. In order to calculate the crack propagation life, the following equation proposed by Klesnil and Lukas (1972) is used.

$$\frac{da}{dN} = C.(\Delta K^m - \Delta K_{th}^m) \quad (4\text{-}23)$$

where $\frac{\mathrm{da}}{\mathrm{dN}}$ is crack growth rate in the stable propagation stage, ΔK is the stress intensity factor range, $\Delta \mathrm{K}_{th}$, C and m are material constants which can be determined for a material by experimental tests and recording crack growth and corresponding number of cycles for each crack growth step.

In a web gap detail in steel multi-girder bridges, the crack first propagates in the weld material and continues into the base metal which is highly affected by the welding process and the material constants used for crack propagation life is different for these zones. Table 4- 2 presents the material properties for weld and Heat-Affected Zone (HAZ) in base metal. These material properties for Mode I are obtained from experimental programs at University of Alberta (Josi & Grondin (2010) and Chen et al. (2005)). These Material properties are used in this study to calculate the fatigue life of the crack in web gap detail.

Table 4- 2: Crack propagation material properties for weld and base metal for Mode I (Chen et al. (2005) and Josi & Grondin (2010))

	Weld Material	Base (HAZ) Material
C	3.87×10^{-13}	3.54×10^{-13}
m	3.0	3.0
$\Delta \mathrm{K}_{th}$	60	60

Knowing the stress intensity factor of a crack in the detail and integrating Equation (4-23) the number of cycle needed for a crack to grow to certain length – crack propagation life - can be calculated. This integration is shown in Equation (4-24).

$$N_p = \int_{a_i}^{a_f} \frac{1}{C.(\Delta K^m - \Delta K_{th}^m)} da \qquad (4\text{-}24)$$

where N_p is the number of stress cycle needed for the crack to grow from a_i to a_f, a_i is the initial length of the crack, a_f is the final length of the crack, ΔK, ΔK_{th}, C, and m are the same as defined previously in Equation (4-23).

Stress intensity factor for crack at weld toe in web gap detail in steel multi-girder bridges must first be found first to investigate fatigue life of the detail. It can be obtained by either experimental tests or finite element analysis. Experimental programs are very costly for this purpose. Therefore, it is decided to use FEA approach to find stress intensity factor for crack at each step of crack propagation phase and calculate the crack propagation life.

In order to find the propagation life of a crack, it is needed to define the initial size of the crack as well as the final crack size. There is no precise and fixed definition for the crack initial length. The initial crack size reported in the literature ranges from 0.01 mm to 1 mm. In web gap detail, the crack initiation and initial stage of crack propagation life is very short and crack grows to a visible size very fast. This is because of the high stress gradient and the huge distortion in the web gap. Therefore, the initial size of the crack does not really affect the crack propagation life and it is decided to use 0.1 mm as a crack initial size. As the crack grows, the web becomes more flexible and this reduces the stress range magnitude which leads to a longer fatigue life.

The final crack size is equal to the length of the crack at which the crack stops growing or the experiment is terminated and the crack length is measured. Δa, or the crack propagation increment, can be defined in several ways. It can be defined as a constant value or a variable parameter. For instance, Equation (4-25) presents a simple way to find a constant value for Δa.

$$\Delta a = \frac{a_f - a_i}{N} \quad (4\text{-}25)$$

where a_f is the final crack size, a_i is the initial crack size, and N is the number of increments that is defined by the assessor. Δa can be variable while crack grows. This is because, at the initial stages of crack growth crack propagates very fast and the smaller crack increments leads to a more accurate result for cycle counting. This trend changes when crack reaches the final stages of crack propagation as it takes numerous cycles for a crack to grow an increment and having variable crack growth increments saves calculation time. This is correct when the crack eventually stops after reaching a certain length and does not propagate anymore. For specimens in which the crack has an unstable crack growth the initiation life and initial stages of crack propagation are longer than the final stages. In this type of crack, the specimen fractures unstably when the crack reaches a certain length, namely the critical length. The crack in the web gap detail eventually stops after it reaches a certain length and does not propagate anymore if the crack propagates toward the center of the web plate. In this study, the variable crack propagation increments are used for crack growth analysis.

In the following section the FEA approach used in this study to obtain stress intensity factor for web gap detail is presented. First of all, the stress intensity factor for a benchmark is obtained using FEA and compared with the stress intensity factor found using the corresponding empirical equation to verify the modeling approach. Then, using the same approach, the stress intensity factor for the web gap detail with an initiated crack is calculated for different crack propagation stages. These results will be used to obtain the crack propagation life of the crack in the detail.

4.2. Verification of FE Models to Calculate SIF

The FEA software ABAQUS 6.13 is used to calculate the stress intensity factor for a benchmark model. This verifies the crack modeling technique as well as SIF calculation for future FE models. The benchmark model is a 2D model containing an edge crack. This is

selected as the analytical equation for this model is driven and is available in the literature. Therefore, it can be used to evaluate the SIF calculation.

4.2.1. SIF for Edge Crack in Finite Plate

The geometry of the model is shown in Figure 4-6 and the SIF for Mode I can be calculated using Equation (4-26). This equation is valid for $\left(\frac{h}{b}\right) \geq 1$, and $\left(\frac{a}{b}\right) \leq 0.6$. Therefore, the dimensions are selected in a way to satisfy these conditions. For the bench mark, h is equal to 100 mm, b is equal to 40 mm, and the 20 mm crack is located at the mid height of the plate. The thickness of the plate is 1 mm. The linear elastic material properties for steel with Young's modules of 200 GPa and Poisson's ratio of 0.3 is used in this model.

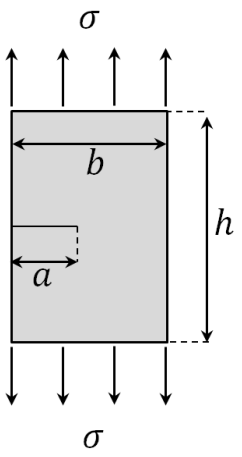

Figure 4- 6: Edge crack in a finite plate under uniaxial stress

$$K_I = \sigma\sqrt{\pi a}\left[1.12 - 0.23\left(\frac{a}{b}\right) + 10.6\left(\frac{a}{b}\right)^2 - 21.7\left(\frac{a}{b}\right)^3 + 30.4\left(\frac{a}{b}\right)^4\right] \quad (4\text{-}26)$$

The plate is modeled using homogeneous solid second-order elements (CPE8) and the crack tip including the integral contour region is meshed using sweep method. A 100 MPa tensile uniform stress is applied to the both top and bottom edges of the plate as shown in Figure 4-6.

A mesh convergence study is also performed for the model and it is decided to use 0.5 mm mesh size. The mesh density for the model and the deformed shape of the model under applied load are shown in Figure 4-7.

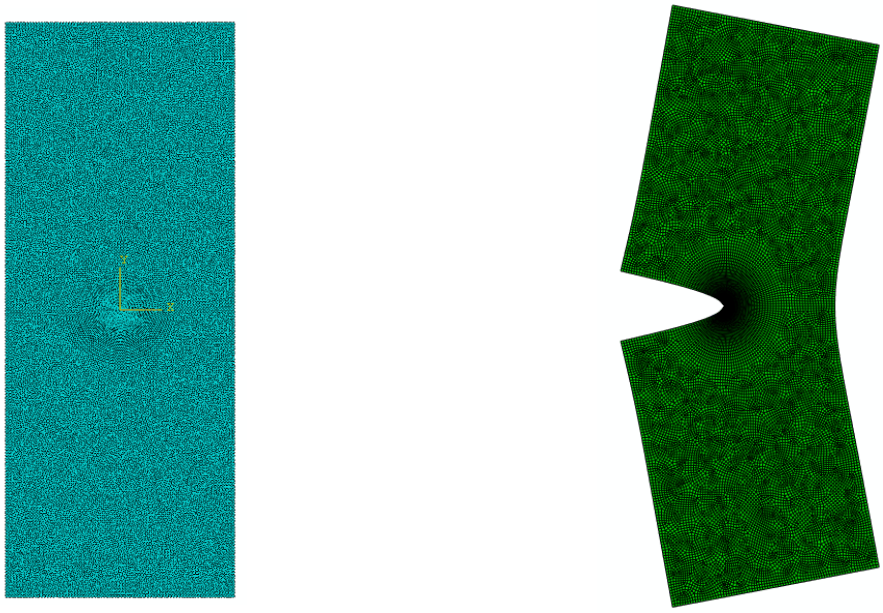

a) b)

Figure 4- 7: a) Mesh density and b) deformed shape of the plate under uniaxial load

For the given dimensions, crack length, and the remote applied stress and by using Equation (4-26), the stress intensity factor for Mode I is calculated and compared to the SIF obtained from finite element analysis in Table 4-3.

Table 4- 3: SIF calculated using Equation (4-26) and Obtained form FEA

	SIF Calculated Using Equation (4-26)	SIF Obtained From FEA
SIF	2253.15	2211.91

As it is shown in Table 4- 3 there is only 1 % difference between the SIF calculated using the Equation (4-26) and SIF predicted by the FEA which confirms the agreement of the two methods.

4.3. Fatigue Life Investigation of Web Gap Detail

In this section, the finite element model of the web gap detail from experimental work conducted at University of Kansas (Hartman et al, 2013) is used to investigate the fatigue life. The 3D finite element model of the three-girder bridge with cross frame braces was created in ABAQUS 6.13. This model is used as a global model for a more refined model of web gap called sub-model to investigate the stress in the detail more accurately and more efficiently. This sub-model is used in order to save computational time as only the region containing the crack is needed to perform fatigue analysis. The global model and the location of the web gap are shown in Figure 4- 8. Further details of the modeling procedure and boundary conditions used for web gap detail are presented in Chapter 3.

4.3.1. Initial Crack Life

According to the finite element analysis performed in Chapter 3, and using Equation (4-1) and crack initiation material properties presented in Table 4- 1, the crack initial life (the number of cycle needed to initiate the crack) is calculated and presented in this section.

The maximum stress in the web gap detail obtained from finite element results (Chapter 3) is 434 MPa at the transverse stiffener weld toe location and the corresponding strain is 0.005. Using Equation (4-1) leads to the total fatigue crack initiation life of 8,340 cycles. The calculation of the crack initiation life is presented in Appendix A.

Base on the experimental program conducted at University of Kansas (Hartman et al, 2013), on the same detail, the initial crack was visible at the weld toe after 15,000 cycles. The difference is from the size of the detected crack and the interval of the visual crack inspection which was at every 5,000 cycles. In the experimental observation, the crack was initiated in earlier stages than it was detected and became visible. Therefore, the reported 15,000 cycle includes some propagation cycles as well.

4.3.2. Initial Crack Location

Stress intensity factor is highly affected by the location of the crack in the web gap. In an ideal web gap detail in which there is no deficiency and imperfection in the weld material, the crack initiates at the weld toe at transverse stiffener location. Then it propagates toward the centroid of the web plate. Figure 4-8 shows the location of crack initiations. In this figure, the global and local models are shown using shell elements in Figure 4-8 a. It must be noted that in order to investigate the crack growth in 3D, solid element must be used. Therefore, at the location of the web gap (local model) the model is replaced with a solid element and the shell elements are tied to the solid elements and the crack is inserted in the solid element model. The solid portion of the model is shown in Figure 4-8 b. The crack location is shown with red line. In reality, the weld is not perfect and this imperfection leads the crack to initiate in the weld body itself. Therefore, the effect of location of the initial crack on the stress intensity factor for these two locations should be investigated. The result of this investigation is presented in this section.

According to the experimental results and observations (Hartman et al, 2013), the crack was initiated in the vertical stiffener weld body in the web gap. This crack location is shown in Figure 4-9.

In this section, two crack locations are investigated; Location 1, which is at the weld toe and Location 2, which is at the weld body. These locations are shown in Figure 4-8 and Figure 4-9.

A semi-circle crack with the radius of 0.1 mm is inserted in these crack locations and the stress intensity factors at the crack tip along the cracks edges are computed. The method and procedure to compute the stress intensity factor are explained in the following section.

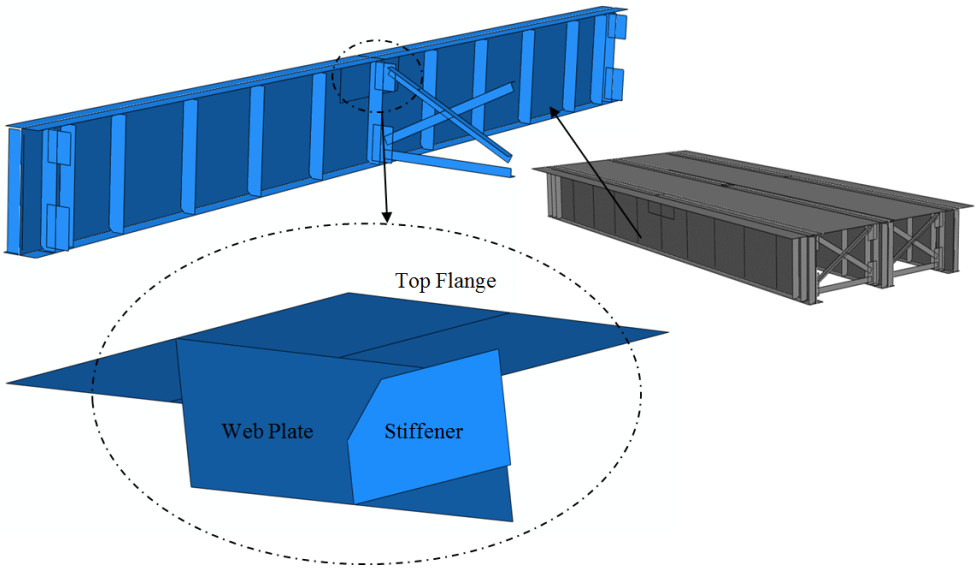

a)

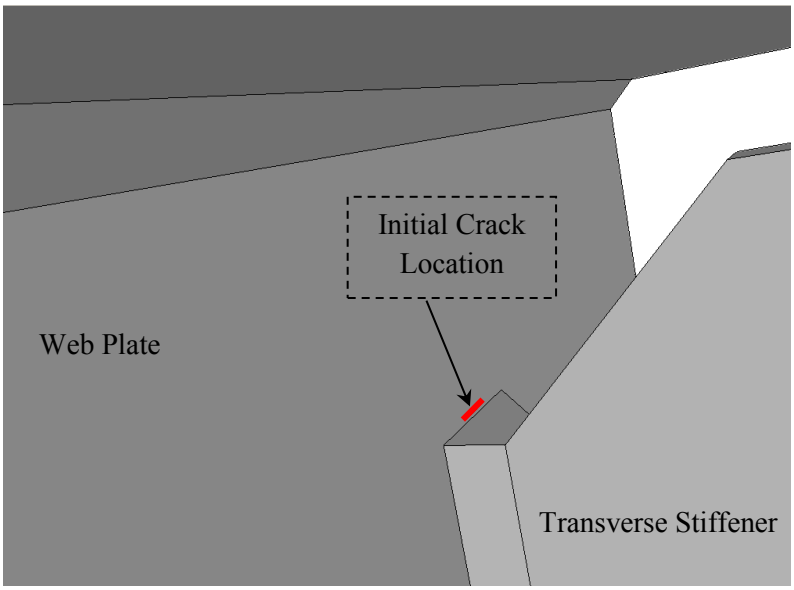

b)

Figure 4- 8: a) The global model and the location of the web gap, b) the initial crack location in the web gap (Location 1)

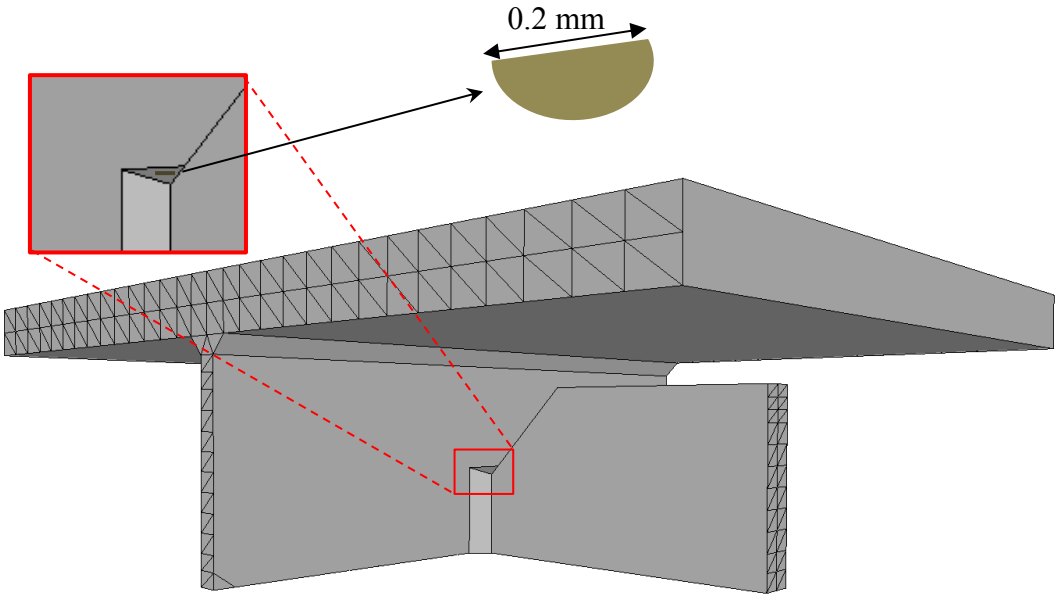

Figure 4- 9: Initial crack location in web gap detail at weld body as reported in the experiment (Location 2).

4.3.3. Using FRANC3D to calculate SIF and J-Integral

The stress intensity factor is defined for the crack tip. When the crack is 2D (semi-circle crack) the stress intensity factor is a function of the crack tip location along the edge of the crack. This makes the calculation of the stress intensity factor even more challenging. Using FE analysis the stress intensity factor along the crack edge can be obtained.

In order to calculate the crack propagation life of a crack, it is needed to grow the crack incrementally (crack propagation step). At the end of crack propagation at each increment the stress intensity factor should be calculated. This process must be performed until the crack reaches the final crack size. This is doable if the crack stays in the same plane and follows the same semi-circle shape as the user can define new crack with the only bigger radios. For example, for the second step, the radios would be equal to the initial crack size plus a crack propagation increment ($r_2 = a_i + \Delta a$).

In web gap detail the crack has a 3D profile. Therefore, only the initial crack can be defined and the crack propagates in the direction of the highest stress at the crack tip along the edge comparing the crack growth criteria that are previously described. Assessing the fatigue life of the web gap detail would be impractical if the crack propagation is done manually for this detail. This is because after the first crack growth increment, the crack propagates out of the plane in which the initial crack was inserted. An alternative solution for this problem is to use a software package that propagates the crack and calculate the stress intensity factor for each increment automatically. FRANC3D is one of the most reliable crack analysis software and is used in this study to propagate the crack and perform fracture analysis.

FRANC3D is developed at Cornell University started in the late 1980's to perform fracture analysis and crack growth analysis in complex 3D structures.

FRANC3D is a software package that can insert a crack in to a model, generate suitable mesh, and extract the model for analysis. It does not perform finite element analysis itself and needs to utilize a FEA package such as ABAQUS, ANSYS, and NASTRAN to run the cracked models in order to obtain the stress around the crack tip. This procedure is explained in the following section.

In order to perform the fracture analysis, a 3D model of the web gap detail with appropriate boundary conditions, material properties and applied load is created and meshed in ABAQUS. This model is imported to FRANC3D for the next steps. A semi-circle crack with the initial radius of 0.1 mm is inserted in the weld body at the vertical stiffener location. Then the crack model is remeshed in FRANC3D. This cracked model is exported to ABAQUS to perform the finite element analysis to calculate the stress in the model. Then, the results imported back into FRANC3D to calculate the stress intensity factors at crack tip along the crack edge. The crack propagates using the crack propagation criteria including critical energy release rate for the material defined in FRANC3D. The model with the new crack is meshed again in FRANC3D and imported to ABAQUS for analysis. This procedure continues till the crack reaches the final length and stops propagating. These steps are graphically presented in in Figure 4-10.

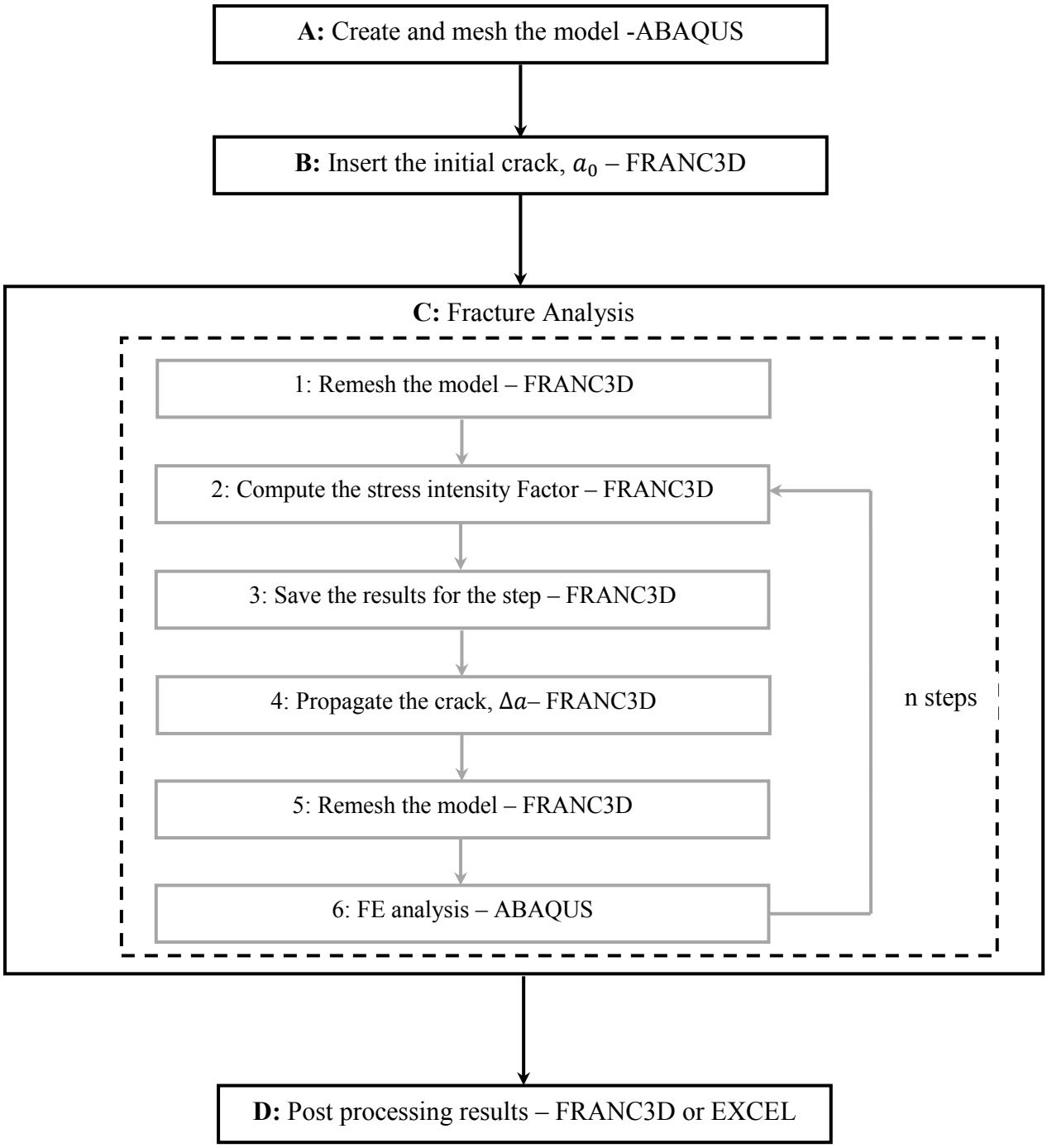

Figure 4- 10: Steps to compute stress intensity factor using FRANC3D and ABAQUS.

4.3.3.1. SIF for Initial Crack at Weld Toe (Location 1)

Using FRANC3D, the stress intensity factor is computed for the semi-circle crack with radios of 0.1 mm at weld toe in transverse stiffener in the web gap detail. The crack geometry and points for which the stress intensity factors are computed are shown in Figure 4- 11. For these crack tip points the stress intensity factors for Mode I, Mode II, Mode III, and J-Integral are computed and the results are presented in Table 4-4. Mixed mode fracture effect is also calculated manually using Equation (4-20) for the mixed mode fracture and presented in Figure 4-15.

The stress intensity factors for Mode I, Mode II, Mode III, the effect of mixed-mode fracture ($K_{Mixed-Mode}$), and J-Integral at crack tip along the crack edge at Location 1 are graphed and shown in in Figure 4-12 to Figure 4-16.

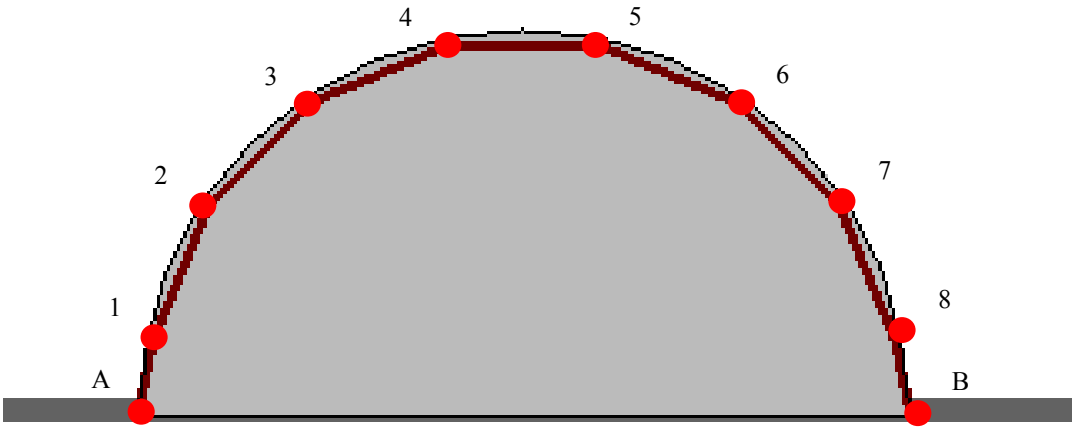

Figure 4- 11: Semi-circle crack geometry and points along the edge for SIFs and J-Integral calculation.

Table 4- 4: Fracture analysis results of the semi-circle crack at the weld toe (Location 1)

Point	D[1]	KI	KII	K111	J-Integral
1	0.06	3097	168	373	39
2	0.19	2491	429	400	24
3	0.31	1987	664	251	15
4	0.44	1747	761	67	12
5	0.56	1747	738	-106	12
6	0.69	1985	600	-287	15
7	0.81	2456	349	-427	24
8	0.94	3048	62	-388	38

[1] D is the normalized distance from point A.

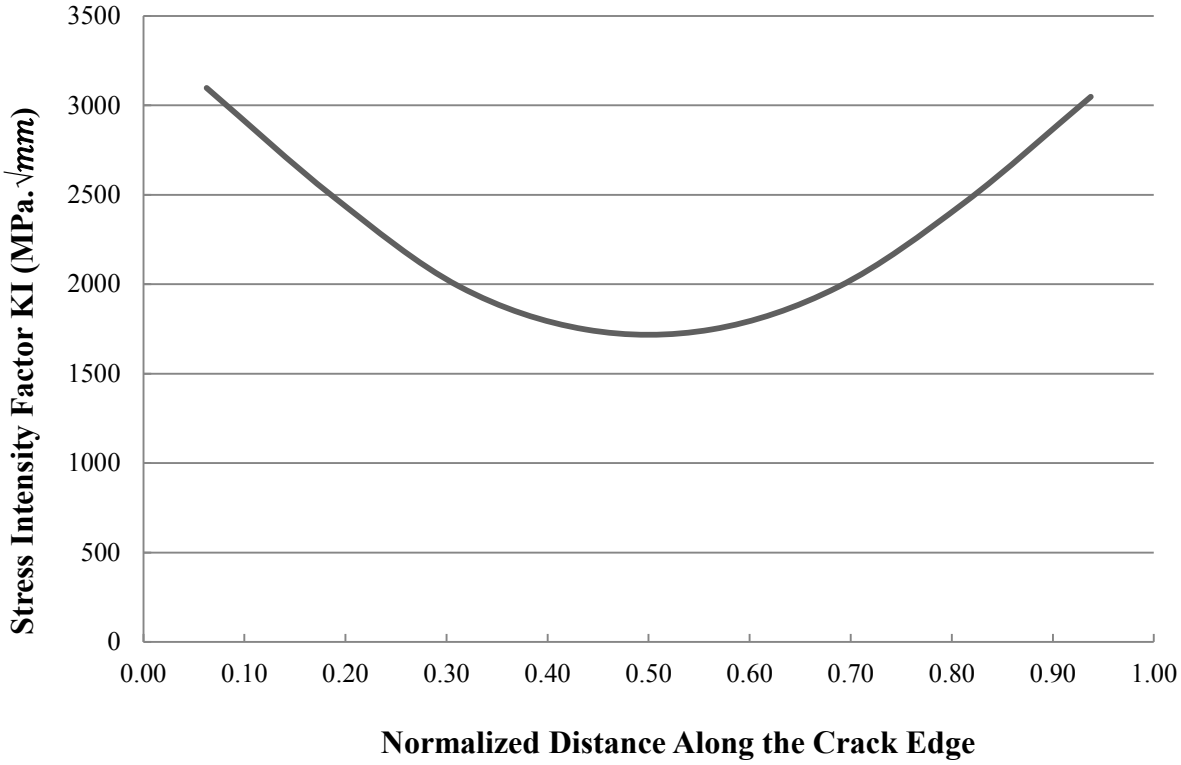

Figure 4- 12: Stress Intensity Factor for Mode I for 0.1 mm Semi-Circle Crack at Transverse Stiffener Weld Toe (Location 1) in Web Gap Detail.

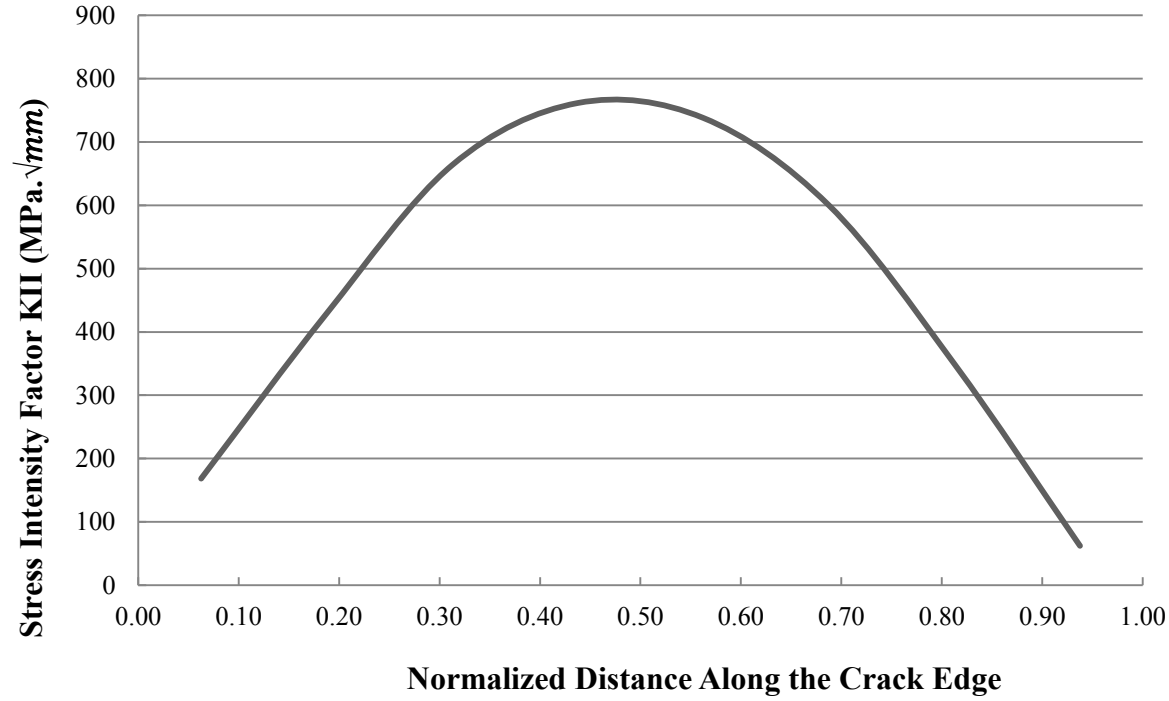

Figure 4- 13: Stress Intensity Factor for Mode II for 0.1 mm Semi-Circle Crack at Transverse Stiffener Weld Toe (Location 1) in Web Gap Detail.

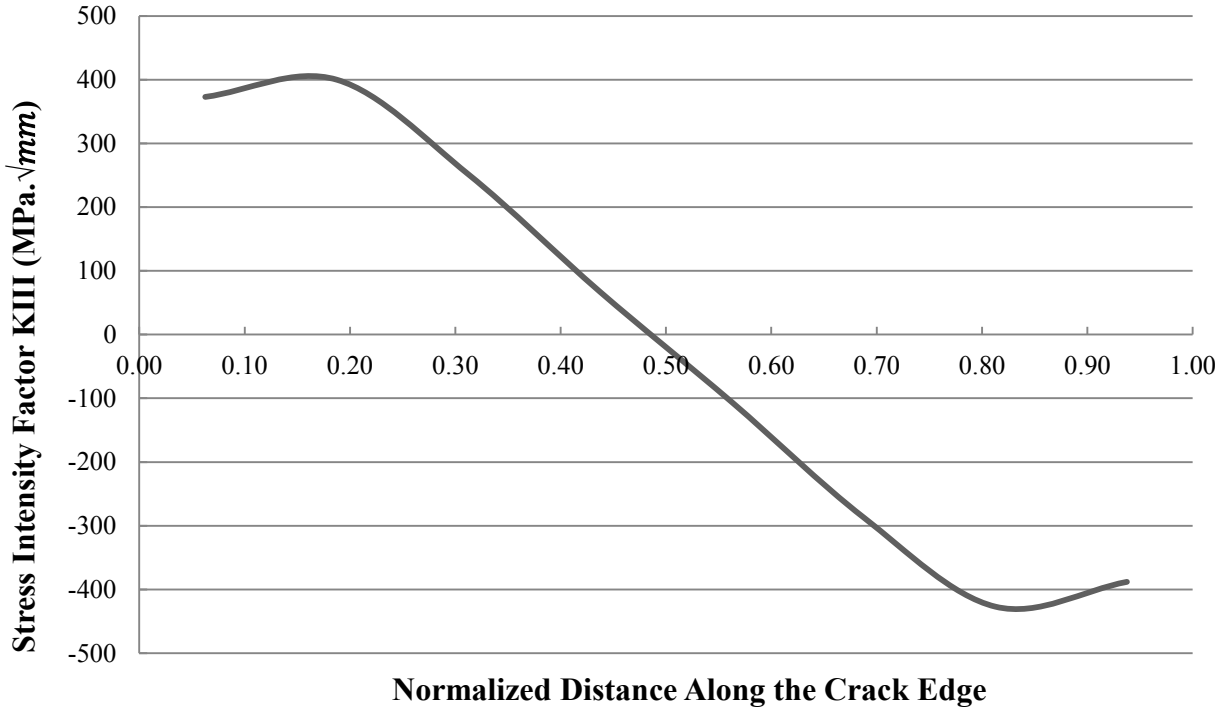

Figure 4- 14: Stress Intensity Factor for Mode III for 0.1 mm Semi-Circle Crack at Transverse Stiffener Weld Toe (Location 1) in Web Gap Detail.

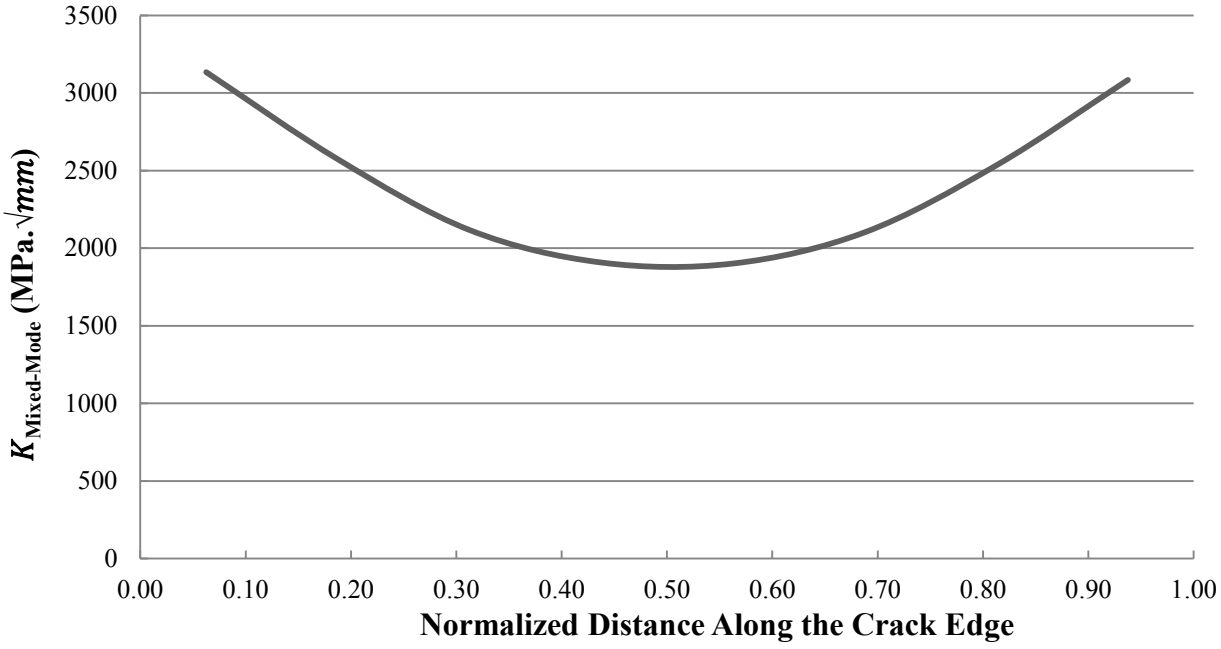

Figure 4- 15: Stress Intensity Factor for Mixed-Modes for 0.1 mm Semi-Circle Crack at Transverse Stiffener Weld Toe (Location 1) in Web Gap Detail.

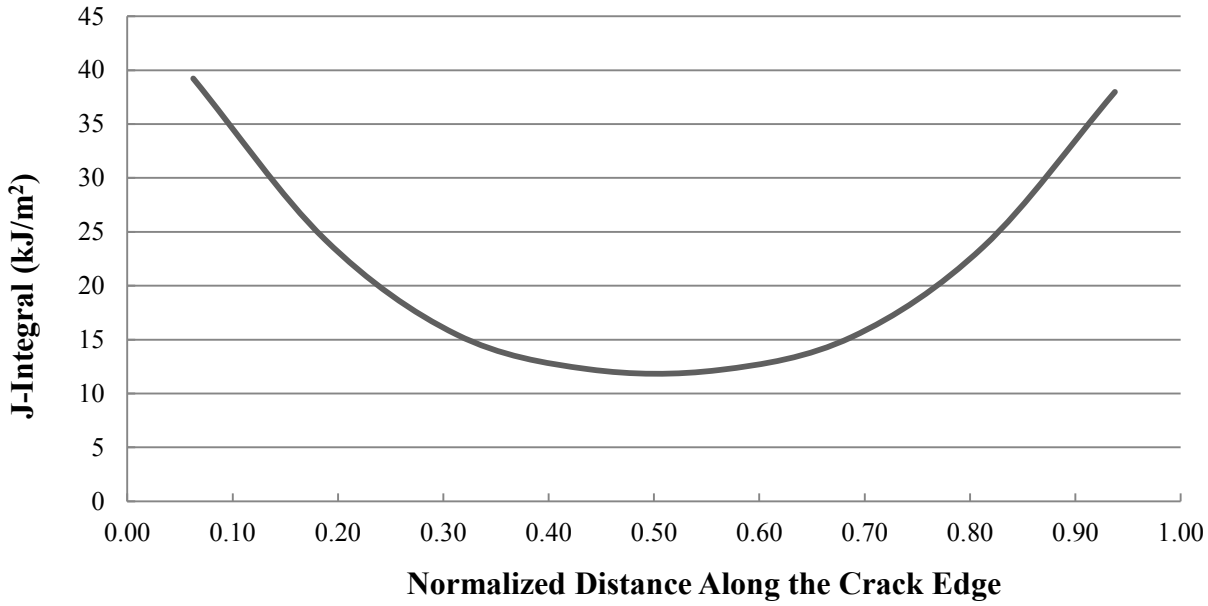

Figure 4- 16: J-Integral Value graphed for 0.1 mm Semi-Circle Crack at Transverse Stiffener Weld Toe (Location 1) in Web Gap Detail.

4.3.3.2. SIF for Initial Crack at Weld Body (Location 2)

The same procedure is performed for crack at the transverse stiffener weld body (Location 2) to obtain stress intensity factors for Mode I, Mode II, Mode III, and J-Integral. The results for the crack at this location are presented in Figure 4-17 to Figure 4-21. The effect of mixed-mode fracture is also calculated using Equation (4-20) for the mixed mode fracture and presented in Figure 4-20.

The effect of each mode of fracture on stress intensity factor can be obtained from these graphs. As it is shown in Figure 4-12 and Figure 4-17, Mode I has the highest stress intensity factor magnitude among the other modes. This shows that the crack opening mode (Mode I) is the governing fracture mode in the web gap detail at the beginning stages of crack propagation. Although the crack shows the same behavior at both crack locations, the magnitude of stress intensity factor is highly affected by location of the crack. At the weld toe (Location 1) the stress intensity factor for Mode I is almost 3 times higher than the crack at the weld body (Location 2). This is the main reason why most of the cracks at web gap locations and under distortion induced fatigue occur at the weld toe.

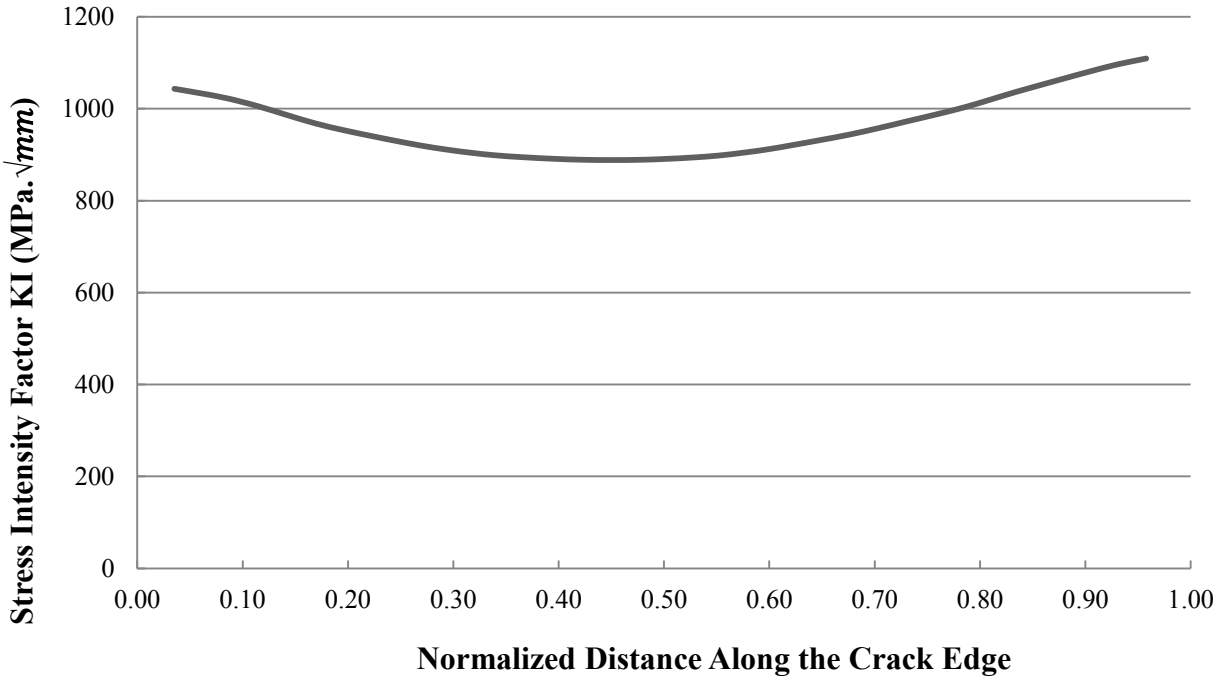

Figure 4- 17: Stress Intensity Factor for Mode I for 0.1 mm Semi-Circle Crack at Transverse Stiffener Weld Body (Location 2) in Web Gap Detail.

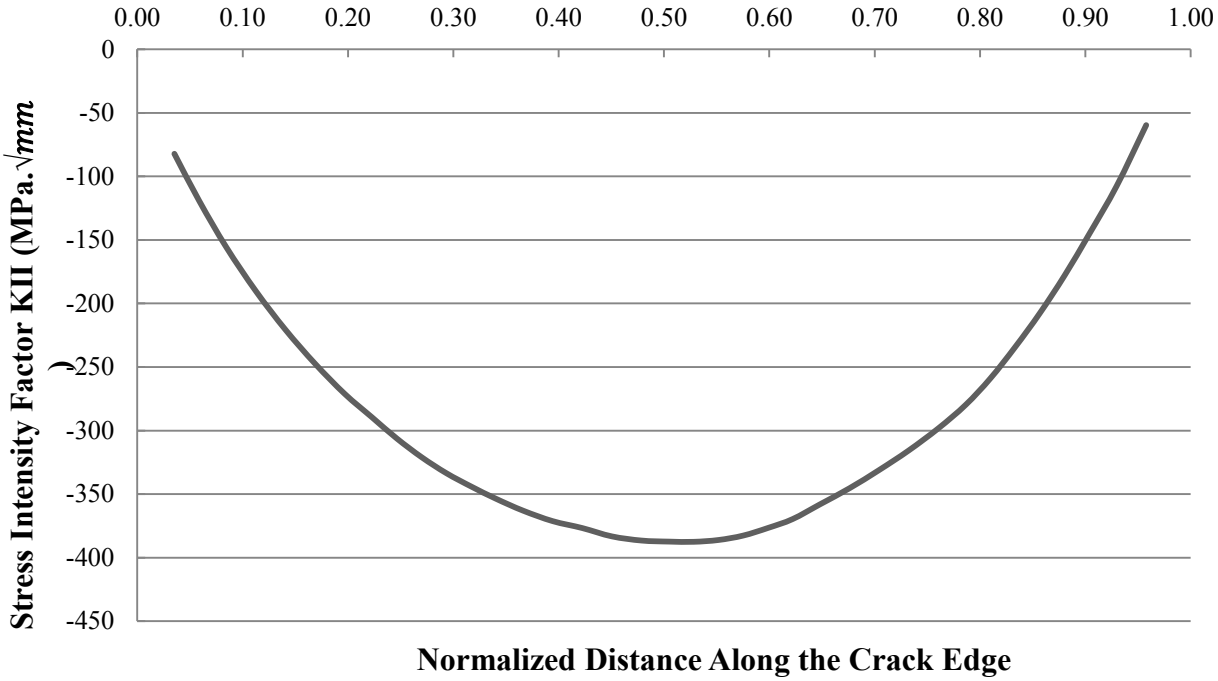

Figure 4- 18: Stress Intensity Factor for Mode II for 0.1 mm Semi-Circle Crack at Transverse Stiffener Weld Body (Location 2) in Web Gap Detail.

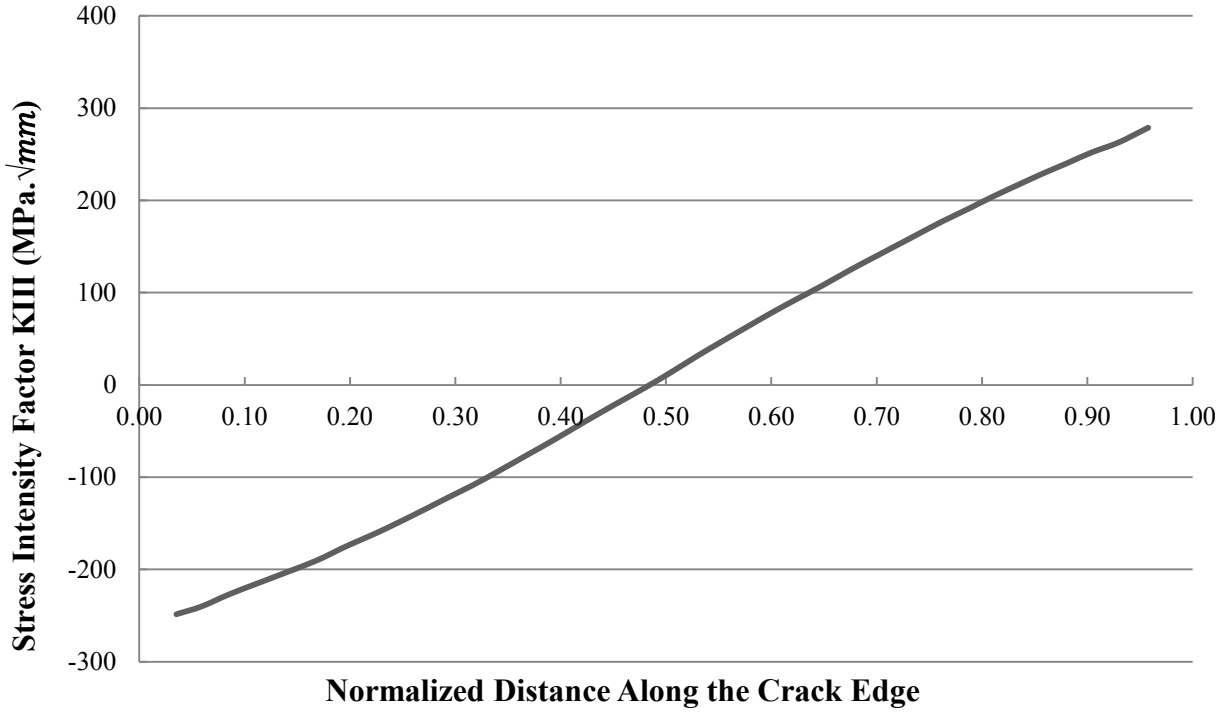

Figure 4- 19 : Stress Intensity Factor for Mode III for 0.1 mm Semi-Circle Crack at Transverse Stiffener Weld Body (Location 2) in Web Gap Detail.

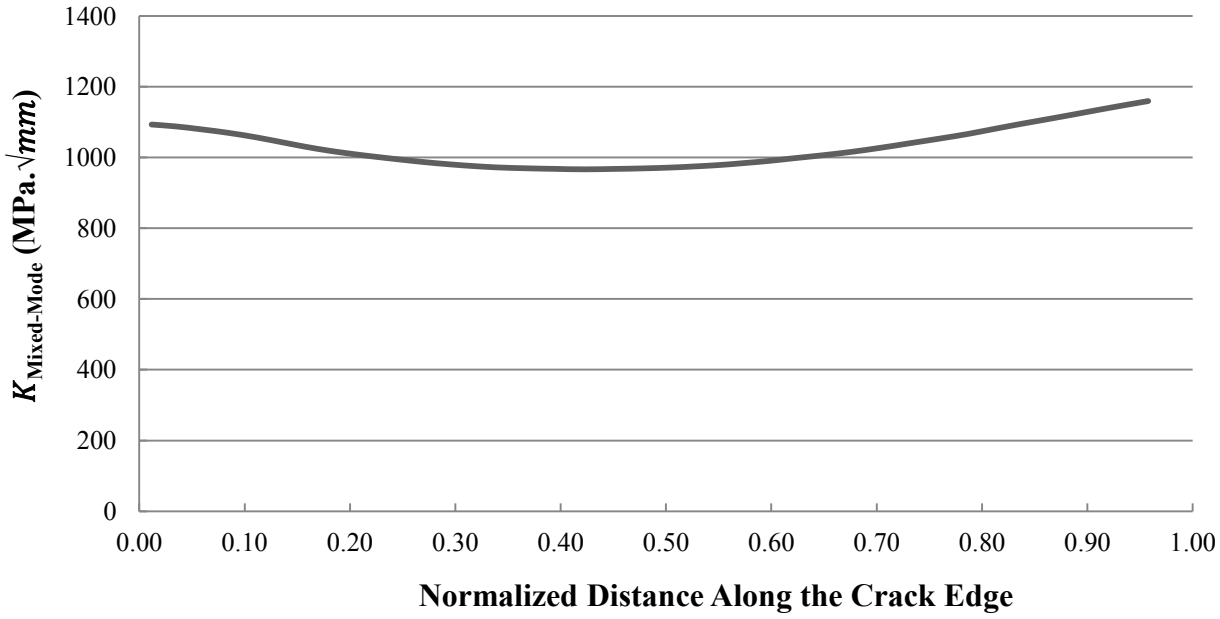

Figure 4-20: Stress Intensity Factor for Mixed-Modes for 0.1 mm Semi-Circle Crack at Transverse Stiffener Weld Body (Location 2) in Web Gap Detail.

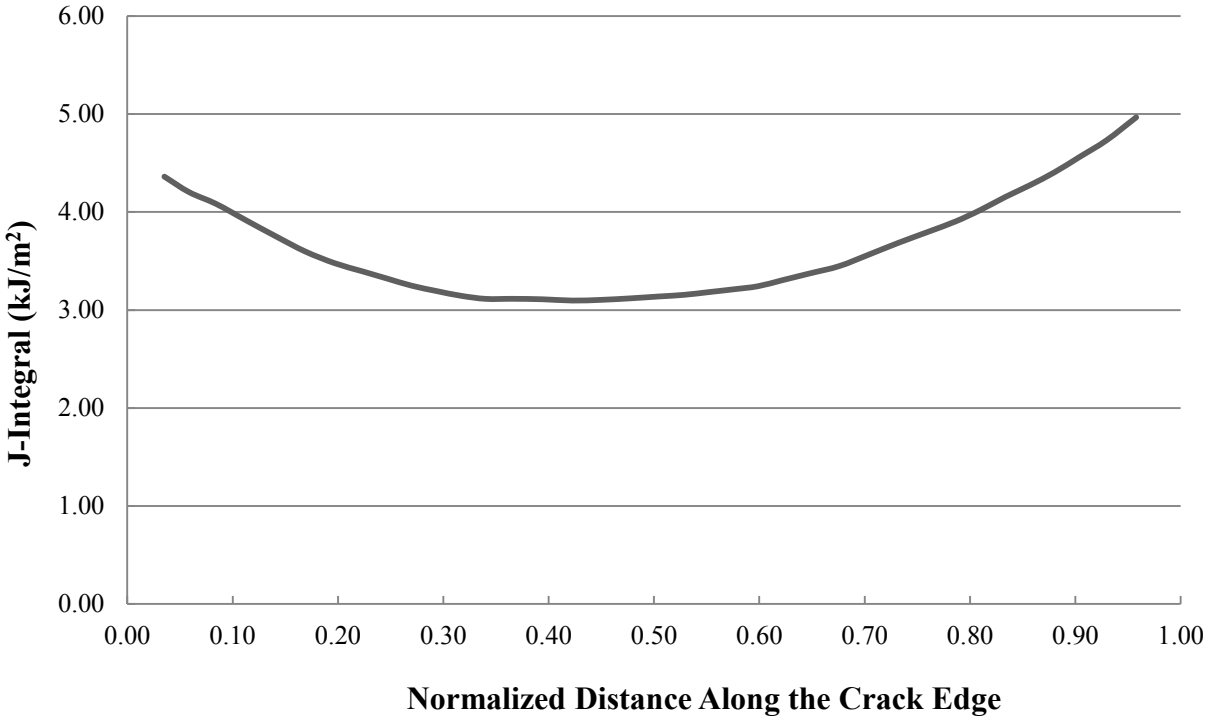

Figure 4- 21: Stress Intensity Factor for Mode I for 0.1 mm Semi-Circle Crack at Transverse Stiffener Weld Body (Location 2) in Web Gap Detail.

As it is shown in Figure 4-15 and Figure 4-20 for 0.1 mm semi-circle crack at both locations (weld toe and weld body) the mixed-mode fracture toughness is mostly governed by Mode I fracture.

4.3.4. Crack Propagation Life

Based on the experimental results obtained from work at University of Kansas (Hartman et al, 2013), the crack initiated at weld body at the transverse stiffener (Location 2). Therefore, the initial crack is decided to be located at Location 2 (weld body) to resemble the experimental test.

To investigate the crack propagation life of the detail, the semi-circle crack with initial radius of 0.1 mm is inserted in the weld body of the web gap detail. The crack propagates with 0.01 mm crack propagation increments for the first 100 crack propagation steps until it reaches 1.1 mm crack length. The crack propagation increment increased to 0.02 mm, 0.05 and 0.1 for next 300 steps (100 steps for each crack propagation increment size). A crack propagation increment size of 0.5 mm is selected for the step size until the end of the analysis in which the crack eventually stops propagating. The analysis performed according to Figure 4-10.

In total 412 crack propagation steps are conducted and the stress intensity factor for each crack increment is recorded. The stress intensity factors for Mode I, Mode II, and Mode III at crack tip along the crack edge for step 412 are graphed and shown in Figure 4-22 to Figure 4-24.

As it is shown in Figure 4-25, Mode I has the most significant effect on the mixed mode failure. Although Mode II and Mode III increase the magnitude of the fracture toughness, the trend of the graph is mostly governed by Mode I.

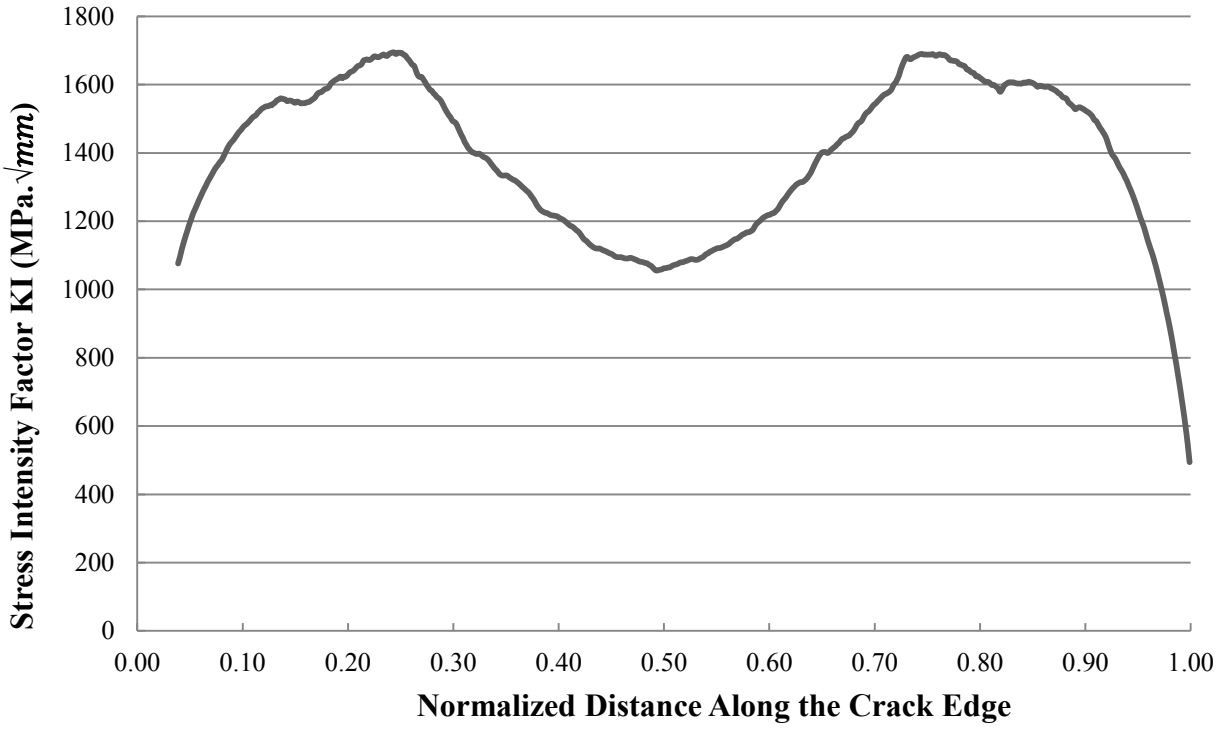

Figure 4- 22: Stress Intensity Factor for Mode I at Step 412 at Crack Tip Along the crack edge in Web Gap Detail.

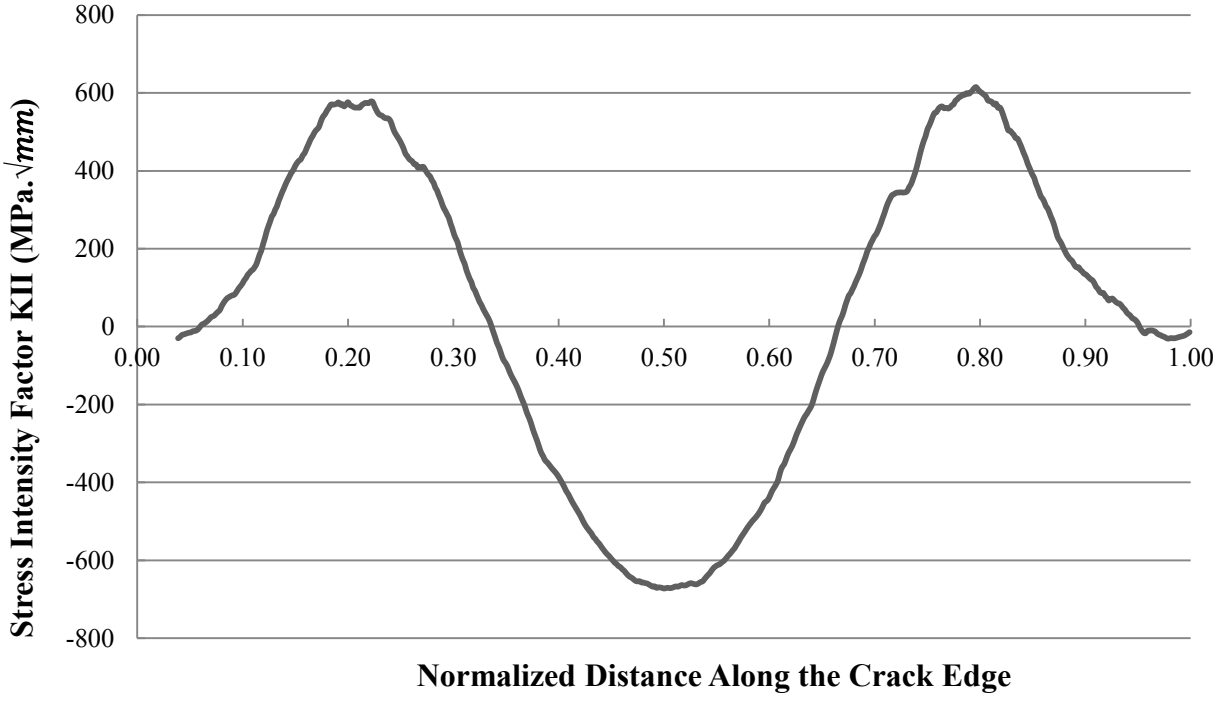

Figure 4- 23: Stress Intensity Factor for Mode II at Step 412 at Crack Tip Along the crack edge in Web Gap Detail.

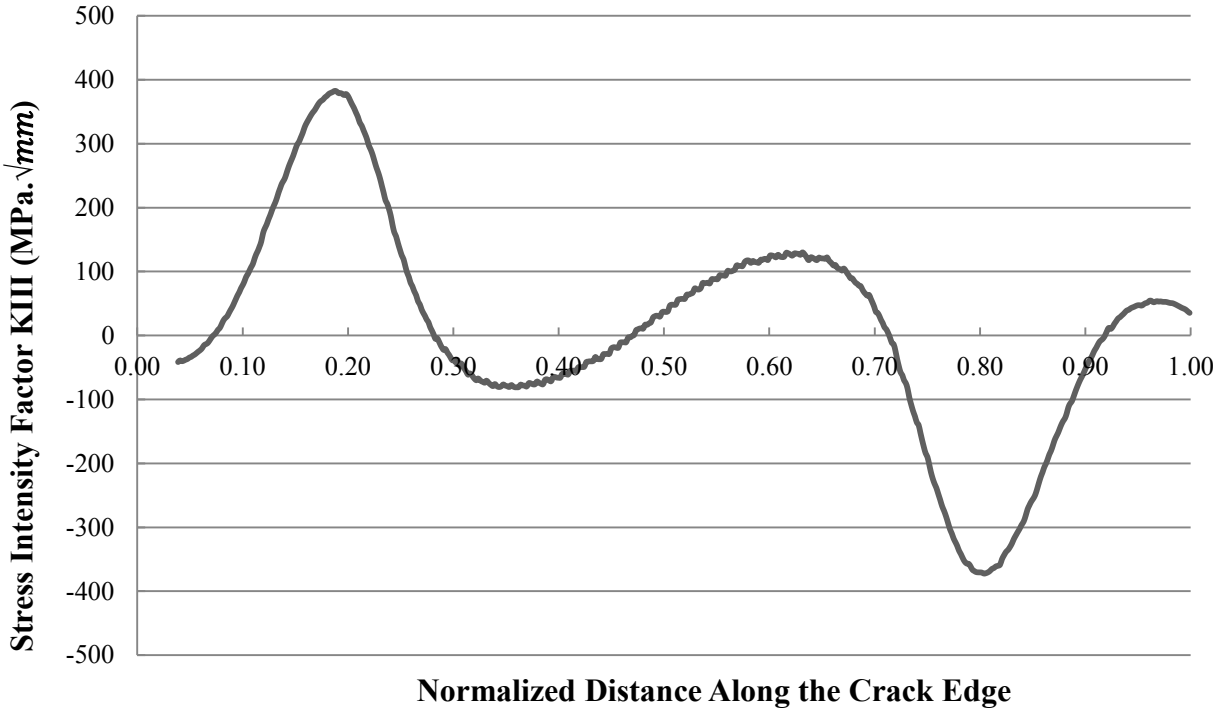

Figure 4- 24: Stress Intensity Factor for Mode III at Step 412 at Crack Tip Along the crack edge in Web Gap Detail.

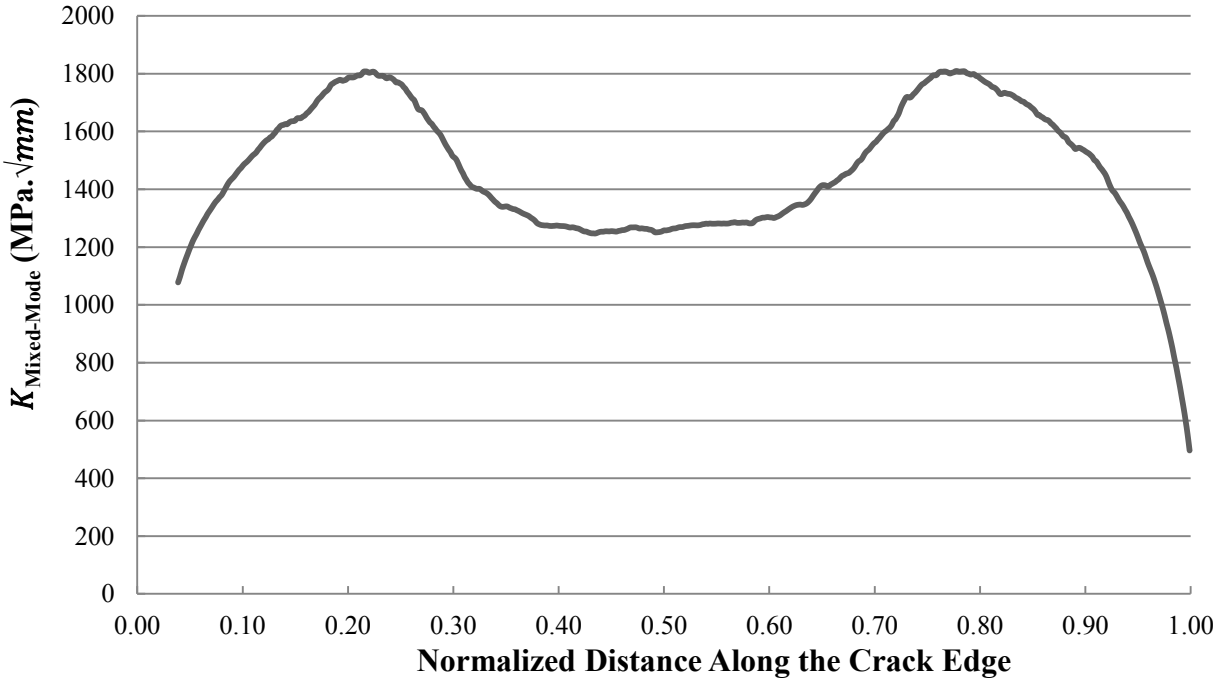

Figure 4- 25: Fracture Toughness for Mixed-Modes at Step 412 at Crack Tip Along the crack edge in Web Gap Detail.

The crack shape and profile at the end of the propagation stage are presented in Figure 4-26 to Figure 4-29. As it is shown in Figure 4-32, the crack propagation length and directions matched very well the experimental observation. The experimental measurements are also shown in Figure 4-32.

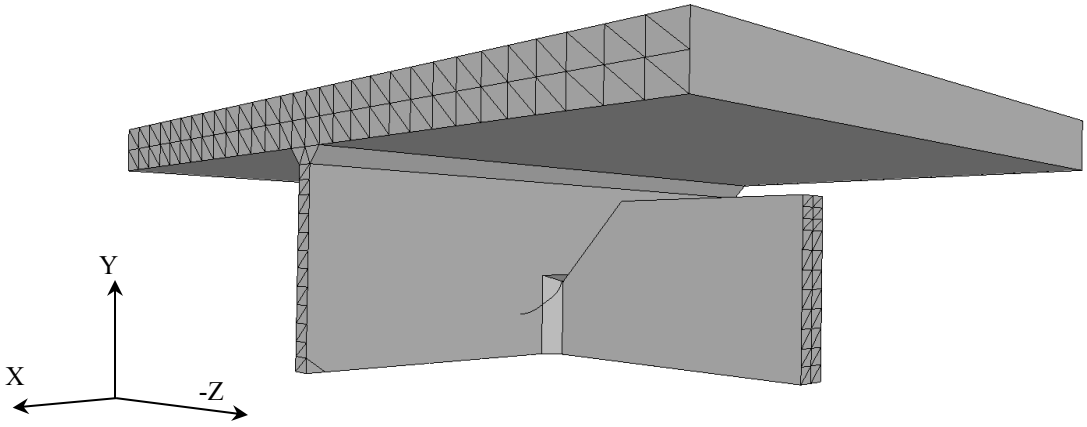

Figure 4- 26: Final crack length and shape at the web gap detail obtained from FEA.

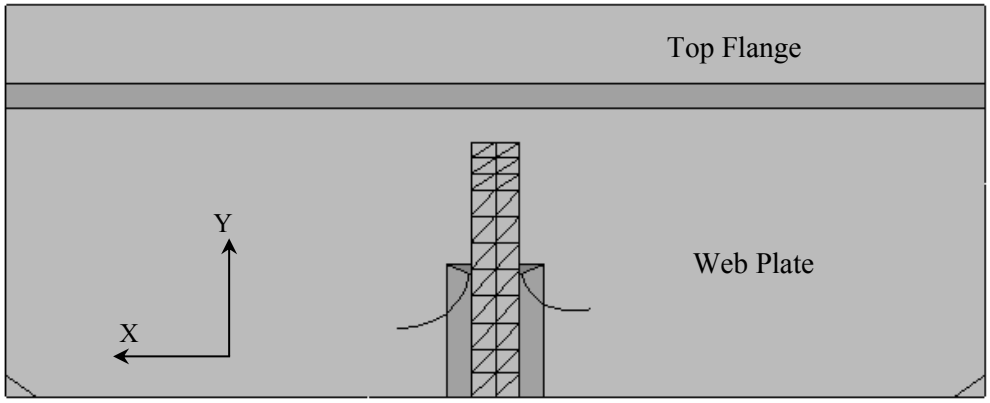

Figure 4- 27: Final crack length and shape at the web gap detail obtained from FEA.

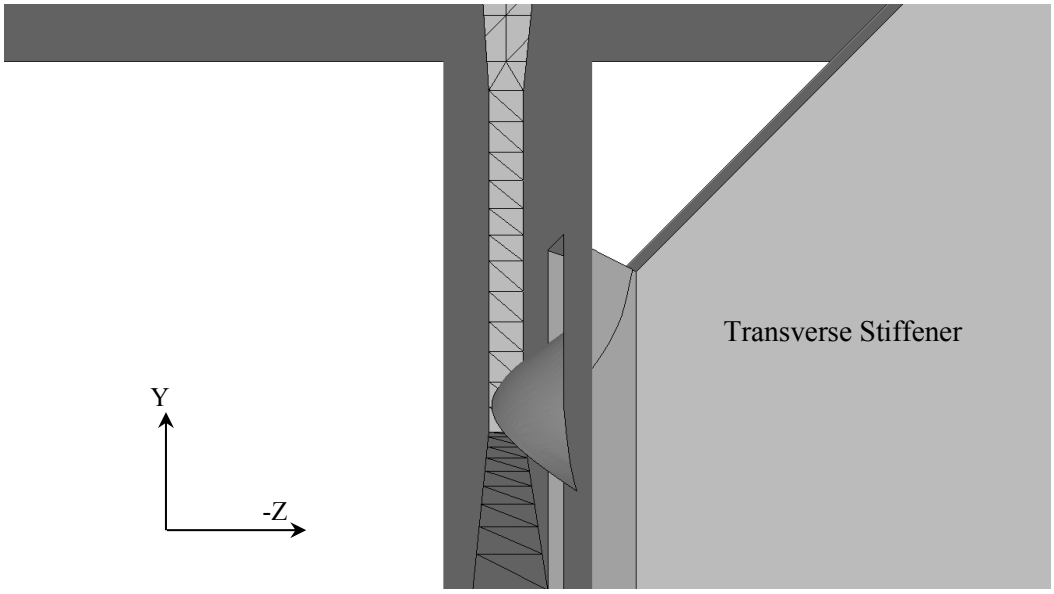

Figure 4- 28: Through thickness crack in the web plate obtained from FEA. Web plate solid elements are removed for the crack presentation purpose.

The crack stops before turning into a complete through thickness crack and as it is shown in Figure 4-28, only 70% of the web plate is cracked.

Figure 4-31 shows the stress intensity factors versus crack length. It is graphed for three different directions of crack propagation, Right, Left, and through thickness directions of crack propagation. These directions are shown in Figure 4-30.

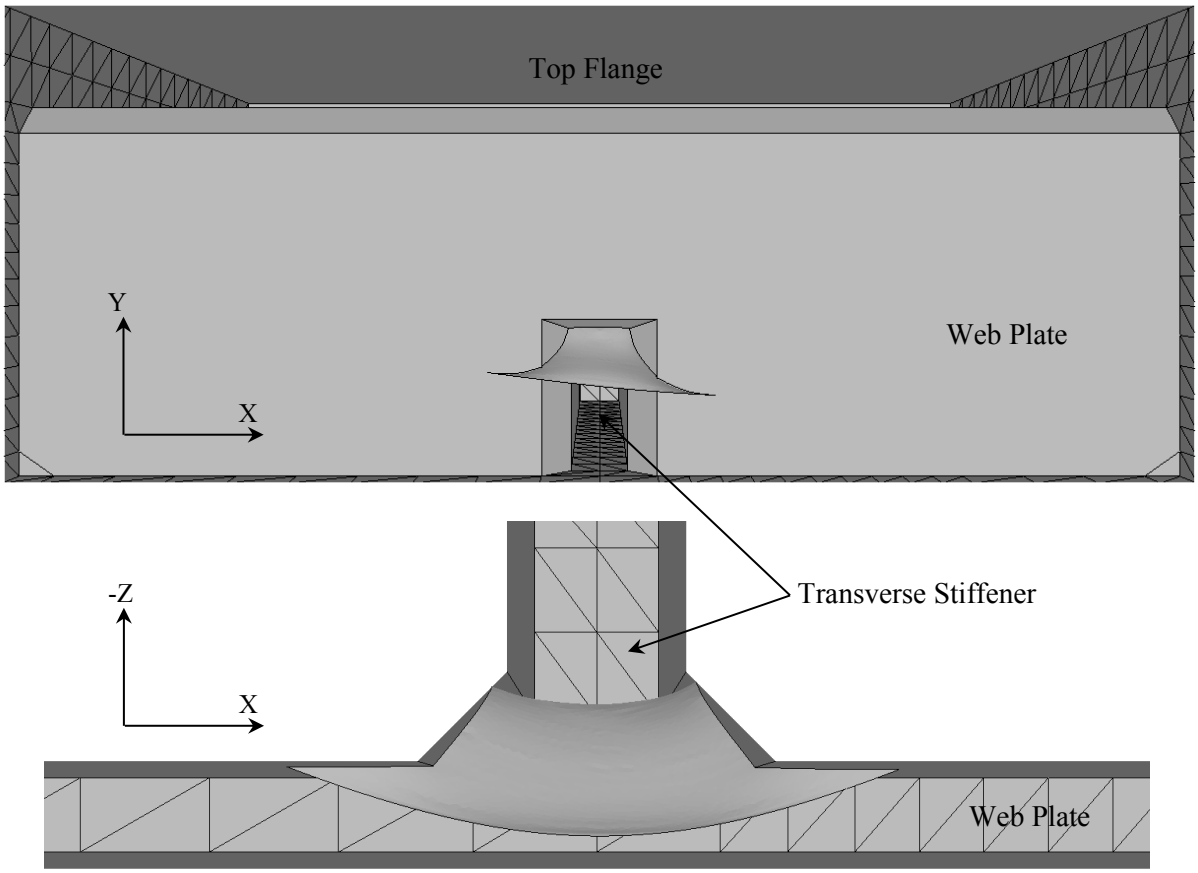

Figure 4- 29: Two different views of the crack profile through the web plate. Solid elements are removed for the crack presentation purpose.

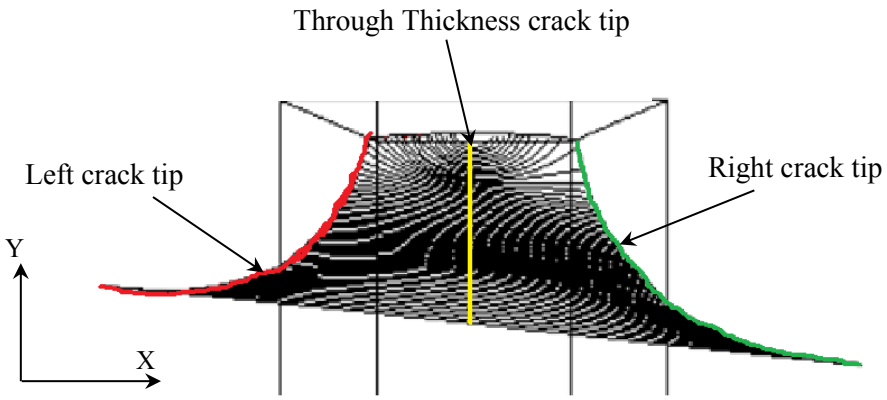

Figure 4- 30: Left, right, and through thickness Crack tip directions.

When the stress intensity factor for a crack is obtained for each crack propagation increment, the crack propagation life can be calculated and the number of cycle to reach the final crack length can be counted using Equation (4-24). In this equation and for this study, $\Delta K=K$ as it is assumed that at the end of each cycle, the load is removed completely and there is no stress reversal effect. K is graphed in Figure 4- 31 versus the crack length. The crack propagation life calculation (N_p counting) can be done either in Excel or in FRANC3D by using the material crack propagation properties as mentioned which are presented in Table 4- 2. In total, after 54,021 cycles the crack reaches to the final length of 13 mm, 21 mm, and 22 mm in thickness, right, and left directions, respectively.

The cycles needed to propagate the crack for an increment is counted and is graphed in Figure 4-33. As it is shown in this figure, at the beginning of the crack propagation stages, for the first 25,000 cycles, the crack only propagates 1mm to 3 mm at each direction. Almost 80% of the crack propagation occurs from 25,000 to 40,000 cycles. The crack growth rate slows down for the rest of the increments and eventually it stopes propagation at 54,021 cycles.

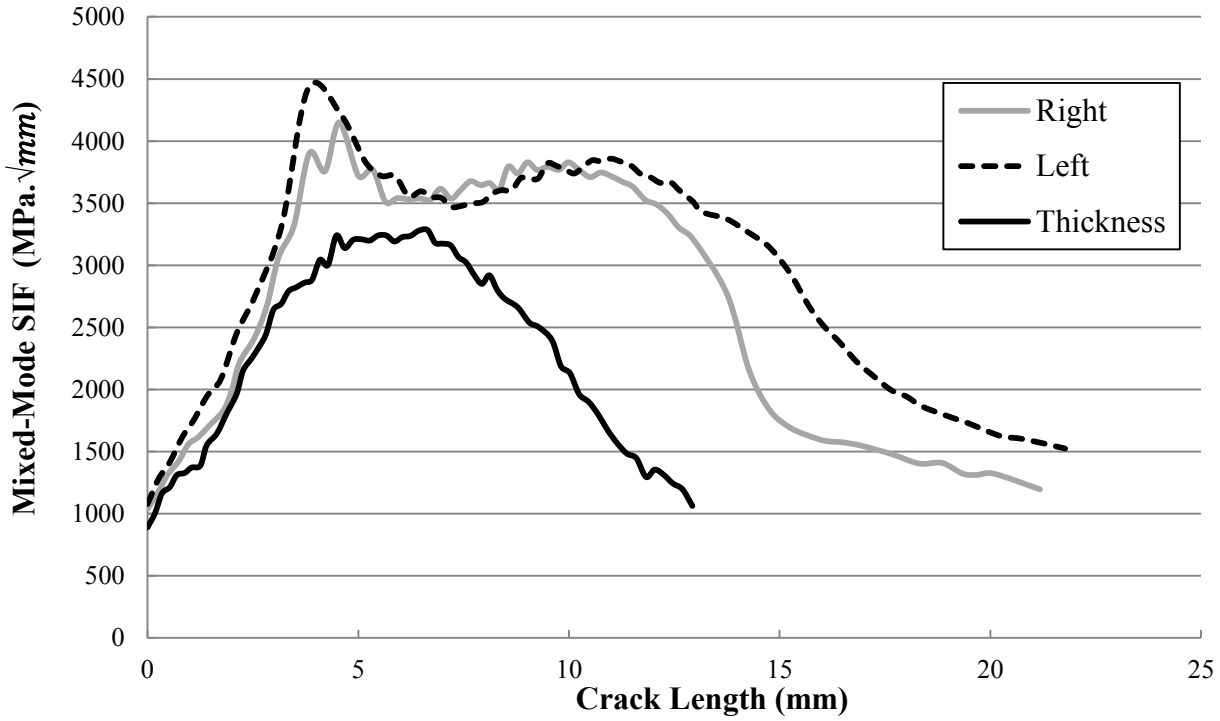

Figure 4- 31: Stress Intensity Factor along the crack at different directions of the crack propagation.

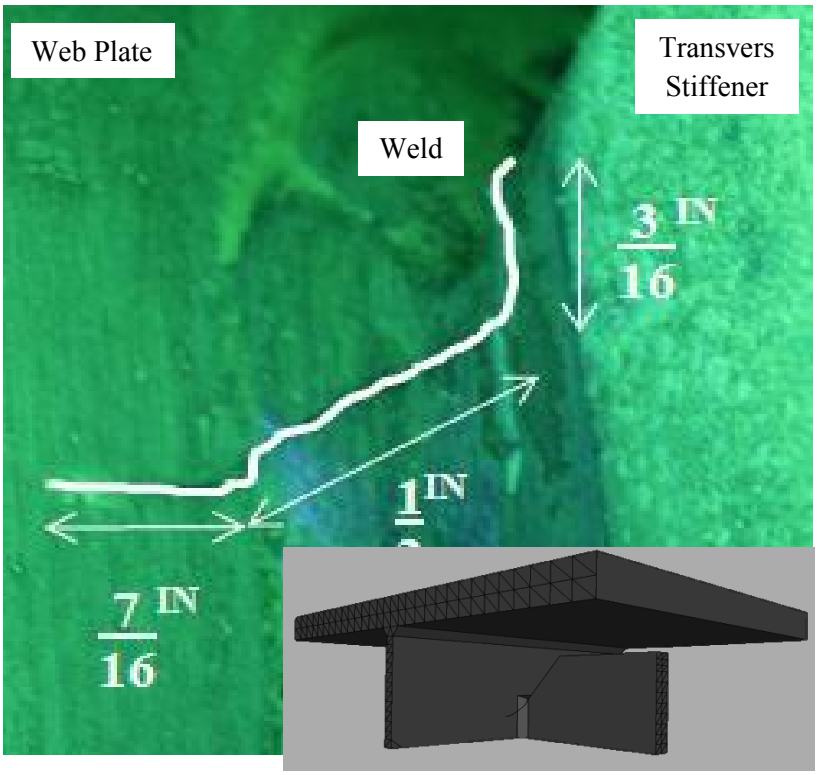

Figure 4- 32: Experimental test and crack observation (Hartman et al, 2013) and comparisan with the FE model.

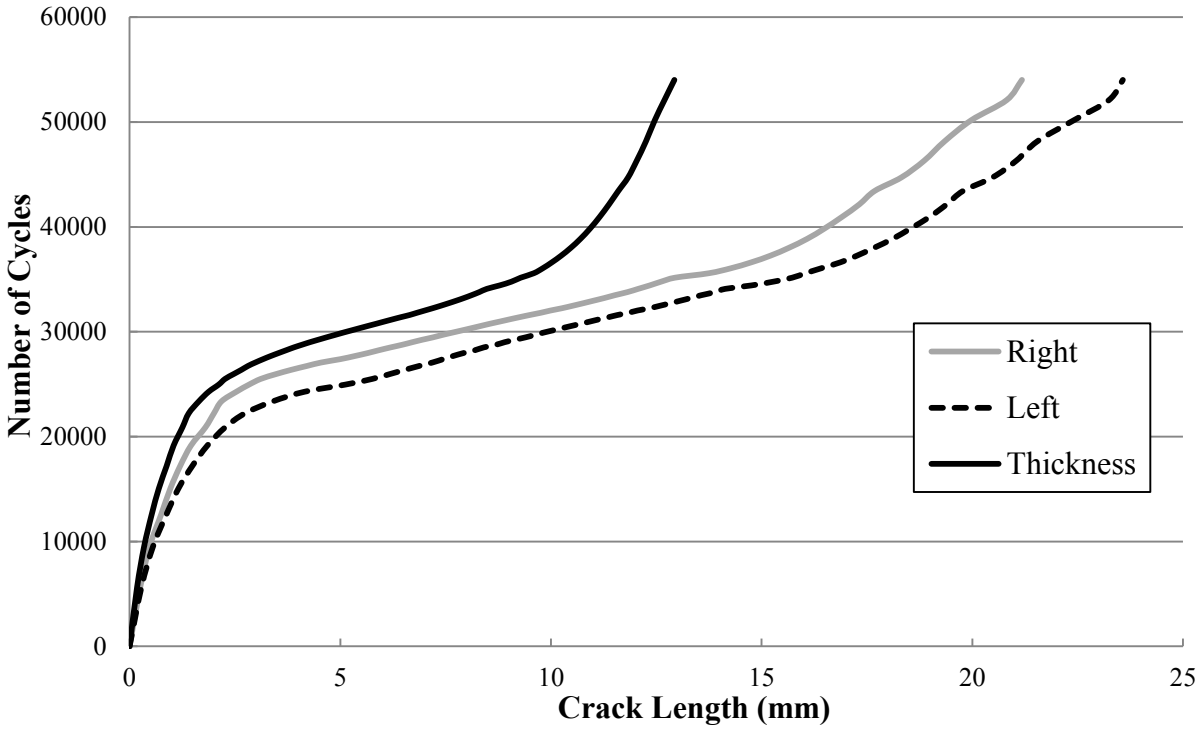

Figure 4- 33: Number of propagation cycles versus crack length for right, left, and through thickness crack tip Obtained from FEA.

The total fatigue life of the crack can be obtained by simply adding the initiation life and propagation life of the detail. This leads to a total life of 62,361 (54,021+8,340) cycles.

The experimental results show that the crack stabilized after about 65,000 cycles (including crack initiation life) at about 29 mm long. It should be noted that there is no imperfection modeled in the FE model of the web gap and this can be a reason that there is slightly difference between the experimental results and finite element analysis results.

As it is presented in this chapter, fracture mechanics is a powerful tool to investigate the behavior of the cracks in web gap detail and can calculate its life even with the very complex stress gradient in the vicinity of the crack.

Although fracture mechanic approach provided an accurate result for crack propagation life, it was very costly in terms of time. Creating, meshing, and analyzing 412 models took two weeks of non-stop computational process. It should be noted that all of these modeling, and analyzing processes were conducted automatically. Otherwise, it is almost impractical to perform this investigation manually and step by step. If the crack size or the location changes, this process should be performed again even for exactly the same web gap detail. Therefore, it is decided to develop an empirical equation in order to predict a representative stress magnitude in the web gap detail in steel multi-girder bridges and find the relation between this stress and the fatigue life of the detail. This approach is explained and presented in Chapter 5.

Chapter 5

Parametric Studies Using Dimensional Analysis

In steel multi girder bridges, web gap stress calculation is fairly complicated as its magnitude is affected by almost all geometrical parameters in the bridge girder, diaphragm plate, and cross brace. Therefore, evaluating stress in the detail is not straightforward. Several attempts have been made to derive a general equation that calculates the stress in the web gap but still only a detailed Finite Element (FE) analysis of the bridge that includes exact boundary conditions of the detail can predict this stress. For such a complex problem it is preferable to drive an empirical equation to include all the parameters affecting the stress in the detail. Thus, data should be collected and analyzed and the equation should be developed such that it closely approximates the observed behavior of the detail.

The objective of this chapter is to derive dimensionless parameters that can be used to develop an empirical equation that calculates the stress in the web gap details in the girders of multi-girder bridges. This equation is developed using the Response Surface Methodology (RSM) and data generated by FE models described in this chapter.

5.1. Response Surface Methodology

The Response Surface Methodology (RSM) uses mathematical and statistical models in order to construct a structured approach to obtain the response functions. It, statistically, looks into the relationships between several explanatory variables and at least one response variable. The objective of utilizing this method is to optimize the response i.e. (output variable) which is influenced by several independent input variables or factors. The first step involved with this method is designing a set of experiments that yield adequate and reliable measurement of the response. After running the experiments, a mathematical model should be determined using

regression analysis which best fits the data collected from the experiments (Khuri & Cornell, 1996).

The mathematical relationship between the response and the factors is known as a response function. For instance, assuming that the true value of the response, η, depends upon k factors, X_1, X_2,…, X_k, such that (DiBattista, 2002):

$$\eta = \phi(X_1, X_2, \ldots, X_k) \tag{5-1}$$

where, ϕ is the true response function. The response function can be represented in different forms. The most common one is linear or first order form. Polynomial functions are also very common for higher accuracy. This is usually done by obtaining data from the design experiments and evaluating the constants for the response function using an error minimization method such as least squares method. Using a polynomial expression for the response equation is useful for continuous function as it does not require prior knowledge of the exact form of the response equation. However, these functions cannot be truly obtained because of the experimental errors. In addition, as they are calculated using one set of data only, a second source of error is introduced to the calculation (DiBattista, 2002).

If a polynomial expression is used, it may be necessary to include many terms in the prediction equation to make a reasonable representation of the response surface, especially in case of large number of factors (DiBattista, 2002) which makes the equation more complicated as it needs higher number of coefficients. The number of coefficients in a complete second-order prediction equation can be obtained using the following relation (Khuri & Cornell, 1996):

$$p = \frac{(k+1)(k+2)}{2} \tag{5-2}$$

where, p, is the number of regression coefficients, and k, is the number of factors.

For complex problems which have several factors involved, polynomial regression needs a huge number of coefficients in order to predict the response. For instance, if there are 5 factors,

based on the equation, 21 coefficients are required. This yields a very long equation which is difficult to derive and use.

An alternative solution to this issue will be a more compact form of the prediction equation that uses nonlinear regression form with less number of coefficients. Nonlinear equations can take many different forms which provide the most flexibility to fit the curve to the data. Although nonlinear regression reduces the number of coefficients and makes the prediction equation more compact, its solution is more difficult to obtain compared to the linear regression one. However, using a computer can overcome this difficulty.

Equation that evaluates stress in the web gap is complicated and involves many geometrical dimensions thus it cannot be determined using a simple linear regression. Therefore, a nonlinear regression is used in this research in order to determine the equation that can predict maximum stress in the web gap. For the multi girder bridges web gap problems maximum stress in the web gap is considered as response while all other geometrical dimensions are considered as factors. In this chapter, the factors are selected properly and the response is predicted using a suitable regression method in the following chapter.

5.2. Design of Experiments

Physical and analytical experiments are used for better understanding of the web gap stress prediction problem. Experimental design is a process that combines expert knowledge of subject area with appropriate statistical techniques to allow an optimal amount of useful data to be obtained in the most efficient possible manner (Box, Hunter, & Hunter, 1978). This will be discussed in more details in Chapter 6.

5.3. Selection of the Parameters Affecting the Response Equation

As it is described in chapter two, the web gap stress is a function of several parameters (e.g. lateral stiffness of the flange, stiffness of the stiffener, magnitude of the differential displacement (Δ), and several other factors that have been identified to affect the stresses developed in the web gap). Therefore, to develop a prediction equation for stress in the web gap, it is necessary to study a set of parameters that reflects a variety of realistic loading conditions and geometric configurations for the detail. In total there are 17 parameters which are likely governing the behavior of the prediction equation. These parameters are:

w: Web Thickness

L: Diaphragm Spacing

h: Stiffener Height

b_s: Stiffener Width

t_s: Stiffener Thickness

b_F: Tension Flange Width

t_F: Tension Flange Thickness

g: Web Gap Length

E: Young's Modulus

G: Shear Modulus

S: Diaphragm Length (Girder Spacing)

t_D: Diaphragm Thickness

h_D: Diaphragm Height

A_X: Cross Section Area for Diagonal Member in Cross Frame Diaphragms

α: Angle Between Cross Frame Diagonal Member and Vertical Member

σ_{wg}: Web Gap Stress

Δ: Differential Deflection

The effect of concrete deck stiffness (concrete slab thickness) is seen in differential deflection parameter. If the slab is rigid, there would not be any differential deflection between

the adjacent girders. Moreover, as HSS approach is used to calculate the stress in the detail, the effect of weld geometry and size is not included in this parametric study.

Although the relation between some of these parameters such as Young's Modulus (E) and the web gap stress is proven to be linear, the interaction of other parameters are not very well established. It is known that for example increasing the web gap length decreases the web gap stress and increasing the web thickness increases the web gap stress but what if both the web gap length and web thickness vary at the same time i.e. web gap length increases and web thickness decreases. Therefore, an experiment should be performed in order to study the effects of these changes as well. The simplest type of experimental design is 'first-order' experiment design, which is generally used in conjunction with first-order regression. In this case, only two levels of each factor are required, because the resulting prediction equation is planar. Of course, such a design is useful only for problems whose response surface is approximately planar within the region of interest (DiBattista, 2002). For this class of experiments the most common form is a 2^k factorial design which requires 2^k design points, where k is the number of factors. This type of experimental design (first-order) may not be able to identify the approximate shape of the response function within the range of interest as each factor is sampled at only two levels. Therefore it is not possible to observe any curvature that may occur in the response surface.

To overcome this issue and to establish a response function which represents any possible curvature, at least three levels of the factors must be sampled and response equation should be at least a second-order polynomial. The approach with three levels is called 3^k factorial experimental design. As it is mentioned previously, 3^k design points are required, where k is the number of factors. In web gap stress problem, if a 3^k factorial design approach is used, in which k is equal to 17, experiments will be impossible to perform due to the size of the problem. Therefore, alternate factors that reduce the number of the actual factors must be selected to represent the practical and physical characteristic of the detail without eliminating effects of the actual factors from the response equation. This study uses non-dimension factors as alternative factors.

Stiffness of a member is an important parameter which needs to be determined in the design stage. Instead of different geometrical dimensions for each member connected in web gap

in multi-girder bridges, the corresponding stiffness of the member is utilized to develop the non-dimensional factors so-called π-parameters. For the web gap detail, the stiffness of each component is listed below in Equations (5-3) to Equation (5-8).

$$K^2{}_{WEB} = \left(\frac{\pi^4}{4}\right)\frac{w^3 E(L^2+h^2)^2}{L^3 h^3 Sin^2\left(\frac{g}{h}\pi\right)} \tag{5-3}$$

$$K_{DIA} = \frac{h_D t_D G}{S} + \frac{E t_D {h_D}^3}{4S^3} \quad Or \quad \frac{2A_X E}{S} Cos^2(\propto) \tag{5-4}$$

$$K_{STF} = \frac{b_s t_s G}{h_s} + \frac{E t_s {b_s}^3}{4{h_s}^3} \tag{5-5}$$

$$K_{LBF} = (4)\frac{E t_F {b_F}^3}{L^3} \tag{5-6}$$

$$K_{TBF} = \left(\frac{1}{3}\right)\frac{b_F {t_F}^3 G}{L} \tag{5-7}$$

where,

K_{WEB}: Web plate Stiffness

K_{TBF}: Bottom Flange Torsional Stiffness

K_{LBF}: Bottom Flange Lateral Stiffness

K_{DIA}: Diaphragm Stiffness

K_{STF}: Stiffener Stiffness

σ_{wg}: Web Gap Stress

g: Web Gap Length

Δ: Differential Deflection

$$2(1+\vartheta) = \frac{E}{G} \tag{5-8}$$

[2] This equation is obtained using shell and plate theory and driven in Appendix A.

In these parameters, variation of shear modulus, G, and Young's modulus, E, will not be considered in the behaviour as the material of the bridge girders is regular structural steel and these parameters are almost constant for most of the constructed bridges. Therefore, they need not be included in the parametric study. Variation of Poisson's ratio, ν, which is a dimensionless measure, has also a constant value for all types of steel and will also be excluded in the parametric study. Using the mentioned parameter (defined in Equations (5-3) to (5-8), web gap length, differential deflection, and web gap stress), the number of factors reduced from 17 to 8. Therefore, only K_{WEB}, K_{TBF}, K_{LBF}, K_{DIA}, K_{STF}, σ_{wg}, g, and Δ will be investigated in the parametric study. Still considering 8 factors for parametric study would require the analysis of almost twenty thousand FE models. To reduce this to a manageable number, it is beneficial to implement dimensional analysis, which is a process that eliminates extraneous information from a relation between quantities. This approach is well described with several applicable examples by Taylor (Taylor, 1974) and summarized in this chapter.

5.4. Dimensional Analysis - Obtaining the π-parameters

Dimensional analysis offers a method for reducing complex physical problems to the simplest (that is, most economical) form prior to obtaining a quantitative answer. "The principal use of dimensional analysis is to deduce from a study of the dimensions of the variables in any physical system certain limitations on the form of any possible relationship between those variables. The method is of great generality and mathematical simplicity" (Bridgman, 1931).

Consider that the behavior of a given physical problem is governed by a set of n quantities $A_1, A_2, \dots A_n$, that includes the entire variables essential (factors) to the solution of the physical problem. The response y to mechanical load can be expressed as a homogeneous function which is a function with multiplicative scaling behaviour:

$$y = F(A_1, A_2, \dots A_n) \tag{5-9}$$

In order to establish this function, it is necessary to vary all the quantities to find their influences on the solution. The higher number of parameters, the more models required for analysis. To make this analysis more practical, the number of parameters can be reduced by means of the Buckingham π theorem. The theorem states that if there is a physically meaningful equation involving a certain number n of physical variables such as in the forgoing example, then the original equation can be rewritten in terms of a set of $p = n - k$ dimensionless parameters $\pi_1, \pi_2, \ldots, \pi_p$ constructed from the original variables where, k is the number of physical dimensions involved and it is obtained as the rank of a particular matrix. Based on this theorem, the response function can be recast in terms of dimensionless independent $\pi - \text{parameters}$ as:

$$y = G(\pi_1, \pi_2, \ldots, \pi_p) \tag{5-10}$$

The importance of this transformation is that the scale effects can be controlled in an experimental or numerical modeling program and the number of parameters that must be considered is reduced by r, in which r is the rank of the dimensional matrix. This can result in a significant saving of cost and effort.

In order to perform dimensional analysis, first, the dimensions for each individual variable should be found, and then, the $\pi - \text{parameters}$ can be defined more conveniently. Using fundamental units of mass (M), length (L), and time (T), the dimensional matrix for the variables is as shown in the following:

Table 5- 1: Dimensions for the Variables (Dimensional Matrix)

Variable	*M*	*L*	*T*	Dimension
K_{WEB}:	1	0	-2	$[MT^{-2}]$
K_{TBF}:	1	2	-2	$[ML^2T^{-2}]$
K_{LBF}:	1	0	-2	$[MT^{-2}]$
K_{DIA}:	1	0	-2	$[MT^{-2}]$
K_{STF}:	1	0	-2	$[MT^{-2}]$
σ_{wg}:	1	-1	-2	$[ML^{-1}T^{-2}]$
g:	0	1	0	$[L]$
Δ:	0	1	0	$[L]$

The values in this table are based on the unit of each parameter. For instance, the unit for g is $[L^1]$ (Length). Therefore, [M] is zero, [L] is one, and [T] is also zero.

The Buckingham π theorem provides a method for computing sets of dimensionless parameters from given variables, even if the form of the equation is still unknown. However, the choice of dimensionless parameters is not unique: Buckingham's theorem only provides a way of generating sets of dimensionless parameters, and will not choose the most 'physically meaningful' ones. These parameters should be selected in a way to consider the effect of the entire factors on the response function and no matter how these parameters are selected; they must be scale independent as well.

The rank of the dimensional matrix shown in Table 5- 1 is also very important to obtain as it directly reduces the number of parameters in the parametric study. The dimensional matrix for this problem has rank two. Therefore, six independent dimensionless (8-2=6) $\pi-$ parameters must be defined to represent all 8 variables.

For the web gap details in multi-girder steel bridges, the parameters chosen are presented in Equations (5-11) to (5-16).

5.4.1. π_1: Relative Parameter of Web Plate Stiffness and Transverse Stiffener Stiffness

This parameter is very important in calculation of stress in the web gap as the stress in this zone is affected directly by the stiffness of the web plate and the transverse stiffener. If there is a flexible web plate, it deflects and dissipates the energy. Therefore, the magnitude of the stress in the web gap reduces. This deflection obviously, is affected by the transverse stiffener stiffness as well. Relatively rigid stiffener plate transfers the displacement directly to the web plate without any reduction and significantly increases the web gap stress as it has almost a rigid rotation. The relative Stiffness of Web Plate to Transverse Stiffener should be considered as a dimensionless parameter and is defined in Equation (5-11).

$$\pi_1 = \frac{K_{WEB}}{K_{STF}} = \frac{4w^3(L^2+h^2)^2{h_s}^3}{L^3h^3(4b_st_s{h_s}^2G/E + t_s{b_s}^3)Sin^2(\frac{g}{h}\pi)} \quad (5\text{-}11)$$

5.4.2. π_2: Relative Parameter of Web Plate Stiffness and Bottom Flange Torsional stiffness

This parameter is also very important in the web gap stress prediction equation because the bottom flange provides a support for the web gap and works as a spring boundary condition and has rotation due to bottom flange torsional flexibility too. The bottom flange rotation helps the web gap distort and dissipate higher energy. Therefore, if there is a rotationally fixable bottom flange connected to web plate, it accommodates the distortion of the web plate and basically reduces the web gap stress. The dimensions of the Web Plate stiffness and Bottom Flange Torsional stiffness do not match and to make the π-parameters dimensionless, the π_2 parameter is modified accordingly by multiplying the relative stiffness by L^2. The relative modified Web Plate Stiffness and Bottom Flange Torsional stiffness is presented in Equation (5-12).

$$\pi_2 = \frac{K_{WEB}.L^2}{1000K_{TBF}} = \frac{w^3(L^2+h^2)^2}{1000h^3 b_F {t_F}^3 Sin^2(\frac{g}{h}\pi)} \quad (5\text{-}12)$$

5.4.3. π_3: Relative Parameter of Web Plate Stiffness and Bottom Flange Lateral Stiffness

This parameter is very similar to the π_2 parameter. The only difference is that the dimensions of Web Plate Stiffness and Bottom Flange Lateral stiffness are the same and by simply dividing Web Plate Stiffness by Bottom Flange Lateral stiffness the π_3 parameter is formed. π_3 is presented in Equation (5-13).

$$\pi_3 = \frac{K_{WEB}}{K_{LBF}} = \frac{w^3(L^2 + h^2)^2}{h^3 t_F {b_F}^3 Sin^2(\frac{g}{h}\pi)} \quad (5\text{-}13)$$

5.4.4. π_4: Relative Parameter of Transverse Stiffener Stiffness and Diaphragm Stiffness

This parameter is selected to study the effect of Diaphragm Stiffness as it has a significant role in transferring the deferential deflection between two adjacent girders and magnitude of distortion to the web gap detail. This deflection is transferred to the web gap through the transverse stiffener. This parameter is presented in Equation (5-14).

$$\pi_4 = \frac{K_{STF}}{K_{DIA}} = \frac{2h^2 + (1+\nu){b_s}^2}{2S^2 + (1+\nu){h_D}^2} * \frac{b_s t_s S^3}{h_D t_D {h_s}^3} \quad (5\text{-}14)$$

5.4.5. π_5: Relative Parameter of Differential Deformation and Web Gap Length

To obtain the magnitude of stress at web gap location, it is needed to measure magnitude of the differential deflection of the adjacent girder. If a bridge is investigated experimentally, its behavior is generally tested in a displacement control conditions where the differential displacement between the two adjacent girders is recorded. π_5 is a well-established dimensionless parameter which includes this measurement. The web gap length (g) is also a known parameter for the detail. This parameter is presented in Equation (5-15). Unlike other so

far mentioned parameters which are function of the bridge geometrical dimensions only, π_5 is the only parameter that includes the loading scenario.

$$\pi_5 = \frac{\Delta}{g} \tag{5-15}$$

5.4.6. π_6: Relative Parameter of Stress in Web Gap and Web Gap Stiffness

This parameter relates the stiffness of the web plate and the magnitude of the stress in the web gap and can be considered as the output of the regression analysis. This parameter which is selected to be dimensionless as well is presented in Equation (5-16).

$$\pi_6 = \frac{\sigma_{wg}.h}{100K_{WEB}} = \frac{\sigma_{wg}L^3h^4}{100E(L^2+h^2)^2w^3}Sin^2(\frac{g}{h}\pi) \tag{5-16}$$

The first five $\pi-$ parameters are the inputs in the new factors set for the experimental design and π_6 is obtained as output or the response function. Although these parameters are not unique and can be defined anyhow as long as they are dimensionless, they should have meaningful physical definitions.

To assess whether all the 17 parameters which have significant effect on response function are taken into account the scale independency test must be performed on $\pi-$ parameters. This is because the set of $\pi-$ parameters is not unique and can be chosen anyhow as long as there is a meaningful and physical definition for each individual $\pi-$ parameter. If

varying the scales of the factors does not affect the response, the selected $\pi-$ parameters are adequately chosen. To conduct this test, identical $\pi-$ parameters are selected and the geometrical dimensions are scaled for each model. This should be done in order to get the same identical $\pi-$ parameters. The response for these two cases (the obtained π_6 for each model), must remain the same. This can be performed for several scales in which the geometrical dimensions are varying within reasonable and practical ranges. After it is assured that $\pi-$ parameters are scale independent, the experimental program can be designed for the problem.

5.5. Scale Independency Test

In order to perform the test, the experimental test data performed at University of Alberta (D'Andrea, Grondin, & Kulak, 2001; Fraser, Grondin, & Kulak, 2000), is used the initial input data (Table 5- 2) for the FE models and to calculate the identical $\pi-$ parameters. This model is named "Base Scale".

Table 5- 2: Geometrical Dimensions Used in the Experimental Program at University of Alberta

Parameters	g	w	h	b_F	t_F	L	S	h_S	t_S	b_s	t_d	h_d
mm	50	9.5	914	254	16	1700	1000	864	10	100	9.5	686

The FE model used to predict the web gap stress and to calculate π_6, includes two girders, stiffeners, as well as bending plate diaphragm as shown in Figure 5- 1.

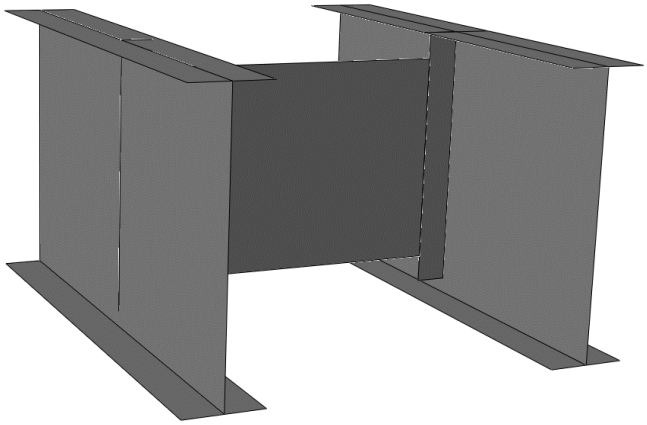

Figure 5- 1: FE Model (Base Scale) Used to Calculate the π-parameters.

The members are modeled as homogeneous shells and governed by cyclic material properties defined in Chapter 3. The girders are simply supported at both ends of bottom flanges. To simulate the effect of bridge concrete deck, a rotation equivalent to the magnitude of differential deflection divided by girder spacing is applied to both top flanges. Mesh sensitivity analysis is performed to obtain an optimal density that ensures consistency of results and efficiency of computation time. Results of the sensitivity analysis are summarized in the Table 5-3. The size of the mesh used in the web gap, the region of interest, is called "local mesh size" while "global mesh size" refers to the one used for the rest of the model. Various densities for local and global meshes are studied (Model 1 through Model 7). Additionally, in Model 8 and Model 9, mesh is gradually increased for both web gap and other parts of the model to reduce the computation time further without affecting results. The differential deflection of 0.31 mm measured experimentally is applied to the middle of one girder during this sensitivity analysis. The magnitude of the stress ($\boldsymbol{\sigma_{y1}}$) that corresponds to the experimental strain produced by the deflection is calculated and compared with the Models predictions (Table 5- 3).

Table 5- 3: Results of Mesh Sensitivity Analysis.

Model	**Local**	**Global Mesh Size**	$\boldsymbol{\sigma_{y1}}$ **(MPa)**		$\boldsymbol{\sigma_{y2}}$ **MPa**	$\boldsymbol{\sigma_{y3}}$ **MPa**	$\boldsymbol{\sigma_{y4}}$ **MPa**	**Running Time**
			Exp	**FE**				
Model 1	10 mm	10 mm	85	1	1	1	1	30 sec
Model 2	5 mm	5 mm		17	15	13	13	2 mins
Model 3	2.5 mm	2.5 mm		30	22	21	20	14 mins
Model 4	2 mm	2 mm		35	24	22	22	1 hr. 17 mins
Model 5	2.5 mm	5 mm		33	24	22	22	6 mins
Model 6	1 mm	5 mm		56	29	29	28	6 mins
Model 7	0.5 mm	5 mm		86	32	33	33	7 hr. 30 mins
Model 8	0.5 to 5 mm	5 mm		86	32	33	33	34 mins
Model 9	0.5 to 5 mm	10-40 mm		86	31	33	33	17 mins

In Table 5- 3, σ_{y1}, σ_{y2}, σ_{y3}, and σ_{y4} are the vertical stresses in the web gap for four preselected locations at the stiffener location (behind of the stiffener), 10 mm below the stiffener weld and 10 mm to the left and right of the stiffener at the weld level, respectively. These locations were picked and used as reference in order to make the comparison the stresses computed in each model. According to the results presented in the mesh sensitivity analysis, the growing mesh size of 0.5 to 5 mm is used for the web gap and 10 to 40 mm is used for the rest of model (Model 9).

The calculated parameters based on the dimensions presented in Table 5- 2 are shown in Table 5- 4.

Table 5- 4: Calculated Factors for the Values Presented in Table 5- 2.

Parameter	Results	Parameter	Results
K_{WEB}	21693	π_1	0.27
K_{TBF}	42839341	π_2	1.46
K_{LBF}	10673	π_3	2.03
K_{DIA}	609534	π_4	0.13
K_{STF}	81794	π_5	0.02

Using the maximum vertical stress at the web gap detail obtained from the FF model the parameter π_6 is calculated and the value 0.26 is obtained.

FE models for eight other scales of the model are created with identical input $\pi-$ parameters. The geometrical dimensions and calculated parameters as well as obtained π_6 from FE analysis are presented in Table 5- 5 and Table 5- 6, respectively. These parameters are chosen in a way to cover wide range for each parameter. For instance, web thickness, w, varies from 3 mm to 21 mm and web gap, g, varies from 10 mm to 300 mm. To obtain identical π parameters, web gap length, g, web thickness, w, and web height, h, are initially chosen while the other geometrical parameters are calculated in a way to obtain similar π parameters. As a result, some of these calculated geometrical parameters do not really make sense in practical point of view and it should be noted that they are selected to provide variety of scales. The finite element models for Scale 1 to Scale 8 are shown in Figure 5- 2.

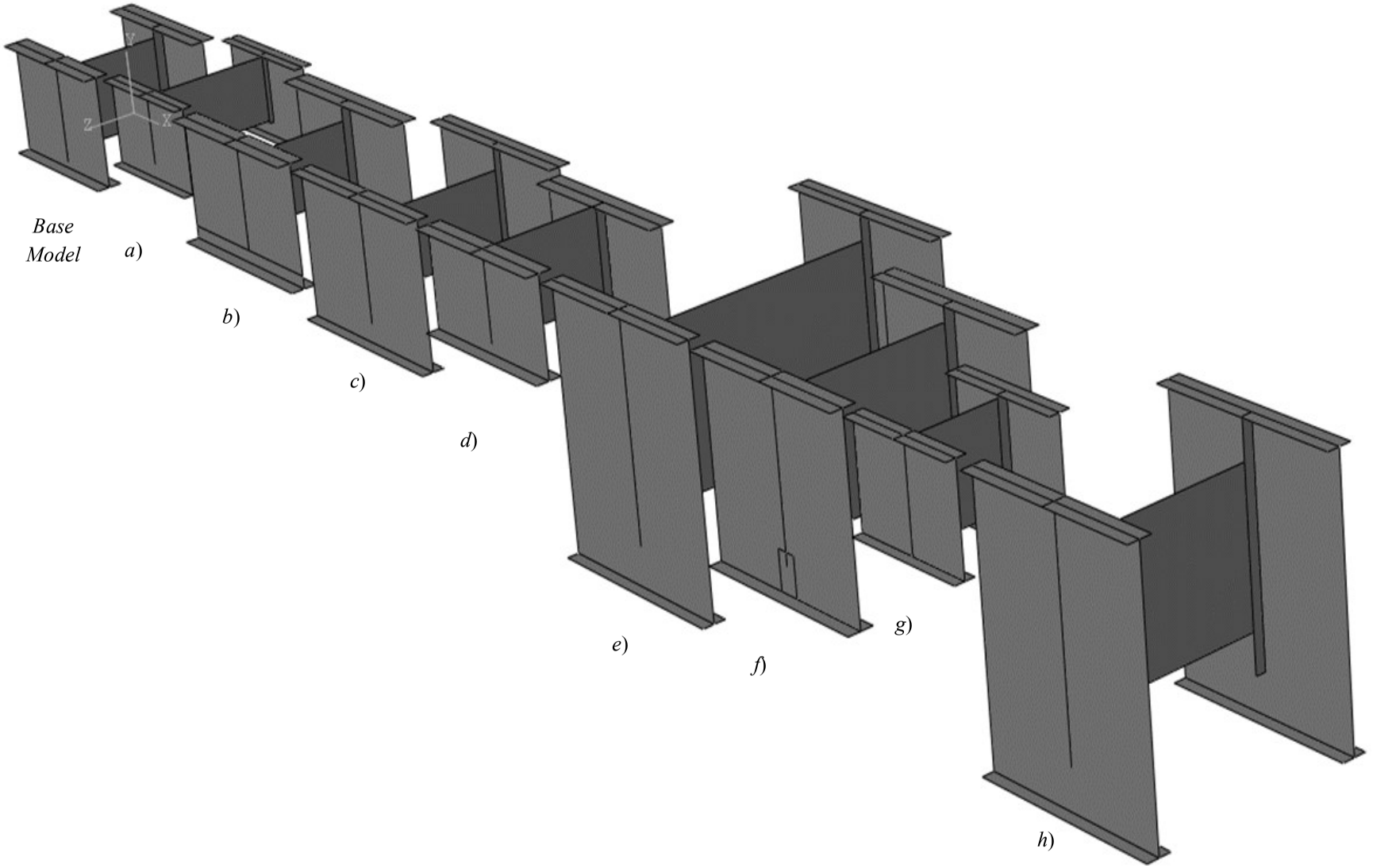

Figure 5- 2: Finite Element Models Used in Scale Independency Tests for a) Scale 1, b) Scale 2, c) Scale 3, d) Scale 4, e) Scale 5, f) Scale 6, g) Scale 7, and h) Scale 8, as well as the Base Model.

Table 5- 5: Geometrical Dimensions Used for Different Model Scales (mm).

	Scale 1	Scale 2	Scale 3	Scale 4	Scale 5	Scale 6	Scale 7	Scale 8
g	120	100	150	80	300	200	10	300
w	13	13	14	12	21	20	3	21
h	700	984	1150	780	2000	1500	800	2000
b_F	189	262	221	255	225	244	195	225
t_F	12	17	14	16	14	15	12	14
L	1416	1970	1987	1740	1970	1844	1249	1866
S	1232	1049	1367	1083	2386	1609	812	1705
h_S	580	884	1000	700	1700	1300	790	1700
t_S	7	9	7	9	9	10	9	10
b_S	49	86	63	87	88	100	90	95
t_d	9	9	6	10	5	7	5	5
h_d	533	586	601	707	1300	1061	738	1112

Table 5- 6: Calculated Parameters for Different Scales and Obtained π_6 From Finite Element Analysis

	Scale 1	**Scale 2**	**Scale 3**	**Scale 4**	**Scale 5**	**Scale 6**	**Scale 7**	**Scale 8**
$\boldsymbol{K_{WEB}}$	11394	15796	7779	20554	8626	14411	19048	10139
$\boldsymbol{K_{DIA}}$	320123	443816	218571	577487	242357	404905	535170	284873
$\boldsymbol{K_{STF}}$	42960	59560	29332	77499	32524	54338	71820	38230
$\boldsymbol{K_{LBF}}$	5606	7772	3828	10113	4244	7091	9372	4989
$\boldsymbol{K_{TBF}}$	15610049	41904803	20994302	42500098	22870341	33481448	20305120	24136311
$\boldsymbol{\pi_1}$	0.27	0.27	0.27	0.27	0.27	0.27	0.27	0.27
$\boldsymbol{\pi_2}$	1.46	1.46	1.46	1.46	1.46	1.46	1.46	1.46
$\boldsymbol{\pi_3}$	2.03	2.03	2.03	2.03	2.03	2.03	2.03	2.03
$\boldsymbol{\pi_4}$	0.13	0.13	0.13	0.13	0.13	0.13	0.13	0.13
$\boldsymbol{\pi_5}$	0.02	0.02	0.02	0.02	0.02	0.02	0.02	0.02
$\boldsymbol{\pi_6}$	0.12	0.11	0.12	0.12	0.12	0.11	0.12	0.12

As it is shown in Table 5-6, for all the models $\boldsymbol{\pi_1}$ to $\boldsymbol{\pi_5}$ parameters are identical while slight discrepancies are found in the response or output ($\boldsymbol{\pi_6}$) parameter. The average value is 0.12. Therefore, the set of these $\pi -$ parameters can be considered as a scale independent and can be used in the parametric study.

5.6. Range of π-parameters for the Parametric Study

An experimental program requires definition of its scope and limitations in advance. It should be clear that experiments are performed and valid for a certain range of parameters. There are generally two sources to define these ranges; the common practice or the practical point of view and the codes of standard. In this section, the ranges of the geometrical dimensions used in the parametric study for multi girder steel bridges web gap are defined.

The requirements given below are generally taken from AASHTO (Minervino, Moses, Mertz, & Edberg, 2004) and Canadian Standard Association (CSA-S6, 2006) and the range are defined in a way to cover wide ranges of variation for each parameter.

According to Canadian Standard Association (CSA-S6, 2006) the slenderness of the flange and the slenderness of the web are both restricted to Class 1 and Class 2 sections. This is simply to prevent local buckling that may occur before the plastic moment of the beam or girder is attained. The minimum web thickness is taken as 1/2" to prevent and reduce potential warping during fabrication.

Webs without longitudinal stiffeners must be proportioned such that ([C6.10.2.1.1]):

$$\frac{h}{w} \leq 150 \qquad (5\text{-}17)$$

where, h is the half of flange width or web height, and w is the flange thickness or the web thickness.

To permit at least 4 lines of bolts for field splices, AASHTO recommends minimum ¾" by 14" flange plate.

The clearance of four to six times the web thickness specified between the end of the stiffener to web weld and the toe of the web to flange weld was also recommended in the code to reduce distortion induced stress in the web gap (CSA-S6, 2006).

For plate girders, flange and web plate thickness AASHTO also recommends selecting values in 1/16" increments for thicknesses up to 1". For thicknesses between 1" and 2 ½", it

recommends the use of 1/8" increments while for thickness range between 2 ½" and 4" the ¼" increments is more suitable.

The minimum flange width $\boldsymbol{b_F}$ and flange thickness $\boldsymbol{t_F}$ are limited to the following relations ([C6.10.2.2]).

$$\frac{h}{b_F} \leq 6 \tag{5-18}$$

$$t_F \geq 1.1\, w \tag{5-19}$$

For stability during shipping and erection the minimum compression flange width b_F is ([C6.10.3.4], [C6.10.2.2]:

$$\frac{b_F}{L} \leq \frac{1}{85} \tag{5-20}$$

$$\frac{b_F}{2t_F} \leq 12 \tag{5-21}$$

Stiffener plate width to thickness ratio is limited to the following to prevent buckling of the plate at a stress below the yield point of the material (AASHO, 1965; AISC, 1963).

$$\frac{b_s}{t_s} \leq \frac{3000}{\sqrt{\sigma_y}} \tag{5-22}$$

For structural steel, this ratio is limited to 16.

Although a maximum cross-frame or diaphragm spacing of 8 m has proven satisfactory in the past to provide girder stability and transfer wind loads, it is no longer mandatory in the code (CSA-S6, 2006). AASHTO recommends 7.5 m to 9 m maximum diaphragm spacing in positive moment segments and 4.5 m to 6 m maximum diaphragm spacing in negative moment

segments. For multi girder bridges, two intermediate diaphragms or cross braces per span is recommended as increasing the number of bracing system beyond this does not provide significant difference (CSA-S6, 2006).

As a rule-of-thumb for the preliminary design of continuous structures, it is recommended to use a steel section depth of 0.033L, where L is the span length. This depth must not be less than 0.0285L ([C2.5.2.6.3]), (Minervino et al., 2004).

AASHTO (2014) recommends that diaphragms or cross-frames for rolled beams and plate girders should be as deep as practicable, but with a minimum value of 0.5 of the beam depth for rolled beams and 0.75 of the girder depth for plate girders at least.

Based on the restrictions and recommendations from AASHTO (2014) (Minervino, Moses, Mertz, & Edberg, 2004) and Canadian Standard Association (CSA-S6, 2006), the ranges of the geometrical dimensions used in this study are defined and presented in Table 5- 7.

Table 5- 7: Ranges of Geometrical Dimensions Used in the Parametric Study

Parameter	Min	Max
g	5 mm	150 mm
w	10 mm	25 mm
h	600 mm	5000 mm
b_F	250 mm	1000 mm
t_F	30 mm	60 mm
L	1000 mm	8000 mm
S	1200 mm	3600 mm
t_S	11 mm	45mm
b_S	100 mm	400 mm
t_d	10 mm	20 mm
h_d	300 mm	4500 mm
A_X	2000 mm^2	10000 mm^2
α	60°	80°

After investigating the FE models, it was found that the diaphragm spacing parameter has almost no effect on the results when the spacing is relatively long. This is simply because the distortion of the web plate and twist of the bottom flange are not transferred beyond a certain point or even close to adjacent diaphragm. Therefore, if this parameter is not available, 1500 mm diaphragm spacing (75 mm each side of the transverse stiffener) seems to provide a reasonable results. This ensures consistency of all FE models as well. Within this distance, the web gap distortion and bottom flange torsional rotation diminish and the web plate and bottom flange do not get influenced by the differential deflection.

To calculate the maximum and minimum stiffness, the parameters are selected based on the range of dimensions of the member affecting the stiffness. It should be noted that this method is not suitable to calculate the maximum and minimum value for π-parameters. For example, to calculate maximum value of π_1, we cannot simply divide maximum of web plate stiffness (K_{WEB}) by minimum of stiffener stiffness (K_{STF})as the detail does not have maximum value for web plate stiffness and minimum value for stiffener stiffness. There must be a logical and practical relation between them to build the connection. Therefore, all the design criteria should be included in the calculations, simultaneously.

In order to get reasonable ranges for these π-parameters, some currently in-service steel multi girder bridges constructed prior to 1985 have been investigated to find the geometric dimensions of the web gap detail and the bridges. Data from this study is presented in Table 5-8. Although this table does not cover all the ranges of geometrical dimensions mentioned in Table 5-7, it is a good guide to consider the relative stiffness of the member in the experimental design.

Table 5- 8: Bridge Survey Data for available Steel Multi Girder Bridges

Bridge #	g	w	h	b_F	t_F	L	S	h_S	t_S	b_S	t_d	h_d
1	50	10	914	254	16	1700	1000	864	10	100	10	686
2	51	15	646	355	25	7620	2667	595	15	154	14	517
3	51	17	719	381	27	6706	2997	668	17	166	15	575
4	51	16	719	268	25	6401	2972	668	16	156	14	575
5	51	15	797	292	22	6096	2438	746	□5	147	13	638
6	38	15	797	292	22	6096	2515	759	1	147	13	638
7	51	19	914	308	32	6706	3048	864	19	194	18	732
8	38	16	863	304	24	6248	2718	825	16	159	14	690
9	38	17	863	305	26	6401	2819	825	17	165	15	690
10	38	11	1118	356	16	5791	2896	1080	11	111	10	894
11	51	18	863	307	30	4877	3048	812	18	184	17	690
12	38	13	1168	356	16	6096	3162	1130	13	127	11	935
13	51	13	1016	356	25	7163	2□□9	965	13	127	11	813
14	51	13	838	356	□5	7010	2438	787	13	127	11	671
15	38	10	1067	356		6706	2718	1029	10	95	9	853
16	38	13	1270	406	19	7010	3099	1232	13	127	11	1016
17	38	13	1372	356	19	6706	2896	1334	13	127	11	1097
18	38	10	1524	457	19	6401	2896	1486	10	95	9	1□19
19	51	14	1524	356	25	7010	3277	1473	14	143	13	1□1
20	51	14	2032	457	25	7620	3124	1981	14	143	13	1626
21	51	13	1778	406	19	7620	3099	1727	13	127	11	1422
22	45	6	876	279	16	1500	1500	831	10	127	10	657
23	70	10	1000	300	30	1500	1500	930	10	100	10	800
24	25	8	100	300	30	1500	1500	975	10	100	10	800
25	64	13	1000	300	32	1500	1500	936	10	100	10	800
26	38-76	10	914	305	25	1500	1500	787-825	10	127	20	800

* The unit for the numbers in the table is mm. For references, see Table 5- 9.

Table 5- 9: References used for bridge inventory in Table 5-8.

Bridge #	Reference	Bridge #	Reference
1	69021	14	66001
2	19898	15	86802
3	19897	16	49011
4	9775	17	27106
5	9452	18	19882
6	27015	19	19816
7	62045	20	19832
8	66809	21	Adams, (2010)
9	31023	22	Shifferaw & Fanous, (2013)
10	55029	23	Zhao & Kim Roddis, (2007)
11	69894	24	27796 (Li & Schultz, 2005)
12	27734	25	Fisher, (1990)
13	62702	26	Fraser et al., (2000)

The numbers in Table 5- 9, indicate the bridge IDs in some Departments of Transformation in USA (Berglund & Schultz, 2001).

Using the parameters in Table 5- 7, the ranges of factors and π-parameters are calculated and presented in Table 5- 10.

Table 5- 10: Ranges of π-parameters Used in the Parametric Study

Parameters	Minimum	Maximum
K_{WEB} (N/mm)	2.E+05	2.E+04
K_{DIA} (N/mm)	6.E+05	2.E+05
K_{STF}(N/mm)	3.E+05	4.E+04
K_{LBF} (N/mm)	1.E+05	2.E+04
K_{TBF} (N. mm)	5.E+08	5.E+07
π_1	0.05	2
π_2	0.05	3.5
π_3	1	4.5
π_4	0.1	1.5
π_5	0	0.02

All of these maximum and minimum limitations are increased and decreased, respectively, by 20 percent to cope with the variability of the dimensions.

Chapter 6

Design of Experiments and the Development of Prediction Equation

The goal of this research is to develop an equation to predict the magnitude of the stress in the web gap detail. This equation would be a fitted mathematical function with estimated coefficients. The first step to develop this equation is to assume a general form for the function whose unknown coefficients can be estimated statistically. The predicted value of the stress obtained using this method is highly sensitive to the general form of the equation. Developing this equation requires a good understanding of the effects that each parameter can have on the output and the overall behavior of the system. Even if the general form of the equation is already known, there are infinite numbers of coefficient values obtained from regression analysis that can potentially be used. Therefore, the best sets of coefficients should be selected among these potential coefficients to predict the output closest to the actual values.

Linear, quadratic, and exponential regressions are investigated for the web gap stress prediction problem and the results of the most accurate regression analysis are presented in this chapter. Least squares criterion is used in order to compare different sets of coefficients for each regression method.

A set of preliminary FE study of the web gap detail is performed to understand the behavior of the model, the effect of each individual parameter on the prediction results, and the general form of the prediction equation. This is mostly known as screening study which roughly clarifies the overall influence of each individual parameter in the prediction equation and gives the assessor a good idea about the preliminary form of the equation. This study is performed and presented in the following section.

To obtain appropriate and acceptable coefficients, numerous sets of experimental data are needed. The more data from experiment we have, the more accurate equation we can get from

the regression analysis and the obtained coefficients lead to more precise predictions. However, it is almost impractical to perform and run unlimited experiments and consider all the possible combinations among the parameters which results the perfect prediction equation. In addition, it is necessary to design experiments that are achievable and provide the satisfying results with minimal costs.

Experimental design or design of experiments (DOE) which is the process of designing and analyzing the experimental program using efficient and effective approach is utilized in this chapter to obtain the essential statistic data. This method combines the expert knowledge and statistical technique to optimize the number of the experimental data and to obtain reasonable and satisfying results.

6.1. Screening Study

Prior to performing any experimental program and design the experiments, all the variables must be considered individually to give an idea to the experimenter about the influence of these parameters on the overall behavior of the response function. In other words, only one variable or one factor is investigated at a time and all other variables are kept constant. This is also known as "one variable at a time" approach. This method helps choose the level of variation at which the variable is needed to be investigated. For instance if the variable shows a linear trend in this step, only two levels are considered for it, and if it shows any curvature trend, at least three levels are needed to represent the effect. Basically, the screening study intends to find the significance of each parameter on the output results or the response function.

If the significance of all the parameters is linear, the experimental design would only be the first-order design where two levels of each factor are needed. This is also known as 2^k factorial design, where k is the number of factors. This approach does not present any possible curvature in the response surface.

If the experimenter expects a curvature in the response surface, the parameters or factors are required to be investigated in at least three levels. This approach is called 3^k factorial design, where k is again the number of all factors. This results in a significant growth in the number of required experiments. For instance, for the web gap stress prediction problem in which the number of factors is 5, 2^k factorial design only needs 32 experiments. However, 3^k factorial design requires 243 experiments. Therefore, it is necessary to understand the effect of each parameter on the response surface and consider the proper levels for the factors as it reduces the number of experiments significantly. If the response shows a linear trend for a specific factor and the experimenter uses three levels for the experimental design for that factor, the number of experiments is increased with no extra gain in the accuracy of the results.

Using one factor at a time approach gives the assessor a good idea about the effect of each factor on the output (response surface) and indicates the levels required for each factor to construct the experiments.

For the web gap stress prediction problem, screening study is performed for all 5 $\pi-$ parameters and the results are presented in this section. The ranges of the $\pi-$parameters are defined in Chapter 5 and the levels at which each parameter is considered, remained within the ranges.

As the effect of the factors in the web gap stress prediction problem is not well established, it is decided to use 3^k factorial design approach to observe the trend of the response surface influenced by each factor. Therefore, three levels for each parameter are selected for this screening study. These factors levels are presented in Table 6-1.

Table 6- 1: π-Parameters levels for parametric study

Factor \ Level	Low	Median	High
π_1	0.12[3]	1	2
π_2	0.12	1.5	3.5
π_3	1	2.5	4.5
π_4	0.1	0.8	1.5
π_5	0	0.01	0.02

L: Lowest Level, **M**: Median Level, **H**: Highest Level

To perform the screening study, a base model is selected and the one factor at a time approach is used to obtain the preliminary idea about the effect of each parameter on the response surface. The base model is formed by using median levels for all $\pi - \text{parameters}$. Each parameter is varied by its three levels and the other parameters are kept the same as the base model. This reduces the number of screening study experiments to 11 models including the base model. The magnitudes of $\pi - \text{parameters}$ for these models are presented in Table 6- 2.

Table 6- 2: Set of variables for screening study of π-Parameters

Model	π_1	π_2	π_3	π_4	π_5
Base	1.00	1.50	2.50	0.80	0.01
1	**0.12**[1]	1.50	2.50	0.80	0.01
2	**2.00**	1.50	2.50	0.80	0.01
3	1.00	**0.12**[1]	2.50	0.80	0.01
4	1.00	**3.50**	2.50	0.80	0.01
5	1.00	1.50	**1.00**	0.80	0.01
6	1.00	1.50	**4.50**	0.80	0.01
7	1.00	1.50	2.50	**0.10**	0.01
8	1.00	1.50	2.50	**1.50**	0.01
9	1.00	1.50	2.50	0.80	**0.005**
10	1.00	1.50	2.50	0.80	**0.02**

[3] 0.12 minimum values are used for the π_1 and π_2 instead of 0.05 (specified in Table 5-10) in this screening study as it was impossible to find the solution for dimensions for models 1 and 3.

In Model 9 the first level of π_5 is zero but it leads to an obvious value of zero for π_6. Therefore, 0.005 is selected for the lowest value for π_5 in this screening study.

The finite element models used for the screening study are the same models as described in Chapter 5. The dimensions for each model were selected and calculated in a manner to obtain the corresponding $\pi - \text{parameters}$. Clearly, there is no unique solution for the dimensions set which leads to the same $\pi - \text{parameters}$. Therefore, some dimensions for each model were randomly selected and the remaining dimensions were calculated such that the goal $\pi -$ parameters were obtained. As the dimensionless parameters are complicated to be equal to a certain values simultaneously, an iterative approach is used to calculate the remaining dimensions of the model. These iteration procedures were performed in Microsoft Excel. The dimensions of these models are presented in Appendix B. These models were created and analyzed in ABAQUS and the results are presented in the following sections. For each $\pi -$ parameter the results of the base model (level M) and two other levels (H and L) for the parameter under consideration are graphed to represent the influence of the parameter on the response surface. The results for the influence of π_1 to π_5 on the response function (π_6) are presented in Figure 6- 1 to Figure 6- 10. To calculate the π_6 for each model, the vertical stress in the web gap detail is obtained from ABAQUS along the web gap detail. The stress is recorded from the weld toe at transverse stiffener and web plate connection for 12 mm toward the bottom flange. The stress at 4 mm, 8 mm, and 12 mm locations are used to calculate the HSS in the web gap detail according to Equation 3-1. This equation is presented in the following as well.

$$HSS = 3\sigma_{4mm} - 3\sigma_{8mm} + \sigma_{12mm} \qquad (3\text{-}1)$$

Using the calculated HSS from the vertical stress at the web gap detail, a corresponding π_6 is calculated for each model using Equation 6-1. This output (π_6) for the model is compared with the outputs from other models.

$$\pi_6 = \frac{HSS \cdot h}{100 K_{WEB}} \quad (6\text{-}1)$$

where h is the web plate height, and K_{WEB} is the web plate stiffeness.

6.1.1. Effect of π_1 on the response (π_6)

In order to find the influence of π_1, which is the relative parameter of web plate stiffness and transverse stiffener stiffness, three levels are considered for $\pi_1(0.12, 1, \text{and } 2)$ in this screening study. The other $\pi -$ parameters are maintained the same as the "Base Model" ($\pi_2 = 1.5, \pi_3 = 2.5, \pi_4 = 0.8, \text{and } \pi_5 = 0.01$). Therefore, Base model, Model 1 and Model 2 are compared in this section. Figure 6- 1 shows the magnitude of π_6 along the web gap using the stress at the web gap location and Figure 6- 2 presents the effect of π_1 on π_6 calculated form HSS using Equation 3-1.

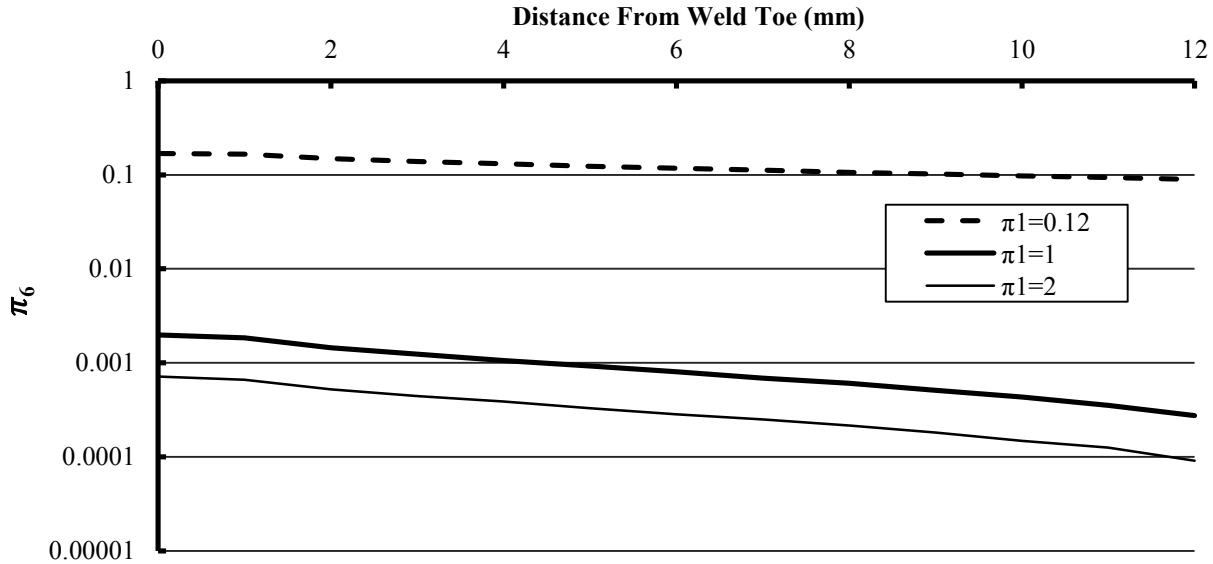

Figure 6- 1: Effect of variation of π_1 on π_6

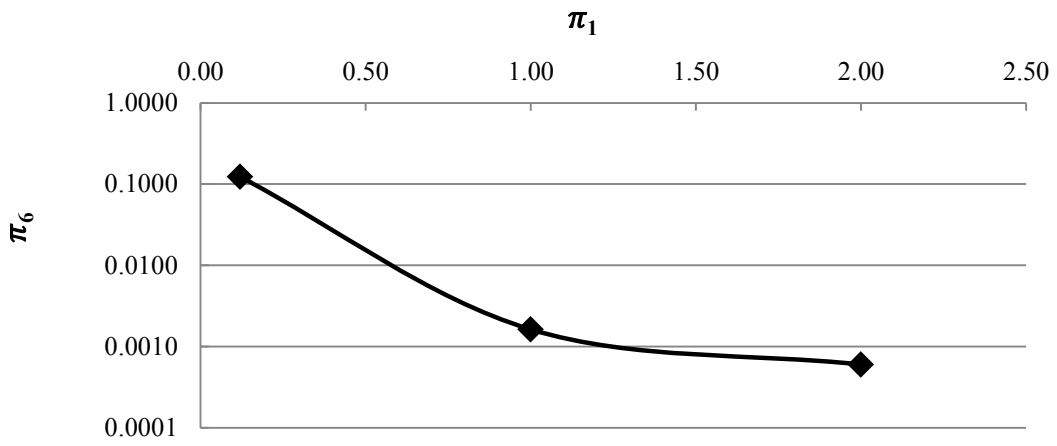

Figure 6- 2: Effect of variation of π_1, obtained from HSS, on π_6

As shown in Figure 6-1 and Figure 6-2, the output (π_6) is highly sensitive to variation of π_1. By increasing π_1, π_6 drops drastically and consequently the stress in the web gap detail decreases. As expected, this means that if the transverse stiffener is more flexible, it absorbs higher deflection and the web gap relatively experiences less load.

6.1.2. Effect of π_2 on the response (π_6)

This parameter relates the web plate stiffness and bottom flange torsional stiffness. It is expected to predict lower stress when there is a more flexible flange in the detail. This is because a flexible flange gives the web plate more flexibility to distort. To find the influence of π_2 on π_6, Model 3 and Model 4 are constructed and π_2 is varied (0.12, 1.5, and 3.5) and the other parameters are again maintained the same as the Base model ($\pi_1 = 1, \pi_3 = 2.5, \pi_4 = 0.8, \text{and } \pi_5 = 0.01$).

The influence of π_2 is shown in Figure 6- 3 and Figure 6- 4. It is clear that by increasing π_2, π_6 decreases up to a certain point and after that it does not significantly affect the output. Although this parameter has some effect on the response function, it is not as considerable as π_1.

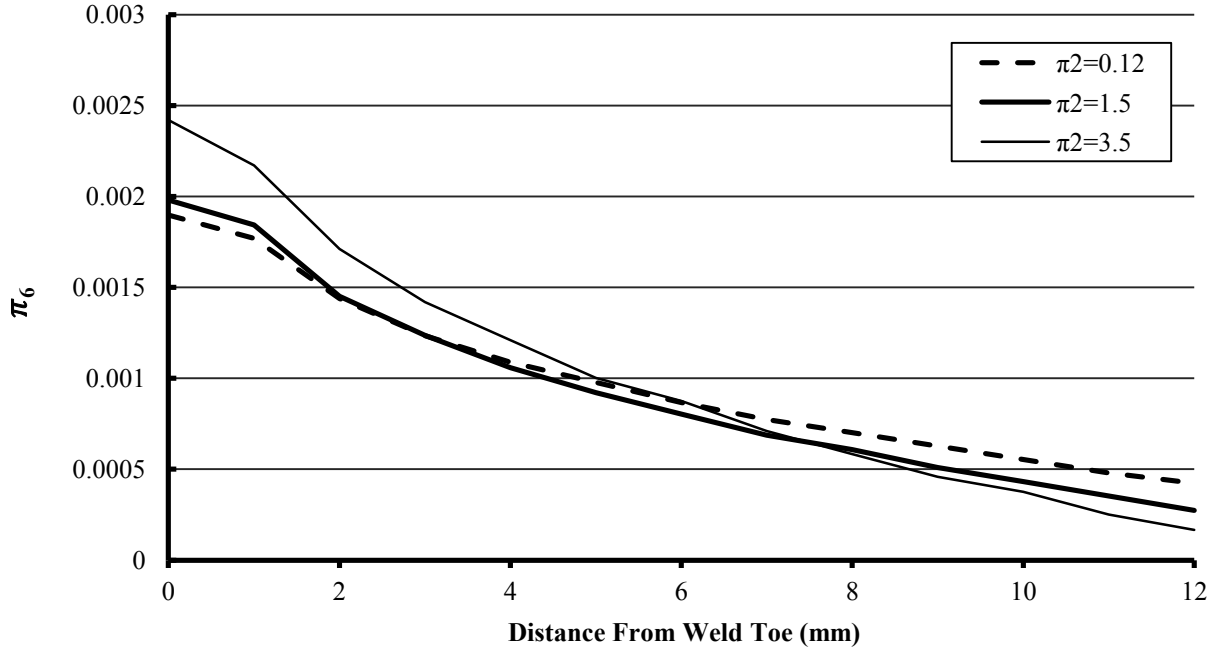

Figure 6- 3: Effect of variation of π_2 on π_6

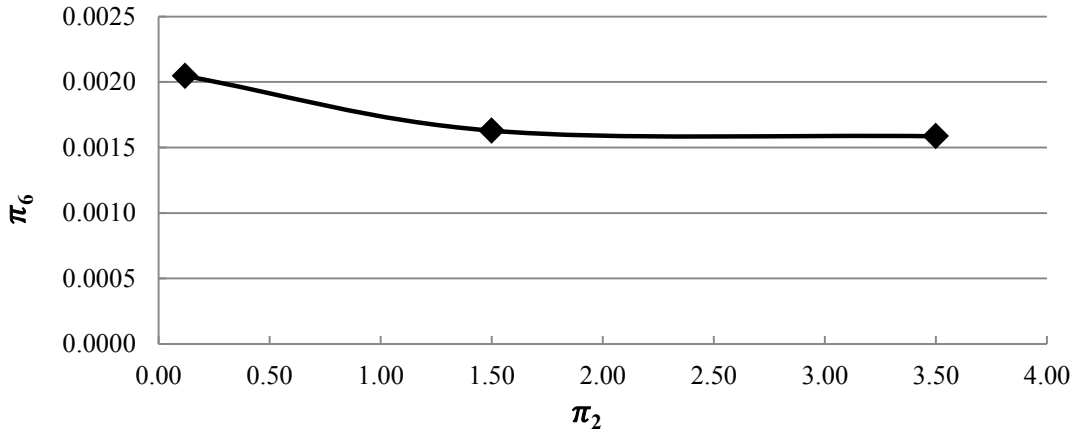

Figure 6- 4: Effect of variation of π_2, obtained from HSS, on π_6

6.1.3. Effect of π_3 on the response (π_6)

To investigate the effect of π_3 on the response function, Model 5 and Model 6 are created. This parameter is the relative parameter of web plate stiffness and bottom flange lateral stiffness. In these models only π_3 is varying in three levels (1, 2.5, and 4.5) and all the $\pi-$ parameters are the same as the ones for Base Model to be able to compare the results ($\pi_1 = 1, \pi_2 = 2.5,\ \pi_4 = 0.8, \text{and } \pi_5 = 0.01$). The results of this investigation are presented in Figure 6- 5 and Figure 6- 6. Decreasing the bottom flange lateral stiffness increases the π_3 and consequently the response function (π_6) decreases. The reason is that as the bottom flange becomes more flexible, the web gap can distort easier and the magnitude of the vertical stress reduces in the detail.

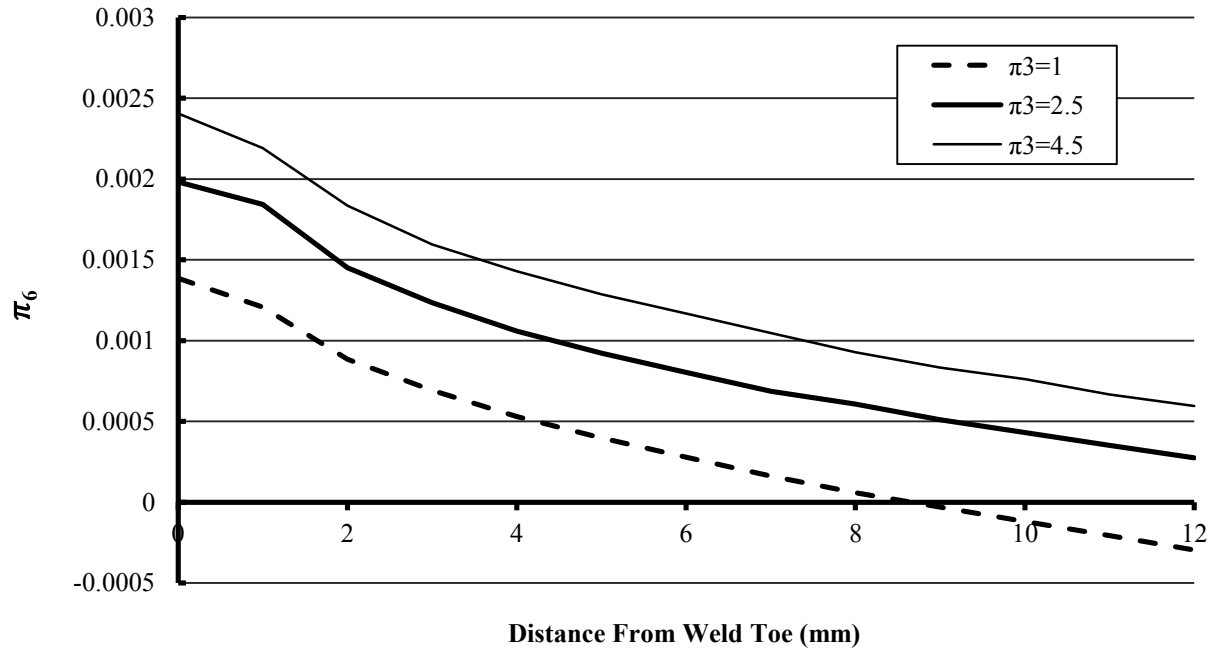

Figure 6- 5: Effect of variation of π_3 on π_6

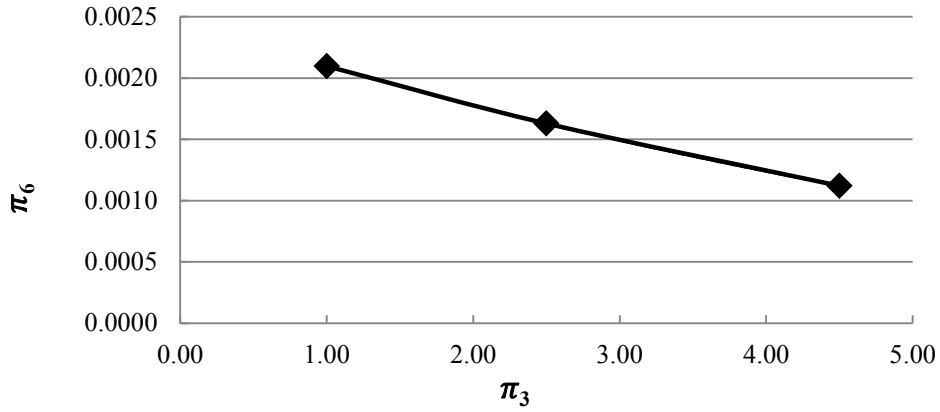

Figure 6- 6: Effect of variation of π_3, obtained from HSS, on π_6

6.1.4. Effect of π_4 on the response (π_6)

This parameter relates the transverse stiffener stiffness and diaphragm stiffness. To assess the influence of this parameter on the output results, Model 7 and Model 8 are constructed. In these models only π_6 is different and is set equal to its three levels (0.1, 0.8, and 1.5) and the other four parameters are kept the same as the ones in Base Model ($\pi_1 = 1, \pi_2 = 2.5,\ \pi_3 = 2.5, \text{and } \pi_5 = 0.01$).

Having a flexible diaphragm in steel multi-girder bridges allows the two adjacent girders to deflect more independently and the lower distortion would be transferred into the web gap detail from the rotation of the diaphragm. This causes less vertical stress in the web gap and consequently, π_6 decreases. This trend of the output is rationally expected and is clearly shown in Figure 6- 8.

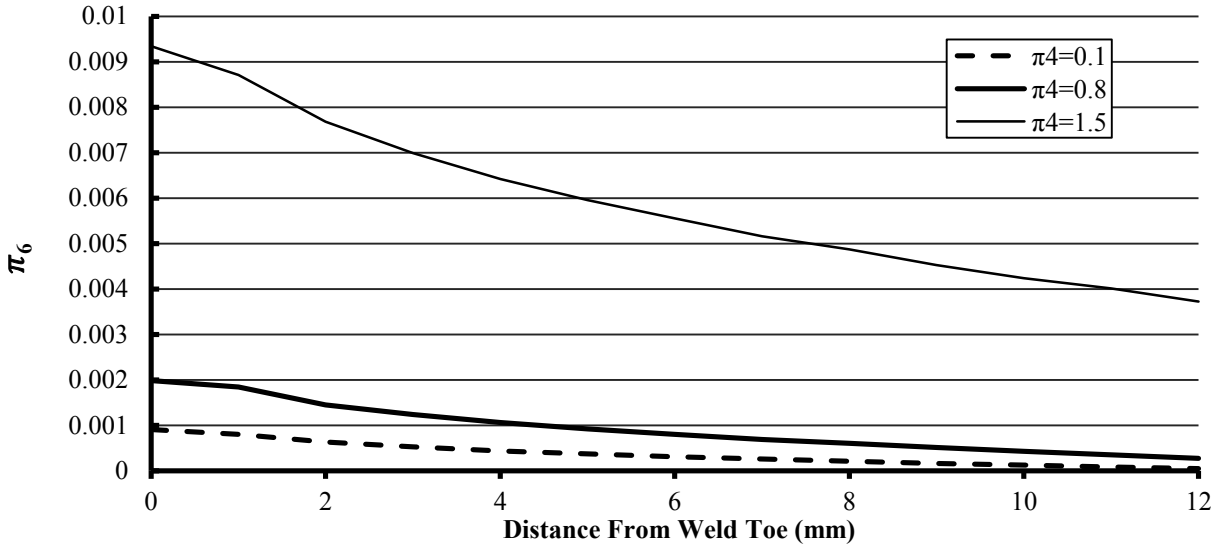

Figure 6- 7: Effect of variation of π_4 on π_6

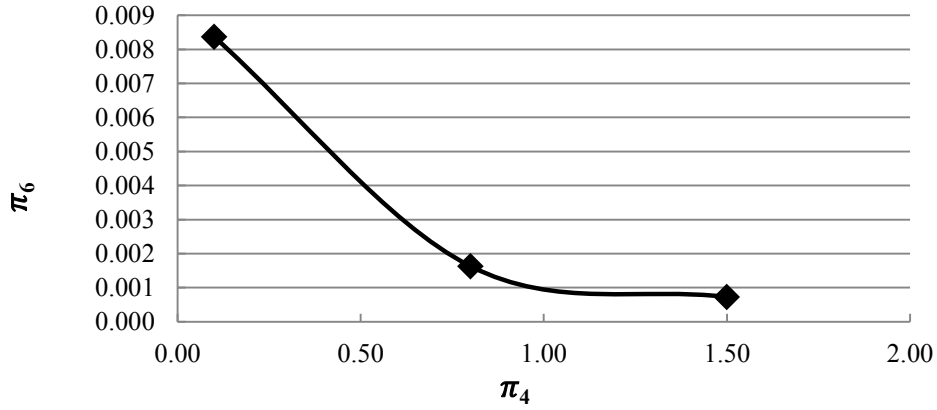

Figure 6- 8: Effect of variation of π_4, obtained from HSS, on π_6

6.1.5. Effect of π_5 on the response (π_6)

This is the final parameter investigated in the screening study. π_5 is the only dimensionless parameter considered as the loading parameter. It represents the differential deflection between two adjacent girders in steel multi-girder bridges. In order to perform the study and realize the influence of this parameter, the "Base Model" is used and only three magnitudes of differential deflections are applied. These differential deflections create the three levels for π_5 (0.005, 0.01, and 0.02). As the same model is used, obviously the other first $\pi-$ parameters were kept unchanged ($\pi_1 = 1, \pi_2 = 2.5,\ \pi_3 = 2.5, \text{and } \pi_4 = 0.8$).

The results for this study are presented in Figure 6- 9 and Figure 6- 10. It is found that the response function varies linearly with changing π_5. By increasing the magnitude of differential deflection, π_5 increases and as it is shown in Figure 6- 10, π_6 increases too. This is clearly because of the magnitude of distortion transferred to the web gap.

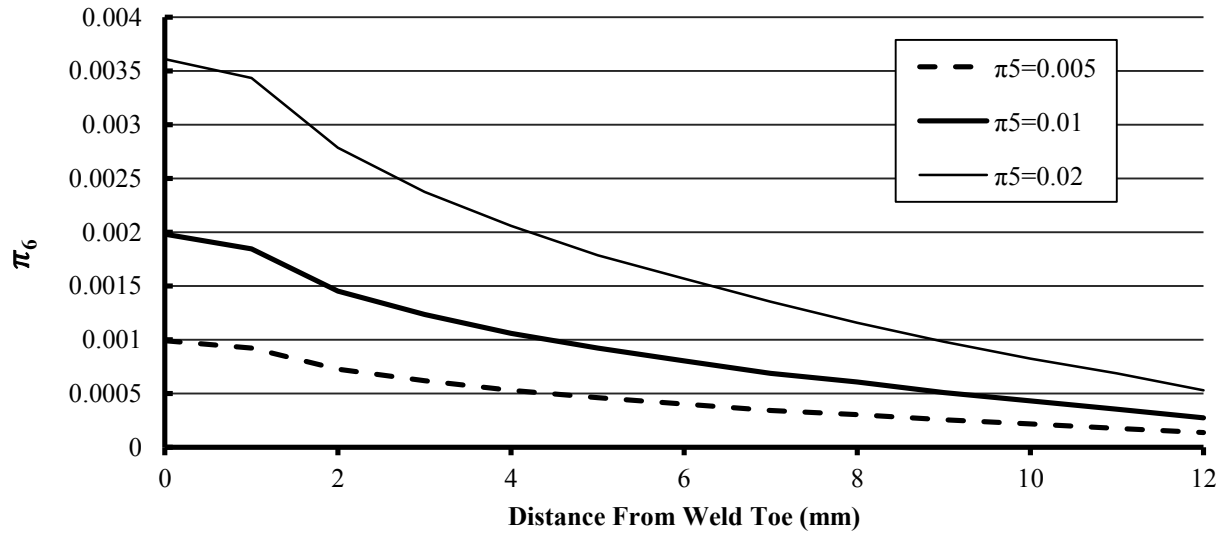

Figure 6- 9: Effect of variation of π_5 on π_6

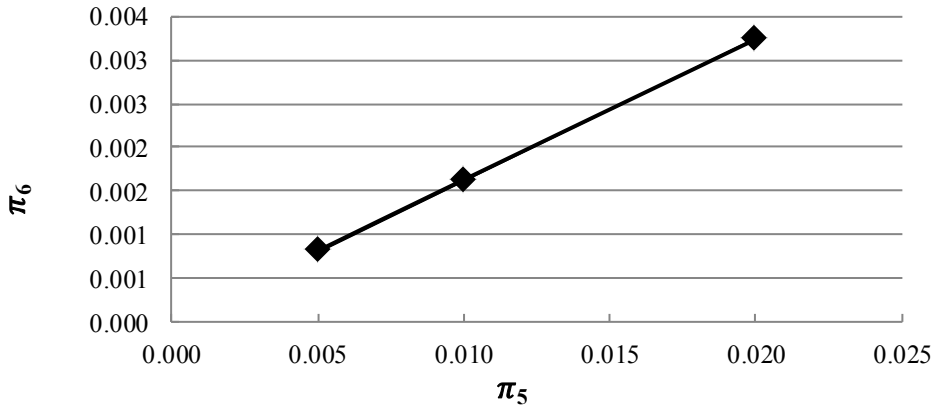

Figure 6- 10: Effect of variation of π_5, obtained from HSS, on π_6

6.2. Design of Experiments

As mentioned in the previous sections, to observe any possible curvature in the response function, at least three levels for each factor are needed. This leads to 3^k full factorial experimental design. In stress prediction problem at web gap detail it leads to 243 (3^5) experiments. According to the screening study performed previously, it was found that the influence of π_5 on the response function is linear and two levels would reflect the influence on the response function. Therefore, the full factorial experiments would be 162 (2×3^4). Although these full factorial experiments provide all possible combination of the relevant factors and parameters, it is very costly to be conducted. Using a fractional factorial design provides an alternative solution to achieve a more doable experimental program without losing the overall accuracy.

Full factorial experiments can require many model executions but a carefully chosen fraction of the models may be all that is necessary. With this method, only a fraction of the models are selected.

In the stress prediction problem at the web gap detail, this fraction factorial experimental design would be a combination of three-level and two-level designs. Therefore, the fractional factorial experimental design would be one factor at two levels and four factors at three levels. According to Taguchi methods which are statistical methods often known as orthogonal arrays

developed by Genichi Taguchi (Cavazzuti, 2012), $L_{18}\,2^1 \times 3^7$ can be the most efficient experimental design for the stress prediction problem in the web gap detail. Taguchi uses the following convention for naming the orthogonal arrays; $L_a\,b^c$, where a is the number of experimental runs, b is the number of levels of each factor, and c is the number of variables. $L_{18}\,2^1 \times 3^7$ consists of one factor at 2 levels and up to 7 factors at three levels each. There are 18 rows in this design of experiments. This method is being successfully implemented in diverse areas such as engineering and science. Using this method, the experiments needed for the stress prediction problem at web gap detail are summarized in Table 6- 3. In this table, "L", "M", and "H" indicate the lowest, median, and highest values for each $\pi - \text{parameter}$, respectively. Run 1 to Run 18 is equivalent to Model 1 to Model 18 in this parametric study.

Table 6- 3: Design of experiments for the stress prediction problem at web gap detail.

Run	π_1	π_2	π_3	π_4	π_5
1	L	L	L	L	L
2	L	M	M	M	L
3	L	H	H	H	L
4	M	L	L	M	L
5	M	M	M	H	L
6	M	H	H	L	L
7	H	L	M	L	L
8	H	M	H	M	L
9	H	L	L	H	L
10	L	L	M	H	H
11	L	M	L	L	H
12	L	H	M	M	H
13	M	L	M	H	H
14	M	M	H	L	H
15	M	H	L	M	H
16	H	L	H	M	H
17	H	L	L	H	H
18	H	H	M	L	H

According to Table 6- 3, 18 finite element models are constructed and the results of this parametric study are presented in the following section. The dimensions of these models are presented in Appendix C. The dimensions for each model were selected and calculated in a manner to obtain the corresponding $\pi - \text{parameters}$. As it was previously mentioned there is no unique solution for the dimensions set which leads to the same $\pi - \text{parameters}$. Therefore, some dimensions for each model were manually selected and the remaining dimensions were calculated such that the goal $\pi - \text{parameters}$ were obtained. The iteration procedures to calculate the dimensions were performed in Microsoft Excel.

6.3. Results of Parametric Study

The results for the parametric study of all the 18 models are presented in this section. To calculate the π_6 for each model, the vertical stress in the web gap detail is obtained from ABAQUS along the web gap detail. The same procedure as the one used in screening study is used to calculate the HSS in the web gap detail. Then, Equation 6-1 is used to calculate π_6 for each model which is used in stress prediction equation for the web gap detail.

Vertical stresses at web gap detail along web plate are extracted from ABAQUS for each model. The stresses for Model 1 to Model 18 are presented in Appendix C from Figure A. 1 to Figure A. 18, respectively. The distance in these graphs are measured from the weld toe at transverse stiffener in perpendicular direction to longitudinal direction along the web plate. The path along which the stress is extracted for each model is also shown in Figure 3- 22. Using the extracted stress from finite element models, HSSs are calculated for each model and from the obtained HSS, π_6's are calculated. These results are presented in Table 6- 4.

Table 6- 4: Calculated HSS and π_6 for Models in Parametric Study.

Run	HSS (MPa)	π_6	Run	HSS (MPa)	π_6
1	372	0.33750	**10**	266	0.02520
2	230	0.02694	**11**	549	0.53545
3	199	0.01270	**12**	277	0.05792
4	65	0.00219	**13**	132	0.00210
5	54	0.00071	**14**	201	0.02761
6	133	0.01114	**15**	152	0.00314
7	65	0.00314	**16**	77	0.00100
8	39	0.00041	**17**	55	0.00081
9	17	0.00038	**18**	93	0.00087

6.4. Prediction Equation Development

Using the results of 18 finite element models obtained from the parametric study as well as the results of 11 models used in the screening study, a regression analysis is conducted in order to obtain the equation to predict stress in the web gap detail. Regardless of the method used for the regression analysis, the form of the prediction equation must be chosen in advance in order to calculate the optimal values for the unknown coefficients. The most common function forms of regression analysis are linear functions, polynomial function, and exponential functions. According to the screening study performed in the previous section for the stress prediction equation, the linear regression and linear combination of the dimensionless parameter do not properly represent the behavior of the detail and cannot provide accurate results for the regression analysis. The same argument is valid for polynomial regression analysis as for some dimensionless parameters such as π_1 and π_4 it is obvious that the trend cannot be described by polynomial functions. Therefore, it is decided to use exponential multi-parameter regression

approach to obtain the equation which best fits the experimental design results and provides the most accurate results for the predicted stress in the web gap detail.

To obtain the coefficients, the residual errors are minimized by using the least squares techniques. The residual error is the difference between the obtained value from experiments or the observed value of the response, and the value given by the prediction equation. The coefficient of determination, R^2, is the most common value that is used to compare the prediction models and the accuracy of the prediction. R^2 is a number between 0 and 1. $R^2 = 1$ means that all the variation in the response function is described in the prediction equation. There are several definitions for R^2 among which the most common definition is used in this study which is presented in Equation (6-2).

$$R^2 = 1 - \frac{SS_{residual}}{SS_{Total}} \tag{6-2}$$

where, R^2 is the coefficient of determination for the prediction equation, $SS_{residual}$ is sum of squared residual error, and SS_{Total} is sum of squared deviations of the observed values about the sample mean. $SS_{residual}$ and SS_{Total} are defined in Equation (6-3) and Equation (6-4).

$$SS_{residual} = \sum_{i=1}^{n} (Y_i - \hat{Y}_i)^2 = \sum_{i=1}^{n} (Error)^2 \tag{6-3}$$

$$SS_{Total} = \sum_{i=1}^{n} (Y_i - \bar{Y})^2 \tag{6-4}$$

where, Y_i is the i^{th} observed value of the response variable, $\hat{Y}_i$ is the i^{th} predicted value of the response variable, $\bar{Y}$ is the mean of observed values of the response variable, and n is the number of observed values.

6.4.1. General Form of the Prediction Equation

Based on the screening study performed in section 6.1 and the results of parametric study, several prediction equations were proposed and investigated. It was found that the equation with the exponential form provides the greatest value for R^2. The general form of the prediction equation is presented in Equation (6-5).

$$\pi_6 = A(\pi_1)^B(\pi_2)^C(\pi_3)^D(\pi_4)^E(\pi_5)^F \quad (6\text{-}5)$$

where, A, B, C, D, E, and F are the regression coefficients and π_1 to π_6 are the dimensionless parameter used as independent variables.

The exponential regression analysis was conducted in Microsoft Excel in order to calculate the regression coefficients which minimize the prediction error and maximizes the R^2. It should be noted that regression coefficient F is manually set to 1 as its corresponding dimensionless parameter (π_5) demonstrated linear influence on the response function (π_6).

6.4.2. Results of Regression Analysis

The regression analyses were performed for two ranges of π_6 as fitting one curve and getting the accurate results were not possible for this set of data. It is simply because the overall behavior of web gap influences the magnitude of the vertical stress in the detail. If the web gap is stiff enough to transfer the distortion to the bottom flange, the lateral and torsional stiffness of the bottom flange affects the boundary condition of the web plate at the web gap location. In contrast, if the web gap is very flexible, it absorbs all the distortion and lets the transverse stiffener deflect without influencing the bottom flange at all. This is taken into consideration by defining a limit for π_6 for flexible and stiff web gaps. Web gaps with π_6 less than 0.01 are

considered as stiff web gap details and the ones with π_6 greater than or equal to 0.01 are defined as flexible web gaps. Therefore, two regression analyses are performed; one for flexible web gaps and one for stiff web gaps. The results are presented in the following sections.

6.5. Prediction Equation for Stiff Web Gaps ($\pi_6 < 0.01$)

By performing the non-linear exponential regression analysis for the results which have π_6 less than 0.01 the regression coefficients and exponents are found for Equation (6-5). Using this regression result, Equation (6-6) and Equation (6-7) are obtained for $\pi_6 < 0.01$.

By combining Equation (6-7) and Equation (6-8) HSS can be obtained from web plate stiffness of each member in the web gap detail. This relation is presented in Equation (6-9).

$$\pi_6 = 0.16\,(\pi_1)^{-1.766}\,(\pi_2)^{-0.124}(\pi_3)^{-0.257}(\pi_4)^{-0.839}(\pi_5)^{1} \qquad (6\text{-}6)$$

$(For\ \pi_6 < 0.01)$

$$\pi_6 = 0.160\,\left(\frac{K_{WEB}}{K_{STF}}\right)^{-1.766}\left(\frac{K_{WEB}.L^2}{1000K_{TBF}}\right)^{-0.124}\left(\frac{K_{WEB}}{K_{LBF}}\right)^{-0.257}\left(\frac{K_{STF}}{K_{DIA}}\right)^{-0.839}\left(\frac{\Delta}{g}\right)^{1} \qquad (6\text{-}7)$$

$(For\ \pi_6 < 0.01)$

$$HSS = \frac{100K_{WEB}}{h}\pi_6 \qquad (6\text{-}8)$$

$$HSS = 16.0\frac{\Delta}{gh}\frac{(K_{STF})^{1.766}}{(K_{WEB})^{-1.147}}\left(\frac{L^2}{1000K_{TBF}}\right)^{-0.124}(K_{LBF})^{0.257}\left(\frac{K_{STF}}{K_{DIA}}\right)^{-0.839} \quad (6\text{-}9)$$

$(For\ \pi_6 < 0.01)$

where, K_{WEB} is the web plate stiffness, K_{TBF} is the bottom flange torsional stiffness, K_{LBF} is the bottom flange lateral stiffness, K_{DIA} is the diaphragm stiffness, K_{STF} is the transverse stiffener stiffness, g is the web gap length, Δ is the differential deflection between the two adjacent girders under investigation, h is the web plate height, L is the transverse stiffener spacing or diaphragm spacing whichever is smaller, and finally HSS is the hot spot stress in vertical direction in the web gap detail.

Figure 6- 11 represent the comparison between predicted responses by Equation (6-7) and the responses obtained from FEA. The regression coefficients (R^2) for response predicted by Equation (6-7) is 0.95 which has reasonable accuracy with all the complication in the web gap stress prediction problem and limited number of experiments.

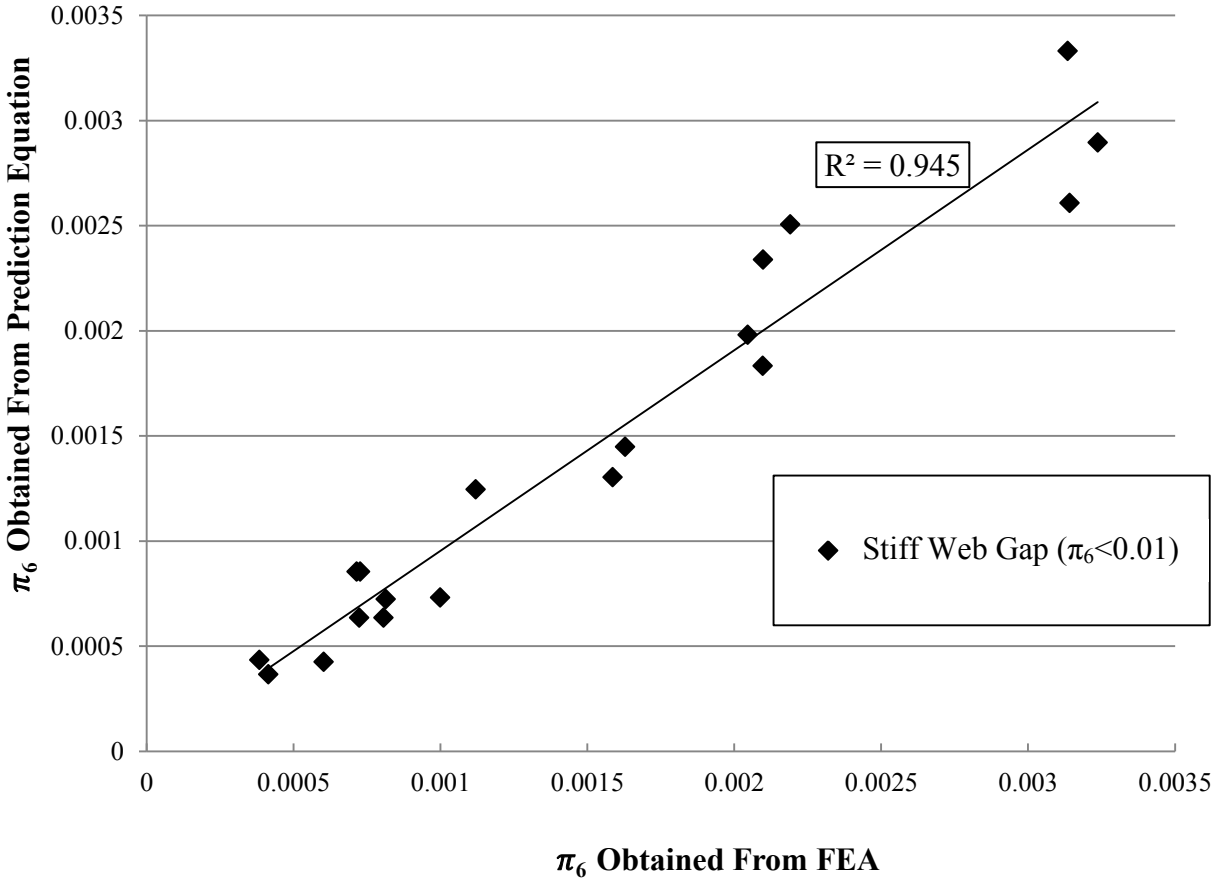

Figure 6- 11: Predicted response by Equation (6-7) versus the response obtained from FEA for stiff web gaps ($\pi_6 < 0.01$).

6.6. Prediction Equation for Flexible Web Gaps ($\pi_6 \geq 0.01$)

When π_6 is greater than 0.01 the torsional and lateral stiffness of the bottom flange does not influence the magnitude of the vertical stress in the web gap. This can be explained as if the web gap is relatively more flexible than bottom flange, the distortion in the web gap is all absorbed in the web gap and the bottom flange does not get exposed to any deflection due to the load from the differential deflection. This is very well observed in the regression analysis. By performing the non-linear regression analysis, the regression coefficients for π_2 and π_3 are very close to

zero. Therefore, it was decided to set these coefficients to zero manually and perform the regression analysis once again to obtain the other unknown coefficients and exponents. These led to even more precise result for the stress prediction. The prediction equation obtained from the regression analysis for $\pi_6 \geq 0.01$ is presented in Equation (6-10) to Equation (6-11). Equation (6-12) is obtained by combining Equation (6-11) and Equation (6-12).

$$\pi_6 = 0.070\ (\pi_1)^{-1.609}\ (\pi_2)^{-0}(\pi_3)^{-0}(\pi_4)^{-1.214}(\pi_5)^{1} \quad (6\text{-}10)$$
$$(For\ \pi_6 \geq 0.01)$$

$$\pi_6 = 0.070\ (\frac{K_{WEB}}{K_{STF}})^{-1.609}(\frac{K_{STF}}{K_{DIA}})^{-1.214}(\frac{\Delta}{g}) \quad (6\text{-}11)$$
$$(For\ \pi_6 \geq 0.01)$$

$$HSS = 7.0\frac{\Delta}{gh}(K_{WEB})^{-0.609}(K_{STF})^{0.395}(K_{DIA})^{1.214} \quad (6\text{-}12)$$
$$(For\ \pi_6 \geq 0.01)$$

where, K_{WEB} is the web plate stiffness, K_{DIA} is the diaphragm stiffness, K_{STF} is the transverse stiffener stiffness, g is the web gap length, Δ is the differential deflection between the adjacent girders under investigation, h is the web plate height, and finally HSS is the hot spot stress in vertical direction in the web gap detail.

Figure 6- 12 represents the comparison between predicted responses by Equation (6-11) and obtained FEA. The regression coefficients (R^2) for the response predicted by Equation (6-11) is 0.99 which indicates that almost all the variation in the response function has been considered and accounted for in the prediction equation.

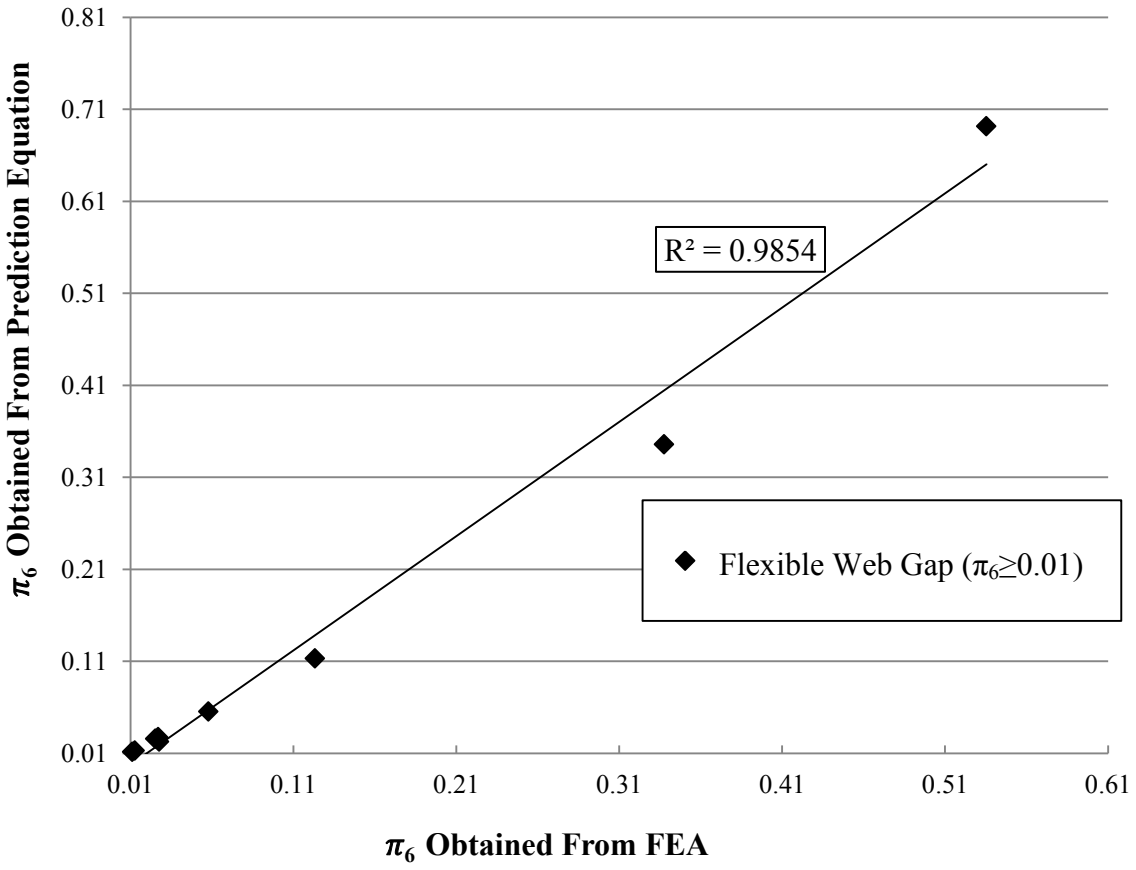

Figure 6- 12 : Predicted response by Equation (6-11) versus the response obtained from FEA for flexible web gaps ($\pi_6 \geq 0.01$).

6.7. Assessment of the Proposed Prediction Equations

The proposed equations (Equation (6-9) and Equation (6-12)) are based on finite element models with some reasonable assumptions. Although the stresses obtained from these equations are in good agreement with the observed stresses from finite element analysis, these equations should be verified against some experimental results and finite element model results available in the literature. Therefore, the results of three research studies available in the literature based on comprehensive experimental tests are used in this section to assess the accuracy of the proposed equations.

The results of the first experimental program used in this section to investigate the proposed equations are obtained from a comprehensive research program conducted at University of Alberta (D'Andrea, Grondin, & Kulak, 2001; Fraser, Grondin, & Kulak, 2000; G. Grondin & Kulak, 2010; G. Y. Grondin, Fraser, & D'Andrea, n.d.). The second experimental result is obtained from a research study performed at University of Kansas (Hartman et al, 2013) and finally the results of a field monitoring and finite element study of a bridge investigated at University of Minnesota (Li & Schultz, 2005) is also used for this purpose. These verifications are presented in the following sections.

The results of the mentioned three experimental and numerical studies are evaluated by stress prediction equations proposed by others as well. These models are presented in Chapter 2 (Fisher (Equation 2-1), Jajich et al. (Equation 2-2), Severtson et al. (Equation 2-4), and Li and Schultz (Equation 2-5)).

6.7.1. Case Study I, Experiments Conducted at University of Alberta

A series of full-scale tests at University of Alberta ((Fraser et al., 2000) and (D'Andrea et al., 2001)) on the specimens obtained from the St. Albert Trail Mile 5.09 Subdivision Bridge was performed to investigate the behaviour of distortion induced fatigue cracks in the steel multi-girder bridges. This Bridge had been replaced with a new structure in 1998 because of the large number of fatigue cracks and the substandard clearance between the roadway and the underside of the bridge. Eight full-size bridge girders with distortion-induced fatigue cracks from field service were tested under constant amplitude cyclic loading. The concrete slab was removed dismantling of the bridge. In order to simulate in the lab the in-situ composite girder properties determined during the field testing, the steel girders were reinforced with a steel wide flange section to bring the neutral axis of the reinforced section to as close as possible to the calculated value of the composite section. Each individual girder was tested with its diaphragms. Therefore, required stiffness to support the free ends of diaphragms was calculated to obtain the stress range and differential displacement in the laboratory test as representative of the field

measured conditions. A total of ten diaphragms were attached to each girder during the laboratory testing. The diaphragms on each side of the girders were staggered, which aggravated the distortion. Two stress ranges of 35 MPa and 50 MPa for midspan bottom fiber were used in their experimental program. LVDTs were mounted beneath the web of the girder and beneath the spring supported end of the diaphragm to measure the differential displacements at each diaphragm. The out of plane web distortion were also measured at the diaphragms located within the constant moment region. Because of limited number of instruments, all the data was not obtained for all the web gap details. In addition, some web gaps were repaired when the bridge was in service and some of them had already cracked. A total of 7 different test results are available from this experimental program which can be used to assess the web gap stress prediction models. They also examined the behavior of the web gap region using finite element analysis. The finite element models were developed and validated using strain measurements and displacements observed during the tests. The ability of the simple beam model used for the derivation of Equation (2-1) to predict the peak stress obtained from a finite element model was assessed through a comparison of stresses obtained from both procedures. They found that simplified calculation based on fixed-ended beam model (Equation 2-1) tend to overestimate the stresses in the web gap region by as much as 400% when the web gap distortion is measured from the experiment. However, it may predict less conservative web gap stresses as the stiffener and tension flange thickness increase. They also numerically investigated the effect of web gap length on the maximum web gap stress and found that increasing the web gap length to double length produced a 50% reduction in vertical stress both at the top and bottom of the web gap.

The dimensions of the model and the results for the vertical stress obtained from both experimental measurements and finite elements investigation is presented in Table 6- 5 and Table 6-6.

Table 6- 5: Geometrical Dimensions Used in the Experimental Program at University of Alberta

Parameters	g	w	h	b_F	t_F	L	S	h_S	t_S	b_s	t_d	h_d
mm	50	9.5	914	254	16	1700	1000	864	10	100	9.5	686

Using differential deflection of 0.31 mm and the equations presented in Chapter 2 the stress in the web gap is calculated and presented in Table 6- 6. As shown in this table, none of the equations predict the results accurately.

Table 6- 6: Comparison of Peak Web Gap Stress Prediction Methods for St. Albert Bridge (University of Alberta)

Peak Web Gap Stress	FE Model Analysis[4]	Fisher (Equation 2-1)	Jajich *et al.* (Equation 2-2)	Severtson *et al.* (Equation 2-4)	Li and Schultz (Equation 2-5)	Field Measurement
σ_{wg} (MPa)	115	457	22	38	33	79

Differential Deflection (Δ) = 0.31 mm.

Using the dimensions from Table 6- 7 and Equation 5-3 to Equation 5-7, K_{WEB}, the web plate stiffness, K_{TBF}, the bottom flange torsional stiffness, K_{LBF}, the bottom flange lateral stiffness, K_{DIA}, the diaphragm stiffness, and K_{STF}, the transverse stiffener stiffness are calculated to obtain the $\pi - parameters$. These results are presented in Table 6-7.

Table 6- 7: Calculated Factors for the Values presented in Table 6-5.

Parameter	Results	Parameter	Results
K_{WEB}	21693	π_1	0.27
K_{TBF}	609534	π_2	1.46
K_{LBF}	81794	π_3	2.03
K_{DIA}	10673	π_4	0.13
K_{STF}	42839341	π_5	0.0062

By using the dimensionless parameters calculated in Table 6-7, Equation 6-8 and Equation 6-10, π_6 and the corresponding HSS are calculated as following. It should be noted that if the calculated π_6 is less than 0.01 then the Equation 6-6 (For $\pi_6 < 0.01$) should be used. Equation 6-10 is chosen first as it has less parameter to calculate and can be obtained faster than Equation 6-6.

[4] G. Grondin & Kulak (2010)

$$\pi_6 = 0.070\ (\pi_1)^{-1.609}\ (\pi_4)^{-1.214}(\pi_5) \quad (6\text{-}10)$$

$(For\ \pi_6 \geq 0.01)$

$$\pi_6 = 0.070\ (0.27)^{-1.609}\ (0.13)^{-1.214}(0.0062)$$

$$= \quad 0.0425$$

$$HSS = \frac{100K_{WEB}}{h}\pi_6 \quad (6\text{-}8)$$

$$HSS = \frac{100 \times (21693)}{914} \times 0.0425$$

$$= \quad 101\ MPa$$

This result is 14 percent less than the stress reported from the finite element analysis by Grondin and Kulak (2010) (115 MPa) and 22 percent greater than the experimental measurements by Fraser *et. al. (2000)* (79 MPa).

6.7.2. Case Study II, Experiments Conducted at University of Kansas

Research at University of Kansas (Hartman et al, 2013) has also been focusing on fatigue performance of web gaps subjected to out-of-plane distortion. This research program mainly investigates the efficiency of different repair and rehabilitation methods on performance of distortion induced fatigue prone details. They also numerically examined the relationships between skew angle, cross-frame spacing, and cross-frame configurations including staggered perpendicular to the girder line as well as parallel to the support skew on distortion induced fatigue susceptibility. It was indicated that several factors such as skew angle of the bridge, lateral brace placement, and geometry of the web gap affect the stresses in the web gap, thus making the stress prediction even more difficult. In addition, there was no clear trend established between skew angle and web-gap stress in their study. In addition, Hartman *et al.* (Hartman et

al., 2010) constructed and tested a 9.1-m (30-ft) long three-girder test bridge (AISI Example 1) spaced at 1.5 m connected with X-type cross frames at the two simple support locations and at mid-span under fatigue loading. The purpose of their study was to investigate the web gap behaviour, and subsequently repair of distortion-induced fatigue cracks. A total of 12 test trials were performed with varying load ranges. Static loading was applied at midspan over the interior girder at rates varying between 1.0 – 2.0 Hz. For each trial test, crack growth, girder deflections as well as strains were monitored and data for girder maximum deflection, girder lateral deflection under different loads, girder maximum bottom flange stress and uncracked and cracked web gap strain as well as crack initiation and propagation life were collected. The results of their first trials for each girder are used to assess the stress prediction models as they were collected before applying any rehabilitation. In order to evaluate the results from this experiments and the predicted stress from the proposed equations, the stiffness of the cross brace for this experimental program is obtained using finite element analysis and the cross brace is replaced with a bend plate diaphragm with the same stiffness.

The dimensions of the model and the results for the vertical stress obtained from both experimental measurements and finite elements investigation as well as models in Chapter 2 are presented in Table 6-8 and Table 6-9.

Table 6- 8: Geometrical Dimensions Used in the Experimental Program at University of Kansas

Parameters	g	w	h	b_F	t_F	L	S	h_S	t_S	b_s	t_d	h_d
mm	45	6	876	279	16	1770	1500	831	10	127	9.5	657

Table 6- 9: Comparison of Peak Web Gap Stress Prediction Methods for Experiment at University of Kansas

Peak Web Gap Stress	FE Model Analysis[5]	Fisher (Equation 2-1)	Jajich *et al.* (Equation 2-2)	Severtson *et al*. (Equation 2-4)	Li and Schultz (Equation 2-5)	Experimental Measurement
σ_{wg} (MPa)	434	1246	43	75	64	183

Deferential Deflection (Δ) = 1.2 mm.

[5] HSS from FEA (Hartman et al (2013))

Using the dimensions from Table 6- 8 and Equation 5-3 to Equation 5-7, K_{WEB}, the web plate stiffness, K_{TBF}, the bottom flange torsional stiffness, K_{LBF}, the bottom flange lateral stiffness, K_{DIA}, the diaphragm stiffness, and K_{STF}, the transverse stiffener stiffness are calculated to obtain the $\pi -$ parameters. These results are presented in Table 6-10.

Table 6- 10: Calculated Factors for the Values presented in Table 6-8.

Parameter	Results	Parameter	Results
K_{WEB}	6828	π_1	0.063
K_{TBF}	331183	π_2	0.47
K_{LBF}	108764	π_3	0.54
K_{DIA}	12533	π_4	0.33
K_{STF}	45194847	π_5	0.0266

Using the dimensionless parameters calculated in Table 6-7, Equation 6-8 and Equation 6-10, π_6 and the corresponding HSS are calculated as following.

$$\pi_6 = 0.070\ (\pi_1)^{-1.609}(\pi_4)^{-1.214}(\pi_5) \quad (6\text{-}10)$$

$(For\ \pi_6 \geq 0.01)$

$$\pi_6 = 0.070\ (0.063)^{-1.609}\ (0.33)^{-1.214}(0.0266)$$

$$= \quad 0.611$$

$$HSS = \frac{100K_{WEB}}{h}\pi_6 \quad (6\text{-}8)$$

$$HSS = \frac{100 \times (6828)}{876} \times 0.611$$

$$= \quad 476\ MP$$

This result is 10 percent higher than the stress reported from the finite element analysis by Hartman et al, (2013) (434 MPa).

6.7.3. Case Study III, Experiments Conducted at University of Minnesota

This study is well reported in Chapter Two and here only the dimensions of the model as well as the results of the study are presented. The dimensions of the finite element model used in this study were based on a bridge which was monitored in the field under service loading condition. These dimensions are presented in Table 6-11.

Table 6- 11: Geometrical Dimensions Used in the Experimental Program at University of Minnesota

Parameters	g	w	h	b_F	t_F	L	S	h_S	t_S	b_s	t_d	h_d
mm	64	13	1000	300	32	1500	2819	936	10	100	10	800

Table 6- 12: Comparison of Peak Web Gap Stress Prediction Methods for Experiment at University of Minnesota

Peak Web Gap Stress	FE Model Analysis[6]	Fisher (Equation 2-1)	Jajich *et al.* (Equation 2-2)	Severtson *et al.* (Equation 2-4)	Li and Schultz (Equation 2-5)	Experimental Measurement
σ_{wg} (MPa)	73	1265	56	98	63	29

Deferential Deflection (Δ) = 1.94 mm.

Stress obtained from their FE model at the location of strain gauges in the field and stress calculated from measured strain in the field are 41 MPa and 37 MPa, respectively. According to Table 6-12, the proposed equation by Li and Schultz (Equation 2-5) predicts the results of FE

[6] Li & Schultz (2005)

analysis accurately. Stress predictions using Equations 2-2 and Equation 2-4 are also in good agreement with the FE results. It should be noted that, these equations are calibrated and developed based on these field data and it is expected to predict the stress reasonably. In contrast, equation proposed by Fisher (Equation 2-1) it is not even close to the results by FE analysis.

Using the dimensions from Table 6- 11 and Equation 5-3 to Equation 5-7, K_{WEB}, the web plate stiffness, K_{TBF}, the bottom flange torsional stiffness, K_{LBF}, the bottom flange lateral stiffness, K_{DIA}, the diaphragm stiffness, and K_{STF}, the transverse stiffener stiffness are calculated to obtain the $\pi - \text{parameters}$ to evaluate the proposed equations in this chapter. These results are presented in Table 6-13.

Table 6- 13: Calculated Factors for the Values presented in Table 6-11.

Parameter	Results	Parameter	Results
K_{WEB}	34481	π_1	0.46
K_{TBF}	210080	π_2	0.17
K_{LBF}	75396	π_3	0.67
K_{DIA}	51200	π_4	0.36
K_{STF}	458752000	π_5	0.03

Using the dimensionless parameters calculated in Table 6-11, Equation 6-8 and Equation 6-10, π_6 and the corresponding HSS are calculated as following.

$$\pi_6 = 0.070\ (\pi_1)^{-1.609}(\pi_4)^{-1.214}(\pi_5) \quad (6\text{-}10)$$

$(For\ \pi_6 \geq 0.01)$

$$\pi_6 = 0.070\ (0.46)^{-1.609}\ (0.36)^{-1.214}(0.03)$$

$$= \quad 0.025$$

$$HS = \frac{100K_{WEB}}{h}\pi_6 \tag{6-8}$$

$$HSS = \frac{100 \times (34481)}{1000} \times 0.025$$

$$= \quad 86 \ MPa$$

This result is 18 percent higher than the stress reported from the finite element analysis by Li & Schultz (2005) (73 MPa).

According to the results obtained from the proposed empirical equations for these three bridges, it can be concluded that these equations can confidently predict the stress at the web gaps in steel multi-girder bridges. In contrast to the available equations proposed by others, the obtained equations in this chapter include the effect of all the parameters in the detail. Although these equations are analytically more complicated than the previously used equations to calculate the stress, they predict the stress in the web gap within 20 percent and cover a wide range of parameters which almost includes all the steel multi-girder bridges with bend plate diaphragm. Considering all the complexity in the web gap details, this is an acceptable accuracy for the stress calculation.

Chapter 7

Summary, Conclusions, and Recommendations

In this chapter, a brief summary of the study, conclusions obtained from the results, and some recommendations for practical application and further researches which can be conducted in this area are presented.

7.1. Summary

In multi-girder steel bridges, to transfer lateral loads and distribute live loads among the girders, diaphragm members are used at the location of transverse stiffeners welded to the girder web. Prior to 1985, connection between these diaphragms connection stiffeners and the girder tension flange was rarely provided to avoid a potential load fatigue prone detail. While applying the traffic load, the diaphragm rotates and this rotation is transferred to this web gap detail and causes distortion in the web plat. This makes the detail susceptible to distortion induced fatigue cracks.

There are two approaches to assess the fatigue life of a detail; Fatigue S-N curves and Fracture Mechanics. Although fracture mechanics can accurately assess any detail, it requires expert's knowledge and sufficient experience. It is also a very challenging and expensive approach when the crack is not 2D and possibly propagates out of the initiation plane as well (cracks with 3D geometry). Using fatigue S-N curves is a straight forward method which has led to acceptable results in fatigue life estimation if and only if the detail matches one of the already available detail categories and the stress range applied to the detail is obtainable. For web gap details there is no distortion induced fatigue curve developed. Even if the fatigue curves were already available for these types of fatigue problems, obtaining the corresponding stress for these

details is a challenge by itself. Obtaining the stress is not possible without using a comprehensive and reliable finite element analysis.

There are several methods and models available to assess the magnitude of the stress in the web gap detail in steel multi-girder bridges. Most of them were developed based on some field measurements for a specific bridge or some experimental tests. Although some of these approaches can predict the stress in the web gap for the identical bridges with the same geometry, they cannot provide reliable results for even slightly different bridge configuration.

At the initial step in this study, the available methods to calculate the magnitude of stress in details prone to distortion induced fatigue were investigated using finite element analysis. This provided a good assessment of the parameters that may influence the behavior of the web gap details and magnitude of the stress in the detail.

Parameters affecting the web gap stress were divided into two categories; Local parameters and Global parameters. Geometrical dimensions of web plate, tension flange, and stiffener directly affect the magnitude of the vertical stress as well as the magnitude of the web gap distortion in the detail. These parameters are considered as local parameters. Global parameters indirectly affect the vertical stress in the web gap details. They play a significant role in the magnitude of the differential deflection which is transformed to the web gap by diaphragm plates or cross frame braces. Girder spacing, deck thickness, span length, angle of skew, and bracing spacing, types, and configurations are grouped as global parameters.

Several finite element modeling techniques using different element types including shell and solid elements were investigated to find the optimum modeling technique which leads to reliable results. A comprehensive finite element model was created based on an experimental program conducted at University of Kansas (Hartman et al, 2013). Steel cyclic material behavior was used in this model which served as a global model in further investigations. Mesh sensitivity analysis is also performed and it was found that using 1 mm mesh size at the web gap and growing mesh density approach provide steady results in calculating HSS.

Fatigue life of the web gap detail in the mentioned experimental program was assessed using fracture mechanics. The initiation life of the detail was obtained using crack initiation material properties presented in Table 4-1 and the maximum vertical stress obtained from the finite

element model. In order to investigate the crack propagation life of the detail, a semi-circle crack with the radius of 0.1 mm is inserted in the weld body and weld toe at the transverse stiffener and web plate weld. These are the locations of maximum vertical stress and the observed location of the crack initiation, respectively. The stress intensity factor was obtained from ABAQUS and the crack propagation procedure was performed in FRANC3D. The fatigue crack propagation life of the detail is obtained using the well-known equation proposed by Paris & Erdogan (1963) and crack propagation material properties presented in Table 4-2.

Almost all the web gap detail dimensions including web thickness, diaphragm spacing, stiffener height, stiffener width, stiffener thickness, tension flange width, tension flange thickness, web gap length deemed to have a significant influence on the magnitude of web gap stress. The influence is understandable and predictable while dealing with only one of these parameters. If these parameters vary at the same time, the influence would be very complicated. To simplify the procedure of the investigation, dimensional analysis using Buckingham Pi theorem was utilized. This led to six dimensionless parameters. These parameters are presented in sections 5.4.1 to 5.4.6.

A series of experiments was designed and conducted using finite element analysis in order to perform a parametric study and investigate the influence of each dimensionless parameter on the magnitude of web gap stress. Using non-linear exponential regression analysis of the obtained data from these experiments, two empirical equations were developed. These proposed equations predict the magnitude of the stress in the web gap. Two experimental test results and a finite element investigation verified the predicted results by these equations. These results were directly compared to FEA results reported in the literature.

7.2. Conclusions

According to a comprehensive investigation of the distortion induced fatigue problems and the results obtained from this study, numerous conclusions have been drawn. Some of these conclusions are presented in the following:

1- Fracture mechanics proved once again that it can be a very powerful and very reliable approach to assess the fatigue life of any details including the ones prone to distortion-induced fatigue cracks. Although fracture mechanics can assess these details accurately, it needs expert knowledge and sufficient experience. It is also a very challenging and expensive approach while dealing with cracks having 3D geometry.

2- Based on the results presented in Chapter 4, the crack propagation mode in the web gap detail is a combination of Mode I, Mode II, and Mode III. Although Mode II and Mode III affect the direction of crack propagation, the governing mode of failure is Mode I which is the opening failure mode. This confirms the previous finding by others.

3- The crack propagates in the web plate but the crack propagation rate in the web thickness direction is much lower than the rate in the girder longitudinal plane. In the assessed web gap detail, the crack did not turn into a complete through thickness crack and eventually stopped prior to be visible from the far side of the transverse stiffener.

4- The available models and equations to predict the web gap stress are based on either limited experimental tests, or field measurements, or finite element results which are only applicable to certain bridge geometry and web gap dimensions. These methods do not take into account the effect of several important parameters which are previously mentioned in this chapter. Therefore, a more comprehensive method considering all the influencing parameters is required to obtain this stress without any experimental test or finite element analysis.

5- It is very expensive and almost impractical to design an experimental program to investigate all the parameters influencing the web gap stress in laboratory with realistic in-situ conditions. Only limited data would be available from these tests which should be full scaled to represent the actual behavior. Therefore, finite element analysis is an alternative to perform the experiments.

6- Finite element model presented in Chapter 3 was verified with the experimental results and served as the global model. This proved the validity of the modeling technique in this study. It was shown that shell element is a powerful tool to model the bridge without

reducing the accuracy of the results. This made the analysis much faster and more efficient in terms of time and computational cost.

7- Material properties represent the real behavior of the detail and directly influence the magnitude of the stress. This is even more significant while assessing the distortion induced fatigue problems as the strain in the detail drastically varies in the detail and the stress concentration is also a concern. Linear elastic material property leads to unrealistic prediction of stress in the web gap details. Therefore, cyclic material properties for steel obtained from a study at University of Alberta were used in this study which provided reasonable and realistic responses in the finite element models.

8- Web plate stiffness, bottom flange stiffness (torsional stiffness and lateral stiffness), diaphragm stiffness, vertical stiffener stiffness, web gap length, magnitude of the differential deflection are shown to have influences in the magnitude of the stress in the detail. These parameters include all the local and global parameters.

9- It was shown that the web gap stiffness has the most significant effect on the magnitude of the stress in the detail. As it is presented in Chapter 6, this parameter governs the overall behavior of the response function (web gap stress).

10- Diaphragm stiffness and transverse stiffener stiffness are also critical parameters while assessing the web gap behavior. These are the members transferring the differential deflection into the web gap and impose out of plane distortion in the web plate. It was revealed that having a flexible diaphragm in steel multi-girder bridges allows the two adjacent girders deflect more independently and as a result lower distortion would be transferred in to the web gap detail through the diaphragm. This decreases the magnitude of the stress in the web gap.

11- While dealing with a relatively rigid web gap located in the bottom of the web plate, the lateral stiffness and torsional stiffness of the bottom flange influence the magnitude of the stress as well. Bottom flange can be assumed as a boundary condition for the web gap plate. If the bottom flange is more flexible, the web gap can distort easier and the magnitude of the stress reduces in the detail.

12- Dimensional analysis is a great approach to investigate the behavior of almost any complex system. Using this method provides a good idea about the relation between all the influencing parameters and the response function. Although in web gap stress calculation problem the effect of each individual parameter can be rationally explained, it is challenging to describe the response when all these parameters are considered simultaneously.

13- Data were generated using finite element analysis of the web gap detail with a reasonable boundary condition explained in Chapter 4. Non-linear exponential regression performed on the data and the stress (σ_{HSS}) is assessed by the following empirical equations:

For the for stiff web gaps ($\pi_6 < 0.01$):

$$\sigma_{HSS} = 16.0\frac{\Delta}{gh}\frac{(K_{STF})^{1.766}}{(K_{WEB})^{-1.147}}\left(\frac{L^2}{1000K_{TBF}}\right)^{-0.124}(K_{LBF})^{0.257}\left(\frac{K_{STF}}{K_{DIA}}\right)^{-0.839} \quad (6\text{-}9)$$

For the for flexible web gaps ($\pi_6 \geq 0.01$):

$$\sigma_{HSS} = 7.0\frac{\Delta}{gh}(K_{WEB})^{-0.609}(K_{STF})^{0.395}(K_{DIA})^{1.214} \quad (6\text{-}12)$$

where, $\pi_6 = \frac{\sigma_{wg}.h}{100K_{WEB}}$, K_{WEB} is the web plate stiffness, K_{TBF} is the bottom flange torsional stiffness, K_{LBF} is the bottom flange lateral stiffness, K_{DIA} is the diaphragm stiffness, K_{STF} is the transverse stiffener stiffness, g is the web gap length, Δ is the differential deflection between the two adjacent girders under investigation, h is the web plate height, L is the transverse stiffener spacing or diaphragm spacing whichever is smaller, and finally HSS is the hot spot stress in vertical direction in the web gap detail.

The average regression coefficients (R^2) for response predicted by these proposed empirical equations is 0.97 which has reasonable accuracy with all the complication in

the web gap stress prediction problem and limited number of experiments. They also predict the results of two experimental tests conducted at University of Alberta and University of Kansas as well as finite element results from the research program at University of Minnesota all within ±20 percent of the observed values. This gives a good confidence in the results obtained from these equations in comparison with other available models presented in Chapter 2.

14- As long as the geometry of the bridge and the web gap detail is available and the differential deflection of the two adjacent girders are measured accurately, the magnitude of the stress can be calculated and used as a nominal stress or hot spot stress to estimate the remaining fatigue life of the detail.

7.3. Recommendations

The proposed equations are developed based on finite element analysis data and can be investigated further by field monitoring and some additional experimental tests which resemble the in-situ condition of the web gap to gain a higher degree of confidence in the results. Although measuring the maximum web gap stress in the field is almost impossible, field monitoring provides the most actual stress at web gap detail considering the in service bridges conditions. These results lead to more realistic finite element models representing the in-situ condition of the bridge from which the hot spot stress can be obtained and used in order to assess the proposed equations.

As it was mentioned in the Chapter 2, angle of skew has shown to have some influence in the differential deflection, web gap distortion and consequently the magnitude of the stress in the web gap detail. This parameter needs to be investigated further and its effect should be included in the general response functions.

These proposed equations are derived for steel multi-girder bridges with bent plate diaphragms as the lateral load resistance system. There are numerous steel bridges with cross braces system instead of bent plate diaphragms. This system of bracing should also be investigated and the stiffness of the cross brace system should be related to an equivalent bent plate in order to use the proposed equations.

These equations provides reliable results for the nominal stress in the web gap detail with a given geometry and loading but even by having these results, the engineers still need to evaluate the fatigue life of the detail. The available fatigue S-N curves are developed for details subjected to stress induced fatigue loadings. A comprehensive study is also required to develop the reliability based method for predicting the fatigue resistance of distortion-induced fatigue details. Although probabilistic models have been developed for stress-induced fatigue cracking, such models are not applicable to distortion induced fatigue.

References:

AASHO, (1965). Standard specifications for highway bridges. American Association of State Highway Officials, Washington, DC, USA.

AASHTO, (2014). Standard specifications for highway bridges. American Association of State Highway Officials, Washington, DC, USA.

Adams, C. A. (2010). Finite Element Study on Bridge Details Susceptible to Distortion-Induced Fatigue.

AISC. (1963). Specifications for the Design, Fabrication and Erection of Structural Steel for Buildings. Including the“ Commentary” and Supplements Thereto as Issued.

Akhlaghi, F. M. A.-E. L. F. (2009). Fatigue testing and analysis of an orthotropic bridge welded detail using structural hot spot stress method. Proc. of the conference Fatigue Design.

Anderson, T. L. (2005). Fracture mechanics: fundamentals and applications. CRC press.

Aygül, M. (2012). Fatigue analysis of welded structures using the finite element method. Chalmers University of Technology.

Aygül, M., Al-Emrani, M., Barsoum, Z. & Leander, J. (2014). Investigation of distortion-induced fatigue cracked welded details using 3D crack propagation analysis. International Journal of Fatigue, 64, 54–66. Elsevier.

Berglund, E. & Schultz, A. E. (2001). Analysis Tools and Rapid Screening Data for Distortional Fatigue in Steel Bridge Girders.

Box, G., Hunter, W. & Hunter, J. (1978). Statistics for experimenters. An introduction to design, data analysis, and model building. Wiley Series in Probability and Mathematical Statistics (USA).

Bridgman, P. W. (1931). Dimensional Analysis. Yale University Press, the University of Michigan.

BSI. (2014). Guide to fatigue design and assessment of steel products (BS 7608.).

Cavazzuti, M. (2012). Optimization Methods: From Theory to Design Scientific and Technological Aspects in Mechanics. Springer Science \& Business Media.

Chen, H., Grondin, G. Y. & Driver, R. G. (2005). Fatigue Resistance of High Performance Steel.

Connor, R. J. & Fisher, J. W. (2006). Identifying effective and ineffective retrofits for distortion fatigue cracking in steel bridges using field instrumentation. Journal of Bridge Engineering, 11(6), 745–752.

CSA-S6. (2006). Canadian highway bridge design code (CSA-S6-06). Canadian Standards Association.

CSA-S6. (2014). Canadian highway bridge design code (CSA-S6-14). Canadian Standards Association.

D'Andrea, M., Grondin, G. Y. & Kulak, G. L. (2001). Behaviour and Rehabilitation of Distortion-Induced Fatigue Cracks in Bridge Girders. Department of Civil and Environmental Engineering, University of Alberta.

Darcy, H. 1857. Recherches Experimentales Relatives au Mouvement de L'Eau dans les Tuyaux, 2 volumes, Mallet-Bachelier, Paris. 268 pages and atlas. ("Experimental Research Relating to the Movement of Water in Pipes")

DiBattista, J. D. (2002). Behaviour of sleeper-supported line pipe. PhD, Thesis, University of Alberta, Edmonton, Alberta.

Fayard, J.-L., Bignonnet, A. & Van, K. D. (1996). Fatigue design criterion for welded structures. Fatigue \& Fracture of Engineering Materials \& Structures, 19(6), 723–729. Wiley Online Library.

Fisher JW. Fatigue cracking in bridges from out-of-plane displacements. Canadian Journal of Civil Engineering. 1978;5(4):542–556.

Fisher JW. Distortion-induced fatigue cracking in steel bridges. Transportation Research Board; 1990.

Fraser, R. E., Grondin, G. Y. & Kulak, G. L. (2000). DISTORTION-INDUCED FATIGUE CRACKS IN BRIDGE GIRDERS.

Gagnon, M., V. Gaudreault, and D. Overton (2008) "Age of Public Infrastructure: A Provincial Perspective" Report 11-621-MIE-067, Investment and Capital Stock Division, Statistics Canada.

Griffith, A. A. (1921). The phenomena of rupture and flow in solids. Philosophical transactions of the royal society of london. Series A, containing papers of a mathematical or physical character, 163–198. JSTOR.

Grondin, G. & Kulak, G. (2010). Distortion-induced fatigue cracking of bridge girders-design issues. Structures Congress 2010 (pp. 484–495).

Grondin, G. Y., Fraser, R. & D'Andrea, M. (n.d.). TESTING AND EVALUATION OF FATIGUE DAMAGED GIRDERS.

Harris, D. (1995). Probabilistic fracture mechanics. Probabilistic structural mechanics handbook (pp. 106–145). Springer.

Hartman et al, H. (2013). Analytical and Experimental Investigation for Distortion-Induced Fatigue in Steel Bridges. University of Kansas.

Hartman, A. S., Hassel, H. L., Adams, C. A., Bennett, C. R., Matamoros, A. B. & Rolfe, S. T. (2010). Effects of Cross-Frame Placement and Skew on Distortion-Induced Fatigue in Steel Bridges. Transportation Research Record: Journal of the Transportation Research Board, 2200(1), 62–68.

Irwin, G. (1965). Onset of fast crack propagation in high strength steel and aluminum. Proc. Sec. Sagamore Conf (Vol. 2, pp. 289–305).

Jajich, D., Schultz, A. E., Bergson, P. M. & Galambos, T. V. (2000). Distortion-induced fatigue in multi-girder steel bridges.

Josi, G. & Grondin, G. Y. (2010). Reliability-Based Management of Fatigue Failures.

Khuri, A. I. & Cornell, J. A. (1996). Response Surfaces: Designs and Analyses (2nd Edition, Vol. 152). Marcel Dekker Inc., New York, New York.

Klesnil, M. and Lukas, P., "Influence of Strength and Stress History on Growth and Stabilisation of Fatigue Cracks." Engineering Fracture Mechanics, Vol. 4, 1972, PP. 77-92.

Li, H. & Schultz, A. E. (2005). Analysis of Girder Differential Deflection and Web Gap Stress for Rapid Assessment of Distortional Fatigue in Multi-Girder Steel Bridges.

Minervino, C. S. B., Moses, F., Mertz, D. & Edberg, W. (2004). AASHTO guide manual for load and resistance factor rating of highway bridges. Journal of Bridge Engineering (Vol. 9, pp. 43–54). American Society of Civil Engineers.

Niemi, E. (1995). Stress determination for fatigue analysis of welded components. Woodhead Publishing.

Paris, P. & Erdogan, F. (1963). A critical analysis of crack propagation laws. Journal of Fluids Engineering, 85(4), 528–533. American Society of Mechanical Engineers.

Severtson, B., Beukema, F. & Schultz, A. E. (2004). Rapid Assessment of Distortional Stresses in Multi-Girder Steel Bridges. Minnesota Department of Transportation, Research Services Section.

Shifferaw, Y. & Fanous, F. (2013). Field testing and finite element analysis of steel bridge retrofits for distortion-induced fatigue. Engineering Structures, 49, 385–395.

Stephens, R. I., Fatemi, A., Stephens, R. R. & Fuchs, H. O. (2000). Metal fatigue in engineering. John Wiley \& Sons.

Taylor, E. (1974). Dimensional Analysis for Engineers. Clarendon Press, Oxford, UK.

Wang .Y, Y. (2010). Fatigue Repair Technique Investigation-Hole Drilling and Expansion Method, PhD Thesis, Department of Civil and Environmental Engineering, University of Alberta, Edmonton, Canada.

Yoda, M. (1980). The J-integral fracture toughness for mode II. International Journal of Fracture, 16(4), R175–R178. Springer.

Zhao, Y. & Kim Roddis, W. (2007). Fatigue Behavior and Retrofit Investigation of Distortion-Induced Web Gap Cracking 1. Journal of Bridge Engineering, 12(6), 737–745.

Appendix A

Obtaining the Web Plate Stiffness using Shell and Plate Theory

In this appendix, the stiffness of the web plate is obtained using shell and plate theory.

Assume a thin plate which is simply supported at all edges and a concentrated load, Q, is applied on a finite area (u×v) at the shown location in Figure A.A- 1.

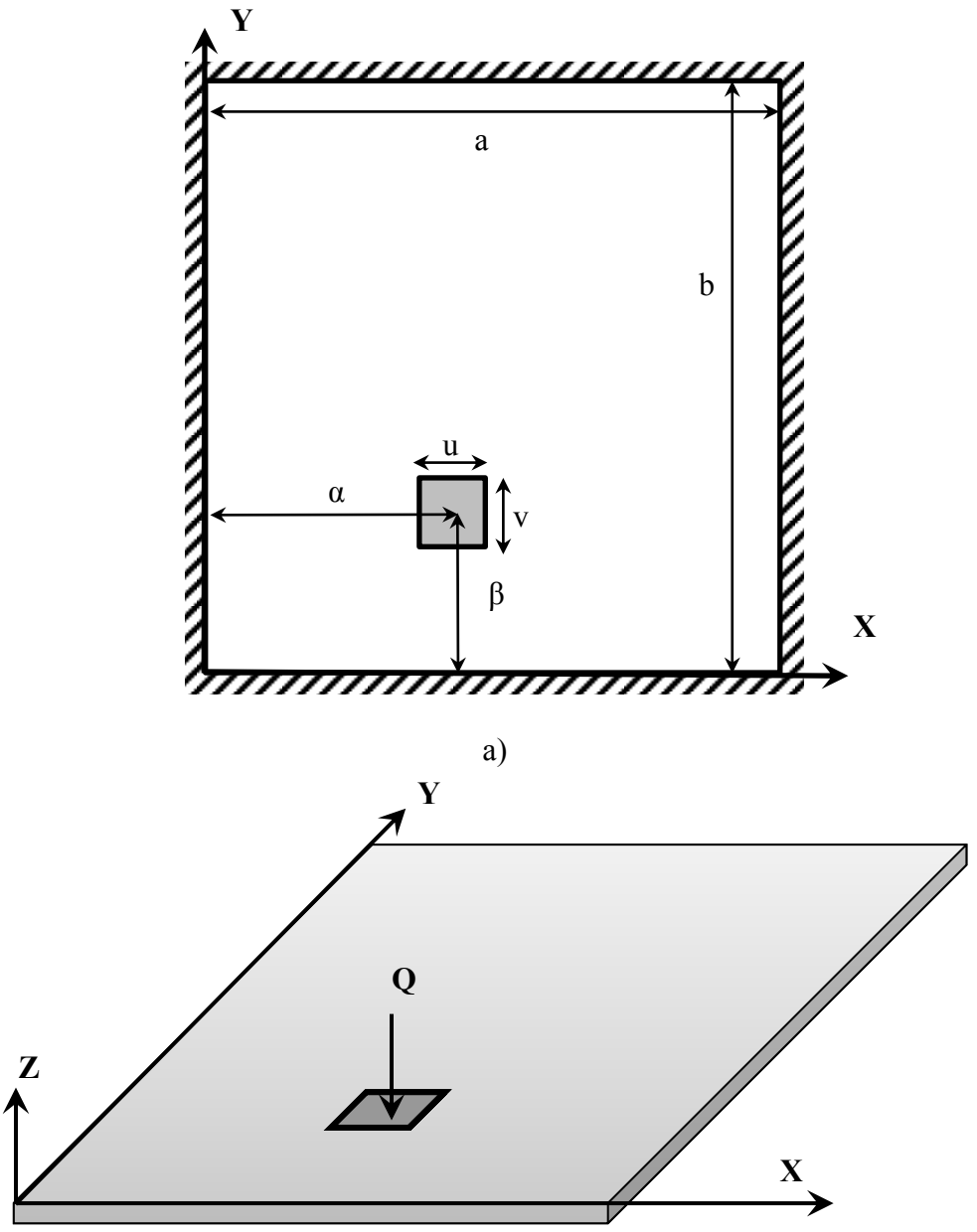

Figure A.A- 1: a) Thin Plate boundary conditions. b) Location of the point load.

Energy method is used to calculate the distortion of the plate under the point load, Q. In order to obtain this distortion, the concentrated load is presented in the Sinusoidal format using Fourier series. This procedure is presented in the following.

$$q(x,y)=\frac{Q}{uv} \quad \Rightarrow \quad \begin{cases} \alpha-\frac{u}{2}\le x\le \alpha+\frac{u}{2} \\ \beta-\frac{v}{2}\le y\le \beta+\frac{v}{2} \end{cases} \quad \Rightarrow \quad q(x,y)=\sum_{m=1}^{\infty}\sum_{n=1}^{\infty} q_{mn} Sin\left(\frac{m\pi x}{a}\right) Sin\left(\frac{n\pi y}{b}\right)$$

Let's assume that the concentrated load is uniformly distributed in X-axis direction with magnitude of $\frac{Q}{u}$ and in Y-axis with the magnitude of $\frac{1}{v}$. Therefore, the loading can be defined as $q(x,y)$ which is presented in the following form.

$$\left.\begin{aligned} q(x)&=\frac{Q}{u} \\ q(y)&=\frac{1}{v} \end{aligned}\right\} \quad \Rightarrow \quad q(x,y)=q(x)\times q(y)=\frac{Q}{u}\times\frac{1}{v}=\frac{Q}{uv}$$

Using Fourier series it can be rewritten as:

$$\left.\begin{aligned} q(x)&=\sum_{m=1}^{\infty} q_m\, Sin\left(\frac{m\pi x}{a}\right) \\ q(y)&=\sum_{n=1}^{\infty} q_n\, Sin\left(\frac{n\pi y}{b}\right) \end{aligned}\right\} \quad \Rightarrow \quad q(x,y)=\sum_{m=1}^{\infty}\sum_{n=1}^{\infty} q_{mn} Sin\left(\frac{m\pi x}{a}\right) Sin\left(\frac{n\pi y}{b}\right)$$

$$q_{mn}=\frac{4Q}{abuv}\left[-\frac{a}{m\pi}Cos\left(\frac{m\pi x}{a}\right)\right]_{\alpha-\frac{u}{2}}^{\alpha+\frac{u}{2}}\times\left[-\frac{b}{n\pi}Cos\left(\frac{n\pi y}{b}\right)\right]_{\beta-\frac{v}{2}}^{\beta+\frac{v}{2}}\quad\Rightarrow$$

$$\frac{4Q}{mnuv\pi^2}\left[Cos\left(\frac{m\pi\left(\alpha+\frac{u}{2}\right)}{a}\right)-Cos\left(\frac{m\pi\left(\alpha-\frac{u}{2}\right)}{a}\right)\right]\times\left[Cos\left(\frac{n\pi\left(\beta+\frac{v}{2}\right)}{b}\right)-Cos\left(\frac{n\pi\left(\beta-\frac{v}{2}\right)}{b}\right)\right]$$

$$\frac{4Q}{mnuv\pi^2}\left[2Sin\left(\frac{m\pi\alpha}{a}\right)Sin\left(\frac{m\pi u}{2a}\right)\right]\times\left[2Sin\left(\frac{n\pi\beta}{b}\right)Sin\left(\frac{n\pi v}{2b}\right)\right]\quad\Rightarrow$$

$$q_{mn}=\frac{16Q}{mnuv\pi^2}Sin\left(\frac{m\pi\alpha}{a}\right)\times Sin\left(\frac{m\pi u}{2a}\right)\times Sin\left(\frac{n\pi\beta}{b}\right)\times Sin\left(\frac{n\pi v}{2b}\right)$$

To have the concentrated load *u* and *v* should approach to Zero.

$$Lim_{u,v\to 0}\quad q_{mn}=\frac{16Q}{mnuv\pi^2}Sin\left(\frac{m\pi\alpha}{a}\right)\times Sin\left(\frac{m\pi u}{2a}\right)\times Sin\left(\frac{n\pi\beta}{b}\right)\times Sin\left(\frac{n\pi v}{2b}\right)\quad\Rightarrow$$

$$q_{mn}=\frac{16Q}{mnuv\pi^2}Sin\left(\frac{m\pi\alpha}{a}\right)\times\frac{m\pi u}{2a}\times Sin\left(\frac{n\pi\beta}{b}\right)\times\frac{n\pi v}{2b}\quad\Rightarrow q_{mn}=\frac{4Q}{ab}Sin\left(\frac{m\pi\alpha}{a}\right)\times Sin\left(\frac{n\pi\beta}{b}\right)$$

$\Rightarrow$

$$\boxed{q(x,y)=\sum_{m=1}^{\infty}\sum_{n=1}^{\infty}\frac{4Q}{ab}Sin\left(\frac{m\pi\alpha}{a}\right)Sin\left(\frac{n\pi\beta}{b}\right)Sin\left(\frac{m\pi x}{a}\right)Sin\left(\frac{n\pi y}{b}\right)}$$

As it was mentioned previously, pin supports are assumed as the boundary condition for all the plate edges. These boundary conditions are shown in the following.

$$@\ x=0\ ,\ x=a\ \Rightarrow\ w=0\ ,\ \frac{d^2w}{dx^2}=0$$

$$@\ y=0\ ,\ y=a\ \Rightarrow\ w=0\ ,\ \frac{d^2w}{dy^2}=0$$

where, w is the distortion or deflection of the plate in Z-axis direction. Therefore, by means of Fourier series the best function that satisfies the boundary conditions and presents the deflection of the plate would be:

$$w(x,y)=\sum_{m=1,3}^{\infty}\sum_{n=1,3}^{\infty}w_{mn}\,Sin\left(\frac{m\pi x}{a}\right)Sin\left(\frac{n\pi y}{b}\right)$$

Potential energy for the system can is the difference between strain energy and the total work done on the system. Using this concept, the deflection of the plate can be obtained as a function of the applied load.

$$T=U-V$$

where, T is the potential energy for the system, U is the strain energy, and V is the total work done on the system. These values are defined as following:

$$U=\frac{D}{2}\int_0^a\int_0^b\left\{\left(\frac{\partial^2w}{\partial x^2}+\frac{\partial^2w}{\partial y^2}\right)^2-2(1-\nu)\left[\left(\frac{\partial^2w}{\partial x^2}\cdot\frac{\partial^2w}{\partial y^2}\right)-\left(\frac{\partial^2w}{\partial x\partial y}\right)^2\right]\right\}dx\,dy$$

$$V=\int_0^a\int_0^b w.q.dx\,dy$$

where, D is the flexural rigidity or is called the bending stiffness coefficient. D and the partial derivatives are defined as following:

$$D = \frac{Et^3}{12\left(1-\nu^2\right)}$$

$$\frac{\partial w}{\partial x} = \sum_{m=1}^{\infty}\sum_{n=1}^{\infty} w_{mn}\left(\frac{m\pi}{a}\right)Cos\left(\frac{m\pi x}{a}\right)Sin\left(\frac{n\pi y}{b}\right),$$

$$\frac{\partial^2 w}{\partial x^2} = \sum_{m=1}^{\infty}\sum_{n=1}^{\infty} w_{mn}\left(-\frac{m^2\pi^2}{a^2}\right)Sin\left(\frac{m\pi x}{a}\right)Sin\left(\frac{n\pi y}{b}\right),$$

$$\frac{\partial w}{\partial y} = \sum_{m=1}^{\infty}\sum_{n=1}^{\infty} w_{mn}\left(\frac{n\pi}{b}\right)Sin\left(\frac{m\pi x}{a}\right)Cos\left(\frac{n\pi y}{b}\right),$$

$$\frac{\partial^2 w}{\partial y^2} = \sum_{m=1}^{\infty}\sum_{n=1}^{\infty} w_{mn}\left(-\frac{n^2\pi^2}{b^2}\right)Sin\left(\frac{m\pi x}{a}\right)Sin\left(\frac{n\pi y}{b}\right),$$

$$\frac{\partial^2 w}{\partial x\,\partial y} = \sum_{m=1}^{\infty}\sum_{n=1}^{\infty} w_{mn}\left(\frac{mn\pi^2}{ab}\right)Cos\left(\frac{m\pi x}{a}\right)Cos\left(\frac{n\pi y}{b}\right),$$

$$U = \frac{D}{2}\int_0^a\int_0^b\left\{\left(\frac{\partial^2 w}{\partial x^2}+\frac{\partial^2 w}{\partial y^2}\right)^2 - 2(1-\nu)\left[\left(\frac{\partial^2 w}{\partial x^2}\cdot\frac{\partial^2 w}{\partial y^2}\right)-\left(\frac{\partial^2 w}{\partial x\partial y}\right)^2\right]\right\}dx\,dy \quad \Rightarrow$$

$$\frac{D}{2}\int_0^a\int_0^b\sum_{m=1}^{\infty}\sum_{n=1}^{\infty}\left\{ {w_{mn}}^2\pi^4\left(\frac{m^2}{a^2}+\frac{n^2}{b^2}\right)^2 Sin^2\left(\frac{m\pi x}{a}\right)Sin^2\left(\frac{n\pi y}{b}\right) - 2(1-\nu)\left({w_{mn}}^2\pi^4\frac{m^2n^2}{a^2b^2}\right)\right.$$

$$\left.\left(Sin^2\left(\frac{m\pi x}{a}\right)Sin^2\left(\frac{n\pi y}{b}\right) - Cos^2\left(\frac{m\pi x}{a}\right)Cos^2\left(\frac{n\pi y}{b}\right)\right)\right\} \Rightarrow$$

$$\frac{D}{2}\sum_{m=1}^{\infty}\sum_{n=1}^{\infty} {w_{mn}}^2\pi^4\left(\frac{m^2}{a^2}+\frac{n^2}{b^2}\right)^2\times\frac{a}{2}\times\frac{b}{2} - 2(1-\nu)\left({w_{mn}}^2\pi^4\frac{m^2n^2}{a^2b^2}\right)\left(\frac{a}{2}\times\frac{b}{2}-\frac{a}{2}\times\frac{b}{2}\right) \Rightarrow$$

$$U = \sum_{m=1}^{\infty}\sum_{n=1}^{\infty}\frac{ {w_{mn}}^2\pi^4 D\,a\,b}{8}\left(\frac{m^2}{a^2}+\frac{n^2}{b^2}\right)^2$$

The total work done on the system is also defined here:

$$V=\int_0^a\int_0^b w.q.dx\,dy \quad\Rightarrow\quad \int_0^a\int_0^b\sum_{m=1}^{\infty}\sum_{n=1}^{\infty} w_{mn}\,\frac{4Q}{ab}\,Sin\left(\frac{m\pi\alpha}{a}\right)Sin\left(\frac{n\pi\beta}{b}\right)Sin^2\left(\frac{m\pi x}{a}\right)Sin^2\left(\frac{n\pi y}{b}\right) \quad\Rightarrow$$

$$\sum_{m=1}^{\infty}\sum_{n=1}^{\infty} w_{mn}\,\frac{4Q}{ab}\,Sin\left(\frac{m\pi\alpha}{a}\right)Sin\left(\frac{n\pi\beta}{b}\right)\times\frac{a}{2}\times\frac{b}{2} \quad\Rightarrow\quad V=\sum_{m=1}^{\infty}\sum_{n=1}^{\infty} w_{mn}Q\,Sin\left(\frac{m\pi\alpha}{a}\right)Sin\left(\frac{n\pi\beta}{b}\right)$$

$$T=U-V \quad\Rightarrow\quad T=\sum_{m=1}^{\infty}\sum_{n=1}^{\infty}\frac{{w_{mn}}^2\pi^4 D\,a\,b}{8}\left(\frac{m^2}{a^2}+\frac{n^2}{b^2}\right)^2-\sum_{m=1}^{\infty}\sum_{n=1}^{\infty} w_{mn}Q\,Sin\left(\frac{m\pi\alpha}{a}\right)Sin\left(\frac{n\pi\beta}{b}\right)$$

To calculate the plate deflection ($w(x,y)$), the potential energy for the system should be minimized. Therefore, $\frac{\partial T}{\partial w_0}=0$.

$$\frac{\partial T}{\partial w_0}=0 \quad\Rightarrow\quad \sum_{m=1}^{\infty}\sum_{n=1}^{\infty}\frac{w_{mn}\pi^4 D\,a\,b}{4}\left(\frac{m^2}{a^2}+\frac{n^2}{b^2}\right)^2-\sum_{m=1}^{\infty}\sum_{n=1}^{\infty} Q\,Sin\left(\frac{m\pi\alpha}{a}\right)Sin\left(\frac{n\pi\beta}{b}\right)=0 \quad\Rightarrow$$

$$w_{mn}=\frac{4Q}{D\,ab\pi^4\left(\frac{m^2}{a^2}+\frac{n^2}{b^2}\right)^2}\,Sin\left(\frac{m\pi\alpha}{a}\right)Sin\left(\frac{n\pi\beta}{b}\right) \quad\Rightarrow$$

$$\boxed{w(x,y)=\sum_{m=1}^{\infty}\sum_{n=1}^{\infty}\frac{4QSin\left(\frac{m\pi\alpha}{a}\right)Sin\left(\frac{n\pi\beta}{b}\right)}{D\,ab\pi^4\left(\frac{m^2}{a^2}+\frac{n^2}{b^2}\right)^2}\,Sin\left(\frac{m\pi x}{a}\right)Sin\left(\frac{n\pi y}{b}\right)}$$

$w(x,y)$ is the deflection of the plate under a consecrated load (Q) at coordinate of (x,y).

In web gap detail, the load is applied from stiffener and it cannot be simplified as a point load at the tip of the transverse stiffener. It has maximum value at this location but it decreases along the transverse stiffener. This condition is shown in

Figure A.A- 2. In this figure, *L* is the diaphragm spacing or the distance between the adjacent stiffeners, whichever is the smallest.

The geometry of the web gap detail as well as the local coordinate system used for the loading is shown in Figure A.A- 3.

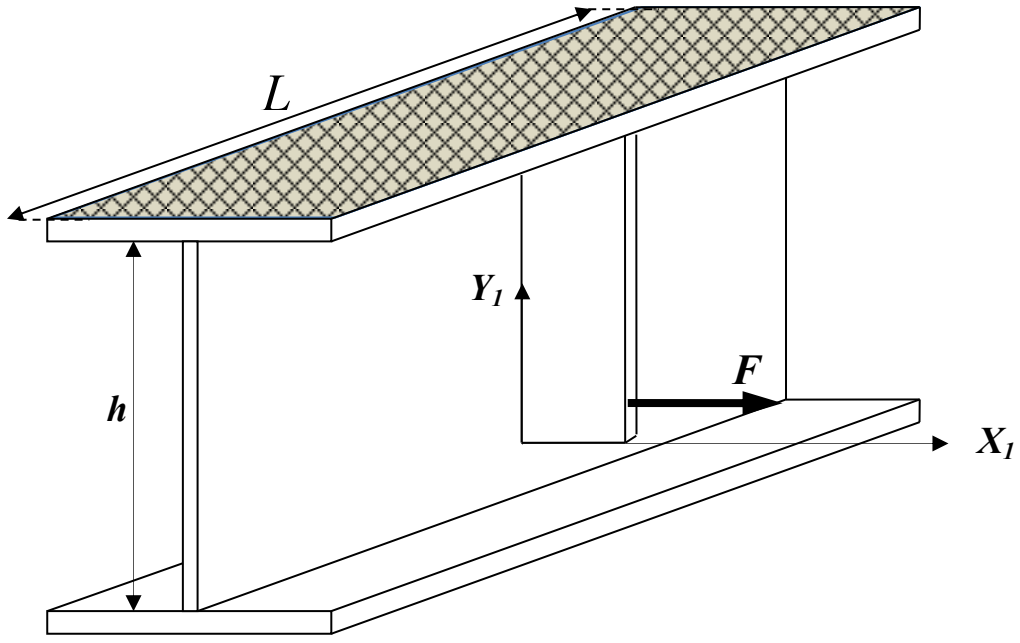

Figure A.A- 2: Loading of the web plate and the location of the transverse stiffener.

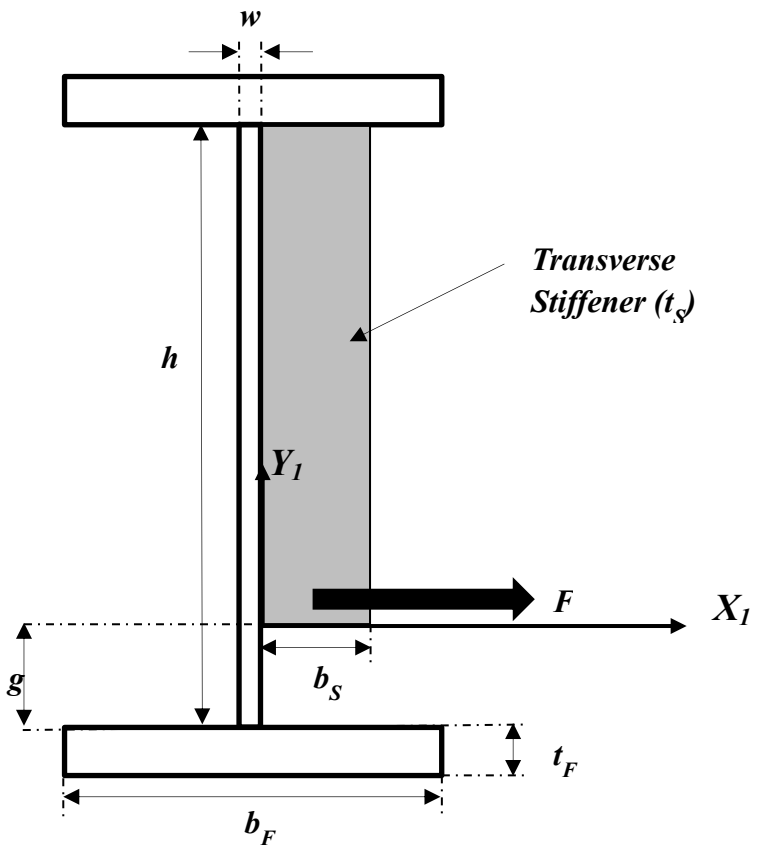

Figure A.A- 3: Web gap detail and web plate dimensions.

The applied load from the transverse stiffener can be assumed as an exponential function which is defined in the following:

$$F(Y_1) = C \times e^{(Y_1)}$$

$$\left.\begin{array}{l} q(x) = 1 \\ q(y) = \dfrac{F(Y_1)}{t_s} \end{array}\right\} \quad \Rightarrow \quad q(x,y) = q(x) \times q(y) = 1 \times \frac{F(Y_1)}{t_s} = \frac{F(Y_1)}{t_s} = \frac{C \times e^{(Y_1)}}{t_s}$$

where, C is the load constant. Using Fourier series the load is presented in terms of Sinusoidal functions for a plate with dimensions of $L \times h$.

$$\left.\begin{aligned} q(x) &= \sum_{m=1}^{\infty} q_m \, Sin\left(\frac{m\pi x}{L}\right) \\ q(y) &= \sum_{n=1}^{\infty} q_n \, Sin\left(\frac{n\pi y}{h}\right) \end{aligned}\right\} \quad \Rightarrow \quad q(x,y) = \sum_{m=1}^{\infty}\sum_{n=1}^{\infty} q_{mn} Sin\left(\frac{m\pi x}{L}\right) Sin\left(\frac{n\pi y}{h}\right)$$

$$\left.\begin{aligned} q_m &= \frac{2}{L}\int_{\alpha-\frac{t_s}{2}}^{\alpha+\frac{t_s}{2}} \frac{F(Y_1)}{t_w} \times Sin\left(\frac{m\pi x}{L}\right) dx \\ q_n &= \frac{2}{h}\int_0^h 1 \times Sin\left(\frac{n\pi y}{h}\right) dy \end{aligned}\right\} \Rightarrow q_{mn} = q_m q_n \Rightarrow q_{mn} = \frac{4}{Lh}\int_{\alpha-\frac{t_s}{2}}^{\alpha+\frac{t_s}{2}}\int_0^h \frac{F(Y_1)}{t_s} Sin\left(\frac{m\pi x}{L}\right) Sin\left(\frac{n\pi y}{h}\right) dx\, dy$$

and $\alpha = \frac{L}{2}$.

Using integration of the load along the transverse stiffener (***Y1***) and calculating the deflection of the web plate at the transverse stiffener tip location (***X1=0***,***Y1=0***) for each load increment, the total deflection of the web plate can be obtained. These steps are shown in the following:

$$w(x,y)_{F(Y_1)} = \sum_{m=1}^{\infty}\sum_{n=1}^{\infty} \frac{4\frac{F(Y_1)}{t_s} Sin\left(\frac{m\pi\alpha}{a}\right) Sin\left(\frac{n\pi\beta}{b}\right)}{Dab\pi^4\left(\frac{m^2}{a^2}+\frac{n^2}{b^2}\right)^2} Sin\left(\frac{m\pi x}{a}\right) Sin\left(\frac{n\pi y}{b}\right)$$

where, $w(x,y)_{(Y_1)}$ is the deflection of the web plate under $F(Y_1)$ at location (x,y) .

To obtain the total deflection the integral should be taken for the above equation for point $\left(x = \frac{L}{2}, y = g\right)$.

$$w(x,y)_{F(Y_1)} = \int \left[\sum_{m=1}^{\infty}\sum_{n=1}^{\infty} \frac{4\dfrac{F(Y_1)}{t_s} Sin\left(\dfrac{m\pi\alpha}{a}\right) Sin\left(\dfrac{n\pi\beta}{b}\right)}{Dab\pi^4\left(\dfrac{m^2}{a^2}+\dfrac{n^2}{b^2}\right)^2} Sin\left(\frac{m\pi x}{a}\right) Sin\left(\frac{n\pi y}{b}\right) \right] dY_1$$

In this equation, $\alpha = g, \beta = \dfrac{L}{2}, a = h,$ and $b = L$.

By setting $m = 1$, 3, and $n = 1$, 3 which is the first two term of the series, the mentioned integration and the stiffness of the web plate can be defined as following the following:

$$K = \frac{Load}{Displacment} \rightarrow K_{Web} = \frac{F(Y_1)}{w(x,y)_{F(Y_1)}}$$

$$K_{Web} = \frac{DhL\pi^4\left(\dfrac{1}{h^2}+\dfrac{1}{L^2}\right)^2}{4Sin\left(\dfrac{\pi}{2}\right)Sin\left(\dfrac{\pi g}{h}\right)Sin\left(\dfrac{\pi}{2}\right)Sin\left(\dfrac{\pi g}{h}\right)} + \frac{DhL\pi^4\left(\dfrac{9}{h^2}+\dfrac{9}{L^2}\right)^2}{4Sin\left(\dfrac{3\pi}{2}\right)Sin\left(\dfrac{3\pi g}{h}\right)Sin\left(\dfrac{3\pi}{2}\right)Sin\left(\dfrac{3\pi g}{h}\right)}$$

The following trigonometric identity is used in order to simplify the web gap stiffness.

$$Sin(3\theta) = 3Sin\theta - 4Sin^3\theta$$

$$K_{Web} = \frac{DhL\pi^4\left(\dfrac{h^2+L^2}{h^2L^2}\right)^2}{4Sin^2\left(\dfrac{\pi g}{h}\right)\left(1+\dfrac{1}{81}(3-4Sin^2(\dfrac{\pi g}{h}))^2\right)} \qquad \text{and,} \quad D = \frac{Ew^3}{12(1-\nu^2)}$$

where, w is the web thickness.

The Term $\left[\frac{12(1-\nu^2)}{81}(3-4Sin^2(\frac{\pi g}{h}))^2\right]$ can be neglected in the equation only to simplify the web gap stiffness equation.

$$K_{Web} = \frac{\pi^4}{4}\frac{Ew^3\left(h^2+L^2\right)^2}{h^3L^3Sin^2\left(\frac{\pi g}{h}\right)}$$

Appendix B

FE Models Dimensions for the Screening Study

Table A.B.1: Models Dimensions for the Screening Study.

Model	Base	1	2	3	4	5	6	7	8	9	10
g	40	85	45	40	40	46	27	64	32	40	40
w	25	10	25	18	25	25	20	24	25	25	25
h	1231	1170	777	946	1128	1099	998	1365	600	1231	1231
b_F	618	628	841	250	664	703	456	435	435	618	618
t_F	43	43	58	60	30	31	42	30	30	43	43
L	2004	6754	2933	1274	1929	1665	1744	1730	1078	2004	2004
S	1200	3600	1200	1991	1913	1416	1456	1200	1200	1200	1200
h_S	1191	1084	732	906	1088	1053	971	1301	568	1191	1191
t_S	45	27	33	29	45	20	23	16	42	45	45
b_S	231	194	108	100	206	323	369	262	176	231	231
t_d	10	20	10	10	19	11	15	20	20	10	10
h_d	937	1053	616	733	922	848	898	1195	500	937	937
Δ	0.40	0.85	0.45	0.40	0.40	0.46	0.27	0.64	0.32	0.20	0.79
K_{WEB}	627229	17376	683423	226650	611993	461360	677047	238197	983226	627229	627229
K_{DIA}	784036	434407	427139	283313	764991	576700	846310	2381974	655484	784036	784036
K_{STF}	627229	347525	341712	226650	611993	461360	677048	238197	983226	627229	627229
K_{LBF}	250892	6951	273369	90660	244797	461360	150455	95279	393290	250892	250892
K_{TBF}	1678764802	528397222	3920120568	2966857890	650649019	852675183	1372369582	475207561	762048247	1678764802	1678764802
π_1	1.00	0.05	2.00	1.00	1.00	1.00	1.00	1.00	1.00	1.00	1.00
π_2	1.50	1.50	1.50	0.12	3.50	1.50	1.50	1.50	1.50	1.50	1.50
π_3	2.50	2.50	2.50	2.50	2.50	1.00	4.50	2.50	2.50	2.50	2.50
π_4	0.80	0.80	0.80	0.80	0.80	0.80	0.80	0.10	1.50	0.80	0.80
π_5	0.01	0.01	0.01	0.01	0.01	0.01	0.01	0.01	0.01	0.005	0.02

Appendix C

FE Models Dimensions and the FEA Results for the Parametric Study

(The Design of Experiment)

M1 to M18 represent Model 1 to Model 18 in the parametric study, respectively.

Table A.C.1: Models Dimensions for the Parametric Study.

Model	M1	M2	M3	M4	M5	M6	M7	M8	M9
g	92	90	80	61	24	41	27	21	50
w	13	25	25	23	17	14	13	17	22
h	1445	1419	1073	735	737	1183	879	714	622
b_F	291	474	495	332	519	262	250	385	389
t_F	45	33	30	51	36	16	60	36	60
L	2406	2429	2690	1196	1650	1222	1370	1398	1369
S	1200	1212	1279	1748	1200	1200	1458	1200	3600
h_S	1354	1329	993	674	713	1142	853	692	572
t_S	13	45	45	17	27	12	11	23	11
b_S	201	400	400	121	201	190	100	138	100
t_d	10	10	13	10	10	18	20	10	10
h_d	1267	1246	966	616	553	937	786	609	466
Δ	0.92	0.90	0.80	0.61	0.24	0.41	0.27	0.21	0.50
K_{WEB}	15932	121164	168185	218225	556669	141307	182342	672837	275256
K_{DIA}	1327676	1262128	934359	272781	371113	1413065	911708	420523	91752
K_{STF}	132750	1009427	1401345	218225	556669	141307	91171	336419	137628
K_{LBF}	15932	48466	37374	218225	222668	31401	72937	149519	275256
K_{TBF}	768583790	476514465	347751728	2600751273	1010631072	60323989	2759348955	876842416	4296058663
π_1	0.12	0.12	0.12	1	1	1	2	2	2
π_2	0.12	1.5	3.5	0.12	1.5	3.5	0.12	1.5	0.12
π_3	1	2.5	4.5	1	2.5	4.5	2.5	4.5	1
π_4	0.1	0.8	1.5	0.8	1.5	0.1	0.1	0.8	1.5
π_5	0.01	0.01	0.01	0.01	0.01	0.01	0.01	0.01	0.01

Table A.C.2: Models Dimensions for the Parametric Study. (Continued)

Model	M10	M11	M12	M13	M14	M15	M16	M17	M18
g	71	79	61	51	93	48	27	60	30
w	19	10	15	25	22	24	17	25	25
h	803	1001	1153	600	1183	836	600	600	1166
b_F	250	275	359	250	267	602	272	895	609
t_F	60	12	16	60	25	27	25	39	28
L	1768	1697	1896	1075	1702	1943	996	2392	1357
S	1200	1200	1420	1481	1307	1292	1200	2368	1320
h_S	732	922	1092	549	1090	788	573	540	1136
t_S	45	11	45	29	11	16	19	15	45
b_S	159	102	157	100	121	260	100	100	218
t_d	10	15	10	11	13	12	10	10	10
h_d	661	770	903	459	901	669	450	450	885
Δ	1.43	1.58	1.21	1.03	1.86	0.96	0.54	1.20	0.60
K_{WEB}	84762	10262	55123	377518	86110	404475	462514	409447	1239968
K_{DIA}	470901	855180	574203	251679	861103	505594	289071	136482	619984
K_{STF}	706352	85518	459362	377518	86110	404475	231257	204723	619984
K_{LBF}	33905	10262	22049	151007	19136	161790	102781	409447	495987
K_{TBF}	2137529540	19710877	56642561	3516879036	166363339	436424227	305713457	1561618399	652827929
π_1	0.12	0.12	0.12	1	1	1	2	2	2
π_2	0.12	1.5	3.5	0.12	1.5	3.5	1.5	1.5	3.5
π_3	2.5	1	2.5	2.5	4.5	2.5	4.5	1	2.5
π_4	1.5	0.1	0.8	1.5	0.1	0.8	0.8	1.5	1
π_5	0.020	0.020	0.020	0.020	0.020	0.020	0.020	0.020	0.020

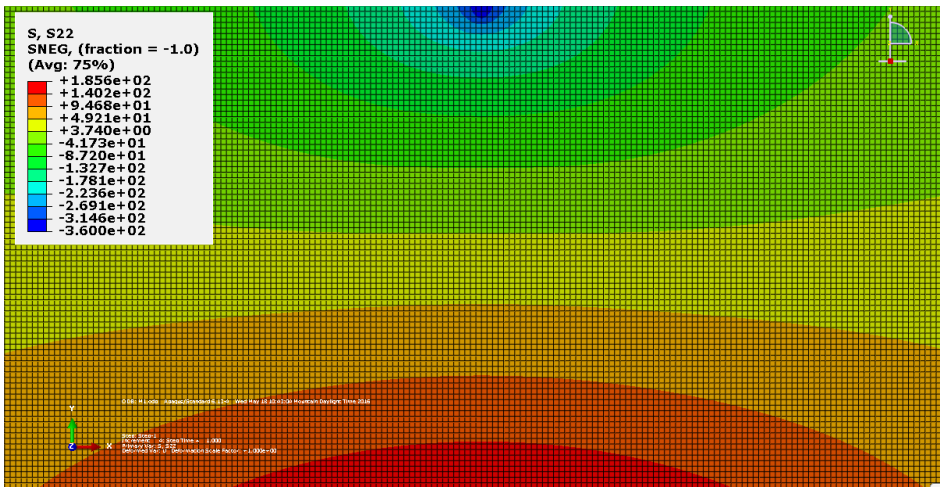

a)

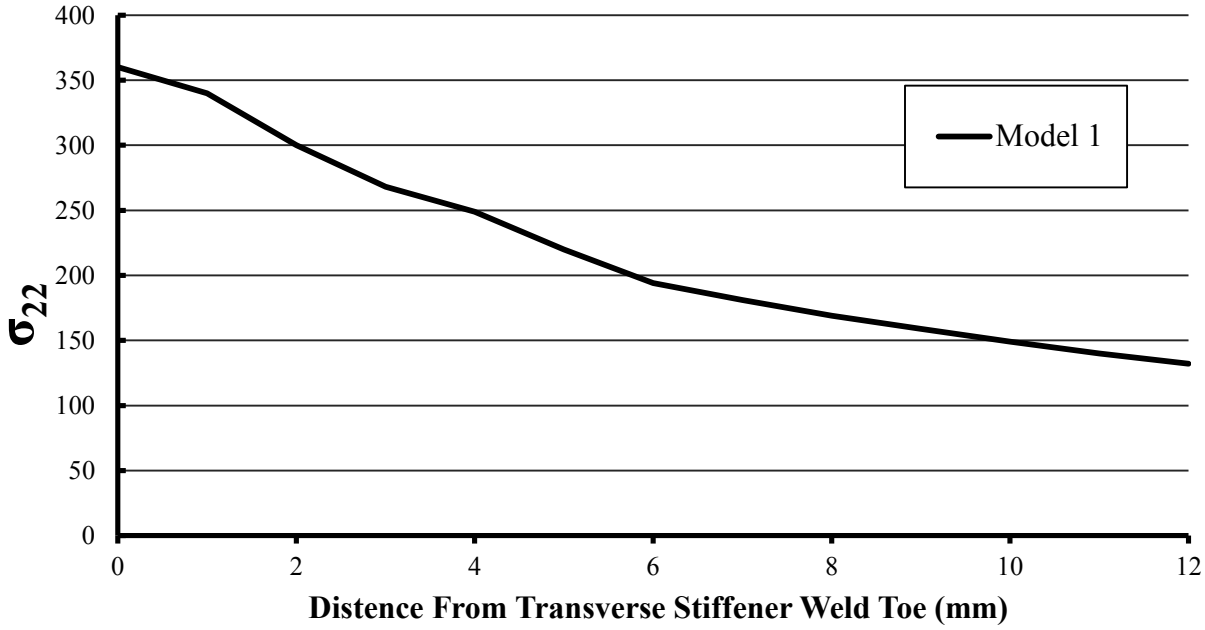

b)

Figure A.C. 1: Vertical stress distribution for Model 1(Run 1) a) in web gap detail, b) along the vertical path at web gap

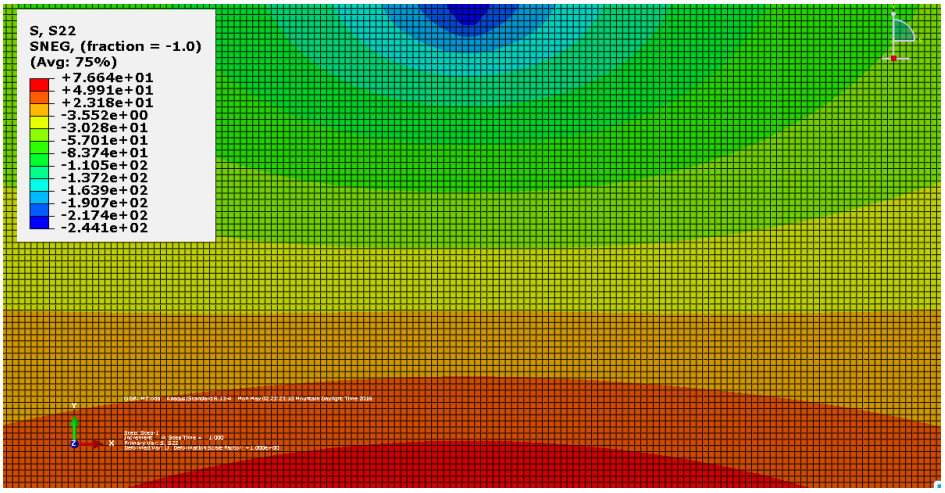

a)

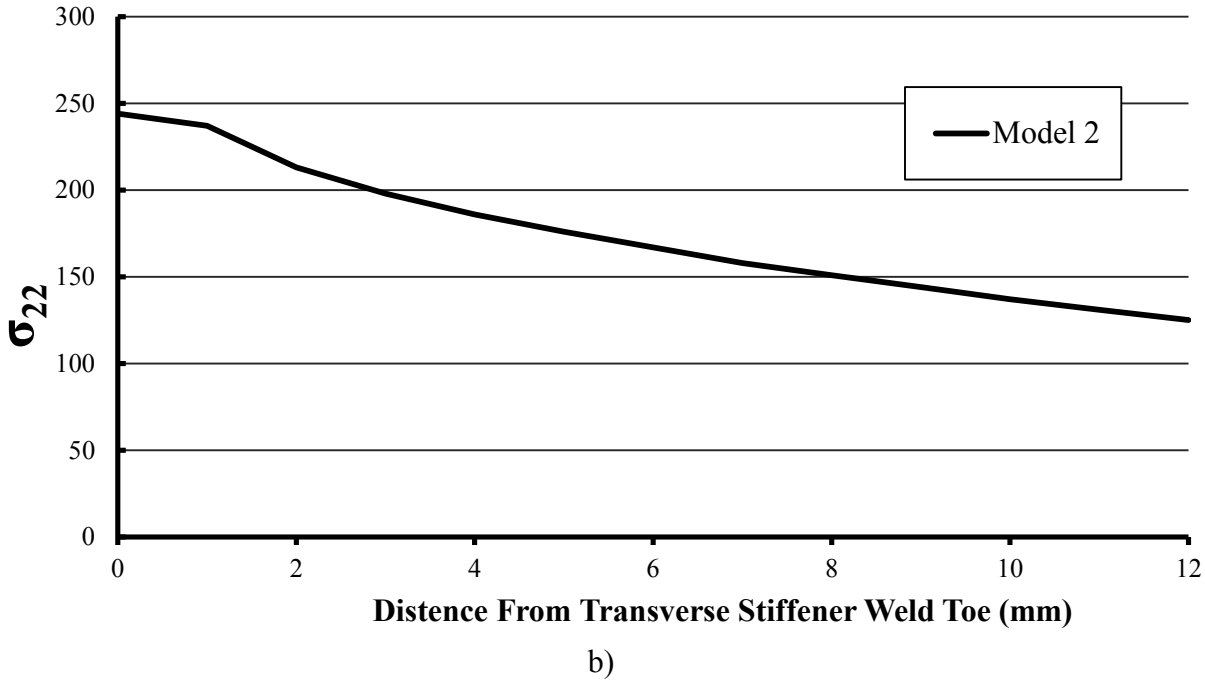

b)

Figure A.C. 2: Vertical stress distribution for Model 2 (Run 2) a) in web gap detail, b) along the vertical path at web gap

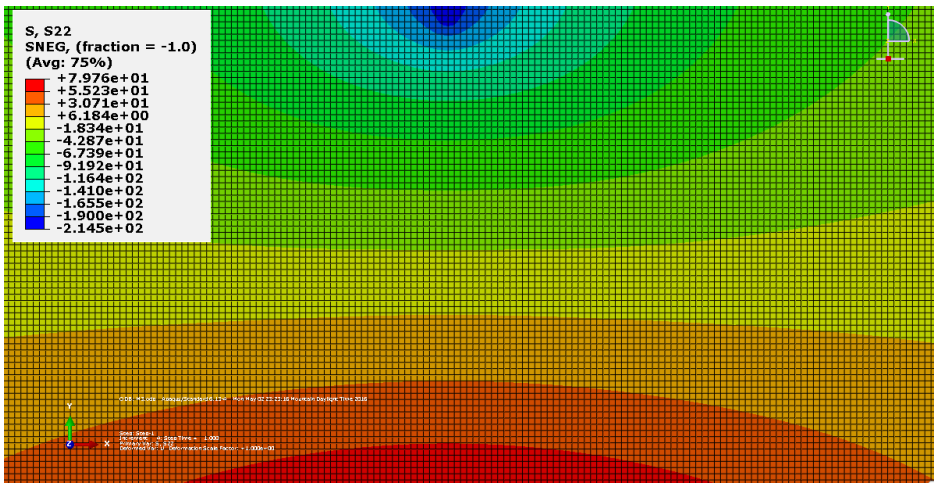

a)

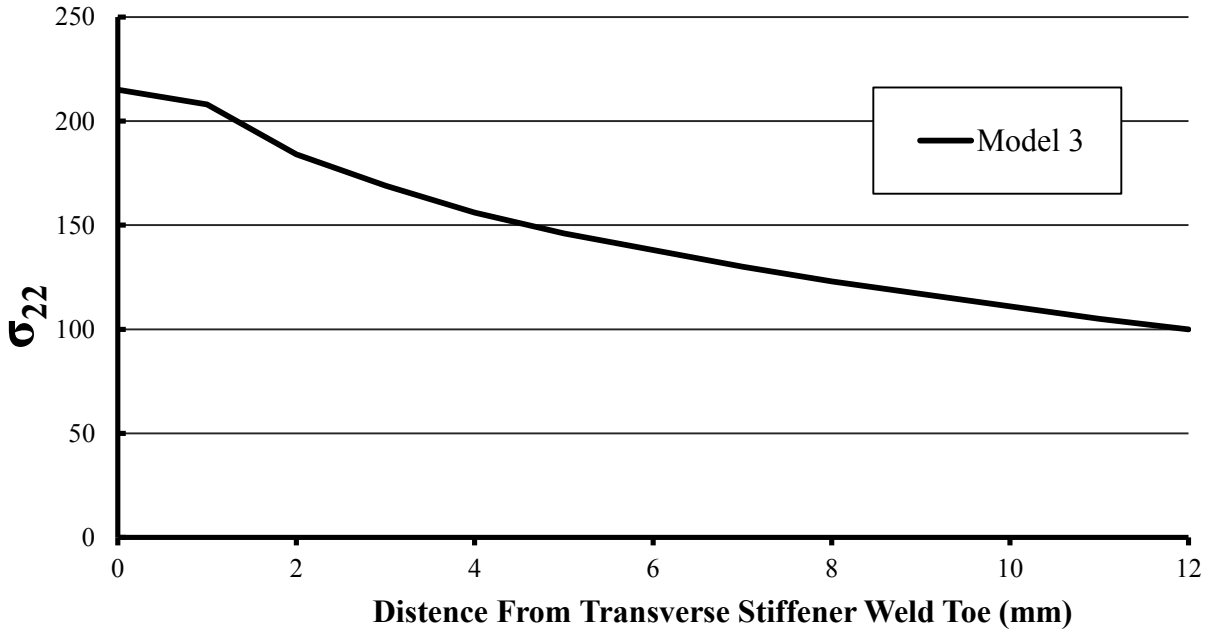

b)

Figure A.C. 3: Vertical stress distribution for Model 3 (Run 3) a) in web gap detail, b) along the vertical path at web gap

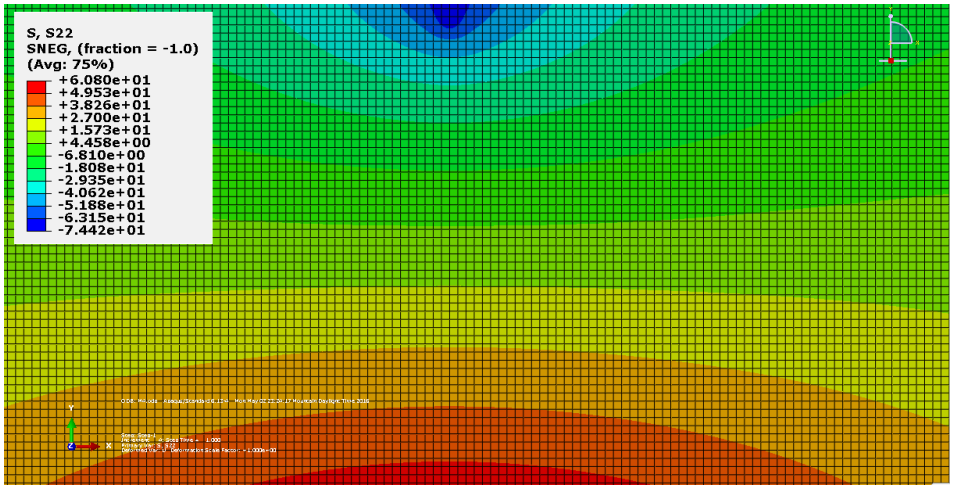

a)

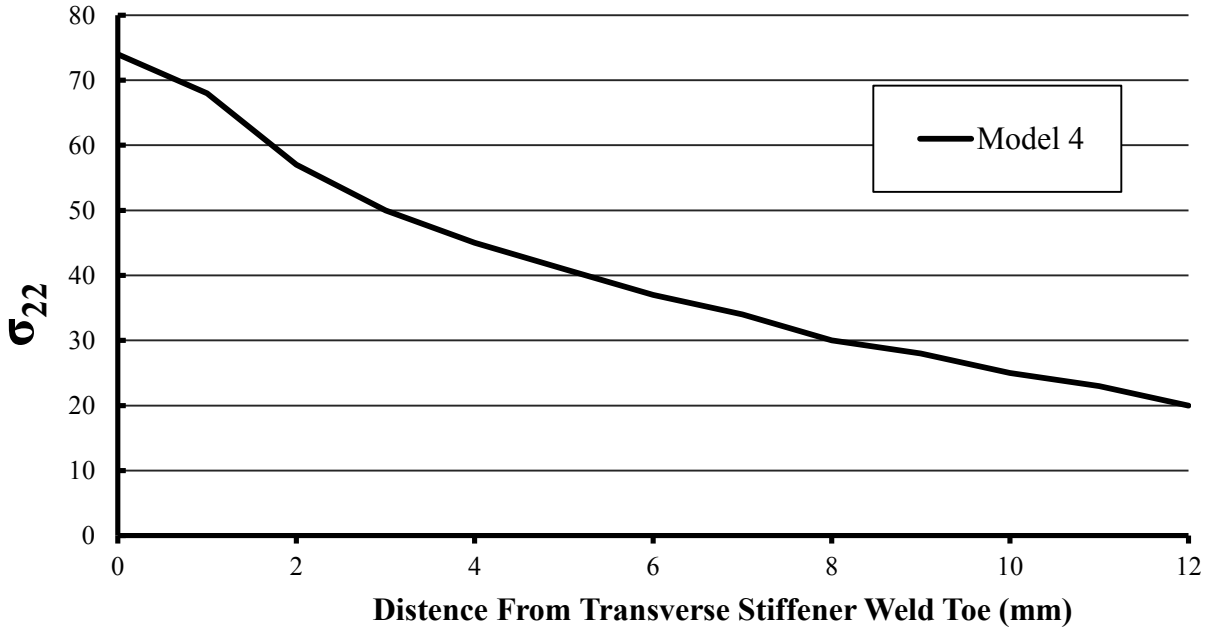

b)

Figure A.C. 4: Vertical stress distribution for Model 4 (Run 4) a) in web gap detail, b) along the vertical path at web gap.

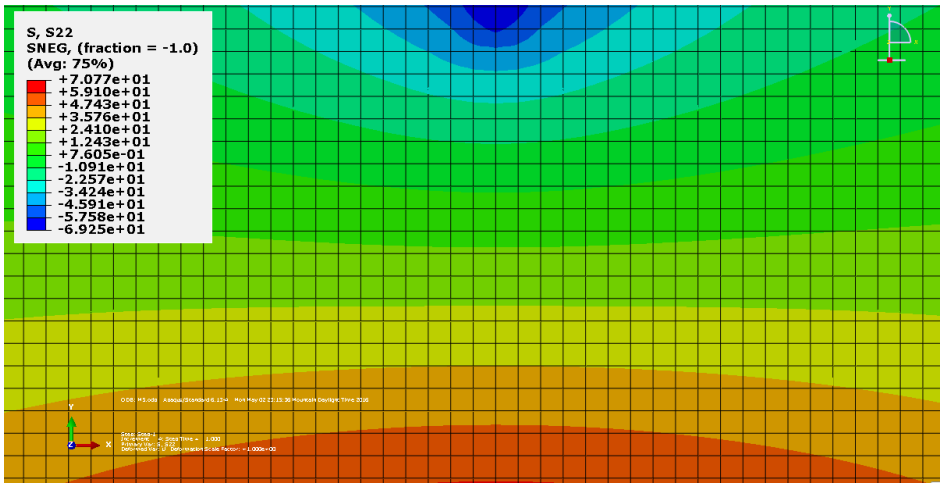

a)

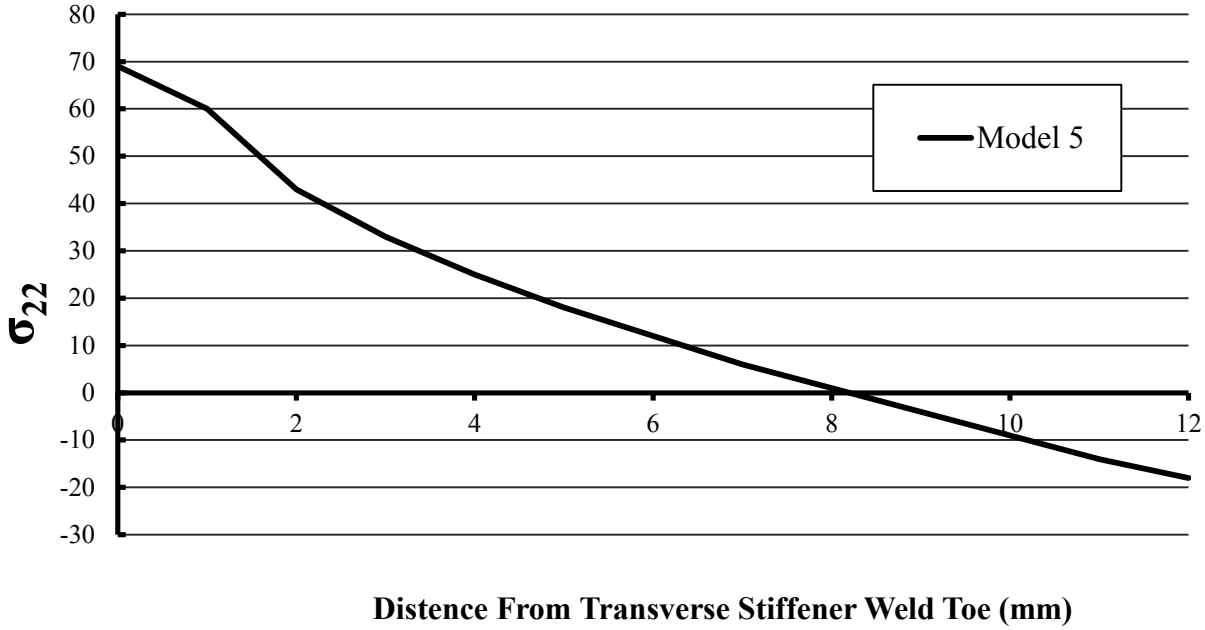

b)

Figure A.C. 5: Vertical stress distribution for Model 5 (Run 5) a) in web gap detail, b) along the vertical path at web gap.

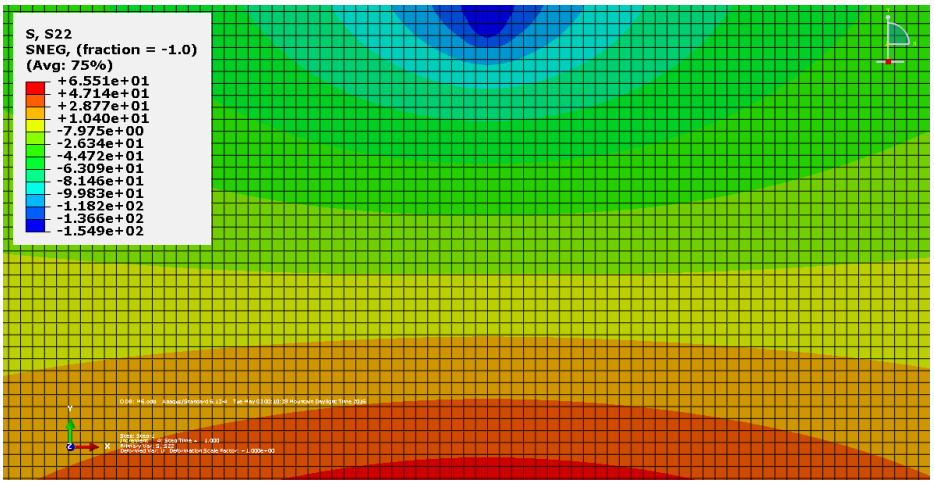

a)

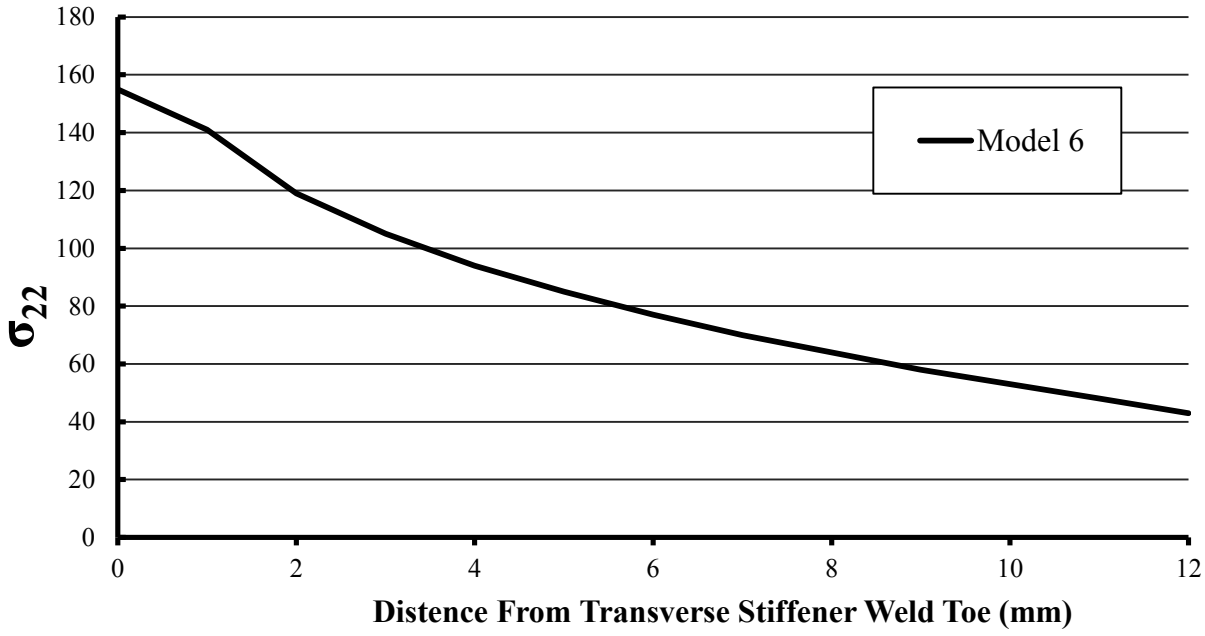

b)

Figure A.C. 6: Vertical stress distribution for Model 6 (Run 6) a) in web gap detail, b) along the vertical path at web gap.

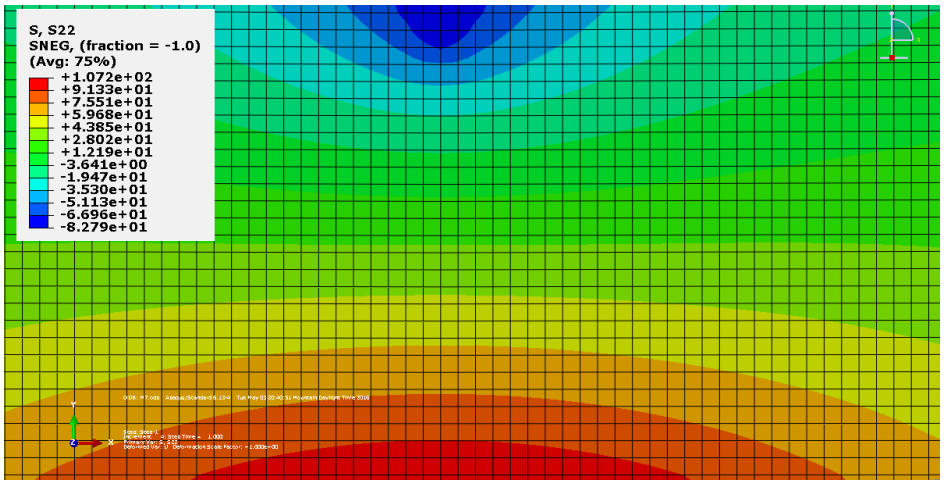

a)

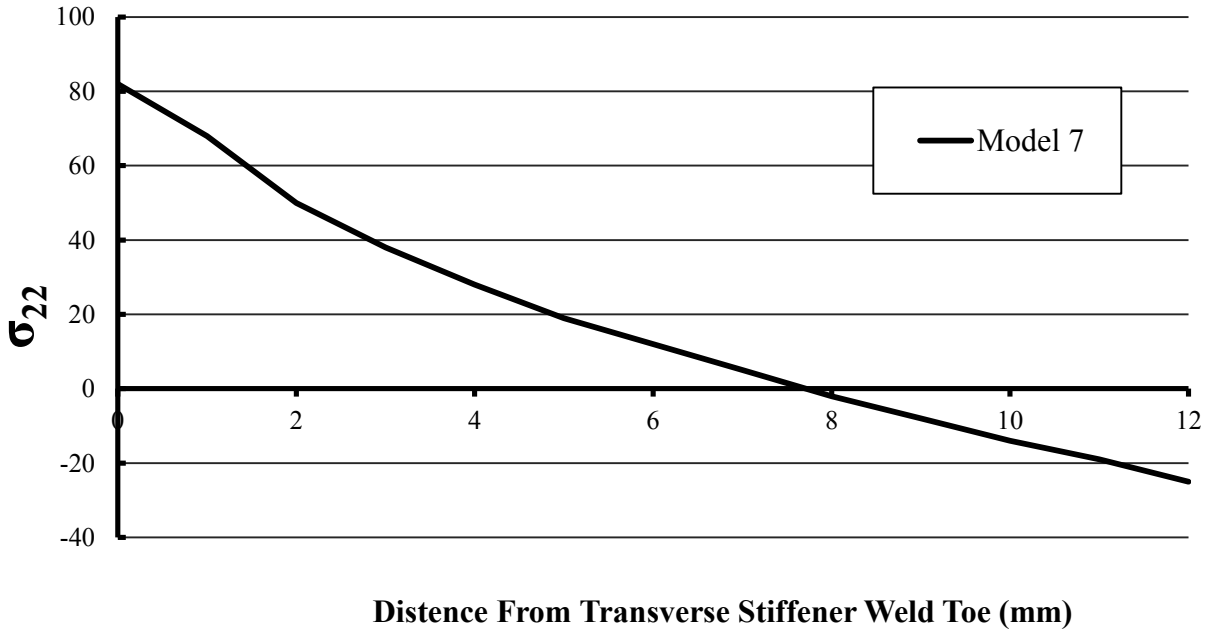

b)

Figure A.C. 7: Vertical stress distribution for Model 7 (Run 7) a) in web gap detail, b) along the vertical path at web gap.

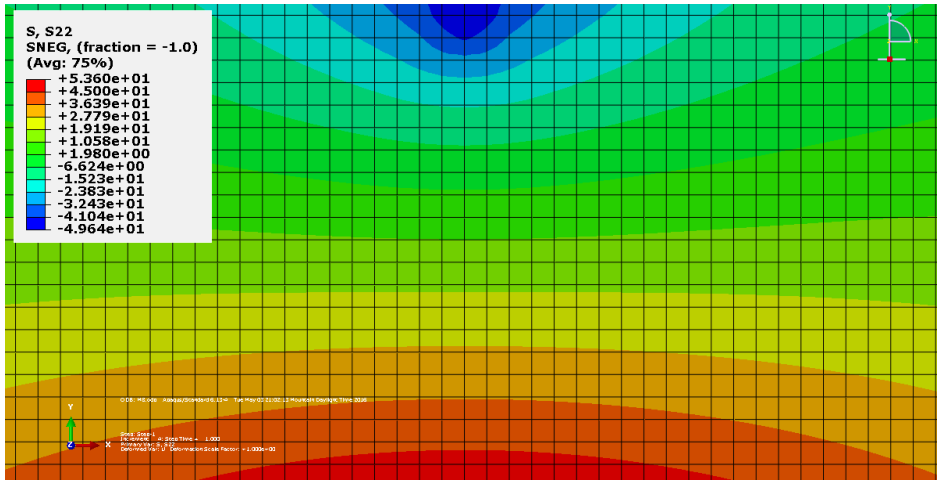

a)

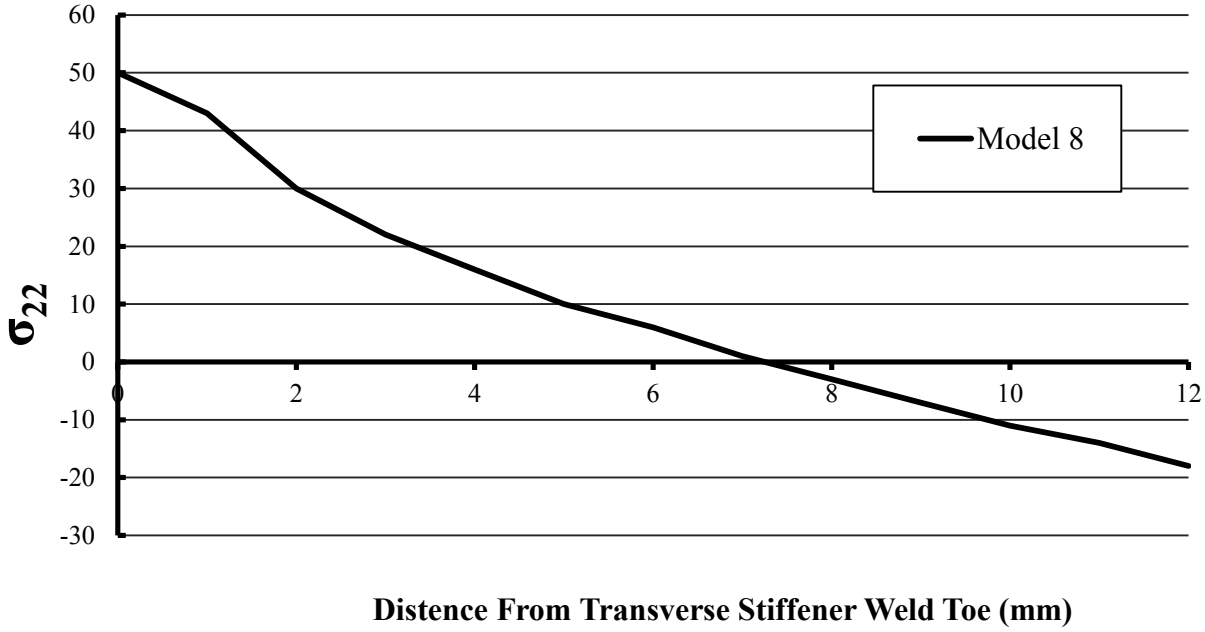

b)

Figure A.C. 8: Vertical stress distribution for Model 8 (Run 8) a) in web gap detail, b) along the vertical path at web gap.

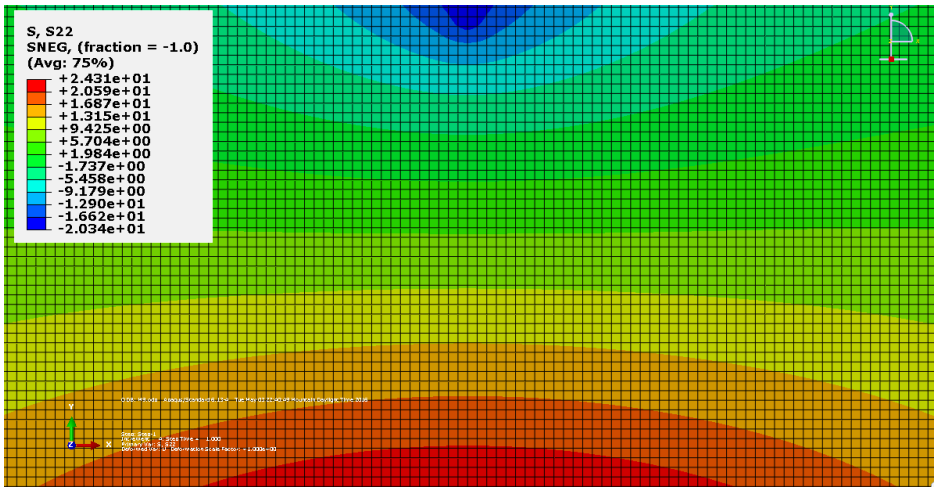

a)

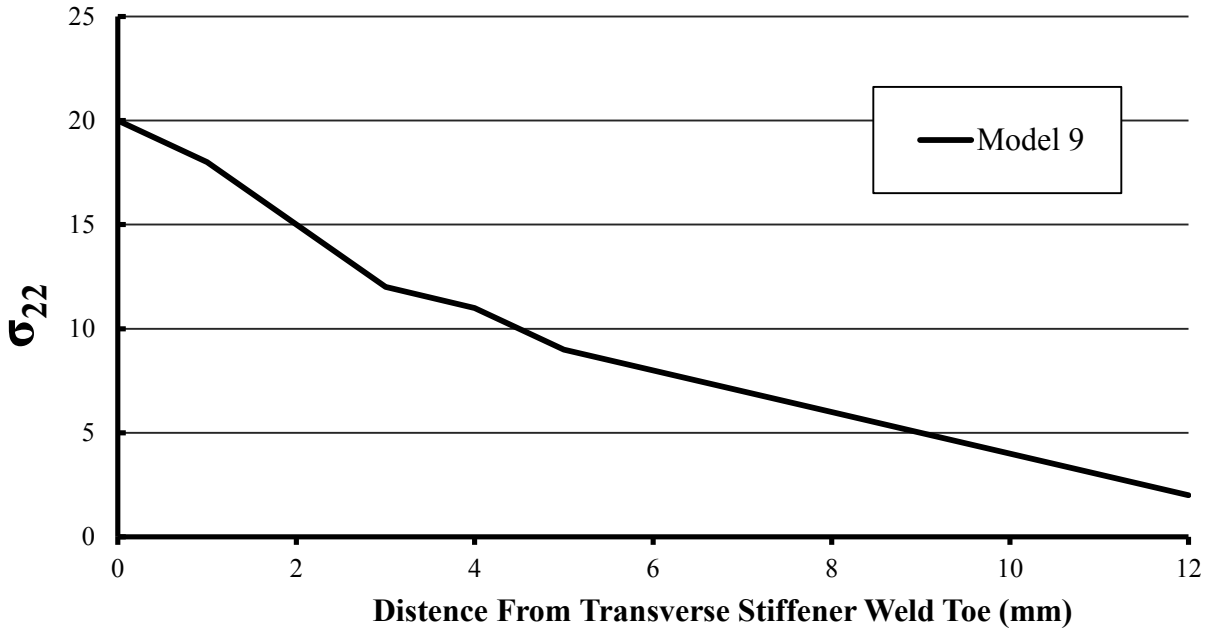

b)

Figure A.C. 9: Vertical stress distribution for Model 9 (Run 9) a) in web gap detail, b) along the vertical path at web gap.

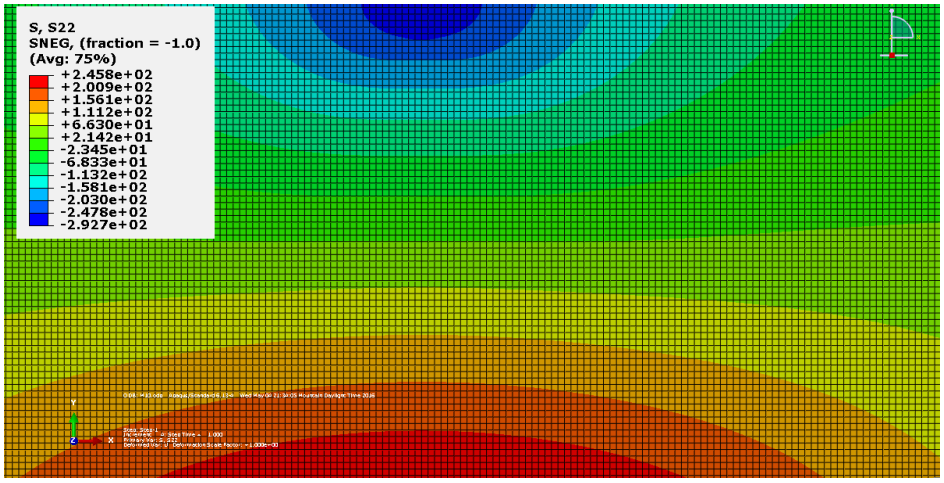

a)

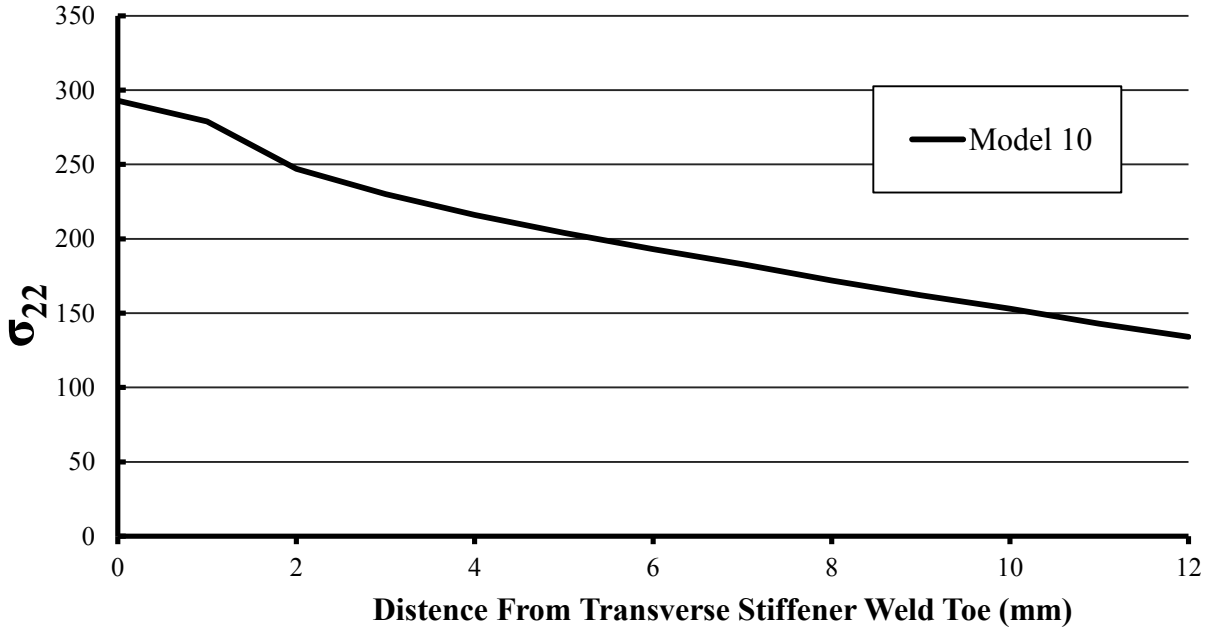

b)

Figure A.C. 10: Vertical stress distribution for Model 10 (Run 10) a) in web gap detail, b) along the vertical path at web gap.

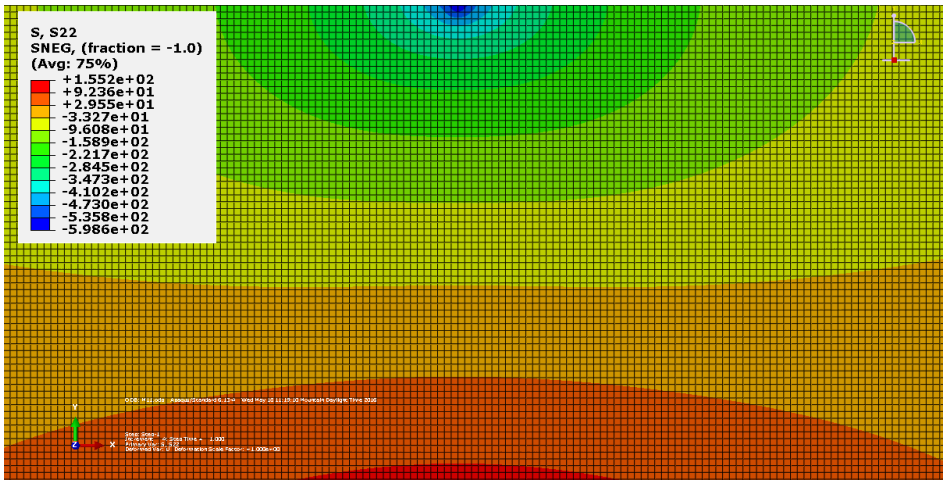

a)

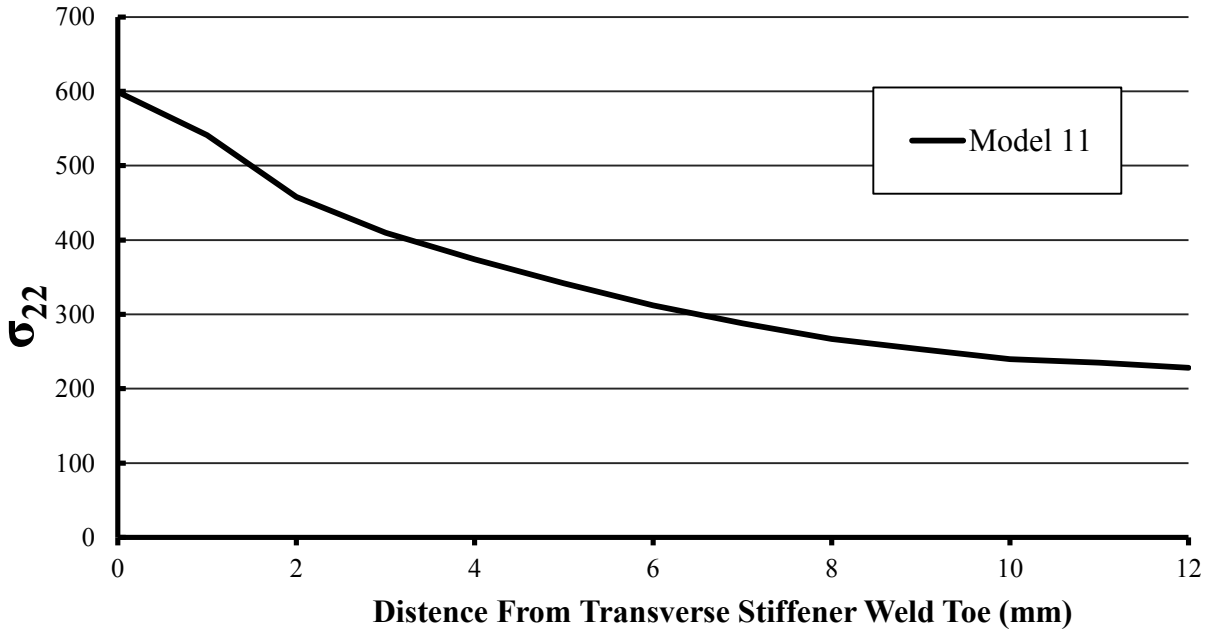

b)

Figure A.C. 11: Vertical stress distribution for Model 11 (Run 11) a) in web gap detail, b) along the vertical path at web gap.

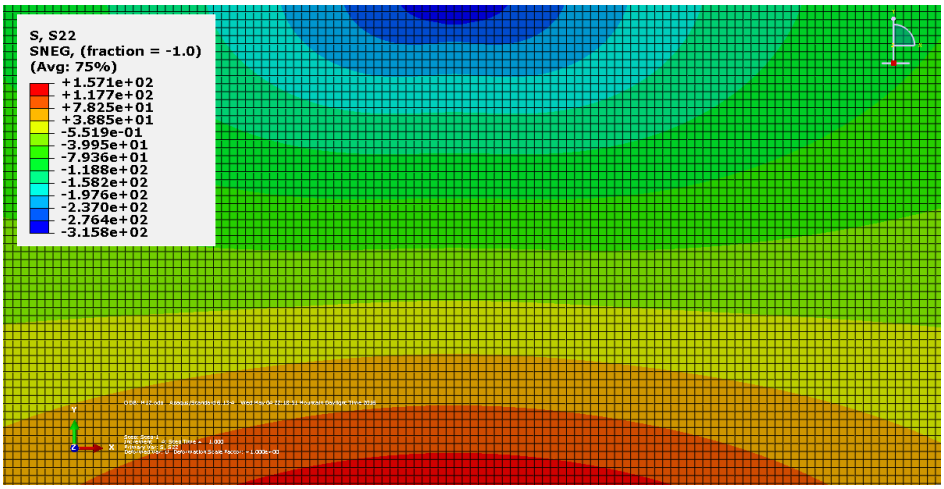

a)

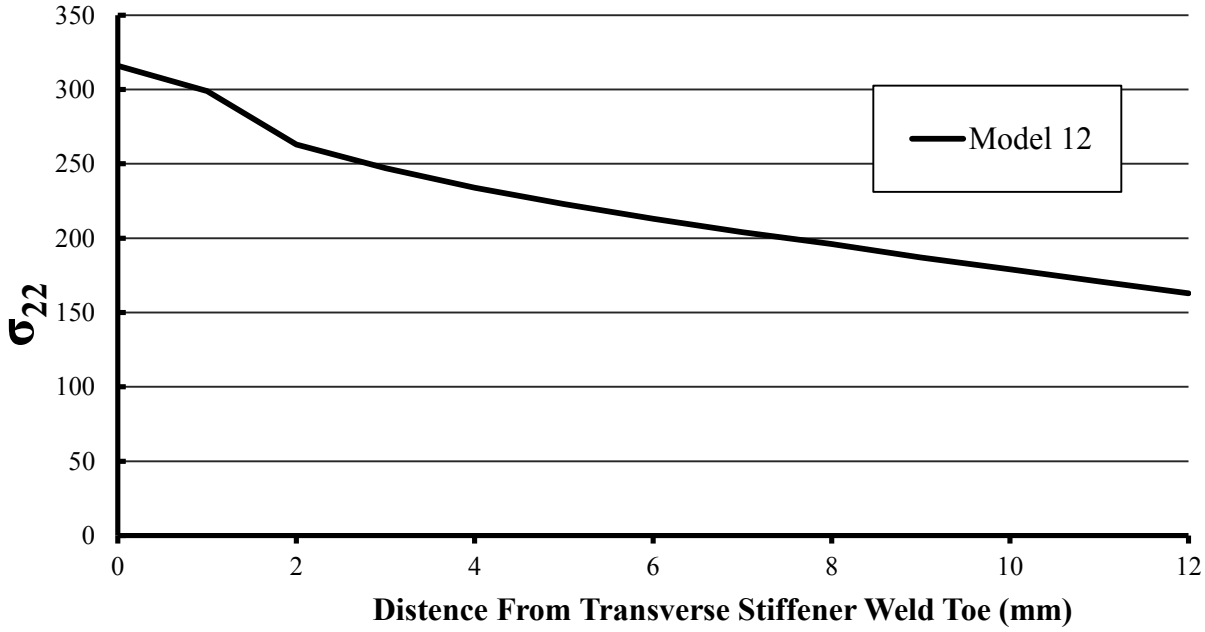

b)

Figure A.C. 12: Vertical stress distribution for Model 12 (Run 12) a) in web gap detail, b) along the vertical path at web gap.

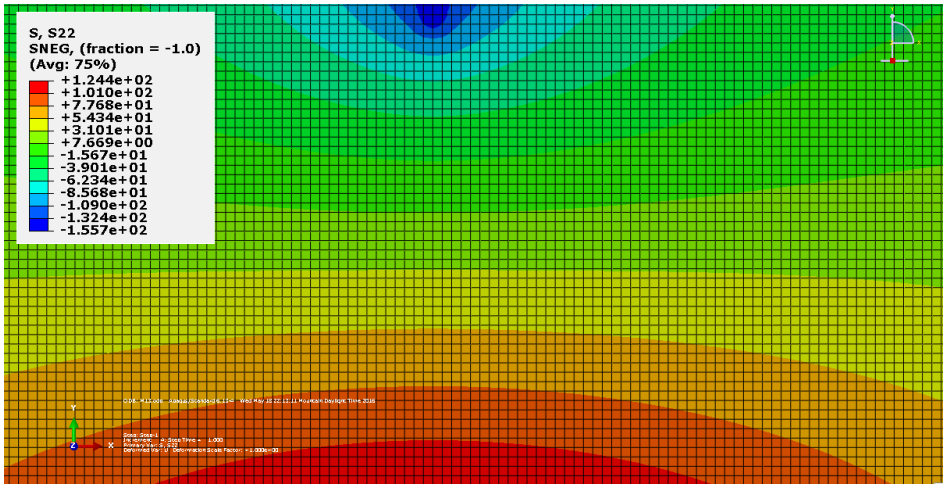

a)

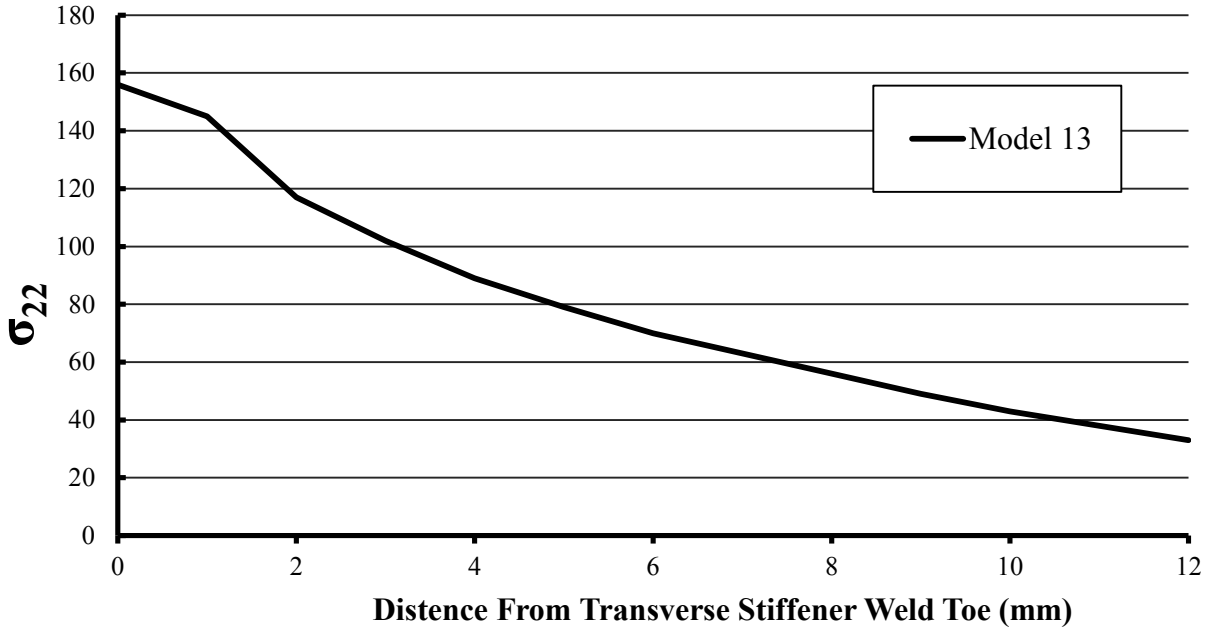

b)

Figure A.C. 13: Vertical stress distribution for Model 13 (Run 13) a) in web gap detail, b) along the vertical path at web gap.

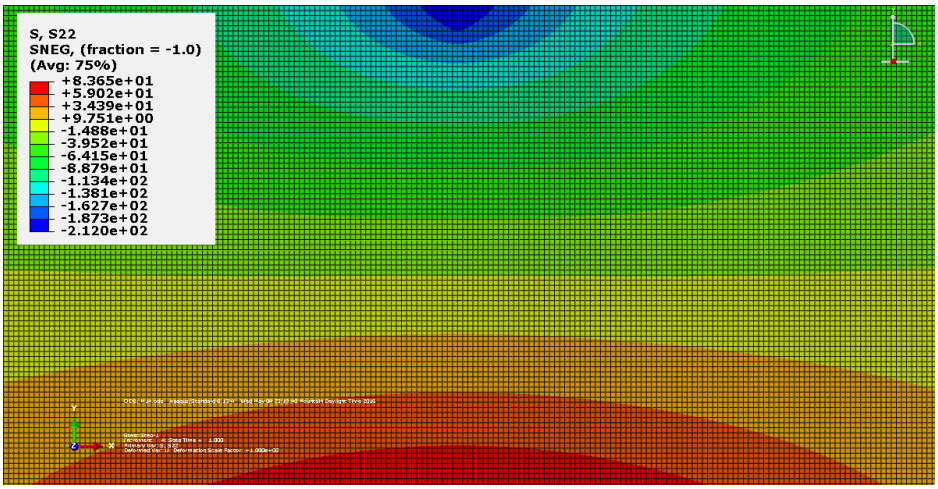

a)

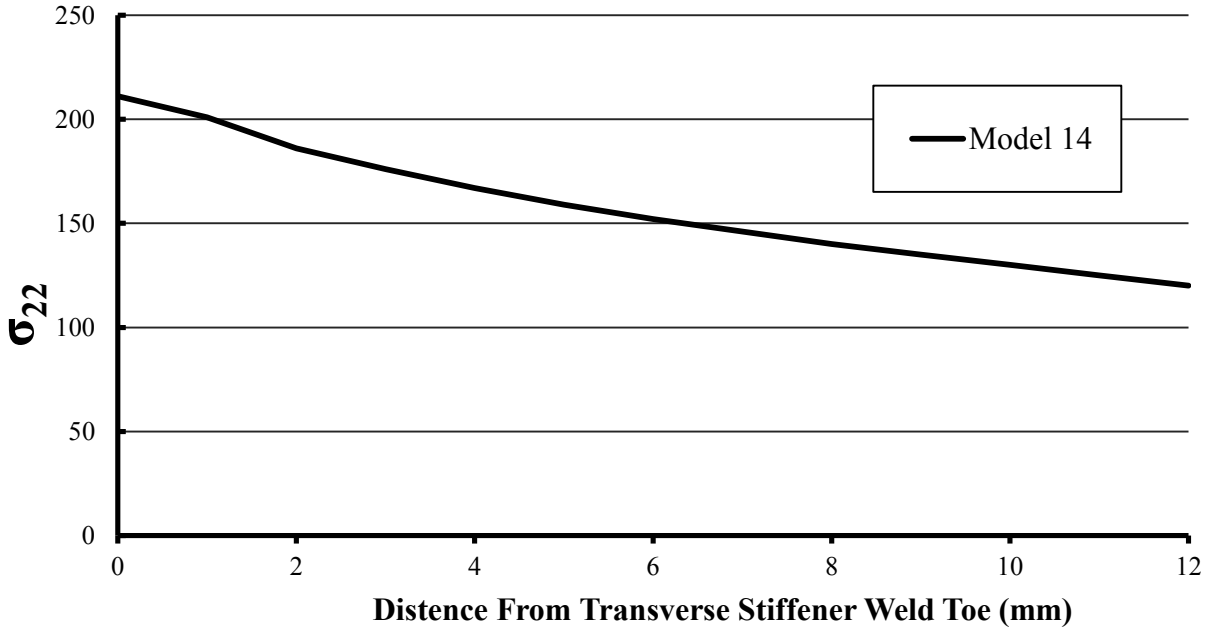

b)

Figure A.C. 14: Vertical stress distribution for Model 14 (Run 14) a) in web gap detail, b) along the vertical path at web gap.

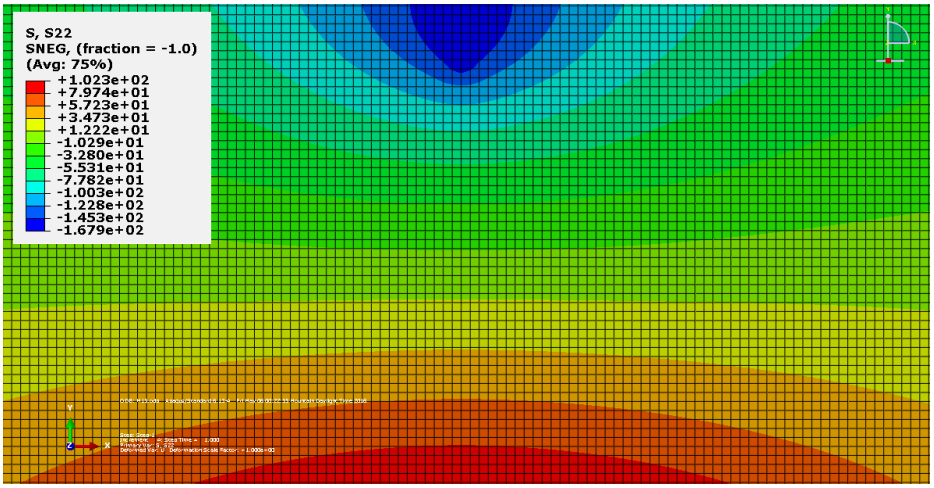

a)

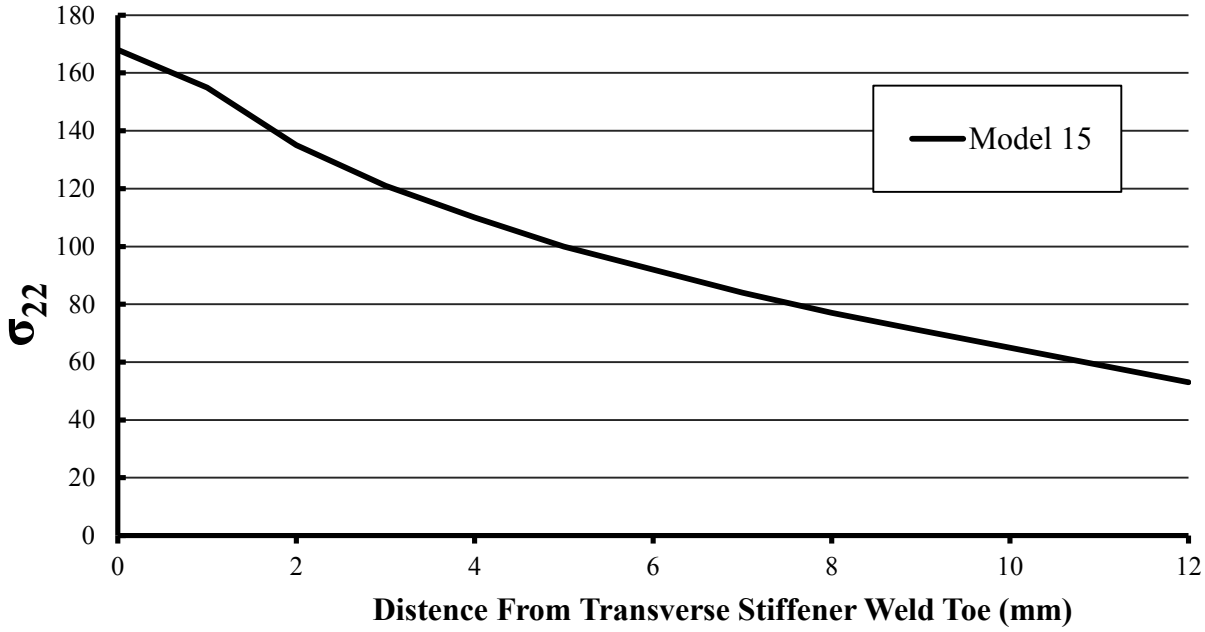

b)

Figure A.C. 15: Vertical stress distribution for Model 15 (Run 15) a) in web gap detail, b) along the vertical path at web gap.

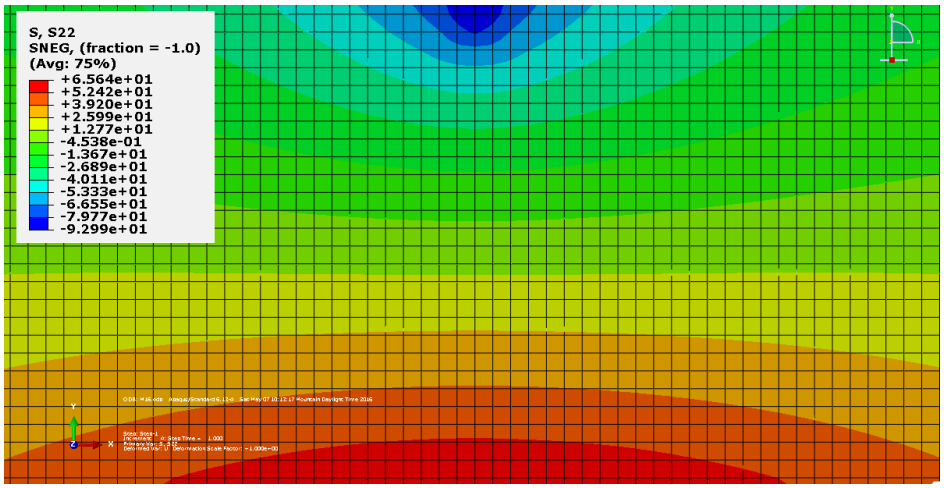

a)

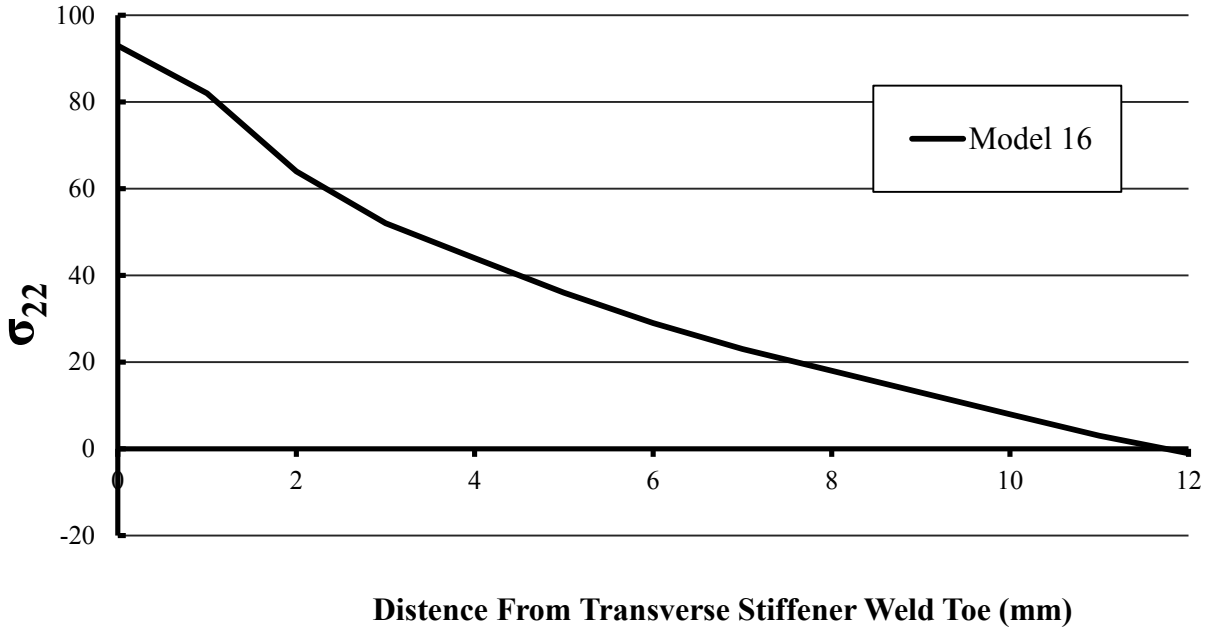

b)

Figure A.C. 16: Vertical stress distribution for Model 16 (Run 16) a) in web gap detail, b) along the vertical path at web gap.

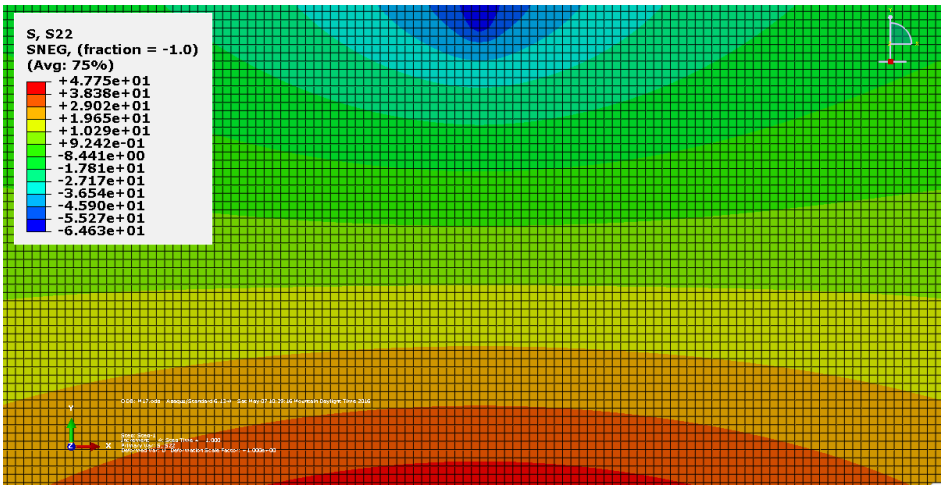

a)

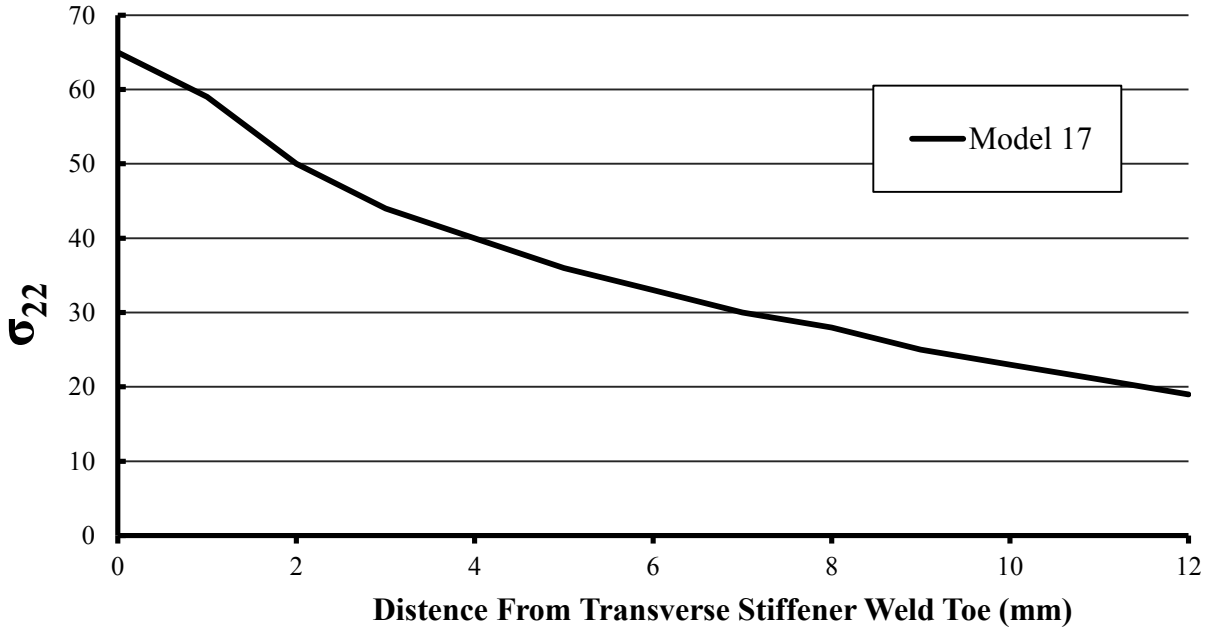

b)

Figure A.C. 17: Vertical stress distribution for Model 17 (Run 17) a) in web gap detail, b) along the vertical path at web gap.

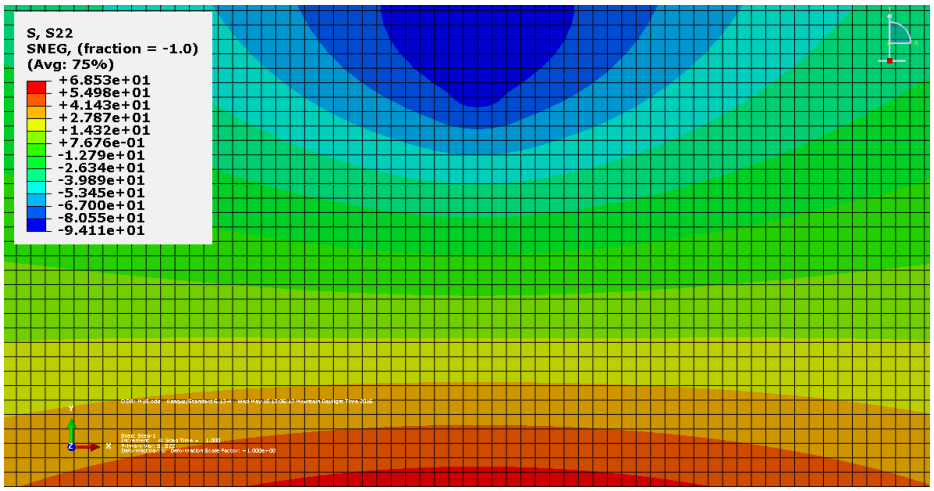

a)

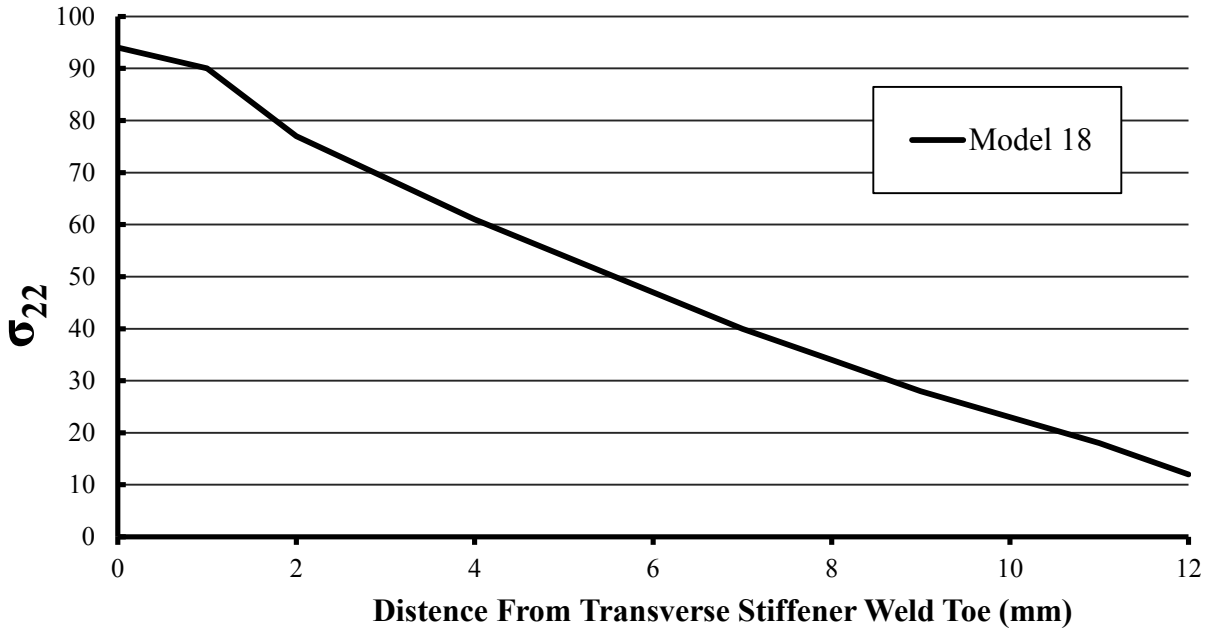

b)

Figure A.C. 18: Vertical stress distribution for Model 18 (Run 18) a) in web gap detail, b) along the vertical path at web gap.